Syntheses and Characterization of Ruthenium(II) Complexes with 5-Methyl-2-(phenylazo)pyridine Ligand

Uraiwan Changsaluk

A Thesis Submitted in Fulfillment of the Requirements
for the Degree of Doctor of Philosophy in Chemistry
Prince of Songkla University
2008

ชื่อวิทยานิพนธ์	การสังเคราะห์และยืนยันโครงสร้างของสารประกอบเชิงซ้อนของโลหะรูทีเนียม โดยมีลิแกนด์ 5-methyl-2-(phenylazo)pyridine
ผู้เขียน	นางสาวอุไรวรรณ ช่างสลัก
สาขาวิชา	เคมี
ปีการศึกษา	2550

บทคัดย่อ

ได้สังเคราะห์ลิแกนด์เอโซอิมีนตัวใหม่ คือ 5-methyl-2-(phenylazo)pyridine (5mazpy) เมื่อนำลิแกนด์ใหม่ 5mazpy มาทำปฏิกิริยากับ $RuCl_3.3H_2O$ ในตัวทำละลายเอทานอล เกิดเป็นสามไอโซเมอร์ของสารประกอบ $[Ru(5mazpy)_2Cl_2]$ ได้แก่ *cis-trans-cis* (*ctc*) *cis-cis-cis* (*ccc*) และ *trans-cis-cis* (*tcc*) มีการสังเคราะห์สารประกอบเชิงซ้อน $[Ru(5mazpy)_2L](PF_6)_2$ $[Ru(5mazpy)_2L']$$(PF_6)_2$ และ $[Ru(L')_2 5mazpy](PF_6)_2$ เมื่อ L คือ 2-(phenylazo)pyridine (azpy) 5-methyl-2-(phenylazo)pyridine (5mazpy) และ L′ คือ 2,2′-bipyridine (bpy) 1,10-phenanthrolene (phen) ได้ศึกษาเคมีของสารประกอบเชิงซ้อนดังกล่าวโดยเทคนิคการวิเคราะห์หาปริมาณธาตุที่เป็นองค์ประกอบ แมสสเปกโทรเมททรี การวัดการดูดกลืนแสง และ อินฟราเรดสเปกโทรสโกปี ศึกษานิวเคลียร์แมกเนติกเรโซแนนซ์สเปกตร้าของสารประกอบเชิงซ้อนโดยใช้เทคนิค ^1H ^{13}C DEPT ^1H-^1H COSY และ ^1H-^{13}C HMQC นิวเคลียร์แมกเนติกเรโซแนนซ์สเปกโทรสโกปี ศึกษาไฟฟ้าเคมีของสารประกอบโดยเทคนิคไซคลิกโวลแทมเมทรี ยืนยันโครงสร้างของลิแกนด์ 5mazpy และ สารประกอบเชิงซ้อน *ctc*, *ccc, tcc*-$[Ru(5mazpy)_2Cl_2]$ และ $[Ru(5mazpy)_2bpy](PF_6)_2$ โดยเทคนิคการเลี้ยวเบนของรังสีเอ็กซ์บนผลึกเดี่ยว ผลจากการศึกษาด้วยเทคนิคอินฟราเรดสเปกโทรสโกปี แถบการยืดของ N=N ในสารประกอบเชิงซ้อนปรากฏที่ความถี่ที่ต่ำกว่าในลิแกนด์อิสระ ซึ่งสนับสนุนอันตรกิริยาการเกิดพันธะไพระหว่างโลหะรูทีเนียมและลิแกนด์ (5mazpy) นอกจากนี้มีการสังเคราะห์สารประกอบเชิงซ้อน $[Ru(5mazpy)_2L](NO_3)_2$ $[Ru(5mazpy)_2L']Cl_2$ และ $[Ru(L')_2 5mazpy]Cl_2$ เพื่อศึกษาคุณสมบัติการจับกันระหว่างดีเอ็นเอกับสารประกอบเชิงซ้อนโดยเทคนิคการไทเทรตวัดการดูดกลืนแสง (absorption titration) การแย่งจับ (competitive binding) การวัดความหนืด (viscosity measurements) และ ไซคลิกโวลแทมเมทรี (cyclic voltammetry) ติดตามการตัดสายพลาสมิดดีเอ็นเอ (pBIND)โดยเทคนิค agarose gel electrophoresis ผลจากการศึกษาแสดงให้เห็นว่าสารประกอบเชิงซ้อนจับกับดีเอ็นเอ แบบการแทรกสอด (intercalation) และตัดสายพลาสมิด

ดีเอ็นเอ นอกจากนี้มีการทดสอบการออกฤทธิ์ทางชีวภาพของสารประกอบเชิงซ้อนของโลหะรูทีเนียมต่อเซลล์มะเร็งปอด (A549 และ Anti-NCl-H187) มะเร็งลำไส้ (WIDR) มะเร็งรังไข่ (IGROV) มะเร็งเต้านม (MCF-7 และ BC) มะเร็งอัณฑะ (PC3) มะเร็งผิวหนัง (SK-MEL-28) มะเร็งเม็ดเลือด (CEM) และ มะเร็งเยื่อบุที่ปาก (KB) พบว่า สารประกอบเชิงซ้อน *ctc*-[Ru(5mazpy)$_2$Cl$_2$] ออกฤทธิ์ต่อเซลล์มะเร็งปอด (A549) และ มะเร็งลำไส้ (WIDR) ได้ดีกว่าซีสพลาติน

Thesis Title	Syntheses and Characterization of Ruthenium(II) Complexes with 5-Methyl-2-(phenylazo)pyridine Ligand
Author	Miss Uraiwan Changsaluk
Major Program	Chemistry
Academic Year	2007

ABSTRACT

The new azoimine functionalized ligand, 5-methyl-2-(phenylazo)-pyridine (5mazpy) was synthesized. It reacted with $RuCl_3.3H_2O$ in ethanolic solution to give three isomers of $[Ru(5mazpy)_2Cl_2]$. These isomers are *cis-trans-cis* (*ctc*), *cis-cis-cis* (*ccc*), *trans-cis-cis* (*tcc*). In addition, the $[Ru(5mazpy)_2L](PF_6)_2$, $[Ru(5mazpy)_2L'](PF_6)_2$ and $[Ru(L')_25mazpy](PF_6)_2$ complexes (L = 2-(phenylazo)pyridine (azpy), 5-methyl-2-(phenylazo)pyridine (5mazpy); L′ = 2,2′-bipyridine (bpy), 1,10-phenanthrolene (phen)) were also synthesized. They were characterized by elemental analysis, mass spectrometry, UV-visible absorption spectroscopy, and infrared spectroscopy. The NMR spectra have been resolved using ^1H, ^{13}C, DEPT, ^1H-^1H COSY, and ^1H-^{13}C HMQC NMR spectroscopy. The electrochemistry of the complexes was investigated by cyclic voltammetry. The structures of 5mazpy, *ctc*-, *ccc*-, *tcc*-$[Ru(5mazpy)_2Cl_2]$, and $[Ru(5mazpy)_2bpy](PF_6)_2$ have been confirmed by X-ray crystallography. Results from infrared spectroscopy show that N=N stretching mode in the complexes appeared at a lower frequency than that in the free ligand supporting Ru-azo nitrogen pi bonding interaction. In addition, the complexes of $[Ru(5mazpy)_2L](NO_3)_2$, $[Ru(5mazpy)_2L']Cl_2$ and $[Ru(L')_25mazpy]Cl_2$ were also synthesized for studing DNA interaction. The DNA-binding properties of the ruthenium complexes were investigated by absorption titration, competitive binding, viscosity measurements, and cyclic voltammetry. In addition, the cleavage reaction on plasmid DNA (pBIND) has been monitored by agarose gel electrophoresis. The experimental results suggest that the ruthenium complexes bind to DNA in an intercalative mode and can cleave the plasmid DNA. Besides, the biological acticity of ruthenium complexes have been also studied with a series of human tumor cell lines, lung cancer (A549 and Anti-NCl-H187), colon cancer (WIDR), ovarian cancer

(IGROV), breast cancer (MCF-7 and BC), prostate cancer (PC3), melanoma cancer (SK-MEL-28), leukemia (CEM) and oral human epidermal carcinoma (KB). The results showed that *ctc*-[Ru(5mazpy)$_2$Cl$_2$] displays high activity in lung cancer (A549) and colon cancer (WIDR) than cisplatin.

Acknowledgements

I would like to thank all people who have helped and inspired me during my doctoral study.

First of all I wish to express my sincere gratitude to my advisor, Asst. Prof. Dr. Kanidtha Hansongnern, who guided this work, suggested and encouraged me in all the time of research and for writing of this thesis.

I would like to thank Asst. Prof. Dr. Chaveng Pakawatchi for suggestion and preparing X-ray cryatallographic data and Asst. Prof. Dr. Adisorn Ratanaphan for suggestion and providing the service of gel electrophoresis technique. I also wish to thank Prof. Selby A. R. Knox and Prof. Neil Connelly for FAB and ESI mass spectrometric data. I would like to thank Dr. John D Allen and his team who gave me an opportunity to do a part of my thesis at Cancer Drug Resistance (CDR) laboratory and the Centenary Institute of Cancer Medicine and Cell Biology, Faculty of Medicine, University of Sydney, Australia and gave me an important guidance about cytotoxicity assay.

I wish to thank all of examination committee of this thesis (Assoc. Prof. Dr. Sutatip Siripaisarnpipat, Asst. Prof. Dr. Kanidtha Hansongnern, Asst. Prof. Dr. Adisorn Ratanaphan, Dr. Walailak Puetpaiboon, and Dr. Nararak Leesakul) for their valuable time. I am grateful to Department of Chemistry, Faculty of Science, Prince of Songkla University for all necessary laboratory apparatus and chemical supplies used throughout this research.

The financial support from the Center for Innovation in Chemistry: Postgraduate Education and Research Program in Chemistry (PERCH-CIC), Commission on Higher Education, Ministry of Education and Thailand Research Fund (Grant No. BRG 4680018), Department of Chemistry Faculty of Science and Graduate School at Prince of Songkla University are gratefully acknowledged. I also thank the Center of Excellence in Nanotechnology under the Southern Thailand Science Park for a grant during my work in Sydney, Australia.

I wish to thank my former and present colleagues of CH439 are grateful for their kindness, help and friendship. I would also like to thank my friends,

Kittiya Muaksang and Jerremy Shearman for all of their help and support during my stay in Sydney. Finally, my deepest gratitude goes to my family for their unflagging love and support throughout my life.

Uraiwan Changsaluk

The Relevance of the Research Work to Thailand

Cancer in Thailand is becoming a significant health problem. It is the leading cause of death in Thailand. The platinun compounds are widely used as chemotherapy drug such as cisplatin and carboplatin. It is most commonly used to treat testicular, bladder, lung, stomach and ovarian cancers. But they have toxic side effects. Therefore, the researcher try to develop the new drugs. In this work we focus on the ruthenium(II) complexes which contain the new bidentate ligand, 5-methyl-2-(phenylazo)pyridine (5mazpy). The $[Ru(5mazpy)_2Cl_2]$, $[Ru(5mazpy)_2L](PF_6)_2$, $[Ru(5mazpy)_2L'](PF_6)_2$, and $[Ru(L')_2 5mazpy](PF_6)_2$ complexes (L = 2-(phenylazo)pyridine (azpy), 5-methyl-2-(phenylazo)pyridine (5mazpy); L′ = 2,2′-bipyridine (bpy), 1,10-phenanthroline (phen)) were synthesized and characterized. In addition, the water soluble complexes, $[Ru(5mazpy)_2L](NO_3)_2$, $[Ru(5mazpy)_2L']Cl_2$, $[Ru(L')_2 5mazpy]Cl_2$, were also synthesized for study of DNA interaction. Furthermore, all complexes, $[Ru(5mazpy)_2Cl_2]$, $[Ru(5mazpy)_2L](PF_6)_2$, $[Ru(5mazpy)_2L'](PF_6)_2$, $[Ru(L')_2 5mazpy](PF_6)_2$, $[Ru(5mazpy)_2L](NO_3)_2$, $[Ru(5mazpy)_2L']Cl_2$, and $[Ru(L')_2 5mazpy]Cl_2$, were investigated cytotoxicity against a series of human tumor cell lines (A549, CEM, IGROV, MCF-7, PC3, SK-MEL-28, WIDR, Anti-NCI-H187, BC, and KB). The result from this work is a basic knowledge for developing the new antitumor agents in the future.

Contents

Contents (Continued)

Contents (Continued)

Contents (Continued)

List of Tables

List of Tables (Continued)

List of Tables (Continued)

List of Tables (Continued)

List of Tables (Continued)

List of Figures

List of Figures (Continued)

List of Figures (Continued)

List of Figures (Continued)

List of Figures (Continued)

List of Figures (Continued)

List of Figures (Continued)

List of Figures (Continued)

List of Figures (Continued)

List of Figures (Continued)

List of Figures (Continued)

List of Figures (Continued)

List of Figures (Continued)

List of Figures (Continued)

List of Figures (Continued)

List of Figures (Continued)

List of Figures (Continued)

Abbreviations and symbols

5mazpy	5-Methyl-2-(phenylazo)pyridine
Å	Angstrom unit (1Å = 10^{-10} meter)
A.R. grade	Analytical reagent grade
azpy	2-(Phenylazo)pyridine
bpy	2,2′-Bipyridine
CD_3OD	Deuterated methanol
$CDCl_3$	Deuterated chloroform
CH_3CN	Acetonitrile
$CHCl_3$	Chloroform
CH_2Cl_2	Dichloromethane
cm^{-1}	Wave number
COSY	Correlation spectroscopy
CT DNA	Calf thymus DNA
CV	Cyclic voltammetry
d	Doublet
dd	Doublet of doublet
ddd	Doublet of doublet of doublet
DEPT	Distortionless Enhancement by Polarization Transfer
DMF	N,N-Dimethylformamide
DMSO	Dimethyl sulfoxide
FAB MS	Fast-atom bombardment Mass Spectrometry
ESI	Electro spray ionization mass spectrometry
g	Gram
h	Hour
HMQC	Heteronuclear Multiple Quantum Correlation experiment
HOMO	Highest Occupied Molecular Orbital

Abbreviations and symbols (Continued)

Hz	Hertz
IC_{50}	Inhibitory concentration of 50%
IR	Infrared
J	Coupling constant
K	Kelvin
LUMO	Lowest Unoccupied Molecular Orbital
mL	Milliliter
mmol	Millimole
mVs^{-1}	Millivolt per second
m/z	A value of mass divided by charge
MLCT	Metal to ligand charge transfer
MW	Molecular weight
nm	Nanometer
NMR	Nuclear Magnetic Resonance
NOESY	Nuclear Overhauser Enhancement Spectroscopy
phen	1,10-Phenanthroline
ppm	Part per million
Rel. Abun.	Relative abundance
s	Singlet
SCE	Saturated Salomel reference Electrode
t	Triplet
td	Triplet of doublet
TMS	Tetramethylsilane
UV-Vis	Ultraviolet-Visible
°	Degree
ε	Molar extinction coefficient
δ	Chemical shift relative to TMS

CHAPTER 1
INTRODUCTION

1.1 Background

The ruthenium(II) complexes containing azoimine (-N=N-C=N-) and imine (-N=C-C=N-) functional units have been chosen for study of their chemistry. These two functions are isoelectronic and π-acidic in character.

Azoimine ligands, such as 2-(phenylazo)pyridine (azpy), which contain the -N=N-C=N- linkage have unusual properties (Velder *et al.*, 2004). The pyridine ring is an intermediate π-accepter, and its nitrogen is a weak σ-donor. The azo group has low σ-donor ability to the metal, but possesses enhanced π-accepting ability through the azo π* orbital. The polypyridyl ligand is a symmetric bidentate ligand, which has σ-donor and π-accepter properties such as 2,2′-bipyridine (bpy) and 1,10-phenantroline (phen). These ligands contain the imine moiety (-N=C-C=N-).

There are a variety of applications of the ruthenium(II) complexes with azoimine and imine ligands. In the research for antitumor-active metal complexes, several ruthenium complexes have been reported to be promising as anticancer drugs. For example, the $[Ru(azpy)_2Cl_2]$ complexes show remarkably high cytotoxicity against a reries of tumor-cell lines (Velder *et al.*, 2004). Furthermore, the $[Ru(azpy)_2L]$ complexes (L = 1,1-cyclobutanedicarboxylate, oxalate, malonate) display a promising cytotoxicity in the A2780 cell line (Hotze *et al.*, 2003). The cytotoxicity data of the mer-$[Ru(azpy)_3](PF_6)_2$, α-$[Ru(azpy)_2bpy](PF_6)_2$, β-$[Ru(azpy)_2$ $bpy](PF_6)_2$ and $[Ru(bpy)_2azpy](PF_6)_2$ complexes show a moderate activity in some particular cell lines (Hotze *et al.*, 2005). In addition, the interaction of the cytotoxic α-$[Ru(azpy)_2Cl_2]$ with DNA-model base has been studied (Hotze *et al.*, 2000).

Over the past decade there has been substantial interest in the design and study of DNA binding properties of a number of potential, substitution inert and redox active ruthenium(II) complexes, in the hope of developing novel probes of the

DNA structure. Particularly, the octahedral ruthenium(II) complexes incorporating the aromatic ligands are suitable for application. They have many unique and convenient features such as strong visible absorbance which provide a convenient, sensitive and powerful spectroscopic for monitoring the DNA binding process.

Recently, a ruthenium(II) polypyridyl derivative, $[Ru(bpy)_2(dppz)]^{2+}$ (bpy = 2,2′-bipyridine; dppz = dipyrido[3,2-*a*:2′,3′-*c*]phenazine) was shown to be a remarkable luminescent light switch for DNA (Hartshorn and Barton, 1992). In addition, the $[Ru(bpy)_2(actatp)](ClO_4)_2.2H_2O$ and $[Ru(phen)_2(actatp)](ClO_4)_2.2H_2O$ (actatp = acenaphthereno[1,2-*b*]-1,4,8,9-tetraazariphenylence) complexes bind to DNA through an intercalative mode (Deng *et al.*, 2003). Zhen *et al*. reported that $[Ru(bpy)_2L]^{2+}$ (L = 4,5, 9,18-tetraazaphenanthreno[9,10-*b*]triphenylene (taptp); 2,3-di-phenyl-1,4,8,9-tetraazatriphenylene (dptatp)) bind enantioselectively to double-stranded calf thymus DNA via the intercalative mode (Zhen *et al*., 1999).

In this work, our interest is to synthesize the complexes of ruthenium(II) with a new azoimine ligand, 5-methyl-2-(phenylazo)pyridine (5mazpy). The 5mazpy is similar to azpy but contains a methyl group ($-CH_3$) at the fifth position on the pyridine ring is an unsymmetric bidentate N,N′-donor center. For this reason the $[Ru(5mazpy)_2Cl_2]$ complexes can theoretically exist in five different isomeric forms. If the coordinating pairs of Cl, N(py), and N(azo) are considered in that order, the configurations of these isomers are *trans-trans-trans* (*ttt*), *trans-cis-cis* (*tcc*), *cis-trans-cis* (*ctc*), *cis-cis-trans* (*cct*) and *cis-cis-cis* (*ccc*). From this work, only three isomers of *ctc*, *ccc* and *tcc* are obtained.

Recently, the chloride atoms of α-$[Ru(azpy)_2Cl_2]$ were replaced by a third azpy and bpy ligand and investigated this series for their cytotoxicity (Hotze *et al*, 2005). Moreover, the $[Ru(azpy)_2Cl_2]$ complexes were under renewed investigation due to their cytotoxic activity in a series of human tumor cell lines (Velder *et al*., 2004). In particular the α-configuration as this isomer displayed a very high cytotoxicity, stability and a reasonable solubility (Velder *et al*., 2000, 2004). Therefore, it is our interest to synthesize and to characterize the $[Ru(5mazpy)_2L](PF_6)_2$, $[Ru(5mazpy)_2L'](PF_6)_2$, $[Ru(L')_25mazpy](PF_6)_2$ complexes (L = 2-(phenylazo) pyridine (azpy), 5-methyl-2-(phenylazo)pyridine (5mazpy); L′ = 2,2′-bipyridine

(bpy), 1,10-phenanthroline (phen)). In addition, the cytotoxicity of these complexes were also investigated.

In order to study DNA-binding properties of ruthenium complexes, the water solubility is required. Therefore, the complexes of $[Ru(5mazpy)_2L](NO_3)_2$, $[Ru(5mazpy)_2L']Cl_2$, and $[Ru(L')_2 5mazpy]Cl_2$ were synthesized and characterized. Besides, the DNA-binding of these complexes were carried out.

1.2 Literature reviews

Syntheses and characterization of the ruthenium(II) complexes with the imine and azoimine ligands

Krause and Krause, (1980) studied the chemistry of the 2-(phenylazo)pyridine (azpy) ligand and $[Ru(azpy)_2Cl_2]$ complexes. Three isomers of these complexes were obtained. The isomers were assigned to be *trans-cis-cis* (γ), *cis-trans-cis* (α) and *cis-cis-cis* (β) with referred to the order of coordination pairs of Cl, N(pyridine), N(azo), respectively. All of three isomers were characterized by infrared spectroscopy, UV-Visible absorption spectroscopy, and ^{13}C NMR spectroscopy. The data from cyclic voltammetry showed that azpy ligand appeared to be a better ligand for stabilizing ruthenium(II) than 2,2′-bipyridine (bpy).

Goswami, *et al*., (1981) reported the two types of ruthenium complexes RuX_2L_2 (green) and $[Ru(bpy)_2L](ClO_4)_2.H_2O$ (red) (X = Cl, Br, I; L = 2-(phenylazo)pyridine of 2-(*m*-tolylazo)pyridine; bpy = 2,2′-bipyridine). Both types of complexes had intense $t_2(Ru) \rightarrow \pi^*(L)$ transition in the visible region. The complexes displayed electrochemical responses on the negative side of SCE due to ligand-based reductions. The azopyridine ligand system greatly stabilized the +2 oxidation state in ruthenium.

Krause and Krause, (1982) studied a series of ruthenium(II) complexes with the strong π-acceptor ligand 2-(phenylazo)pyridine (azpy), $[Ru(azpy)_2(AB)]^{n+}$ (AB = 2-(phenylazo)pyridine, 2,2′-bipyridine, 4,4′-bithiazole, 1,2-diaminoethane, 2,4-pentanedione; X = NO_2^-, CN^-, Br^-, N_3^-, thiourea). Infrared spectra showed the azo stretching mode (N=N) to be diagostic of the coligand (AB) π-accepting behaviour. For a very strong π-acid coligand, the azo mode could approach the free ligand value, while with a π-base coligand a single bond order might be approached for the azo linkage.Visible spectra of the complexes appeared to be typical charge-transfer(CT) spectra. The CT band energy should be indicative of the metal-ligand interaction. Emission spectra could be obtained three compounds, one compound appearing to give multiple emission. Cyclic Voltammetric data supported the strong π-stabilization.

Goswami, *et al*., (1983) examined the reactions of the $[Ru(OH_2)_2L]^{2+}$ (L = 2-(phenylazo)pyridine and 2-(*m*-tolylazo)pyridine) with a number of bidentate ligands (2,2′-bipyridine (bpy), ethylenediamine (en) , acetylacetone (Hacac). The stereochemistries have been established with the help of ^1H NMR data. The metal oxidation and ligand reduction behaviour of the complexes were studied electrochemically in acetonitrile.

Bag, *et al.*, (1992) reported the $Ru(RQc)(tap)_2$ complexes which were synthe- sized by reaction $[Ru(OH_2)_2(tap)_2](ClO_4)_2.H_2O$ with catechols in the presence of base (RQc = catecholate, R = H, 4-*t*-Bu, 3,5-(*t*-Bu)$_2$ or 3,4,5,6-Cl_4; tap = 2-(*m*-tolylazo)pyridine). The X-ray structure of $[\{Ru(RQc)(tap)_2\}_2H_2O].CH_2Cl_2$ (R = H) was reported. Results from UV-Visible absorption spectra showed MLCT excitation Ru(dπ)→ RQc(pπ) at near 1000 nm. Besides, cyclic voltammetry was used to study their redox properties. The interligand charge-transfer transition (RQc(pπ)→tap(azo pπ*) and Ru^{II}(dπ)→RQc(pπ) energies qualitatively correlated with the relevant reduction potentials.

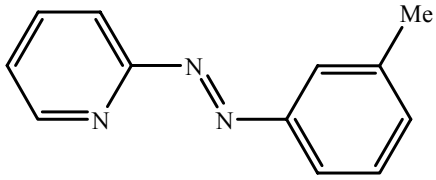

Figure 1.1 2-(*m*-Tolylazo)pyridine)

Choudhury, *et al.*, (1992) studied the reaction of 2-arylpyridinecarboxaldimine [$RH_4C_6NC(H)Py$, L] with hydrated RuX_3 (X = Cl, Br) in ethanol afforded crystals of RuX_2L_2. Two isomers of complex have been isolated and characterized by analytical and spectroscopic data. From the IR data, the green isomer is *trans* with respect to two chlorides and the other isomer has a *cis*-$RuCl_2$ geometry. The high-resolution ^1H NMR spectra of the compounds were used to examine the geometry of the isomeric RuX_2L_2. All the complexes have multiple $t_2 \rightarrow \pi^*(L)$ transition in the visible region. The data from cyclic voltammetry showed that E^0_{298} of the Ru^{III}/Ru^{II} couple in $RuCl_2L_2$ depends on the nature of substitution (R) in the ligand L.

Boelrijk, *et al.*, (1995) investigated the oxidation of octyl α-D-glucopyranoside by $NaBrO_3$. The complexes of $[Ru(azpy)_2(H_2O)_2]^{2+}$ (azpy = 2-(phenylazo)pyridine and $[Ru(naz)_2(H_2O)_2]^{2+}$ (naz = 2-(*p*-nitrophenyl)azopyridine) were used to be active catalyst yielding octyl glucopyranoside (OGP). Results from reactions with cyclobutanol in combination with spectroscopic data indicated that Ru(IV)=O species was the active catalyst species. The two new complexes were synthesized, $[Ru(terpy)(azpy)(H_2O)](ClO_4)_2$ and $[Ru(terpy)(naz)(H_2O)](ClO_4)_2$. Besides the both complexes were less active than the first two complexes.

Misra, *et al.,* (1998) synthesized the RuL_2Cl_2 complex which contained the new azoimidazoles, 1-methyl-2-(arylazo)imidazoles and 1-benzyl-2-(arylazo)-imidazoles (R = H, Me, OMe, Cl, NO_2). Two isomers of this complex were chromatographyically separated. The isomeric structures were confirmed by X-ray crystallography. The compounds exhibited $t_2(Ru) \rightarrow \pi^*(L)$ MLCT transitions in the

visible region. Results from cyclic voltammetry revealed that the Ru(III)/Ru(II) couple was shifted to more positive potential on going from azoimidazole to azopyridine-ruthenium(II) complexes due to the decrease π-acidity of the five-membered heterocycle imidazole compared to the six-membered pyridine ring.

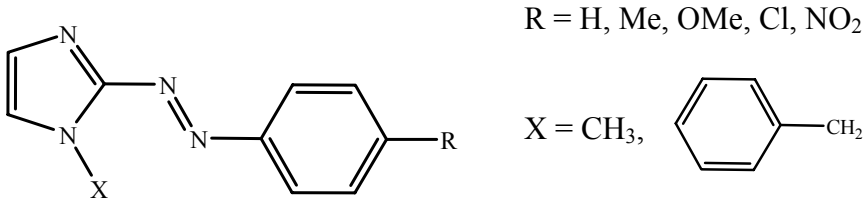

Figure 1.2 1-Methyl-2-(arylazo)imidazoles

Santra, *et al*., (1999) reported the new N,N′-chelating ligands, 2-(aryl-azo)pyrimidine. These ligands reacted with $RuCl_3$ in ethanol to give three isomers. There were *trans-cis-cis* (*tcc*), *cis-trans-cis* (*ctc*), and *cis-cis-cis* (*ccc*) configurations with reference to the order of coordination paire as Cl, N(pyridine), and N(azo). Two of the three isomeric structure (*tcc*-Ru(papm)$_2$Cl$_2$, *ccc*-Ru(papm)$_2$Cl$_2$; papm = 2-(phe-nylazo)pyrimidine) were confirmed by X-ray crystallography. The ^{1}H NMR spectra of the ligands and complexes were compared to determine the binding mode and stereochemistry of the complexes. The electronic spectra of complexes exhibited allowed MLCT transitions in the visible region. Results from cyclic voltammetry showed that the azopyrimidine ligands stabilize ruthenium(II) better than the azopyridines.

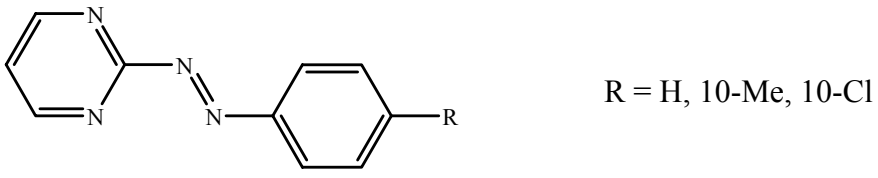

Figure 1.3 2-(Arylazo)pyrimidine

Hotze, *et al*., (2000) studied the α-[Ru(azpy)$_2$(NO$_3$)$_2$] complex (azpy = 2-(phe nylazo)pyridine). The structure of this complex was determined using X-ray crystallography. Besides, the binding of the DNA-model bases 9-ethylguanine (9equa) and guanosine (guo) was studied and compared with previously obtained results for the binding of model bases to the *cis*-[Ru(bpy)$_2$Cl$_2$] complex. The orientations of 9equa and guo in ruthenium complexes were proven using 2D NOESY NMR spectroscopy.

Peneerselvam, *et al*., (2000) reported the crystal structures of the [protonated 2-(phenylazo)pyridine and protonated 2-(4-hydroxyphenylazo)pyridine (3:1)]tetrafluoroborate compound. The results from X-ray showed that the protonation occurred at N(azo) atom and it was more basic than N(pyridine). The azpy compound was normally liquid at room temperature but intramolecular H bonding, N-H-N, and van der waals forces stabilized this crystal structure.

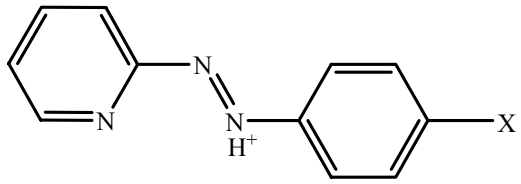

Figure 1.4 Protonated azpy X = H (75%) and OH^- (25%)

Hotze, *et al*., (2002) found that adenine base coordinates to the cytotoxic α-[Ru(azpy)$_2$Cl$_2$] complex in the rare imine form, stabilized by N6, N7-didentate coordination. In addition, the α-[Ru(azpy)$_2$(3-MeAde$_{-H}$)](PF$_6$)$_2$ was proven by X-ray crystallography (azpy = 2-(phenylazo)pyridine; 3-MeAde$_{-H}$ = deprotonate-3-methyladenine)

Hotze, *et al*., (2002) studied the coordination of the DNA model base 9-methyladenine (9-MeAde) with *cis*-[Ru(bpy)$_2$Cl$_2$] and α-[Ru(azpy)$_2$(NO$_3$)$_2$]. The structure were confirmed by using 2D NMR techniques and variable-temperature NMR studies between 25 and -55°C. As the binding mode of 9-MeAde to both *cis*-

$[Ru(bpy)_2Cl_2]$ and α-$[Ru(azpy)_2(NO_3)_2]$ is the same, this binding mode does not explain the earlier observed difference in cytotoxicity between *cis*-$[Ru(bpy)_2Cl_2]$ and α-$[Ru(azpy)_2Cl_2]$.

Hansongnern, *et al.*, (2003) reported the crystal structure of 2-(4′,N,N-Diethyl aminephenylazo)pyrimidine. The azo group, being coplanar with the attached benzene rings and the -N-C group of the substituent $-N(CH_2CH_3)_2$ on the phenyl ring, supported extensive delocalization of electron density. The substituent donated electron to the conjugated system via benzene ring into π* orbital of the azo moiety which, decreased the bond order of the azo leading to a longer bond of 1.283(2)Å.

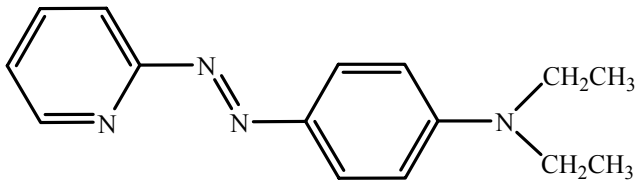

Figure 1.5 2-(4′,N,N-Diethylaminephenylazo)pyrimidine (deazpym)

Byabartta, (2003) isolated the $[Ru(phen)(RaaiR')_2](ClO_4)_2$ complexes (phen = 1,10-phenanthroline; RaaiR′ = 1-alkyl-2-(arylazo)imidazole, *p*-R-C_6H_4-N=N-C_3H_2-NN-1-R′, R = H, Me, Cl and R′=Me, Et, CH_2Ph). The structure of $[Ru(phen)(RaaiR')_2](ClO_4)_2$ was confirmed by X-ray diffraction study. Besides the structure and stereochemistry of the complexes were supported by ^1H NMR data. The absorption spectra of the complexes exhibited a strong MLCT transition in visible region. Electrochemical properties of all the complexes were studied by cyclic voltammetry.

Lu, *et al.*, (2003) studied the isomeric of the $[RuL_2Cl_2]$ complex (L = 1-(phenylazo)isoquinoline). The reaction of $RuCl_3$ with 1-(phenylazo)isoquinoline produced two isomeric form. There were *trans-cis-cis* (*tcc*) and *cis-cis-cis* (*ccc*) in order of the coordinating pairs: (Cl, Cl); (N, N); (N′, N′) where N represented N(isoquinoline), N′ represents N(azo). The configuration of two isomers was described by X-ray crystallography.

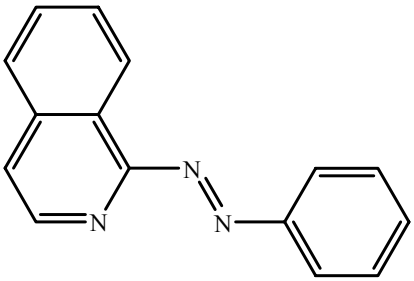

Figure 1.6 1-(Phenylazo)isoquinoline

Hotze, *et al*., (2004) studied the synthesis and characterization of the new water soluble ligand, 2-phenylazopyridine-5-sulfonic acid (Hsazpy), and its ruthenium complexes, α and β-$[NEt_4]_2[Ru(sazpy)_2Cl_2]$. The compounds were characterized by 2D NMR spectroscopy. Only α-$[NEt_4]_2[Ru(sazpy)_2Cl_2].2H_2O$ was determined by single-crystal structure analysis. The α-$[NEt_4]_2[Ru(sazpy)_2Cl_2]$ complex was classified as non-toxic in A2780 cell line.

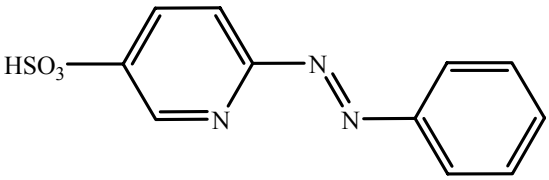

Figure 1.7 2-Phenylazopyridine-5-sulfonic acid (Hsazpy)

Jasimuddin, *et al.*, (2004) studied $[Os(bpy)(RaaiR')_2](PF_6)_2$ (RaaiR′ = 1-alkyl-2-(arylazo)imidazole, *p*-R-C_6H_4-N=N-C_3H_2NN-1-R′, where R = H, Me, Cl, and R′ = Me, Et and CH_3Ph; bpy = 2,2′-biypridine). The $[Os(bpy)(MeaaiMe)_2](PF_6)_2.4H_2O$ complex was confirmed by X-ray crystallography. The υ(N=N) and υ(C=N) appeared at 1370-1390 and 1590-1610 cm^{-1}, respectively. UV-Visible absorption spectra of all complexes in acetonitrile solution displayed ligand-centred transitions in UV region, and metal-to-ligand charge transfer (MLCT) transition in visible region. The cyclic voltammogram exhibited Os(IV)/Os(III) and Os(III)/Os(II) at the positive side which were quasireversible reduction couples at the negative side.

They were due to gradual addition of electron into two azoimine chelates from RaaiR′ and one diimine chelate ring in the complex.

Jasimuddin, *et al*., (2004) prepared the $[Ru(o/p\text{-}RaaiR')_3]Cl_2$ (RaaiR′ = 1-alkyl-2-(arylazo)imidazole, R = H, *p*-Me, *p*-Ome, *o*-Ome; R′ = Me, Et, CH_2Ph) by microwave technique. The complexes were characterized by IR, UV-Visible and ^1H NMR spectral data. In the case of $[Ru(o\text{-}OmeaaiCH_2Ph)_3]Cl_2$, single crystals were obtained. The metal-to-ligand charge transfer transition was observed at visible region. Cyclic voltammetry of the complexes showed one metal oxidation Ru(II)/ Ru(III) at the positive side and three successive ligand reduction couples negative to SCE as the reference electrode.

Kooijman, *et al*., (2004) reported the crystal structure of the $[Ru(dazpy)_2Cl_2]$ complex (dazpy = 2-phenylazo-4,6-dimethylpyridine). The dazpy ligand coordinated to ruthenium in the so-call α-configuration, meaning that the coordinating pairs of Cl, N_{py}, and N_{azo} are in *cis*, *trans*, and *cis* orientations, respectively.

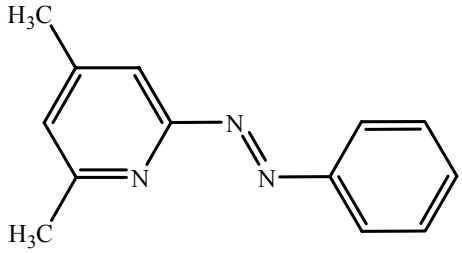

Figure 1.8 2-Phenylazo-4,6-dimethylpyridine (dazpy)

Velders, *et al*., (2004) reported the fourth isomer of $[Ru(azpy)_2Cl_2]$ (azpy = 2-(phenylazo)pyridine). The structure of this isomer was determined by ^1H NMR spectroscopy and single-crystal X-ray diffraction analysis. Besides, the UV-Visible and infrared spectroscopies were used to study chemistry of this isomer.

Hotze, *et al*., (2005) studied the complexes of $[Ru(L_3)](PF_6)_2$ (L = 2-(phenylazo)pyridine (azpy), *o*-tolylazopyridine (tazpy) and $[Ru(L')_2L'](PF_6)_2$ (L′, L″

= 2-(phenylazo)pyridine, 2,2′-bipyridine). They were structurally characterized and investigated the cytotoxicity. The structures of mer-$[Ru(azpy)_3](PF_6)_2$ and mer-$[Ru(tazpy)_3](PF_6)_2$ were determined by X-ray diffraction. NMR spectra of these series of compounds were resolved using 2D COSY and NOESY NMR spectroscopy. The cytotoxicity data against a series of human tumor cell lines (A498, EVSA-T, H226, IGROV, M19, MCF-7, and WIDR) showed a moderate cytotoxicity for these series of complexes.

Jasimuddin, *et al.,* (2005) reported the $[Os(phen)(RaaiR')_2](PF_6)_2$ complexes (phen = 1,10-phenanthroline; RaaiR′ = 1-alkyl-2-(arylazo)imidazole, *p*-R-C_6H_4-N=N-C_3H_2-NN-1-R′ where R = H, Me, Cl and R′ = Me, Et, CH_2Ph). The single crystal of the complexes $[Os(phen)(ClaaiEt)_2](PF_6)_2$ was obtained. In addition, the structure of all complexes was confirmed by ^1H NMR spectroscopy. Electronic spectra of the complexes showed ligand centered (LC) transitions in the UV region and metal-to-ligand charge transfer transition in visible region. Cyclic voltammetry of all complexes exhibited two metal redox couple, Os(III)/Os(II) and Os(IV)/Os(III), at the positive side versus SCE, and three successive ligand reductions.

Dinda, *et al.*, (2006) reported the heteroleptic tris-chelates, $[Ru(bpy)_2(\alpha/\beta\text{-NaiR})](ClO_4)_2$ complexes (bpy = 2,2′-bipyridine; α-NaiR = 1-alkyl-2-(naphthyl-α-azo)imidazole; β-NaiR = 1-alkyl-2-(naphthyl-β-azo)imidazole). The electronic spectra of NaiR were recorded in CH_3CN in the UV-Visible region. The ^1H NMR spectra were collected in CD_3CN. The structure of $[Ru(bpy)_2(\alpha\text{-NaiEt})](ClO_4)_2$ was confirmed by single crystal X-ray diffraction technique. The voltammograms of all complexes displayed Ru(III)/Ru(II) couple at the positive side and the ligand reductions at the negative side to reference electrode, SCE. Three successive reduction may be expected to involve the ligand having the most stable lowest unoccupied molecular orbital, which was dominated by azo function of naphthyl azoimidazole than bpy.

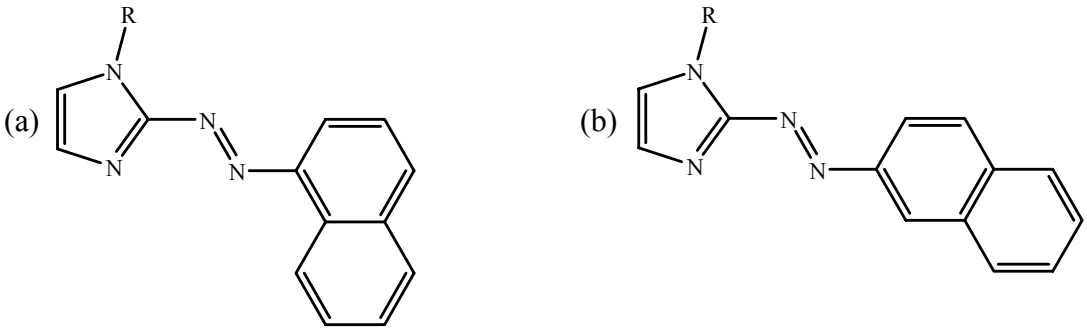

R = H, Me, Et, CH_2Ph

Figure 1.9 (a) 1-Alkyl-2-(naphthyl-α-azo)imidazole (α-NaiR)
(b) 1-Alkyl-2-(naphthyl-β-azo)imidazole (β-NaiR)

Al-Noaimi, *et al*., (2007) studied three novel families of azomethine ligands (L) of the type $C_6H_5N{=}NC(R){=}N(4\text{-}YC_6H_4)$ (6), $C_6H_5N{=}NC(R){=}N(4\text{-}YC_6H_4)$ (7) and $4\text{-}ClC_6H_4N{=}NC(R){=}N(4\text{-}YC_6H_4)$ (8). These ligands reacted with $RuCl_3$, 2,2′-bipyridine (bpy) and lithium chloride in ethanol to produce *trans*-$[Ru^{II}(bpy)LCl_2]$ complexes. These ligands were characterized by IR, ^1H NMR, mass spectra and elemental analysis, UV-Visible spectroscopy. The structures of the two complexes, *trans*-$[Ru^{II}(bpy)(C_6H_5N{=}NC(COCH_3){=}N(4\text{-}C_{10}H_7C_6H_4)Cl_2].0.25C_7H_8$ and *trans*-$[Ru^{II}$ $(bpy)(4\text{-}ClC_6H_4N{=}NC(CO_2CH_3){=}N(4\text{-}C_6H_5)Cl_2].0.5$acetone were studied by X-ray crystallography. Results from crystallographic, electrochemical, electronic spectral data and DFT calculations were consistent with azomethine ligands possessing strong π-acceptor properties.

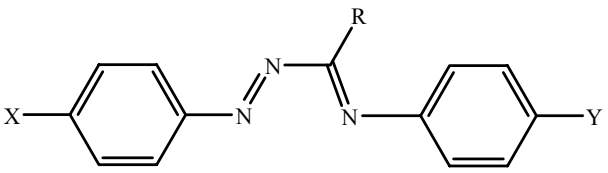

(6, 7, 8)

(6) : X = H, R = $COCH_3$
(7) : X = H, R = CO_2CH_3
(8) : X = Cl, R = CO_2CH_3

Y= H (a), CH_3 (b), Cl (c),
Br (d), $C_{10}H_7$ (e),
OCH_3 (f), NO_2 (g)

Figure 1.10 Azomethine ligands

Byabartta, (2007) reported the $[Ru(bpy)_2(RaaiR')_2](ClO_4)_2$ complexes (RaaiR′ = 1-alkyl-2-(arylazo)imidazole, *m*-R-C_6H_4-N=N-C_3H_2-NN-1-R′ where R = H, OMe, NO_2 and R′ = Me, Et, CH_2Ph; bpy = 2,2′-bipyridine). The molecular weight of all complexes was confirmed by FAB mass spectrum. IR spectra showed -N=N- stretching at 1370 cm^{-1} which was red shift 90 cm^{-1} from the free ligand value. The absorption spectra were studied within 200-1100 nm. The emission spectra was frozen glass (77K) which were sharper and considerably more intense than the room temperature spectra. The ^1H NMR, ^{13}C NMR, and ^1H-^1H COSY NMR were used to support the structure of complexes. In addition, the ^1H-^{13}C HMQC NMR spectrum was used to assign quaternary carbons. One redox couple was observed at positive to SCE which refered to Ru(III)/Ru(II) couple. Besides, three redox couples at negative to SCE were due to reductions of ligand. Electrochemical parameterisation of Ru(III)/Ru(II) redox potential was carried out and calculated ligand potential $E_L(L)$.

The interactions of the ruthenium(II) complexes with calf thymus DNA (CT DNA)

Nair, *et al*., (1998) reported the synthesis and characterization of $[Ru(NH_3)_4dppz]^{2+}$ (dppz = dipyridophenazine) and also explored the interactions of the complex with DNA. Results from DNA-binding studies showed that the addition of DNA clearly yielded an absorbance hypochromism of 13.6%, which was possibly associated with intercalated binding of the complexes to the helix.

Zhen, *et al*., (1999) reported the synthesis of the $[Ru(bpy)_2L]^{2+}$ complexes (L = 4,5,9,18-tetraazaphenanthreno[9,10-b]triphenylene (taptp), 2,3-diphenyl-1,4,8,9-tetraazatriphenylene (dptatp)) and characterization by using elemental analyses, ^1H NMR, and mass spectra. The interactions of the complexes with calf thymus DNA were investigated by viscosity measurement, absorption titration, emission titration and circular dichroism. All data indicated that both complexes bind enantioselectively to double-stranded calf thymus DNA via the intercalative mode.

Vaidyanathan and Nair, (2002) reported the $[Ru(bzimpy)_2]Cl_2$ complex (bzimpy = 2,6-bis(benzimidazole-2-yl)pyridine). It was characterized by ESI-MS, UV -Visible, ^1H NMR and fluorescence spectra. The interaction of this complex with calf thumus DNA was studied by absorption titration, thermal denaturation, viscosity measurement and fluorescence spectroscopy.

Deng, *et al.*, (2003) reported the two novel ruthenium complexes, $[Ru(bpy)_2(actatp)](ClO_4)_2.2H_2O$, $[Ru(phen)_2(actatp)](ClO_4)_2.2H_2O$ (actatp = acenaph-thereno-[1,2-*b*]-1,4,8,9-tetraazariphenylence; phen = 1,10-phenanthroline). These complexes were characterized by UV-Visible, ^1H NMR, and mass spectra. The cyclic voltammetry was used to study electrochemical behavior of the two complexes. The interaction of the two complexes with calf thymus DNA was investigated by spectrophotometric methods and viscosity measurements. The experimental results supported that the actatp ligand strongly intercalated into the DNA helix. Besides, both complexes were found the photo cleavage of plasmid pBR322.

Jiang, *et al.*, (2003) reported the synthesis of ruthenium complexes with the two novel tridentate ligand, 2-(2-benzimidazole-1,10-phenanthroline (PHBI), 2-(2-naphthoimidazole-1,10-phenanthroline (PHNI). The $[Ru(tpy)(PHBI)](ClO_4)_2.2H_2O$ and $[Ru(tpy)(PHNI)](ClO_4)_2.2H_2O$ complexes (tpy = 2,2′:6′,2′′-terpyridyl) were characterized by elemental analysis, mass spectra, ^1H NMR, absorption spectroscopy and also studied electrochemical behaviours by cyclic voltammetry. The interaction of these complexes with calf thymus DNA was investigated by spectroscopic methods and viscosity measurements. Results from DNA interaction study indicated that the two complexes interact with DNA in different binding mode.

Deng, *et al.*, (2005) reported the series of Ru(II) polypyridyl complexes, $[Ru(bpy)_2(ptdb)](ClO_4)_2$, $[Ru(bpy)_2(ptda)](ClO_4)_2$, $[Ru(bpy)_2(ptdp)](ClO_4)_2$ (bpy = 2,2′-bipyridine; ptdb = 3-(pyridine-2-yl)5,6-diphenyl-*as*-triazine; ptda = 3-(pyridine-2-yl)-*as*-triazino-[5,6-*f*]phenanthrene; ptda = 3-(pyridine-2-yl)-*as*-triazi-no-[5,6-f]acenaphthylene. They were characterized by elemental analysis, mass spectra, ^1H NMR, and cyclic voltammetry. The structure of $[Ru(bpy)_2(ptdb)](ClO_4)_2$

was determined. The DNA-binding properties of the complexes were investigated by absorption titration, luminescence spectroscopy, and viscosity measurements. The experimental results suggested that all complexes bind to DNA in an intercalation mode.

Mazumder, *et al.*, (2005) reported a series of the $[Ru(M)_2U]^{2+}$ complexes (M = 2,2′-bipyridine, 1,10-phenanthroline; U = tpl (Ru1), 4-Cl-tpl (Ru2), 4-CH_3-tpl (Ru3), 4-CH_3-O-tpl (Ru4), 4-NO_2-tpl (Ru5), pai (Ru(6); tpl = thiopicolinanilide and pai = 2-phenylazoimidazole). All of complexes were characterized by IR, UV-Visible, ^{1}H NMR, ^{13}C NMR, FAB mass spectrophotometer, and elemental analysis. The complexes displayed the tumor inhibitory activity of ruthenium complexes against transplantable murine tumor cell line, EAC. The study of in vitro antibacterial activity revealed the significant activity of Ru1-Ru4 against microorganisms compared of the standard drug chloramphenicol.

Tan, *et al.*, (2005) synthesized and characterized the $[Ru(phen)_2(NMIP)]^{2+}$ complex (NMIP = 2′-(2′′-nitro-3′′-4′′-methylenedioxyphenyl)imidazo-[4′,5′-*f*][1,10]-phenanthroline. This complex were characterized by mass spectrometry, ^{1}H NMR spectroscopy and cyclic voltammetry. Binding of the complex to calf thymus DNA was investigated by spectroscopic methods, viscosity and electrophoresis measurements. Results from this study indicated that $[Ru(phen)_2(NMIP)]^{2+}$ binds to DNA via partial intercalative mode. In addition, it was also found to promote cleavage of plasmid pBR322 DNA.

The cytotoxicity of the ruthenium(II) complexes

Velders, *et al.*, (2000) studied the cytotoxicity of the three isomers of the $[Ru(azpy)_2Cl_2]$ complexes (azpy = 2-(phenylazo)pyridine). They found that these complexes showed different in vitro cytotoxicity. The α-$[Ru(azpy)_2Cl_2]$ complex showed remarkably high cytotoxicity against a series of tumor-cell lines (MCF-7, EVSA-T, WIDR, IGROV, M19, A498, and H226). It was in contrast to the low

cytotoxicity of β-[Ru(azpy)$_2$Cl$_2$] and γ-[Ru(azpy)$_2$Cl$_2$] and the structurally related complex *cis*-[Ru(bpy)$_2$Cl$_2$] (bpy = 2,2′-bipyridine).

Hotze, *et al*., (2003) reported the new water-soluble bis(2-phenylazopyridine)ruthenium(II) complexes. The α-[Ru(azpy)$_2$(cbdca-O,O′)], α-[Ru(azpy)$_2$(ox)], and α-[Ru(azpy)$_2$(mal)] (cbdca-O,O′ = 1,1-cyclobutanedicarboxylate, ox = oxlate, mal = malonate) were synthesized and characterized. The structures of first two complexes were confirmed by X-ray crystallography. The cytotoxicity of these complexes was determined in A2780 human ovarian carcinoma and A2780cisR, the corresponding cisplatin-resistant cell line. Results from cytotoxicity showed that all the water-soluble carboxylato complexes displayed a cytotoxicity of a factor 10 less than the α-[Ru(azpy)$_2$Cl$_2$] in the A2780 and A2780cisR cell lines.

Hotze, *et al*., (2004) reported the most common isomers, α-, β-, and γ-[RuL$_2$Cl$_2$] (L = *o*-tolylazopyridine (tazpy) and 4-methyl-2-phenylazopyridine (mazpy)). All complexes were synthesized and characterized by NMR spectroscopy. The molecular structures of γ-[Ru(tazpy)$_2$Cl$_2$] and α-[Ru(mazpy)$_2$Cl$_2$] were investigated by X-ray diffraction analysis. The IC$_{50}$ values of the geometrically isomeric [Ru(tazpy)$_2$Cl$_2$] and [Ru(mazpy)$_2$Cl$_2$] complexes were compared with those of the parent [Ru(azpy)$_2$Cl$_2$] complexes which were determined in the series of human tumour cell lines (MCF-7, EVSA-T, WIDR, IGROV, M19, A498 and H266). These data unambiguously showed for all complexes the following trend: the α isomer showed a very high cytotoxicity, where the β isomer was a factor 10 less cytotoxic. The γ isomer of [Ru(tazpy)$_2$Cl$_2$] and [Ru(mazpy)$_2$Cl$_2$] displayed a very high cytotoxicity comparable to that of the γ isomer of the parent compound [Ru(azpy)$_2$Cl$_2$] and to that of the α-isomer.

Chen, *et al.*, (2006) studied the electronic and geometric structures of a series of isomeric complexes α, β, γ, δ, and ε-[Ru(azpy)$_2$Cl$_2$] using the density functional theory (DFT) method. The computed results showed that: (i) The main-body (azopyridine) planes of two conjugative ligands (azpy) in γ-[Ru(azpy)$_2$Cl$_2$] were

almost located on the same plane; therefore it must be advantageous for the conjugative ligand to intercalate between DNA-base pairs whereas those in α- and β-$[Ru(azpy)_2Cl_2]$ were almost inter-vertical; thus it must be disadvantageous to their DNA-binding affinities due to their greater steric hindrance. (ii) The energies (ε_L) of the LUMO were in sequence of $\varepsilon_L(\beta) > \varepsilon_L(\alpha) > \varepsilon_L(\gamma)$. The energy differences ($\Delta\varepsilon_{L\text{-}H}$) between LUMO and HOMO were in sequence of $\Delta\varepsilon_{L\text{-}H}(\gamma) < \Delta\varepsilon_{L\text{-}H}(\alpha) < \Delta\varepsilon_{L\text{-}H}(\beta)$. (iii) The total dipole moments (μ) of the isomers were in sequence of $\mu(\beta) > \mu(\alpha) > \mu(\gamma)$. (iv) The positive charges (Q_L) in the ligand azpy were in sequence of $Q_L(\gamma) > Q_L(\alpha) > Q_L(\beta)$.

Dougan, *et al.*, (2006) studied the ruthenium(II) η^6-arene complexes containing *p*-cymene (*p*-cym), tetrahydronaphthalene (thn), benzene (bz), or biphenyl (bip), as the arene, phenylazopyridine derivatives ($C_5H_4NN{:}NC_6H_5R$; R = H (azpy), OH (azpy-OH), NMe_2 (azpy-NMe_2)) or a phenylazopyrazole derivatives (NHC_3H_2 $NN{:}NC_6H_5NMe_2$ (azpy-NMe_2)) as N,N-chelating ligands and chloride as a ligand. All complexes displayed intense transitions in the visible region assignable to MLCT from the filled 4d orbitals of Ru(II) to the empty π* ligand orbital. The structure of these complexes was characterized by ^{1}H NMR spectroscopy and X-ray crystallography. None of the azpy complexes were cytotoxic toward A2780 human ovarian or A549 human lung cancer cells, but several of the azpy-NMe_2, azpy-OH, and azpyz-NMe_2 complexes were active (IC_{50} values 18-88 μM).

1.3 Objectives

1. To synthesize and characterize a new bidentate ligand, 5-methyl-2-(phenylazo)-pyridine (5mazpy).
2. To synthesize and characterize the $[Ru(5mazpy)_2Cl_2]$ complexes.
3. To synthesize and characterize the $[Ru(5mazpy)_2L](PF_6)_2$, $[Ru(5mazpy)_2L'](PF_6)_2$ and $[Ru(L')_2 5mazpy](PF_6)_2$ complexes (L = azpy, 5mazpy; L′ = bpy, phen).

4. To synthesize and characterize the $[Ru(5mazpy)_2L](NO_3)_2$, $[Ru(5mazpy)_2L']Cl_2$ and $[Ru(L')_25mazpy]Cl_2$ complexes (L = azpy, 5mazpy; L′ = bpy, phen).
5. To study the interactions of the $[Ru(5mazpy)_2L](NO_3)_2$, $[Ru(5mazpy)_2L']Cl_2$ and $[Ru(L')_25mazpy]Cl_2$ complexes with calf thymus DNA.
6. To test the cytotoxicity of the $[Ru(5mazpy)_2Cl_2]$, $[Ru(5mazpy)_2L](PF_6)_2$, $[Ru(5mazpy)_2L'](PF_6)_2$, $[Ru(L')_25mazpy](PF_6)_2$, $[Ru(5mazpy)_2L](NO_3)_2$, $[Ru(5mazpy)_2L']Cl_2$ and $[Ru(L')_25mazpy]Cl_2$ complexes with cell lines.
7. To analyze and to summarize the chemistry of all complexes.

CHAPTER 2
MATERIALS AND METHODS

2.1 Materials

2.1.1 Chemical substances

Materials from Fluka AG, Switzerland

6-amino-3-picoline $C_6H_8N_2$, AR grade
Nitrosobenzene, C_6H_5NO, AR grade
2,2′-bipyridine, $C_{10}H_8N_2$, AR grade
Ruthenium(III)chloride trihydrate, $RuCl_3.3H_2O$, AR grade
Tetrabutylammonium hexafluorophosphate, $C_{16}H_{36}F_6NP$, AR grade
Ethidium Bromide, $C_{21}H_{20}BrN_3$, AR grade

Materials from Merck

Silica gel 60 (0.040-0.063 nm) GF_{254}
Sodium hydroxide, NaOH, AR grade
Tetra-*n*-butylammoniumchloride, $C_{16}H_{36}NCl$, AR grade
1,10-phenanthroline, $C_{12}H_8N_2$, AR grade

Materials from Aldrich Chemical Company, Inc.

Ammoniumhexafluorophosphate, NH_4PF_6, AR grade
Ferrocenemethanol, $C_{11}H_{12}FeO$, AR grade

Materials from BDH Laboratory Supplies, Poole

Silver nitrate, $AgNO_3$, AR grade

Lithium chloride, LiCl, AR grade

Materials from Lab-Scan analytical sciences

Sodium chloride, NaCl, AR grade

Hydrochloric acid, HCl, AR grade

Materials from Sigma-Aldrich Laborchemkalien

Deoxyribonucleic acid (CT DNA), AR grade

Trisbase, $C_4H_{11}NO_3$, AR grade

2.1.2 Solvents

Solvents from Lab-Scan analytical sciences

Acetonitrile, CH_3CN, AR grade

Acetone, C_3H_6O, AR grade

Benzene, C_6H_6, AR grade

Chloroform, $CHCl_3$, AR grade

Dimethylsulfoxide, C_2H_6OS, AR grade

Ethanol, C_2H_5OH, AR grade

Ethyl acetate, $C_4H_8O_2$, AR grade

Methanol, CH_3OH, AR grade

N,N-dimethylformamide, C_3H_7NO, AR grade

Solvents from Merck

Dichloromethane, CH_2Cl_2, AR grade

Hexane, C_6H_{14}, AR grade

The solvents for column chromatography, dichloromethane and hexane, were reagent grade and purified by distillation prior to use.

2.2 Instruments

2.2.1 Melting Point Apparatus

Melting Points of the complexes were measured on an Electrothermal melting point apparatus (Electrothermal 9100).

2.2.2 Elemental Analysis

Elemental analysis was measured by CE Instruments Flash 1112 Series EA CHNS-O Analyzer.

2.2.3 The Fast-atom bombardment (FAB) Mass Spectrometry

The Fast-atom bombardment (FAB) mass spectra were measured on a VG Autospec instrument and ESI mass spectrometry (University of Bristol, UK.).

2.2.4 Infrared Spectroscopy

Infrared spectra were measured on a Perkin Elmer Spectrum GX FT-IR spectrophotometer from 370 to 4,000 cm^{-1}. All samples were prepared in the KBr pellets.

2.2.5 UV-Visible Absorption Spectroscopy

Ultraviolet and visible absorption spectra were measured on UV-Vis Spectrophotometer SPECORD S100.

2.2.6 Fluorescence Spectroscopy

Emission spectra were recorded with Hellet packard L55S Spectrofluorometer.

2.2.7 1D and 2D Nuclear Magnetic Resonance Spectroscopy

1D and 2D NMR spectra were measured in $CDCl_3$, acetone-d_6, and CD_3OD with a Varian UNITY SNOVA 500 MHz FT-NMR spectrometer at ambient temperature with Me_4Si as an internal standard.

2.2.8 Cyclic Voltammetry

Electrochemical experiments were measured using MacLab (4e AD Instruments) with potentiostat (Serial No p068). The program was EChem 1.5.1. A glassy carbon working electrode, platinum wire auxillary electrode, and platinum reference electrode were used in three-electrode configuration. The supporting electrolyte was tetra-*n*-butylammonium hexafluorophosphate ($[NBu_4]PF_6$) in CH_3CN and dichloromethane. Ferrocene was added at the end of each experiment as an internal standard. All potentials were quoted vs the ferrocene/ferrocenium couple (Fc/Fc^+). The solvent was used as received. The argon gas was bubbled through the solution prior to each measurement.

2.2.9 X-ray Diffractometer

The X-ray structures of 5-methyl-2-(phenylazo)pyridine, *ctc*-[Ru $(5mazpy)_2Cl_2$], *ccc*-[Ru$(5mazpy)_2Cl_2$], *tcc*-[Ru$(5mazpy)_2Cl_2$], and [Ru$(5mazpy)_2$bpy] $(PF_6)_2$ complexes were determined by Smart APEX CCD diffractometer.

2.3 Syntheses of ligands

2.3.1 Synthesis of the 2-(phenylazo)pyridine (azpy) ligand

The 2-(phenylazo)pyridine ligand was prepared by modified literature method (Krause and Krause, 1980).

The 2-(phenylazo)pyridine ligand was prepared by literature method (Krause and Krause, 1980). 2-Aminopyridine (0.45 g, 4.78 mmol) reacted with nitrosobenzene (0.60 g, 5.60 mmol) in the mixture of 20 M NaOH 13.5 mL and 10 mL of benzene with stirring. The reaction mixture was heated on the water bath for 45 min. The reaction mixture was extracted five times with 5 mL portions of benzene, then the solvent was removed by rotary evaporation. The residue was purified by column chromatography on a silica gel. A mixture of hexane and ethyl acetate as the eluting solvent. The orange band was collected. The yield was 35%.

2.3.2 Synthesis of the 5-methyl-2-(phenylazo)pyridine (5mazpy) ligand

The 5-methly-2-(phenylazo)pyridine ligand was prepared by using literature procedure (Changsaluk and Hansongnern, 2005). 6-Amino-3-picoline (0.34 g, 3.13 mmol) was added to the benzene solution and the mixture was stirred on water bath. Then NaOH was added to the reaction. Nitrosobenzene (0.34 g, 3.16 mmol) in small portions was added to the reaction then the reaction mixture was refluxed for 8 h. The green solution became brown. The product was extracted with benzene and evaporated to dryness. The residue was purified by column chromatography on silica gel. The orange band was eluted with the mixture of CH_2Cl_2 : Hexane (1:9 v/v). The yield of 5mazpy ligand was 62 %.

2.4 Syntheses of the ruthenium complexes

2.4.1 Synthesis of the $[Ru(5mazpy)_2Cl_2]$ complex

The $[Ru(5mazpy)_2Cl_2]$ complex was prepared by modified literature method (Krause and Krause, 1980).

The ruthenium complex, $[Ru(5mazpy)_2Cl_2]$, was prepared by the reaction between $RuCl_3.3H_2O$ (0.05 g, 0.24 mmol) and 5mazpy (0.10 g, 0.53 mmol) in ethanol. After the mixture was refluxed for 6 h, the solution was evaporated to dryness. The dried product was dissolved in a small volume of $CHCl_3$ and purification of the compound was carried out by column chromatography on silica gel by using a mixture of chloroform and hexane (9:1) as the eluting solvent. Three isomers were collected as blue (% yield = 28), purple (% yield = 20), and green (% yield = 35) isomers.

2.4.2 Synthesis of the *cis*-$[Ru(bpy)_2Cl_2]$ complex

The *cis*-$[Ru(bpy)_2Cl_2]$ complex was prepared by using literature method (Sullivan *et al.*, 1978).

The $RuCl_3.3H_2O$ (0.10 g, 5 mmol), 2,2′-bipyridine (1.56 g, 10 mmol), and LiCl (2.12 g, 50 mmol) were heated by refluxing in dimethylformamide (25 mL) for 4 h. The reaction was stirred magnetically throughout this period. The reaction mixture was cooled to room temperature and a mixture of 200 mL 1:1 acetone-water was added. Dark green solid was obtained by filtration. The product was washed with water and ether, and then it was dried by suction. The yield was 80%.

2.4.3 Synthesis of the *cis*-$[Ru(phen)_2Cl_2]$ complex

The *cis*-$[Ru(phen)_2Cl_2]$ complex was prepared by using literature method (Sullivan *et al.*, 1978).

The $RuCl_3.3H_2O$ (0.50 g, 2.4 mmol), 1,10-phenanthroline (0.99 g, 5 mmol), and LiCl (0.03 g, 0.6 mmol) were heated at reflux in dimethylformamide (30

mL) for 4 h. After the reaction mixture was cooled to room temperature, 70 mL of acetone was added and the resultant solution cooled at 0°C overnight. The solid was filtered and washed with 75 mL of water followed by 75 mL of diethyl ether. The yield was 33.8%.

2.4.4 Synthesis of the $[Ru(5mazpy)_3](PF_6)_2$ complex

ctc-$[Ru(5mazpy)_2Cl_2]$ (0.07 g, 0.13 mmol), and $AgNO_3$ (0.05 g, 0.29 mmol) were suspended in 50 mL of methanol. After the solution was refluxed 2 h, AgCl was removed by filtration. The 5-methyl-2-(phenylazo)pyridine (0.03 g, 0.16 mmol) ligand was added into the solution mixture. Then the solution was refluxed for 7 h, AgCl was removed by filtration. The aqueous solution of NH_4PF_6 (0.042 g, 0.27 mmol) was added to the filtrate. The solvent was removed by rotary evaporation, the resulting precipitate from methanol was separated by filtration, washed with hexane and ether, respectively. Thenit was dried at 80 °C. The yield was 79%.

2.4.5 Synthesis of the $[Ru(5mazpy)_2azpy](PF_6)_2$ complex

This complex was synthesized by using the same method as the $[Ru(5mazpy)_3](PF_6)_2$ complex, but the 5-methyl-2-(phenylazo)pyridine ligand was replaced by 2-(phenylazo)pyridine. The yield was 75%.

2.4.6 Synthesis of the $[Ru(5mazpy)_2bpy](PF_6)_2$ complex

This complex was synthesized by using the same method as the $[Ru(5mazpy)_3](PF_6)_2$ complex, but the 5-methyl-2-(phenylazo)pyridine ligand was replaced by 2,2′-bipyridine ligand. The yield was 76%.

2.4.7 Synthesis of the $[Ru(5mazpy)_2phen](PF_6)_2$ complex

This complex was synthesized by using the same method as the $[Ru(5mazpy)_3](PF_6)_2$ complex, but the 5-methyl-2-(phenylazo)pyridine ligand was

replaced by 1,10-phenanthroline ligand. The yield was 78%.

2.4.8 Synthesis of the $[Ru(bpy)_2 5mazpy](PF_6)_2$ complex

The *cis*-$[Ru(bpy)_2Cl_2]$ complex (0.05 g, 0.13 mmol), and $AgNO_3$ (0.05 g, 0.29 mmol) were suspended in 50 mL of methanol. After the solution was refluxed 2 h, AgCl was removed by filtration. The 5-methyl-2-(phenylazo)pyridine (0.03 g, 0.16 mmol) ligand was added into the solution mixture. Then the solution was refluxed for 10 h, AgCl was removed by filtration. The aqueous solution of NH_4PF_6 (0.042 g, 0.27 mmol) was added to the filtrate. The solvent was removed by rotary evaporation, the resulting precipitate from methanol was separated by filtration, washed with hexane and ether respectively, and dried at 80 °C. The yield was 85%.

2.4.9 Synthesis of the $[Ru(phen)_2 5mazpy](PF_6)_2$ complex

This complex was synthesized by using the same method as the $[Ru(bpy)_2 5mazpy](PF_6)_2$ complex, but the *cis*-$[Ru(bpy)_2Cl_2]$ was replaced by *cis*-$[Ru(phen)_2Cl_2]$. The yield was 86%.

2.4.10 Synthesis of the $[Ru(5mazpy)_3](NO_3)_2.5H_2O$ complex

ctc-$[Ru(5mazpy)_2Cl_2]$ (0.07 g, 0.13 mmol), and $AgNO_3$ (0.05 g, 0.29 mmol) were suspended in 50 mL of methanol. After the solution was refluxed 2 h, AgCl was removed by filtration. The 5-methyl-2-(phenylazo)pyridine (0.03 g, 0.16 mmol) ligand was added into the solution mixture. Then the solution was refluxed for 7 h, AgCl was removed by filtration. The solid was obtained by slow diffusion of ether in to a mixture of acetone and ethanol. The product was washed with hexane and ether respectively, and dried at 75 °C. The yield was 72%.

2.4.11 Synthesis of the $[Ru(5mazpy)_2azpy](NO_3)_2.4H_2O$ complex

This complex was synthesized by using the same method as the $[Ru(5mazpy)_3]$ $(NO_3)_2$ complex, but the 5-methyl-2-(phenylazo)pyridine ligand was replaced by 2-(phenylazo)pyridine ligand. The yield was 70%.

2.4.12 Synthesis of the $[Ru(5mazpy)_2bpy]Cl_2.6H_2O$ complex

The saturated tetra-*n*-butylammoniumchloride in acetone was added into the solution of $[Ru(5mazpy)_2bpy](PF_6)_2$ in a small volumn of acetone. After the solution was centrifuged, the solid was obtained. The product was washed with acetone and diethyl ether, respectively and dried at 50 °C. The yield was 72%.

2.4.13 Synthesis of the $[Ru(5mazpy)_2phen]Cl_2.7H_2O$ complex

This complex was synthesized by using the same method as the $[Ru(5mazpy)_2bpy]Cl_2$ complex, but the $[Ru(5mazpy)_2bpy](PF_6)_2$ complex was replaced by $[Ru(5mazpy)_2phen](PF_6)_2$. The yield was 72%.

2.4.14 Synthesis of the $[Ru(bpy)_25mazpy]Cl_2.6H_2O$ complex

This complex was synthesized by using the same method as the $[Ru(5mazpy)_2bpy]Cl_2$ complex, but the $[Ru(5mazpy)_2bpy](PF_6)_2$ complex was replaced by $[Ru(bpy)_25mazpy](PF_6)_2$. The yield was 73%.

2.4.15 Synthesis of the $[Ru(phen)_25mazpy]Cl_2.9H_2O$ complex

This complex was synthesized by using the same method as the $[Ru(5mazpy)_2bpy]Cl_2$ complex, but the $[Ru(5mazpy)_2bpy](PF_6)_2$ complex was replaced by $[Ru(phen)_25mazpy](PF_6)_2$. The yield was 74%.

2.5 DNA-binding and cleavage experiments

The DNA-binding and cleavage experiments were performed at room temperature. Concentrated stock solutions of DNA were prepared in buffer and sonicated for 25 cycles, where each cycle consisted of 30 s with 1 min intervals (Maheswari and Palaniandavar, 2004). The DNA concentration was determined by absorption spectroscopy using the known molar extinction coefficient value of 6,600 $M^{-1}cm^{-1}$ at 260 nm (Reichmann *et al.*, 1954). Solutions of calf thymus DNA in the buffer gave a ratio of UV absorbance at 260 and 280 nm in the range 1.8 to 1.9 : 1 indicating that DNA is free form protein (Marmur, 1961).

2.5.1 Absorption titration

This experiments were carried out in 10 mM Tris buffer pH 7.4. The absorption titration was carried out by keeping the concentration of the complex (40 μM) and varying the concentration of CT DNA (3 to 300 μM). The metal-to-ligand charge transfer (MLCT) bands were monitored to follow the interaction of the complexes with CT DNA. Ruthenium-DNA solutions were allowed to incubate for 10 min before the absorption spectra were recorded.

2.5.2 Competitive binding

Fluorescence quenching experiments were conducted by adding small aliquots of 20 μM Ru(II) complexes solution to the samples containing 2 μM ethidium bromide (EB) and 40 μM CT DNA in buffer. This experiment was carried out using 5mM Tris base and 50 mM NaCl pH 7.1. Samples were excited at 340 nm and fluorescence spectra were recorded between 500-670 nm.

2.5.3 Viscosity measurements

This experiment was carried out using 5 mM Tris base and 50 mM NaCl pH 7.1 and maintained at a constant temperature at 29 °C. Data were presented as $(\eta/\eta_0)^{1/3}$ versus binding ration, where η is the viscosity of calf thymus DNA alone.

Viscosity values were calculated from the observed flow time of DNA containing solution (t) corrected for that of buffer alone (t_0), $\eta=(t-t_0)/t_0$.

2.5.4 Cyclic voltammetry

The supporting electrolyte was 50 mM NaCl and 5 mM Tris base buffer at pH 7.1. Solutions were deoxygenated by purging with argon gas for 15 min prior to the measurements; during the measurements, a stream of argon was passed over the solution. The experiments were carried out in 0.5 mM ruthenium(II) complexes in the absence and presence of 2.5 mM CT DNA.

2.5.5 DNA cleavage study

In this experiment, supercoiled pBIND DNA (0.5 μg/8 μL) was treated with ruthenium(II) complexes (20, 40, 60, 80 and 100 μM). The samples were analysed by electrophoresis for 1 h at 75 V on a 1% agarose gel in TAE buffer. The gel was stained with ethidium bromide and photographed under UV light.

2.6 Cytotoxicity assay

The cell lines used were the phoenix amphotropic packing cell lines (ϕNX-A cells). Cells were grown as adherent monolayers in medium (DMEM, RPMI-1640) plus 10% (v/v) supplemented hyclone cosmic calf serum, 100 μg/mL penicillin and 100 μg/mL streptomycin in a humid atmosphere of 5 % CO_2 at 37°C and unless otherwise stated. The cell lines used here were human breast cancer (MCF-7), human colon cancer (WiDr), human melanoma (sk-mel-28), human ovarian cancer (Igrov), human prostate cancer (PC3), human lung cancer (A549), and leukemia (CEM).

Cells were counted and seeded into 96 well at 1000 cells/well in 100 μL complete medium. Cells were allowed to attach for approximately 12 h. Each complex was added in a dilution series of 2 fold concentration steps to quadruplicate

wells in a final volume. 100 μL medium cells were allowed to 4 days when cells in control wells still subconfluent. Cells were lysed in a hypotonic buffer with detergent, (200 mM Tris pH 8.0, 50 mM EDTA, 2% triton X-100), also containing the nucleic acid stain Sybr I green (1:1000 molecular Probes). Fluorescence was read on a victor^2 1420 multilabel counter (wallac) with 485 nm excitation and 530 nm emission filters.

Because the ruthenium(II) complexes in this work are poorly water-soluble, a DMSO stock solution was used for all compounds to perform a proper comparison between the compounds. The positive control is cisplatin (0.25, 0.5, 1.0, 2.0, 4.0, 8.0, and 16.0 μM).

CHAPTER 3
RESULTS AND DISCUSSION

3.1 Syntheses of the 5mazpy ligand and the $[Ru(5mazpy)_2Cl_2]$ complexes

The 5-methyl-2-(phenylazo)pyridine (5mazpy) is used as ligand. The 5mazpy was synthesized by using literature procedure (Changsaluk and Hansongnern, 2005). This ligand was generally obtained by the condensation of nitrosobenzene with 6-amino-3-picoline in the presence of sodium hydroxide in dry benzene under refluxing condition for 8 h. Purification was carried out by column chromatography on silica gel. The reaction are shown in equation (1).

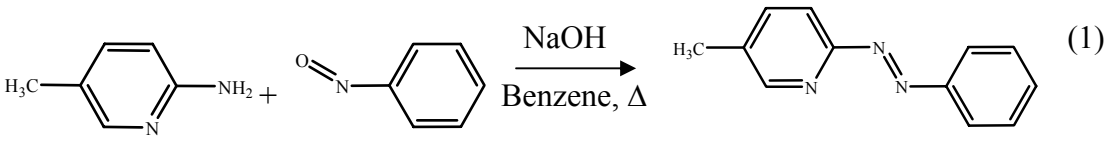

(1)

6-amino-3-picoline nitrosobenzene 5-methyl-2-(phenylazo)pyridine (5mazpy)

The yield of the 5mazpy ligand was 62%. The 5mazpy is a new bidentate ligand and acts as an unsymmetrical bidentate chelating ligand.

Ethanolic solutions of 5mazpy with $RuCl_3.3H_2O$ under reflux afford three isomers of the $[Ru(5mazpy)_2Cl_2]$ complex (equation (2)). There are *ctc*, *ccc*, and *tcc*-$[Ru(5mazpy)_2Cl_2]$. Because the 5mazpy has unsymmetric bidentate N,N′-donor centres, the pseudo-octahedral dichloro species, $[Ru(5mazpy)_2Cl_2]$, can occur in five geometrically isomeric forms: *trans-cis-cis* (*tcc*); *trans-trans-trans* (*ttt*); *cis-trans-cis* (*ctc*); *cis-cis-trans* (*cct*); *cis-cis-cis* (*ccc*) (Figure 3.1). Two (*tcc* and *ttt*) of these have the $RuCl_2$ group in the trans geometry and the other three (*ctc*, *cct*, and *ccc*) have the $RuCl_2$ group in the cis geometry. Either the *ctc* or *cct* configuration has been indicated

in the case of one blue isomer (herein refered to as the C_2 isomer, owing to the nominal two fold symmetry of the complex), while the other (the C_1 isomer) appeares to be of the *ccc* variety (Goswami *et al*., 1981).

$$RuCl_3.3H_2O + 2(5mazpy) \longrightarrow [Ru(5mazpy)_2Cl_2] \quad (2)$$

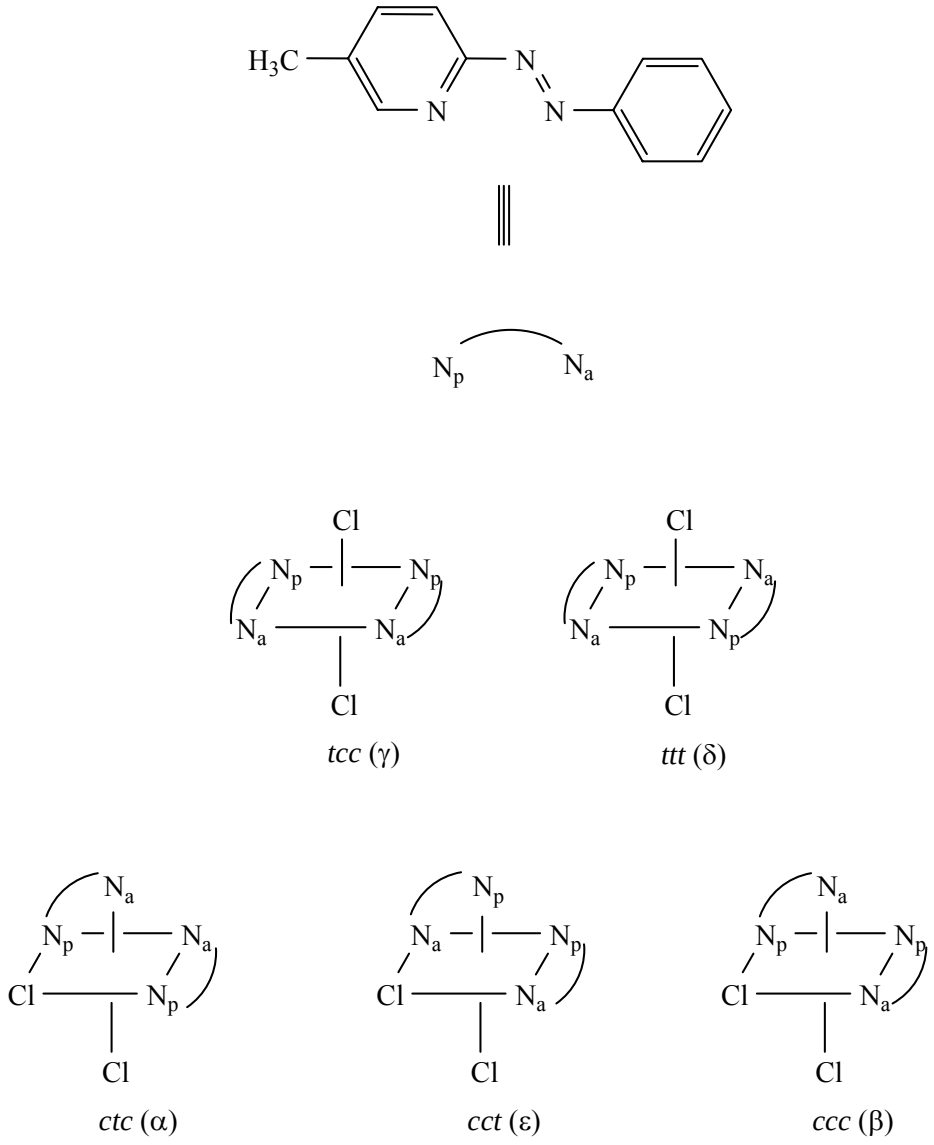

Figure 3.1 The five possible $[Ru(5mazpy)_2Cl_2]$ isomers

The physical properties of the 5mazpy ligand and its complexes are summarized in Table 3.1.

Table 3.1 The physical properties of the 5mazpy ligand and the $[Ru(5mazpy)_2Cl_2]$ complexes

Compounds	Physical properties		
	Appearance	Color	Melting point (°C)
5mazpy	Solid	Red orange	77-78
ctc-$[Ru(5mazpy)_2Cl_2]$	Solid	Blue	320-322
ccc-$[Ru(5mazpy)_2Cl_2[$	Solid	Purple	327-328
tcc-$[Ru(5mazpy)_2Cl_2]$	Solid	Green	326-327

3.2 Characterization of the 5mazpy ligand and the $[Ru(5mazpy)_2Cl_2]$ complexes

The chemistry of the 5mazpy ligand and the $[Ru(5mazpy)_2Cl_2]$ complexes were investigated by using following techniques:

3.2.1 Elemental analysis

3.2.2 FAB mass spectrometry

3.2.3 Infrared spectroscopy

3.2.4 UV-Visible absorption spectroscopy

3.2.5 1D and 2D Nuclear Magnetic Resonance spectroscopy

3.2.6 Cyclic voltammetry

3.2.7 X-ray Crystallography

3.2.1 Elemental analysis

Elemental analysis is a technique to investigate the composition of elements in the compounds. Results from this technique show that the analytical data of the compounds correspond to the calculated values. The elemental analysis data of the 5mazpy ligand and the *ctc*, *ccc*, and *tcc*-[$Ru(5mazpy)_2Cl_2$] complexes are listed in Table 3.2.

Table 3.2 Elemental analysis data of the 5mazpy ligand and the [$Ru(5mazpy)_2Cl_2$] complexes

Compounds	%C		%N		%H	
	Calc.	Found	Calc.	Found	Calc.	Found
5mazpy	73.08	72.66	21.30	22.53	5.62	5.54
ctc-[$Ru(5mazpy)_2Cl_2$]	50.89	50.82	14.84	15.27	3.91	3.96
ccc-[$Ru(5mazpy)_2Cl_2$]	50.89	50.71	14.84	15.40	3.91	3.99
tcc-[$Ru(5mazpy)_2Cl_2$]	50.89	50.79	14.84	14.99	3.91	3.89

3.2.2 Fast Atom Bombardment (FAB) mass spectrometry

FAB mass spectrometry is a technique to confirm molecular mass of the compounds. The FAB mass spectra of 5mazpy, *ctc*-[$Ru(5mazpy)_2Cl_2$], *ccc*-[$Ru(5mazpy)_2Cl_2$], and *tcc*-[$Ru(5mazpy)_2Cl_2$] are displayed in Figure 3.2, 3.3, 3.4 and 3.5, respectively. The results from FAB mass spectrometric data of the 5mazpy ligand and the *ctc*, *ccc*, and *tcc*-[$Ru(5mazpy)_2Cl_2$] complexes are summarized in Table 3.3.

Table 3.3 FAB mass spectrometric data of the 5mazpy ligand and the $[Ru(5mazpy)_2Cl_2]$ complexes

m/z	Stoichiometry	Equivalent species	Rel. Abun. (%)
5mazpy			
197	[5mazpy]	[L]	20
169	[5mazpy-phenyl+2Na$^+$]	[L-phenyl+2Na$^+$]	48
76	[phenyl-H]$^+$	[phenyl-H]$^+$	100
ctc-$[Ru(5mazpy)_2Cl_2]$			
566	$[Ru(L)_2Cl_2]$	[M]	30
531	$[Ru(L)_2Cl_2]$-Cl]$^+$	[M-Cl]$^+$	12
495	$[Ru(L)_2Cl_2]$-2Cl]$^+$	[M-2Cl]$^+$	18
77	[phenyl]	[phenyl]	100
ccc-$[Ru(5mazpy)_2Cl_2]$			
568	$[Ru(L)_2Cl_2]$+2H]$^+$	[M+2H]$^+$	50
531	$[Ru(L)_2Cl_2]$-Cl]$^+$	[M-Cl]$^+$	56
495	$[Ru(L)_2Cl_2]$-2Cl]$^+$	[M-2Cl]$^+$	54
tcc-$[Ru(5mazpy)_2Cl_2]$			
567	$[Ru(L)_2Cl_2]$+H]$^+$	[M+H]$^+$	40
496	$[Ru(L)_2Cl_2]$-2Cl+H]$^+$	[M-2Cl+H]$^+$	20
77	[phenyl]	[phenyl]	100

L = Molecular weight of the 5mazpy ligand = 197.21 g/mol

M = Molecular weight of the $[Ru(5mazpy)_2Cl_2]$complex = 566.45 g/mol

The FAB mass spectrum of the 5mazpy ligand is shown in Figure 3.2 From the data, the most intense peak at m/z 76, which give 100% relative abundance

is assigned to the one protonation phenyl ring. The peak at m/z 197 consistents with the molecular weight of the 5mazpy ligand.

The molecular weight of the *ctc*-[Ru(5mazpy)$_2$Cl$_2$] complex is 566 g/mol and the mass spectrum exhibits peak at m/z 566. It means that the peak at m/z 566 is used to confirm the molecular weight of this complex.

In the mass spectrum of the *ccc*-[Ru(5mazpy)$_2$Cl$_2$] complex, The peak at m/z 495 (54%) is observed which is assigned to this complex lost two chloride atoms from molecule.

The *tcc*-[Ru(5mazpy)$_2$Cl$_2$] complex gives the intense peak at m/z 567 (40%) which corresponds to protonated *tcc*-[Ru(5mazpy)$_2$Cl$_2$].

3.2.3 Infrared spectroscopy

Infrared spectroscopy is a technique to study functional groups in the compounds. Infrared spectra were recorded in a KBr pellet in the range 4000-370 cm^{-1} region. The infrared spectroscopic data of the 5mazpy ligand and the *ctc*, *ccc*, and *tcc*-[$Ru(5mazpy)_2Cl_2$] complexes are listed in Table 3.4.

Table 3.4 Infrared spectroscopic data of the 5mazpy (L) ligand and the [$Ru(L)_2Cl_2$] complexes

Vibration modes	Frequencies (cm^{-1})			
	5mazpy (L)	*ctc*-[$Ru(L)_2Cl_2$]	*ccc*-[$Ru(L)_2Cl_2$]	*tcc*-[$Ru(L)_2Cl_2$]
C=C, C=N stretching	1586(m) 1485(m) 1443(m)	1560(m) 1483(m) 1452(s)	1560(m) 1482(m) 1453(s)	1599(m), 1473(s), 1454(m)
N=N stretching	1389(s)	1334(s)	1299(s)	1307(s)
C-H bending of monosubstituted benzene	835 (s) 773 (s) 686 (s)	847(s), 776(s), 695(s)	830(s), 763(s), 692(s)	832(s), 761(s), 693(s)

s = strong, m = medium, w = weak

The free 5mazpy ligand shows the medium peaks at 1605-1440 cm^{-1}, corresponds to C=C and C=N stretching in the pyridine ring and phenyl ring in the free ligand. The sharp band at 1389 cm^{-1} is assigned to the N=N stretching, which occurs at a lower frequency than that in azpy ligand (1421 cm^{-1}) (Krause and Krause, 1980). The stretching frequencies of the C=C and C=N modes in the three isomers display three medium peaks in the range 1599-1452 cm^{-1}. The most important peak is

the N=N stretching mode which is used to be considered the π-acid property in the azo complexes. The *ctc*, *ccc*, and *tcc*-[Ru(5mazpy)$_2$Cl$_2$] complexes exhibit $\upsilon_{(N=N)}$ at 1334, 1299, and 1307 cm^{-1}, respectively, red shifted by 55-90 cm^{-1} from the free 5mazpy ligand. This suggests that less double-bond character in the N=N group in the complexes. This is strong evidence for substantial π-bonding to ruthenium through an azo nitrogen (Krause and Krause, 1980). The infrared spectra of the 5mazpy ligand and the *ctc*, *ccc*, and *tcc*-[Ru(5mazpy)$_2$Cl$_2$] complexes are shown in Figure 3.6, 3.7, 3.8, and 3.9, respectively.

3.2.4 UV-Visible absorption spectroscopy

UV-Visible absorption spectroscopy is a technique to study the electronic transitions of compounds. UV-Visible spectral studies of the compounds revealed absorptions within the range 200-800 nm in CH_2Cl_2, $CHCl_3$, CH_3CN, DMSO, and DMF. The UV-Visible absorption spectroscopic data of the 5mazpy ligand and the *ctc*, *ccc*, and *tcc*-[Ru(5mazpy)$_2$Cl$_2$] complexes are summarized in Table 3.5.

Table 3.5 UV-Visible absorption spectroscopic data of the 5mazpy (L) ligand and the [Ru(L)$_2$Cl$_2$] complexes

Compounds	λ_{max} nm, ($\varepsilon^a \times 10^{-4}$ $M^{-1}cm^{-1}$)				
	$CHCl_3$	CH_3CN	DMF	DMSO	CH_2Cl_2
5mazpy	321(2.1) 449(0.04)	322 (2.0) 448 (0.05)	326 (1.8) 450 (0.05)	326 (2.0) 450 (0.06)	324 (4.25) 448 (0.06)
ctc-[Ru(L)$_2$Cl$_2$]	322 (2.9) 582 (1.3)	318 (2.5) 588 (1.1)	322 (2.4) 588 (0.9)	322 (2.9) 594 (1.2)	322 (2.1) 582 (0.9)
ccc-[Ru(L)$_2$Cl$_2$]	342 (3.1) 576 (1.7)	332 (2.0) 578 (10.1)	322 (2.2) 578 (1.1)	336 (2.4) 576 (1.3)	338 (2.1) 576 (1.2)
tcc-[Ru(L)$_2$Cl$_2$]	302 (1.9) 406 (1.2) 630 (1.5)	300 (2.9) 392 (1.7) 636 (1.9)	304 (1.5) 396 (8.7) 640 (0.9)	302 (1.8) 638 (1.3)	302(1.8) 400(1.1) 638(1.2)

[a] Molar extinction coefficient

In CH_2Cl_2, the 5mazpy ligand exhibits transition at 448 nm ($\varepsilon \sim 600$ $M^{-1}cm^{-1}$) and 324 nm ($\varepsilon \sim 42{,}500$ $M^{-1}cm^{-1}$), corresponds to intraligand transitions, $n \rightarrow \pi^*$ and $\pi \rightarrow \pi^*$, respectively, centred primarily on the azo group. Therefore, the transitions in the complexes at around 400 nm are probably of ligand origin and are not considered further. The *trans* (*tcc*) complex shows an intense band ($\varepsilon \sim 12{,}000$ M^{-}

$^{1}cm^{-1}$) in the region 636-640 nm, are assigned to the $t_2(Ru) \rightarrow \pi^*(L)$ MLCT transition, where the π^* orbital has a large azo character (Santra *et al.*, 1999). The *cis* complexes (*ctc* and *ccc*-[Ru(5mazpy)$_2$Cl$_2$]) exhibit hightly intense (ε ~ 9,000-17,000 $M^{-1}cm^{-1}$) MLCT transitions at higher energies compare to the trans complex. The *cis* complexes display two different intense band characters. The most intense bands are in the range 318-342 nm and the less intense bands are in the range 576-594 nm while the spectrum of trans complex shows two similar band characters. The *ccc*-[Ru(5mazpy)$_2$Cl$_2$] isomer exhibits a transition at a higher energy (~ 10 nm) than that of the *ctc*-[Ru(5mazpy)$_2$Cl$_2$] isomer. The UV-visible absorption spectra of the 5mazpy ligand and the *ctc*, *ccc*, and *tcc*-[Ru(5mazpy)$_2$Cl$_2$] complexes in CH_2Cl_2 are shown in Figure 3.10, 3.11, 3.12, and 3.13, respectively.

3.2.5 1D and 2D Nuclear Magnetic Resonance spectroscopy

The Nuclear Magnetic Resonance spectroscopy is a technique to support the structure of compounds. The NMR spectra of compound were carried out in $CDCl_3$ and the tetramethylsilane ($Si(CH_3)_4$) was used as an internal reference. The structures of compound were explained by using 1D and 2D NMR spectroscopic techniques (^{1}H NMR, ^{13}C NMR, DEPT 135 NMR, ^{1}H-^{1}H COSY NMR, and ^{1}H-^{13}C HMQC NMR). The NMR spectroscopic studies of each compound were described as below.

(a) Nuclear Magnetic Resonance spectroscopy of the 5mazpy ligand

The ^{1}H and ^{13}C NMR spectroscopic data of the 5mazpy ligand are listed in Table 3.6.

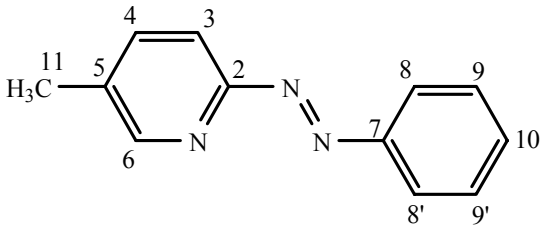

Table 3.6 ^{1}H and ^{13}C NMR spectroscopic data of the 5mazpy ligand

H-C Position	^{1}H NMR			^{13}C NMR
	δ (ppm)	J (Hz)	Number of H	δ (ppm)
6	8.56 (*d*)	2.0	1	149.81
8, 8′	8.04 (*dd*)	7.5, 2.0	2	123.48
3	7.76 (*d*)	8.5	1	115.23
4	7.69 (*dd*)	8.0, 2.0	1	138.74
9, 9′, 10	7.52 (*m*)	-	3	129.11, 131.88
11	2.43 (*s*)	-	3	18.39

Table 3.6 (continued)

H-C Position	^{1}H NMR			^{13}C NMR
	δ (ppm)	J (Hz)	Number of H	δ (ppm)
Quaternary Carbons				161.07, 152.42, 135.58

d = doublet, *dd = doublet of doublet*, *m = multiplet* and *s = singlet*

The ^{1}H NMR spectrum of 5mazpy is shown in Figure 3.14. There are two types of protons, aliphatic proton and aromatic proton. The ^{1}H NMR spectrum exhibited six signals for eleven protons. The detail of each proton signal could be explained below.

The proton H3 appears at 7.76 ppm as *doublet* because of coupling with H4 (J = 8.5 Hz). The proton H4 locates next to H3, the signal of H4 appears at 7.69 ppm which *doublet of doublet* peak is observed due to coupling with H3 (J = 8.0 Hz) and long range coupling with H6 (J = 2.0 Hz). The signals of proton H6 exhibit at 8.56 ppm. The splitting pattern is doublet (J = 2.0 Hz) by long range coupling with proton H4. The proton H6 locates next to nitrogen atom on pyridine ring, therefore this signal appears at the most downfield. The proton H8 and H8′ are two equivalent proton on the phenyl ring. The signal shows *doublet of doublet* peaks at 8.04 ppm. This signal appears at the lower field than other proton (H9, H9′, H10) on the phenyl ring because it locates close to the azo nitrogen. The signal of proton H9 occurs at 7.52 ppm. The splitting pattern is *multiplet* at the same position of proton H10. In comparison, the 5-methyl-2-(phenylazo)pyridine (5mazpy), 2-(phenylazo)pyridine (azpy) (Changsaluk and Hansongnern, 2005) and 5-Clazpy-2-(phenylazo)pyridine (Clazpy) ligands (Sahavisit and Hansongnern, 2005), the proton signals in 5mazpy appear at the highfield than azpy and Clazpy due to the effect of donating group (methyl group) in pyridine ring. The signal of protons on methyl group is observed at 2.43 ppm. In addition, all proton resonance signals are confirmed by ^{1}H-^{1}H COSY NMR experiments and the ^{1}H-^{1}H COSY NMR spectrum is given in Figure 3.15.

The results from ^{13}C NMR spectrum (Figure 3.16) correspond to the results from DEPT 135 NMR spectrum (Figure 3.17). The ^{13}C NMR spectrum of the 5mazpy ligand shows ten signals for twelve carbons. The signals at 138.74 ppm (C4) and 115.23 ppm (C3) are observed. The signals of carbon C6 (149.81 ppm) occur at lower field than that of other methine carbons because is located next to the nitrogen atom on pyridine ring. The carbons C8 and C9 (123.48 and 129.11 ppm) in phenyl ring resonate symmetrically at different position. The carbon signal at 131.88 ppm is attributed to the carbon C10. The methyl carbon appears at the highest field 18.39 ppm. Furthermore, the ^{1}H-^{13}C HMQC NMR spectroscopy was used to assign all signals. Contour peaks in the ^{1}H-^{13}C HMQC NMR spectrum (Figure 3.18) in 5mazpy ligand, the absence of any contours at 161.07, 152.42, and 135.58 ppm assign them to the carbon C2, C7 and C5, respectively.

(b) Nuclear Magnetic Resonance spectroscopy of the *ctc*-[Ru(5mazpy)$_2$Cl$_2$] complex

The ^{1}H and ^{13}C NMR spectroscopic data of the *ctc*-[Ru(5mazpy)$_2$Cl$_2$] complex are summarized in Table 3.7.

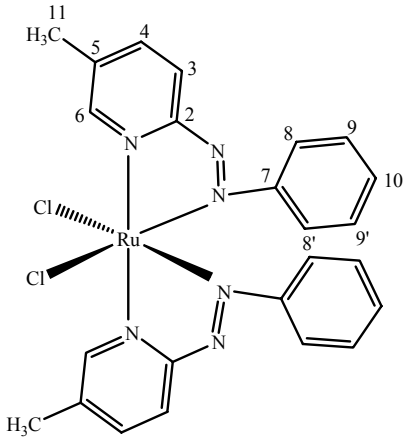

Table 3.7 ^{1}H and ^{13}C NMR spectroscopic data of the *ctc*-[Ru(5mazpy)$_2$Cl$_2$] complex

H-C Position	^{1}H NMR			^{13}C NMR
	δ (ppm)	*J* (Hz)	Number of H	δ (ppm)
6	9.13 (*d*)	1.5	1	150.93
3	8.37 (*d*)	8.0	1	126.10
4	7.75 (*dd*)	8.5, 2.0	1	137.94
10	7.25 (*td*)	7.5, 7.5	1	129.72
9, 9′	7.10 (*dd*)	8.5, 7.5	2	128.36
8, 8′	6.80 (*dd*)	8.5, 1.0	2	121.92
11	2.35 (*s*)	-	3	19.24
Quaternary Carbons				164.62, 155.31, 136.61,

d = doublet, *dd = doublet of doublet*, *s = singlet*, and *td = triplet of doublet*

The ^{1}H NMR spectrum of the *ctc*-[Ru(5mazpy)$_2$Cl$_2$] complex is shown in Figure 3.19. The signals of protons on the *ctc*-[Ru(5mazpy)$_2$Cl$_2$] complex appear only one set of ligand peaks, indicating two equivalent 5mazpy ligands, so the complex must be symmetric due to its C_2 axis. The assignment was made with the use of ^{1}H-^{1}H COSY NMR spectroscopy (Figure 3.20). The ^{1}H NMR spectrum shows that the pyridine protons are mostly affected when compares to the phenyl protons. The aromatic protons at 9.13, 8.37, 7.75, 7.25, 7.10, and 6.80 ppm are attributed to H6, H3, H4, H10, H9,9′, and H8,8′, respectively on the basis of ^{1}H-^{1}H COSY NMR spectrum. The signals of proton H3, H4, and H6 are shifted to downfield while H8,8′, H9,9′, H10, and H11 are shifted upfield from those of the free ligand. The signal of proton H6 in pyridine rings occurs at the lowest field because of the influence of coordinated nitrogen atoms. One methyl signal is observed at 2.35 ppm (*singlet*). This indicates that the *ctc*-[Ru(5mazpy)$_2$Cl$_2$] complex has C_2-symmetry.

The results of ^{13}C NMR (Figure 3.21) correspond to the DEPT 135 NMR (Figure 3.22). The ^{13}C NMR spectrum contains ten signals from twenty-two carbons. Three signals of quaternary carbon at 164.62, 155.31, and 136.61 ppm are assigned as quaternary carbon C2, C7, and C5, respectively. The methine carbons on the pyridine rings appear at the lower field than that the phenyl rings. It is due to the effected of nitrogen atoms. The methine carbons display at 150.93, 126.10, 137.94, 129.72, 128.36, and 121.92 ppm which are assigned to carbon C6, C3, C4, C10, C9,9′, and C8,8′ positions, respectively. In addition, the ^{1}H-^{13}C HMQC NMR spectroscopy was carried out and the ^{1}H-^{13}C HMQC NMR spectrum is shown in Figure 3.23.

(c) Nuclear Magnetic Resonance spectroscopy of the *ccc*-[Ru(5mazpy)$_2$Cl$_2$] complex

The ^{1}H and ^{13}C NMR spectroscopic data of the *ccc*-[Ru(5mazpy)$_2$Cl$_2$] complex are summarized in Table 3.8.

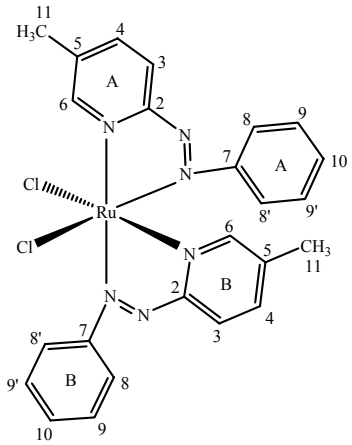

Table 3.8 ^{1}H and ^{13}C NMR spectroscopic data of the *ccc*-[Ru(5mazpy)$_2$Cl$_2$] complex

H-C Position	^{1}H NMR			^{13}C NMR
	δ (ppm)	*J* (Hz)	Number of H	δ (ppm)
6A	9.58 (*s*)	-	1	149.48
3A	8.40 (*d*)	8.0	1	124.19
3B	8.27 (*d*)	8.0	1	125.82
4A	7.93 (*dd*)	8.0, 1.5	1	139.62
8, 8′B	7.77 (*dd*)	8.5, 1.5	2	125.61
4B	7.69 (*dd*)	8.0, 1.0	1	139.27
10B	7.45 (*td*)	7.5, 7.5	1	130.87
9, 9′B	7.38 (*dd*)	8.5, 1.0	2	127.60
10A	7.34 (*t*)	8.0	1	129.63

Table 3.8 (continued)

H-C Position	^{1}H NMR			^{13}C NMR
	δ (ppm)	J (Hz)	Number of H	δ (ppm)
9, 9′A	7.18 (*dd*)	8.0, 7.5	2	128.71
6B	7.00 (*s*)	-	1	148.14
8, 8′A	6.68 (*dd*)	8.5, 1.0	2	121.34
11A	2.56 (*s*)	-	3	19.63
11B	2.20 (*s*)	-	3	19.02
Quaternary Carbons				165.16, 163.45, 157.24, 155.40, 136.80, 136.18,

d = doublet, *dd = doublet of doublet*, *s = singlet*, and *td = triplet of doublet*

The ^{1}H NMR spectrum of the *ccc*-[Ru(5mazpy)$_2$Cl$_2$] complex is displayed in Figure 3.24. The spectrum of the *ccc*-[Ru(5mazpy)$_2$Cl$_2$] complex is more complex than that of the *ctc*-[Ru(5mazpy)$_2$Cl$_2$] complex. The peaks assignments are supported by using simple correlation ^{1}H-^{1}H COSY NMR spectroscopy (Figure 3.25). The ^{1}H NMR spectrum of *ccc*-[Ru(5mazpy)$_2$Cl$_2$] shows twice the number of signals, as this isomer has no C_2 axis, which results in two inequivalent 5mazpy ligands. From all 5 theoretically possible isomers only the *ccc* isomer has no C_2 axis; so already from this ^{1}H NMR spectrum the configuration has been proven. This is also confirmed by the methyl signals in aliphatic region. From the parent complex, [Ru(azpy)$_2$Cl$_2$], only *ccc*-isomer has C_1-symmetry (Seal and Ray *et al*., 1984). Thus, the *ccc*-configuration should exhibit two CH_3 signals of equal intensities. From the ^{1}H NMR spectrum CH_3 signals appear as *singlet* at 2.56 ppm for proton 11A and 2.20 ppm for proton 11B. The H3(A, B) and H6(A) signals are shifted to downfield while H6(B), H8,8′(A,B), H9,9′(A, B) and H10(A, B) are shifted to upfield from those of the free ligand. The proton H6(A) appears at the lower filed than H6(B) because it is

trans to the N=N mode (electron withdrawing group) while proton H6(B) is trans to chloride (Velder *et al*., 2004). This is similar to the result of *ccc*-[$Ru(azpy)_2Cl_2$] which was carried out in the same solvent ($CDCl_3$) (Changsaluk and Kanidtha, 2005). In comparison between *ccc*-[$Ru(5mazpy)_2\ Cl_2$] and *ccc*-[$Ru(azpy)_2Cl_2$] in the same solvent ($CDCl_3$), the proton signals of the 5mazpy complex occur at the higher field relative to azpy complex because of the electron donating substituent (CH_3 group) on the pyridine ring.

The ^{13}C NMR spectrum (Figure 3.26) contains twelve methine carbons, six quaternary carbons, and two methyl carbons. This results support with the DEPT 135 NMR spectrum (Figure 3.27) which present only signal of methine carbons (14 signals) and methyl carbons (2 signals). The carbon C8,8′ C9,9′ in phenyl ring A and B in this complex resonate symmetrically at different position. The signals of carbon C6 occur at a lower field than that of other methine carbons because it is located next to the nitrogen atoms on pyridine ring. The carbon C6(A), C3(A), C3(B), C4(A), C8,8′(A), C4(B), C10(B), C9,9′(B), C10(A), C9,9′(A), C6(B), and C8,8′(A) are found at 149.48, 124.19, 125.82, 139.62, 125.61, 139.27, 130.87, 127.60, 129.63, 128.71, 148.14, and 121.34 ppm, respectively. The signal carbons of CH_3 appear at the highest field 19.02 ppm (ligand B) and 19.63 ppm (ligand A). The quaternary carbons are observed at 136.80, 136.18, 157.24, 155.40, 165.16, and 163.45 ppm. In addition, the ^{13}C NMR signal assignments are based on the ^{1}H-^{13}C HMQC NMR spectrum (Figure 3.28).

(d) Nuclear Magnetic Resonance spectroscopy of the *tcc*-[Ru(5mazpy)$_2$Cl$_2$] complex

The ^{1}H and ^{13}C NMR spectroscopic data of the *tcc*-[Ru(5mazpy)$_2$Cl$_2$] complex are summarized in Table 3.9.

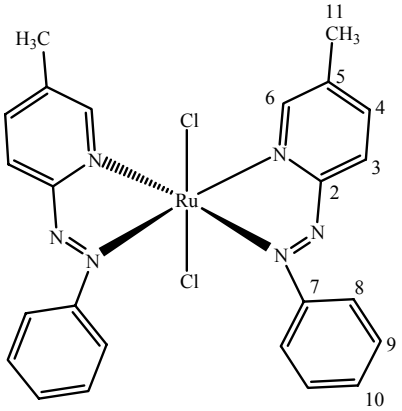

Table 3.9 ^{1}H and ^{13}C NMR spectroscopic data of the *tcc*-[Ru(5mazpy)$_2$Cl$_2$] complex

H-C Position	^{1}H NMR			^{13}C NMR
	δ (ppm)	*J* (Hz)	Number of H	δ (ppm)
6	8.76 (*s*)	-	2	148.92
3	8.48 (*d*)	7.0	2	124.38
4	7.98 (*d*)	7.0	2	141.31
8, 8′	7.52 (*d*)	7.0	4	122.85
10	7.16 (*m*)	-	2	129.43
9, 9′	6.97 (*m*)	-	4	128.15
11	2.55 (*s*)	-	6	19.40
Quaternary Carbons				164.33, 157.72, 134.73

d = doublet, *m = multiplet*, and *s = singlet*

The ^{1}H NMR spectrum of the *tcc*-[Ru(5mazpy)$_2$Cl$_2$] complex (Figure 3.29) is similar to the *ctc*-[Ru(5mazpy)$_2$Cl$_2$] complex which is simpler than that of the *ccc*-[Ru(5mazpy)$_2$Cl$_2$] complex. The two 5mazpy ligands in this complex are magnetically equivalent because this molecule also has C_2-symmetry. The proton spectrum is clearly divided in two portions; the downfield part is due to pyridine protons (H3, H4, and H6) and the upfield signals refer to phenyl protons (H8,8′, H9,9′, and H10). The pyridine protons in the complex are shifted downfield by 0.20-0.72 ppm compare to the free ligand values. This supports the tight binding of Ru(II) with heterocyclic-N. The *singlet* signal at approximately 8.76 ppm refers to H6 because of the closest position to the metal centre and deshielding effect of nearby Cl ligand follow by the H3 (8.48 ppm, J = 7 Hz) and H4 shows *doublet* at approximately 7.98 ppm (*doublet*, J = 7 Hz). The proton H8,8′ (7.52 ppm, *doublet*, J = 7 Hz) appears at lower field compare to proton H9,9′ (6.97 ppm, *multiplet*) and H10 (7.16 ppm, *multiplet*) due to the closest position of the electron withdrawing azo group. This complex displays single CH_3 signal (2.55 ppm), suggesting that the C_2-symmetry is retained. This complex is also confirmed by using simple correlation ^{1}H-^{1}H COSY NMR spectroscopy (Figure 3.30).

The ^{13}C NMR spectrum is given in Figure 3.31. Ten carbon signals are observed in the spectrum. The signals of methine carbons and quaternary carbons are supported by the results from DEPT 135 NMR spectrum (Figure 3.32). The methine carbon signals appear in the range 122-149 ppm. The quaternary carbons C5, C7, and C2 are observed at 134.73, 157.72, and 164.33 ppm, respectively. The highfield resonance at 19.40 ppm belongs to methyl carbon (C11). In addition, the resonances have been assigned using ^{1}H-^{13}C HMQC NMR spectroscopy and this spectrum is given in Figure 3.33.

3.2.6 Cyclic voltammetry

Electron transfer properties of the 5mazpy ligand and the $[Ru(5mazpy)_2Cl_2]$ complexes have been investigated by using cyclic voltammetry in dichloromethane (0.1 M TBAH). In this experiment, the working electrode is glassy carbon. The reported potential data were compared with the values for the ferrocenium-ferrocene couple, under our experimental conditions. The voltammograms displayed metal oxidations at the positive side and the ligand reductions at the negative side. Voltammetric data are collected in Table 3.10 and representative voltammograms are displayed in Figure 3.34, 3.35, 3.36, and 3.37.

In order to check the couple or redox reaction, the different scan rate were used. The couple which have almost equal anodic and cathodic current was refered as reversible couple. While, the unequal currents were refered to the unequally transfer of electron in reduction and oxidation. This is irreverible couple. In addition, the different scan rates were applied, these currents gave anodic and cathodic currents at the higher scan rate. This led to quasi-reversible couple.

Table 3.10 Cyclic voltammetric[a] data of the 5mazpy ligand and the $[Ru(5mazpy)_2Cl_2]$ complexes in CH_2Cl_2 (0.1 M TBAH) at scan rate 100 mVs^{-1}

Compounds	$E_{1/2}$ (V) (ΔE_p (mV))		
	Oxidation	Reduction	
5mazpy	-	-1.62 (94)	
ctc-$[Ru(5mazpy)_2Cl_2]$	0.65 (65)	-1.17 (95)	-1.65 [b]
ccc-$[Ru(5mazpy)_2Cl_2]$	0.60 (85)	-1.16 (95)	-1.61[b]
tcc-$[Ru(5mazpy)_2Cl_2]$	0.47 (90)	-1.20 (115)	-1.57[b]

[a] $E_{1/2} = (E_{pa}+E_{pc})/2$, where E_{pa} and E_{pc} are anodic and chathodic peak potentials, respectively; $\Delta E_p = E_{pa}-E_{pc}$; [b] cathodic peak

Oxidation Range

In the potential range 0 to 1.0 V, the 5mazpy shows no signal in this potential range and the complexes display a one-electron cyclic voltammetric response due to the electrode reactions shown in equation (3).

$$[Ru(5mazpy)_2Cl_2]^+ + e^- \rightarrow [Ru(5mazpy)_2Cl_2] \quad (3)$$

The data reveal that the *ctc*-isomer and *ccc*-isomer exhibit higher potentials by 0.13-0.18 V than the *tcc*-isomer. The *ctc*-isomer displays a slightly higher Ru(III)/ Ru(II) couple (0.65 V, ΔE_p = 65 mV) than that the *ccc*-isomer (0.60 V, ΔE_p = 85 mV). In the $[Ru(5mazpy)_2Cl_2]$ complexes, the ability of the 5mazpy ligand to stabilize the complex is as follow *cis* (*ctc* and *ccc*) > *trans* (*tcc*).

Reduction Range

In the potential range 0 to -2.0 V at the scan rate 100 mVs^{-1} in dichloromethane, all complexes display one reversible to quasireversible (peak-to-peak separation peak ΔE_p = 65-90 mV) and one irreversible peak. It is believed that the reduction peaks correspond to the reduction of the organic ligand possibility at the azo function. The free ligand displays one quasireversible two electron response with peak-to-peak separation at 94 mV, corresponds to the couple in equation (4).

$$5mazpy \xrightarrow{2e^-} 5mazpy^{2-} \quad (4)$$

The free ligand, 5mazpy displays one reduction wave at -1.62 V (ΔE_p = 94 mV). This value is slightly lower than azpy (-1.60 V) by 0.02 V and higher than 4-methyl-2-(phenylazo)pyridine (4mazpy) (-1.68 V, ΔE_p = 94 mV) (Muaksang, K., 2005). All the three complexes exhibit one quasireversible and one irreversible peak of one electron. In addition, the potential shows a positive shifted from the free ligand

value. The first reduction couple of *ccc*-[Ru(5mazpy)$_2$Cl$_2$] (-1.16 V, ΔE_p =95 mV) occurs at the higher potential than that in *tcc*-[Ru(5mazpy)$_2$Cl$_2$] (-1.20 V, ΔE_p = 115 mV) and comparable to *ctc*-[Ru(5mazpy)$_2$Cl$_2$] (-1.17 V, ΔE_p = 95 mV). This results can be implied that the *ccc* isomer accepts electron better than the *tcc* isomer and comparable to *ctc* isomer. Table 3.11 lists the cyclic voltammetric data of the 4mazpy, and 5mazpy and its complexes in dichloromethane at 100 mVs^{-1}.

Table 3.11 Cyclic voltammetric data of 4mazpy, and 5mazpy and its complexes in CH_2Cl_2 at scan rate 100 mVs^{-1}

Compounds	Reduction potential (V)
5mazpy	-1.62 (94)
[Ru(5mazpy)$_2$Cl$_2$]	(-1.16) to (-1.20)
4mazpy	-1.68 (94)
[Ru(4mazpy)$_2$Cl$_2$]	(-1.02) to (-1.22)

In comparison with the 5mazpy and 4mazpy complexes (Table 11), the [Ru(4mazpy)$_2$Cl$_2$] complexes exhibit the first reduction couple in the range -1.02 V to -1.22 V, while the [Ru(5mazpy)$_2$Cl$_2$] complexes display at -1.16 to -1.20 V. So the 4mazpy complexes show the higher potential than the 5mazpy complexes. The π-acidity order of those ligand are as follows: 4mazpy > 5mazpy.

3.2.7 X-ray crystallography

The X-ray crystallography is the most important technique to identify the structure of compounds, 5mazpy, *ctc*-, *ccc*-, and *tcc*-[Ru(5mazpy)$_2$Cl$_2$].

(a) X-ray structure of the 5-methyl-2-(phenylazo)pyridine ligand

The single crystals of 5mazpy were grown by slow diffusion of hexane into ethanol solution of the 5mazpy ligand. The detailed measurement consitions and the crystal data are listed in Table 3.12. The selected bond lengths and bond angles are given in Table 3.13. Figure 3.38 shows the ORTEP and atom numbering scheme for the 5mazpy ligand.

Table 3.12 Crystallographic data of the 5mazpy ligand

Empirical formula	C_{12} H_{11} N_3
Formula weight	197.24
Crystal system	monoclinic
Z	4
Space group	$P2_1/c$
a = 6.3957(7)Å	$\alpha = 90^o$
b = 8.4112(9)Å	$\beta = 95.430(2)^o$
c = 19.931(2)Å	$\gamma = 90^o$
Temperature	293(2)K
Radiation	Mo K_α (λ = 0.71073 Å)
Crystal size	0.269 x 0.197 x 0.138 mm
Volume	1067.4(2)Å^3
Density (calculated)	1.227 Mg/m^3
F(0 0 0)	416
Goodness-of-fit on F^2	1.083
Completeness to theta	25.00^o

Table 3.12 (continued)

Reflections collected	7434
Refinement method: Full-matrix least-squares on F^2	
R indices (all data)	*R1* = 0.0560; *wR2* = 0.1386
Measurement: Bruker SMART CCD diffractometer	
Program system: SHELX-97	
Structure determination: Direct methods (SHELXS-97)	
Refinement: full-matrix least-squares (SHELXL-97)	

Table 3.13 Selected bond lengths (Å) and bond angles (°) of the 5mazpy ligand

N(1)-C(5)	1.329(2)	N(1)-C(1)	1.330(3)
N(2)-N(3)	1.228(2)	N(2)-C(5)	1.442(3)
N(3)-C(6)	1.445(3)	C(1)-C(2)	1.381(3)
C(2)-C(3)	1.382(3)	C(2)-C(12)	1.500(3)
C(3)-C(4)	1.373(3)	C(4)-C(5)	1.385(3)
C(6)-C(7)	1.379(3)	C(6)-C(11)	1.381(3)
C(7)-C(8)	1.379(3)	C(8)-C(9)	1.378(4)
C(9)-C(10)	1.376(4)	C(10)-C(11)	1.371(3)
C(5)-N(1)-C(1)	116.45(18)	N(3)-N(2)-C(5)	112.75(17)
N(2)-N(3)-C(6)	113.70(18)	N(1)-C(1)-C(2)	125.8(2)
C(1)-C(2)-C(3)	115.75(19)	C(1)-C(2)-C(12)	121.8(2)
C(3)-C(2)-C(12)	122.5(2)	C(4)-C(3)-C(2)	120.44(19)
C(3)-C(4)-C(5)	118.38(19)	N(1)-C(5)-C(4)	123.13(19)
N(1)-C(5)-N(2)	111.88(17)	C(4)-C(5)-N(2)	125.00(18)
C(7)-C(6)-C(11)	120.0(2)	C(7)-C(6)-N(3)	115.1(2)
C(7)-C(6)-C(11)	120.0(2)	C(7)-C(6)-N(3)	115.1(2)
C(11)-C(6)-N(3)	124.90(19)	C(8)-C(7)-C(6)	120.0(2)

Table 3.13 (continued)

C(9)-C(8)-C(7)	119.9(2)	C(10)-C(9)-C(8)	119.8(2)
C(11)-C(10)-C(9)	120.6(3)	C(10)-C(11)-C(6)	119.6(2)

In the molecule, the benzene ring (C6, C7, C8, C9, C10, C11), azo (N2, N3), and C12 atom lie in a plane. The C-N=N-C in 5mazpy is *trans*-conformation. The pyridine ring is also planar and the maximum deviation of any atom from mean plane passing through the ring is 0.008(3)Å for C3. In addition, atom C8 of benzene ring deviates from C6-C7-C8-C9-C10-C11 by 0.010(4)Å. The azo(N2, N3) is in the same plane as benzene ring with torsion angle N1-C5-N2-N3 is 172.73(17)° and C7-C6-N3-N2 is 170.89(19)°. In addition, the azo (N2, N3) is coplanar with pyridine ring. This is also reflected in the angle between planes of pyridine ring and benzene ring is 17.31(1)°. Then electrons from substituent can delocalize into the conjugated system in the molecule. This can give the some property of this compound for coordinating with metal ions in the future study.

The N2-N3 distance of the title compound is 1.228(2)Å, shorter than that of the protonated azpy (1.248(4)Å) due to the hydrogen bond interaction between N(azo) and the protonated proton (Panneerselvam *et al*., 2000). This results in decreasing the electron density in azo moiety and lengthening the azo bond. According to Harada *et al*, there are an orientation disorder in azobenzene, resulting in a shortening of the N=N bond and elongation of N-Ph bond. From this result the 5mazpy ligand could be orientation disorder in the crystal but we carried out the experiment only at room temperature (Harada *et al*, 1997). In addition, the C5(pyridine)-N2(azo) bond distance (1.442(3)Å) is comparable to N3(azo)-C6(benzene) (1.445(3)Å) which indicateds the same interaction of azo with pyridine and benzene group. However, in the case of 2-phenylazo-5-nitro-6-methyl-pyridine, both bond lengths are different (1.430(4), 1.421(4)Å) which were confirmed by density functional theory (DFT) calculation (Michalski *et al*, 2005). Moreover, result from vibrational dynamics showed that vibration of the -CNNC- core are strongly

coupled with the vibrations of the pyridine, phenyl and their substituents. This means that strong π electron aromatic systems influence the vibrations of the azo-bridging group (Michalski *et al*, 2005).

(b) X-ray structure of the *ctc*-[Ru(5mazpy)$_2$Cl$_2$] complex

The single crystals of the *ctc*-[Ru(5mazpy)$_2$Cl$_2$] complex were grown by slow diffusion of hexane into chloroform solution of the complex. The molecular structure of *ctc*-[Ru(5mazpy)$_2$Cl$_2$] is shown in Figure 3.39. Table 3.14 lists the crystallographic data of *ctc*-[Ru(5mazpy)$_2$Cl$_2$] and relevant bond distances and angles are given in Table 3.15.

Table 3.14 Crystallographic data of the *ctc*-[Ru(5mazpy)$_2$Cl$_2$] complex

Empirical formula	$C_{24}H_{22}Cl_2N_6Ru$
Formula weight	566.49
Crystal system	Monoclinic
Z	4
Space group	C2/c
a = 10.9692(5)Å	$\alpha = 90^o$
b = 15.6115(7)Å	$\beta = 91.0011(10)^o$
c = 14.4450(7)Å	$\gamma = 90^o$
Temperature	293(2) K
Wavelength	0.71073 Å
Volume	2473.3(2)Å^3
Density (calculated)	1.521 Mg/m^3
Absorption coefficient	0.874 mm^{-1}
F(000)	1144
Goodness-of-fit on F^2	1.05
Reflections collected	2707
Refinement method	Full-matrix least-squares on F^2
Completeness to theta	28.05^o
R indices (all data)	*R1* = 0.035, *wR2* = 0.042
Measurement: Bruker SMART CCD diffractometer	
Program system: SHELX-97	

Table 3.14 (continued)

Structure determination: Direct methods (SHELXS-97)
Refinement: full-matrix least-squares (SHELXL-97)

Table 3.15 Selected bond lengths (Å) and bond angles (°) of the *ctc*-[Ru(5mazpy)$_2$ Cl$_2$] complex

Ru(1)-Cl(1)	2.4102(7)	Ru(1)-N(1)	2.043(2)
Ru(1)-N(3)	1.972(2)	Ru(1)-Cl(1)	2.4102(7)
Ru(1)-N(1)	2.043(2)	Ru(1)-N(3)	1.972(2)
N(2)-N(3)	1.284(3)	N(1)-C(1)	1.344(3)
N(1)-C(6)	1.356(3)	N(2)-C(6)	1.391(3)
N(3)-C(7)	1.439(3)		
Cl(1)-Ru(1)-N(1)	88.70(6)	Cl(1)-Ru(1)-N(3)	171.64(6)
Cl(1)-Ru(1)-Cl(1)	91.24(2)	Cl(1)-Ru(1)-N(1)	95.53(6)
Cl(1)-Ru(1)-N(3)	85.17(6)	N(1)-Ru(1)-N(3)	99.14(8)
N(1)-Ru(1)-Cl(1)	95.53(6)	N(1)-Ru(1)-N(1)	173.96(8)
N(1)-Ru(1)-N(3)	76.87(8)	N(3)-Ru(1)-Cl(1)	85.17(6)
N(3)-Ru(1)-N(1)	76.87(8)	N(3)-Ru(1)-N(3)	99.36(8)
Cl(1)-Ru(1)-N(1)	88.70(6)	Cl(1)-Ru(1)-N(3)	171.64(6)
N(1)-Ru(1)-N(3)	99.14(8)		

The Ru(II) ion is six coordinated with four nitrogen atoms of bidentate ligand and two chloride atoms in a distorted octahedron geometry. The atomic arrangement around the ruthenium center involved sequentially two *cis*-chlorides, *trans*-N(pyridine), and *cis*-N(azo). If the coordinating pairs Cl, N(py), and N(azo) are considered in that order, the configuration of this complexes is *cis*-*trans*-*cis* (*ctc*), the so-called α-configuration. In the coordianation octahedra, the Ru-Cl distances are

2.410(1)Å, it is similar to those found in *ctc*-[Ru(azpy)$_2$Cl$_2$] (2.399(1)Å) (Seal and Ray, 1987). The Ru-N(azo) distances (1.972(2) Å) are shorter than those of Ru-N(pyridine) (2.043(2)Å). The shortening may be due to greater π-backbonding, dπ(Ru) → π*(azo), offered by the azo group. Moreover, in the title complex the average N=N distance of 5mazpy is 1.284(3)Å which is slightly longer than that of the free 5mazpy (N=N 1.228(2)Å). The coordination of azoimine ligand leads to a decrease in the N=N bond order due to the σ-donor and the π-acceptor character of the ligand. The angle Cl-Ru-Cl in this complex (91.24(2)°) is slightly bigger than in *ctc*-[Ru(azpy)$_2$Cl$_2$] (89.52(6)°) (Seal and Ray, 1987). The chelate angles extended by 5mazpy were 76.87(8)° reveal a considerable distorsion of octahedron, as was found for the complexes [Ru(azpy)$_2$Cl$_2$] (76.3(2)°), [Ru(azpy)$_2$(NO$_3$)$_2$] (76.5(1)°) (Hotze *et al*., 2000), and [Ru(Hsazpy)$_2$Cl$_2$] (77.2(3)°) (Hotz *et al*., 2004). As a consequence of the constraint of the bite angle, the ligands are bent back from the coordinated chlorides.

(c) X-ray structure of the *ccc*-[Ru(5mazpy)$_2$Cl$_2$] complex

The single crystals of the *ccc*-[Ru(5mazpy)$_2$Cl$_2$] complex were obatined by slow diffusion of hexane into chloroform solution of the complex. The molecular structure of *ccc*-[Ru(5mazpy)$_2$Cl$_2$] is shown in Figure 3.40. Tthe crystallographic data and selected bond lengths and bond angles for *ccc*-[Ru(5mazpy)$_2$Cl$_2$] are given in Table 3.16 and 3.17, respectively.

Table 3.16 Crystallographic data of the *ccc*-[Ru(5mazpy)$_2$Cl$_2$] complex

Empirical formula	$C_{24}H_{22}Cl_2N_6Ru$
Formula weight	566.49
Crystal system	monoclinic
Z	4
Space group	$P2_1/c$
a = 14.3480(6)Å	$\alpha = 90°$
b = 12.7046(5)Å	$\beta = 111.1790(10)°$
c = 13.9682(6)Å	$\gamma = 90°$
Temperature	293(2) K
Wavelength	0.71073Å
Volume	2374.22(17)Å^3
Density (calculated)	0.396 Mg/m^3
Crystal size	0.157 x 0.102 x 0.069 mm^3
Absorption coefficient	0.228 mm^{-1}
F(000)	286
Reflections collected	27888
Completeness to theta	28.04°
Refinement method	Full-matrix least-squares on F^2
Goodness-of-fit on F^2	0.91
R indices (all data)	*R1* = 0.0486, *wR2* = 0.1217

Table 3.16 (continued)

Measurement: Bruker SMART CCD diffractometer
Program system: SHELX-97
Structure determination: Direct methods (SHELXS-97)
Refinement: full-matrix least-squares (SHELXL-97)

Table 3.17 Selected bond lengths (Å) and bond angles (°) of the *ccc*-[Ru(5mazpy)$_2$Cl$_2$] complex

Ru(1)-N(1)	2.028(3)	Ru(1)-N(3)	2.009(3)
Ru(1)-N(4)	2.060(3)	Ru(1)-N(6)	1.982(3)
Ru(1)-Cl(1)	2.397(1)	Ru(1)-Cl(2)	2.397(1)
N(1)-C(1)	1.339(4)	N(1)-C(6)	1.355(5)
N(2)-N(3)	1.286(4)	N(2)-C(6)	1.387(4)
N(3)-C(7)	1.446(4)	N(4)-C(13)	1.347(4)
N(4)-C(18)	1.344(5)	N(5)-N(6)	1.288(5)
N(5)-C(18)	1.386(5)	N(6)-C(19)	1.433(4)
N(1)-Ru(1)-N(3)	76.8(1)	N(1)-Ru(1)-N(4)	96.6(1)
N(1)-Ru(1)-N(6)	89.5(1)	N(1)-Ru(1)-Cl(1)	88.59(9)
N(1)-Ru(1)-Cl(2)	177.58(8)	N(3)-Ru(1)-N(4)	171.9(1)
N(3)-Ru(1)-N(6)	98.6(1)	N(3)-Ru(1)-Cl(1)	90.98(9)
N(3)-Ru(1)-Cl(2)	100.83(8)	N(4)-Ru(1)-N(6)	76.6(1)
N(4)-Ru(1)-Cl(1)	93.46(9)	N(4)-Ru(1)-Cl(2)	85.79(8)
N(6)-Ru(1)-Cl(1)	169.59(9)	N(6)-Ru(1)-Cl(2)	90.65(9)
Cl(1)-Ru(1)-Cl(2)	91.65(4)		

The ruthenium(II) ion is six coordinated with four nitrogen atoms of bidentate ligand and two chloride atoms in a distorted octahedron geometry. The

atomic arrangement around the ruthenium center involved sequentially two *cis*-chlorides, *cis*-N(pyridine), and *cis*-N(azo). Therefore, the configuration of this complex is *cis*-*cis*-*cis* (*ccc*). The mononuclear complex is a neutral molecule due to the two coordinated chloride ions. The chelate angles extended by 5-methyl-2-(phenylazo)pyridine were 76.82(7)° and 76.4(7)° and deviate considerably from the ideal geometry (90°). As a consequence of the constraint of the bite angle, the ligands are bent back from the coordinated chlorides. The *cis*-chloro angle of 91.65(4)° is very nearly the ideal octahedral angle and is comparable to the reported values (Seal and Ray, 1984). The angles between the pyridine ring and phenyl ring of complex are 39.146° and 44.545°. In the complex *ccc*-[$Ru(5mazpy)_2Cl_2$], the phenyl rings are inclined at angles of 40.591° and 44.625° relative to the chelated azo pyridine plane. The N-N distances of azo function are 1.286(4) and 1.288(5)Å. The Ru-N(azo) distances (1.982(3), 2.009(3)Å) are shorter than those of Ru-N(pyridine) (2.028(3), 2.060(3) Å). The shortening may be due to greater π-backbonding, $d\pi(Ru) \rightarrow \pi^*$(azo), offer by the azo group. The average N-N distance is 1.287 Å which is longer than some reported values of free azo ligands (N-N ~ 1.248 Å) (Panneerselvam *et al*., 2000). The coordination can lead to decrease in the N-N bond order due to both σ-donor and π-accepter characters of the ligand. Thus, the elongation of the N-N distance and shortening of Ru-N(azo) bond length are an indication of the existance of considerable Ru-5mazpy π-bonding with major involvement of the azo group. The Ru-Cl distance in this complex (2.397(1)Å, 2.397(1)Å) is comparable with the reported values in *ccc*-[$Ru(azpy)_2Cl_2$] (2.401(4)Å, 2.410(3)Å) (Seal and Ray, 1987) and *ccc*-[$Ru(papm)_2Cl_2$] (2.394(1)Å, 2.401(1)Å) (Santra *et al*., 1999).

(d) X-ray structure of the *tcc*-[Ru(5mazpy)$_2$Cl$_2$] complex

The single crystals of the *tcc*-[Ru(5mazpy)$_2$Cl$_2$] complex were grown by slow diffusion of acetonitrile into chloroform solution of the complex. The molecular structure of *tcc*-[Ru(5mazpy)$_2$Cl$_2$] is shown in Figure 3.41. The crystallographic data of *tcc*-[Ru(5mazpy)$_2$Cl$_2$] are listed in Table 3.18 and the relevant bond distances and angles are given in Table 3.19.

Table 3.18 Crystallographic data of the *tcc*-[Ru(5mazpy)$_2$Cl$_2$] complex

Empirical formula	$C_{28}H_{28}Cl_2N_8Ru$
Formula weight	648.55
Crystal system	Monoclinic
Z	4
Space group	*C*2/*c*
a = 14.8241(16) Å	$\alpha = 90^o$
b = 13.8388(15) Å	$\beta = 117.020(2)^o$
c = 15.2462(16) Å	$\gamma = 90^o$
Temperature	293(2) K
Wavelength	0.71073 Å
Volume	2786.3(5) Å^3
Density (calculated)	1.546 Mg/m^3
Absorption coefficient	0.788 mm^{-1}
F(000)	1320
Goodness-of-fit on F^2	1.138
Crystal size	0.134 x 0.105 x 0.06 mm^3
Completeness to theta	26.37^o
Reflections collected	10996
Refinement method	Full-matrix least-squares on F^2
R indices (all data)	*R1* = 0.0800, *wR2* = 0.1905

Table 3.18 (continued)

Measurement: Bruker SMART CCD diffractometer
Program system: SHELX-97
Structure determination: Direct methods (SHELXS-97)
Refinement: full-matrix least-squares (SHELXL-97)

Table 3.19 Selected bond lengths (Å) and bond angles (°) of the *tcc*-[Ru(5mazpy)$_2$ Cl$_2$] complex

Ru(1)-N(3)	1.990(5)	Ru(1)-N(3)#1	1.990(5)
Ru(1)-N(1)	2.102(5)	Ru(1)-N(1)#1	2.102(5)
Ru(1)-Cl(1)#1	2.377(2)	Ru(1)-Cl(1)	2.377(2)
N(1)-C(6)	1.342(7)	N(1)-C(1)	1.344(8)
N(2)-N(3)	1.286(7)	N(2)-C(6)	1.390(8)
N(3)-C(7)	1.448(8)	N(4)-C(14)	0.784(19)
N(3)-Ru(1)-N(3)#1	105.2(3)	N(3)-Ru(1)-N(1)	75.5(2)
N(3)#1-Ru(1)-N(1)	179.31(19)	N(3)-Ru(1)-N(1)#1	179.31(19)
N(3)#1-Ru(1)-N(1)#1	75.5(2)	N(1)-Ru(1)-N(1)#1	103.9(3)
N(3)-Ru(1)-Cl(1)#1	95.26(15)	N(3)#1-Ru(1)-Cl(1)#1	88.40(14)
N(1)-Ru(1)-Cl(1)#1	91.33(14)	N(1)#1-Ru(1)-Cl(1)#1	84.94(14)
N(3)-Ru(1)-Cl(1)	88.40(14)	N(3)#1-Ru(1)-Cl(1)	95.27(15)
N(1)-Ru(1)-Cl(1)	84.94(14)	N(1)#1-Ru(1)-Cl(1)	91.33(14)
Cl(1)#1-Ru(1)-Cl(1)	173.97(9)		

The crystal structure of the *tcc*-[Ru(5mazpy)$_2$Cl$_2$] complex consists of a *tcc*-[Ru(5mazpy)$_2$Cl$_2$] and a lattice CH_3CN molecule. The central ruthenium(II) ion is six-coordinated by four nitrogen donors of two 5mazpy molecules and two chloride anions. The atomic arrangement in *tcc*-[Ru(5mazpy)$_2$Cl$_2$] involves sequentially *trans*-

chlorides, *cis*-N(pyridine), and *cis*-N(azo) and corresponds to a *tans-cis-cis* (*tcc*) configuration. The ruthenium ion forms two five membered chelated rings with two 5mazpy ligands. The bite angles N3-Ru1-N1 and N3A-Ru1-N1A (75.52(2)°) reveal a considerable distortion in octhahedral around ruthenium and are similar ones found for *tcc*-[$Ru(azpy)_2Cl_2$]. The trans chloride angle is 173.97(9)° and is corroborates with a distorted octhahedral structure. The Ru-N(azo) bond (1.990(5)Å) is shorter than the Ru-N(pyridine) (2.102(5)Å). The shortening may be due to greater π-back-bonding, dπ(Ru)→π*(azo) (Bag *et al.*, 1992). In the *tcc*-[$Ru(azpy)_2Cl_2$] complex, the N-N distance is 1.286(7)Å which longer than that the free 5mazpy ligand (1.228(2)Å). This suggests that the coordination can lead to a decrease in the N-N bond order due to both σ-donor and π-acceptor character of the ligands. The Ru-Cl distance is comparable with the reported values (Bag *et al.*, 1992).

3.3 Syntheses of the $[Ru(5mazpy)_2L](PF_6)_2$, $[Ru(5mazpy)_2L']$ $(PF_6)_2$ and $[Ru(L')_2 5mazpy](PF_6)_2$ complexes (L = azpy, 5mazpy; L′= bpy, phen)

The series of the $[Ru(5mazpy)_2L](PF_6)_2$ and $[Ru(5mazpy)_2L'](PF_6)_2$ complexes were prepared from the reaction of the *ctc*-$[Ru(5mazpy)_2Cl_2]$ complex with L ligands (L = 2-(phenylazo)pyridne (azpy), 5-methly-2-(phenylazo)pyridne (5mazpy); L′ = 2,2′-bipyridine (bpy), and 1,10-phenanthroline (phen)) in refluxing methanol in the presence of $AgNO_3$ to afford $[Ru(5mazpy)_2L]^{2+}$ and $[Ru(5mazpy)_2L']^{2+}$, respectively. These complexes were isolated as the PF_6^- salts, $[Ru(5mazpy)_2L](PF_6)_2$, and $[Ru(5mazpy)_2L'](PF_6)_2$. The synthetic reaction is shown in equation (5).

$$\textit{ctc}\text{-}[Ru(5mazpy)_2Cl_2] \xrightarrow[\text{MeOH, L or L'}]{AgNO_3,\ NH_4PF_6} [Ru(5mazpy)_2L](PF_6)_2,\ [Ru(5mazpy)_2L'](PF_6)_2 \qquad (5)$$

For the series of the $[Ru(L')_2 5mazpy](PF_6)_2$ complexes (L′= bpy, phen), the *cis*-$[Ru(bpy)_2Cl_2]$ and *cis*-$[Ru(phen)_2Cl_2]$ complexes were used as precursor for synthesis of the $[Ru(bpy)_2 5mazpy](PF_6)_2$ and $[Ru(phen)_2 5mazpy](PF_6)_2$ complexes, respectively. The reactions of the *cis*-$[Ru(bpy)_2Cl_2]$ or *cis*-$[Ru(phen)_2Cl_2]$ complexes with 5mazpy ligand in methanol in the presence of NH_4PF_6 generated the $[Ru(bpy)_2 5mazpy](PF_6)_2$ and $[Ru(phen)_2 5mazpy](PF_6)_2$ complexes, respectively. The synthetic detail is shown in equation (6).

$$\textit{cis}\text{-}[Ru(L')_2Cl_2] \xrightarrow[\text{MeOH, 5mazpy}]{AgNO_3,\ NH_4PF_6} [Ru(L')_2 5mazpy](PF_6)_2 \qquad (6)$$

The structures of the ligands, 2-(phenylazo)pyridine (azpy), 5-methly-2-(phenylazo)pyridne (5mazpy), 2,2′-bipyridine (bpy), 1,10-phenanthroline (phen), in this work are illustrated in Figure 3.42. The physical properties of the complexes of

$[Ru(5mazpy)_2L](PF_6)_2$, $[Ru(5mazpy)_2L']](PF_6)_2$ and $[Ru(L')_25mazpy](PF_6)_2$ are summarized in Table 3.20.

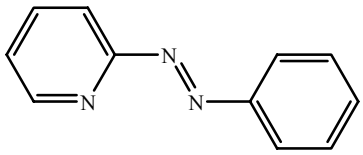

2-(phenylazo)pyridine (azpy)

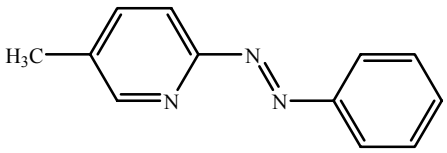

5-methyl-2-(phenylazo)pyridine (5mazpy)

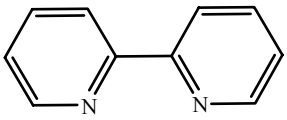

2,2′-bipyridine (bpy)

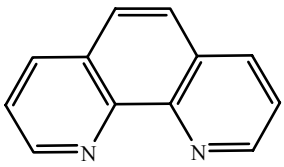

1,10-phenanthroline (phen)

Figure 3.42 The structure of the 2-(phenylazo)pyridine (azpy), 5-methyl-2-(phenylazo)pyridine (5mazpy), 2,2′-bipyridine (bpy), and 1,10-phenanthroline (phen) ligands

Table 3.20 The physical properties of the $[Ru(5mazpy)_2L](PF_6)_2$, $[Ru(5mazpy)_2L']](PF_6)_2$ and $[Ru(L')_25mazpy](PF_6)_2$ complexes

Complexes	Physical properties		
	Appearance	Color	Melting point (°C)
$[Ru(5mazpy)_3](PF_6)_2$	Solid	Red-brown	293-296
$[Ru(5mazpy)_2azpy](PF_6)_2$	Solid	Red-brown	288-290
$[Ru(5mazpy)_2bpy](PF_6)_2$	Solid	Dark-Red	298-300
$[Ru(5mazpy)_2phen](PF_6)_2$	Solid	Dark-Red	331-333
$[Ru(bpy)_25mazpy](PF_6)_2$	Solid	Red-brown	325-328

Table 3.20 (continued)

Complexes	Physical properties		
	Appearance	Color	Melting point (°C)
$[Ru(phen)_2 5mazpy](PF_6)_2$	Solid	Red-brown	330-333

3.4 Characterization of the $[Ru(5mazpy)_2L](PF_6)_2$, $[Ru(5mazpy)_2L']](PF_6)_2$ and $[Ru(L')_2 5mazpy](PF_6)_2$ complexes (L = azpy, 5mazpy; L′= bpy, phen)

The chemistry of the $[Ru(5mazpy)_2L](PF_6)_2$, $[Ru(5mazpy)_2L']](PF_6)_2$ and $[Ru(L')_2 5mazpy](PF_6)_2$ complexes (L = azpy, 5mazpy, bpy; L′= bpy, phen) was studied by following techniques.

3.4.1 Elemental analysis
3.4.2 ESI mass spectrometry
3.4.3 Infrared spectroscopy
3.4.4 UV-visible absorption spectroscopy
3.4.5 1D and 2D Nuclear Magnetic Resonance spectroscopy
3.4.6 Cyclic voltammetry
3.4.7 X-ray Crystallography

3.4.1 Elemental analysis

Elemental analysis data are consistent with the general formula of the complexes, $[Ru(5mazpy)_3](PF_6)_2$, $[Ru(5mazpy)_2azpy](PF_6)_2$, $[Ru(5mazpy)_2bpy](PF_6)_2$, $[Ru(5mazpy)_2phen](PF_6)_2$, $[Ru(bpy)_2 5mazpy](PF_6)_2$, and $[Ru(phen)_2 5mazpy](PF_6)_2$. Results from elemantal analysis are listed in Table 3.21.

Table 3.21 Elemental analysis data of the $[Ru(5mazpy)_2L](PF_6)_2$, $[Ru(5mazpy)_2L']$$(PF_6)_2$ and $[Ru(L')_2 5mazpy](PF_6)_2$ complexes

Complexes	%C		%N		%H	
	Calc.	Found	Calc.	Found	Calc.	Found
$[Ru(5mazpy)_3](PF_6)_2$	43.99	43.81	12.83	13.05	3.36	3.25
$[Ru(5mazpy)_2azpy](PF_6)$	43.39	43.38	13.02	13.15	3.20	3.04
$[Ru(5mazpy)_2bpy](PF_6)_2$	43.35	43.76	11.90	12.10	3.19	3.15
$[Ru(5mazpy)_2phen](PF_6)_2$	44.76	44.93	11.60	11.62	3.11	3.20
$[Ru(phen)_2 5mazpy](PF_6)_2$	45.57	44.62	10.34	10.53	2.85	2.49
$[Ru(bpy)_2 5mazpy](PF_6)_2$	42.64	43.66	10.89	10.40	3.02	3.17

3.4.2 Electro Spray Ionization (ESI) mass spectrometry

The results from ESI mass spectrometry supported the molecular weight of complexes. The ESI mass spectrometric data are summarized in Table 3.22 and ESI mass spectra are illustrated in Figure 3.43, 3.44, 3.45, and 3.46.

Table 3.22 ESI mass spectrometric data of the $[Ru(5mazpy)_2L](PF_6)_2$ and $[Ru(5mazpy)_2L']$$(PF_6)_2$ complexes

m/z	Stoichiometry	Equivalent species	Rel. Abun. (%)
$[Ru(5mazpy)_3](PF_6)_2$			
838	$[Ru(5mazpy)_3](PF_6)]^+$	$[M\text{-}PF_6^-]^+$	10
346	$[Ru(5mazpy)_3]^{2+}$	$[M\text{-}2PF_6^-]^{2+}$	100

Table 3.22 (continued)

m/z	Stoichiometry	Equivalent species	Rel. Abun. (%)
$[Ru(5mazpy)_2azpy](PF_6)_2$			
824	$[Ru(5mazpy)_2azpy](PF_6)]^+$	$[M\text{-}PF_6^-]^+$	11.4
339	$[Ru(5mazpy)_2azpy]^{2+}$	$[M\text{-}2PF_6^-]^{2+}$	100
$[Ru(5mazpy)_2bpy](PF_6)_2$			
797	$[Ru(5mazpy)_2bpy](PF_6)]^+ + H^+]$	$[M\text{-}PF_6^- + H^+]^+$	23.1
326	$[Ru(5mazpy)_2bpy]^{2+}$	$[M\text{-}2PF_6^-]^{2+}$	100
$[Ru(5mazpy)_2phen](PF_6)_2$			
821	$[Ru(5mazpy)_2phen](PF_6)]^+$	$[M\text{-}PF_6^- + H^+]^+$	100
338	$[Ru(5mazpy)_2bpy]^{2+}$	$[M\text{-}2PF_6^-]^{2+}$	78.6

M = Molecular weight (MW) of each complex

MW of $[Ru(5mazpy)_3](PF_6)_2$ (M) = 982.07 g/mol

MW of $[Ru(5mazpy)_2azpy](PF_6)_2$ (M) = 968.07 g/mol

MW of $[Ru(5mazpy)_2bpy](PF_6)_2$ (M) = 941.07 g/mol

MW of $[Ru(5mazpy)_2phen](PF_6)_2$ (M) = 965.07 g/mol

The maximum molecular peak of the $[Ru(5mazpy)_3](PF_6)_2$ complex is observed at m/z 346 (100 %), which corresponds to the molecular ion, $[Ru(5mazpy)_3]^{2+}$. In addition, this complex exhibits peak at m/z 838 (10 %) which is assigned to the $[Ru(5mazpy)_3](PF_6)]^+$ ion. In the ESI mass spectrum of the $[Ru(5mazpy)_2azpy](PF_6)_2$ complex shows the base peak at m/z 339 due to the complex cation, $[Ru(5mazpy)_2azpy]^{2+}$. This complex also shows a peak at m/z 824 (11.4 %) which corresponds to the $[Ru(5mazpy)_2azpy](PF_6)]^+$ ion pair. For the $[Ru(5mazpy)_2bpy](PF_6)_2$ complex, its spectrum exhibits two major peaks at m/z 797 and 326 of which the response at 797 is assigned to $[M\text{-}PF_6^- + H^+]$ (23.1 %) while, that

at 326 is due to the $[M\text{-}2PF_6^-]^{2+}$ (100%). Similar to $[Ru(5mazpy)_2bpy](PF_6)_2$, the mass spectrum of $[Ru(5mazpy)_2phen](PF_6)_2$ also shows two major ions, the most intense peak at m/z 821 is due to the $[M\text{-}PF_6^-+H^+]$ (100%), the second intense peak at m/z 338 is assigned to the $[M\text{-}2PF_6^-]^{2+}$ with 78.6 % relative abundance.

3.4.3 Infrared Spectroscopy

The important functional groups in the complexes, $[Ru(5mazpy)_2L](PF_6)_2$, $[Ru(5mazpy)_2L']$ $(PF_6)_2$ and $[Ru(L')_2 5mazpy](PF_6)_2$ (L = azpy, 5mazpy; L′ = bpy, phen), are N=N, C=N, C=C, and PF_6^-. The characteristic group frequencies are collected in Table 3.23.

Table 3.23 Infrared spectroscopic data of the $[Ru(5mazpy)_2L](PF_6)_2$, $[Ru(5mazpy)_2L'](PF_6)_2$ and $[Ru(L')_2 5mazpy](PF_6)_2$ complexes

Vibration modes	Wave number (cm^{-1})					
	$[Ru(5mazpy)_2L](PF_6)_2$		$[Ru(5mazpy)_2L'](PF_6)_2$		$[Ru(L')_2 5mazpy](PF_6)_2$	
	5mazpy	azpy	bpy	phen	bpy	phen
C=C, C=N stretching	1600 (m), 1572 (m), 1474 (m), 1456 (m)	1601 (m), 1572 (m), 1456 (s)	1585 (m), 1608 (s) , 1571(s), 1471(s), 1447(s)	1602 (m), 1572 (m), 1429 (m), 1474 (m)	1603(m) 1585(m) 1517(m) 1430(s)	1606(m) 1570(m) 1468(s) 1448(s)
N=N stretching	1365 (s)	1363 (s)	1337 (s)	1349 (s)	1338(s)	1332(s)
C-H bending In mono substituted benzene	558 (s) 691 (s) 767 (s)	557 (s), 691 (s), 779 (s)	557 (s), 696 (s), 763 (s)	557 (s), 694 (s), 765 (s)	557 (s), 695 (s), 769 (s)	557 (s) 694(s) 761(s)
PF_6^-	835	840	834	836	840	834

s = strong, m = medium

For IR spectrum of all complexes shows medium peak at 1601-1429 cm^{-1}, corresponding to C=C and C=N stretching frequencies. The N=N stretching frequencies of free ligand, 5mazpy, occur at 1389 cm^{-1} which appear at a lower frequencies than that in azpy (Changsaluk, U., 2002). This stretching mode is used to be consider the π-acid property in azo complexes. The N=N stretching frequencies of the azpy, 5mazpy ligands, the *ctc*-$[Ru(5mazpy)_2Cl_2]$, $[Ru(5mazpy)_2L](PF_6)_2$, $[Ru(5mazpy)_2L']$ $(PF_6)_2$ and $[Ru(L')_2\ 5mazpy](PF_6)_2$ complexes are listed in Table 3.24.

Table 3.24 The N=N stretching frequency in the azpy, 5mazpy ligands, the *ctc*-$[Ru(5mazpy)_2Cl_2]$, $[Ru(5mazpy)_2L](PF_6)_2$, $[Ru(5mazpy)_2L'](PF_6)_2$ and $[Ru(L')_2 5mazpy](PF_6)_2$ complexes

Compounds	$\upsilon_{(N=N)}$ (cm^{-1})
5mazpy	1389
azpy	1421
ctc-$[Ru(5mazpy)_2Cl_2$	1334
$[Ru(5mazpy)_3](PF_6)_2$	1365
$[Ru(5mazpy)_2azpy](PF_6)_2$	1363
$[Ru(5mazpy)_2bpy](PF_6)_2$	1337
$[Ru(5mazpy)_2phen](PF_6)_2$	1349
$[Ru(bpy)_2 5azpy](PF_6)_2$	1338
$[Ru(phen)_2 5azpy](PF_6)_2$	1332

The azoimine orbitals in these compounds are strongly involved in π-interactions. Thus the $\upsilon_{(N=N)}$ stretching frequencies in the complexes of 5mazpy are appreciably lower as compare to that for the free 5mazpy. In the precursor complex, *ctc*-$[Ru(5mazpy)_2Cl_2]$, the N=N stretching frequencies appear at 1334 cm^{-1} which

lower energy than of mixed ligand complexes, $[Ru(5mazpy)_2L](PF_6)_2$. In addition, the N=N stretching mode in the $[Ru(5mazpy)_3](PF_6)_2$ and $[Ru(5mazpy)_2azpy](PF_6)_2$ complexes occurs at the higher frequencies than those of the $[Ru(5mazpy)_2bpy](PF_6)_2$ and $[Ru(5mazpy)_2phen](PF_6)_2$ complexes. These may be due to better π-acceptor properties of 5mazpy, azpy, bpy, and phen. It results in less π back donation to the azo function.

As the employed coligand becomes a better π-acceptor, there is competition for the ruthenium t_{2g} electrons and less π back donation to the azo ligand raising the azo bond order. Thus, with a very strong π-acid coligand, the azo mode could approach the free ligand value, while with a low π-acid coligand a single bond order might be approached for the azo linkage. In comparison of $[Ru(5mazpy)_2L](PF_6)_2$, $[Ru(5mazpy)_2L']](PF_6)_2$ and $[Ru(L')_25mazpy](PF_6)_2$, the υ(N=N) in $[Ru(L')_25mazpy]$ $(PF_6)_2$ (L′ = bpy, phen) appears at the lower frequencies than that the $[Ru(5mazpy)_2L](PF_6)_2$ (L′= bpy and phen) because the $[Ru(L')_25mazpy]$ $(PF_6)_2$ complexes contain one azo ligand. The infrared spectra of the $[Ru(5mazpy)_2$ $L](PF_6)_2$, $[Ru(5mazpy)_2L']](PF_6)_2$ and $[Ru(L')_25mazpy](PF_6)_2$ complexes are shown in Figure 3.47 to 3.52.

3.4.4 UV-Visible absorption spectroscopy

The complexes of $[Ru(5mazpy)_2L](PF_6)_2$, $[Ru(5mazpy)_2L']$ $(PF_6)_2$ and $[Ru(L')_2 5mazpy](PF_6)_2$ (L = azpy, 5mazpy; L′ = bpy, phen), appear to be typical charge-transfer (CT) spectra with molar extinction coefficients of the lowest energy band near 10^4 $M^{-1}cm^{-1}$. Absorption spectroscopic data of solutions of the complexes in MeOH, EtOH, CH_3CN, DMSO, and CH_2Cl_2 are reported in Table 3.25.

Table 3.25 UV-Visible absorption spectroscopic data of the $[Ru(5mazpy)_2L](PF_6)_2$, $[Ru(5mazpy)_2L'](PF_6)_2$ and $[Ru(L')_2 5mazpy](PF_6)_2$ complexes in CH_3CN

Complexes	λ_{max} nm, ($\varepsilon^a \times 10^{-4}$ $M^{-1}cm^{-1}$)				
	CH_3OH	CH_3CN	DMSO	CH_2Cl_2	C_2H_5OH
$[Ru(5mazpy)_3](PF_6)_2$	284 (3.6) 322 (4.3) 374 (6.2)	282(2.2) 320 (2.6) 372(3.8) 496(1.4)	374(3.6) 322(2.8) 498(1.3)	282(1.6) 326(1.9) 380(3.1) 496(1.4)	282(1.9) 322(2.2) 376(3.2) 496(1.1)
$[Ru(5mazpy)_2azpy](PF_6)_2$	280(2.2) 320(2.4) 374(3.9)	282(2.0) 322(2.2) 372(3.2) 496(1.3)	282(2.4) 322(2.7) 374(4.0) 498(1.5)	282(2.1) 324(2.2) 380(3.8) 496(1.3)	280(2.2) 322(2.4) 376(3.7) 496(1.4)
$[Ru(5mazpy)_2bpy](PF_6)_2$	286(3.9) 372(3.4) 512(1.5)	286(0.7) 372(2.6) 514(1.1)	374(4.5) 520(2.1)	286(2.7) 378(2.4) 516(1.0)	286(2.6) 374(2.2) 514(1.0)
$[Ru(5mazpy)_2phen](PF_6)_2$	274(2.9) 362(2.2) 506(1.2)	274(5.5) 362(4.0) 506(2.1)	360(3.6) 512(2.0) 452(1.2)	270(4.2) 370(3.3) 510(1.7)	274(3.9) 366(2.8) 508(1.5)

Table 3.25 (continued)

Complexes	λ_{max} nm, ($\varepsilon^a \times 10^{-4}$ $M^{-1}cm^{-1}$)				
	CH_3OH	CH_3CN	DMSO	CH_2Cl_2	C_2H_5OH
$[Ru(bpy)_2 5mazpy](PF_6)_2$	207(9.6) 263(5.5) 357(1.5) 494(0.9)	224(7.8) 262(8.6) 355(2.1) 494(1.2)	358(1.6) 500(0.9)	262(9.2) 631(2.8)	205(7.8) 264(6.4) 356(1.7) 496(0.9)
$[Ru(phen)_2 5mazpy](PF_6)_2$	206(4.6) 279(4.2) 498(0.9)	243(5.5) 280(10) 362(2.8) 495(2.0)	282(4.7) 500(1.1)	280(3.6) 368(1.4) 500(0.9)	205(4.2) 280(3.8) 363(1.3) 495(0.8)

[a] Molar Extinction coefficient

The electronic spectra of the complexes were recorded in the range 200-800 nm reveal that the absorptions <400 nm are due to n→π* and π→π* transitions. The visible region of the spectrum shows one high intense absorptions near 500 nm. The transitions are of typical metal-to-ligand charge transfer type (MLCT) with high molar extinction coefficients (ε ~ 10^4 $M^{-1}cm^{-1}$). The absorption spectra of $[Ru(5mazpy)_3](PF_6)_2$, $[Ru(5mazpy)_2azpy](PF_6)_2$, $[Ru(5mazpy)_2bpy](PF_6)_2$, and $[Ru(5mazpy)_2phen](PF_6)_2$ in CH_3CN displays intense bands at λ_{max} 496, 496, 514, and 506 nm, respectively. The MLCT band for the $[Ru(5mazpy)_3](PF_6)_2$ and $[Ru(5mazpy)_2azpy](PF_6)_2$ complexes occurs at the higher energies than that the $[Ru(5mazpy)_2bpy](PF_6)_2$, and $[Ru(5mazpy)_2phen](PF_6)_2$ complexes. Owing to the azoimine ligands (5mazpy and azpy) are good π-acceptor ligand, and back bonding from Ru(II) to 5mazpy or azpy results in stabilization of the dπ levels relative to π*(bpy and phen) and an increase in the MLCT band energy. The π* orbital of azoimine ligand is lower than in imine ligand (Krause and Krause, 1980). Then, the lowest energy of each complexes is attributable to the MLCT transition

d(Ru)→π*(azomine ligand). The lowest energy of MLCT absorptions bands of complexes in acetonitrile is listed in Table 3.26.

Table 3.26 The lowest energy of MLCT absorption bands of the $[Ru(5mazpy)_2L](PF_6)_2$, $[Ru(5mazpy)_2L']$ $(PF_6)_2$ and $[Ru(L')_2 5mazpy](PF_6)_2$ complexes in CH_3CN

Complexes	λ_{max} nm, ($\varepsilon^a \times 10^{-4}$ $M^{-1}cm^{-1}$)
$[Ru(5mazpy)_3](PF_6)_2$	496
$[Ru(5mazpy)_2azpy](PF_6)_2$	496
$[Ru(5mazpy)_2bpy](PF_6)_2$	514
$[Ru(5mazpy)_2phen](PF_6)_2$	506
$[Ru(bpy)_2 5mazpy](PF_6)_2$	494
$[Ru(bpy)_3](PF_6)_2$ [b]	450
$[Ru(phen)_2 5mazpy](PF_6)_2$	495
$[Ru(phen)_3](PF_6)_2$ [c]	446

[a] Molar Extinction coefficient

[b] (Tempiam, S., 2002); [c] (Rattanawit, N., 2002)

According to MLCT bands in visible region of the $[Ru(bpy)_2 5mazpy](PF_6)_2$ complex only one intense band is observed in the visible region. In comparison of the MLCT band in this complex with $[Ru(bpy)_3](PF_6)_2$ (450 nm), the $[Ru(bpy)_2 5mazpy](PF_6)_2$ (494 nm) complex displays at the lower energy than $[Ru(bpy)_3](PF_6)_2$ (Tempiam, S., 2002). Besides, the MLCT band in $[Ru(phen)_2 5mazpy](PF_6)_2$ was compared with $[Ru(phen)_3](PF_6)_2$. The complex of $[Ru(phen)_2 5mazpy](PF_6)_2$ (495 nm) has MLCT band at the lower energy than that $[Ru(phen)_3](PF_6)_2$ (446 nm) (Rattanawit, N., 2002). For the $[Ru(bpy)_2 5mazpy](PF_6)_2$ and [Ru

$(phen)_2$5mazpy]$(PF_6)_2$ complexes, they are expected that the π^* levels of 5mazpy are lower than that bpy and phen. Therefore, the energy of the d(Ru)$\rightarrow\pi^*$(azomine ligand) transition shifts to the red when compares with [Ru$(bpy)_3$]$(PF_6)_2$, and [Ru$(phen)_3$]$(PF_6)_2$, respectively. The absorption spectra of [Ru$(5mazpy)_2$L]$(PF_6)_2$, [Ru$(5mazpy)_2$L′]$(PF_6)_2$ and [Ru$(L')_2$5mazpy]$(PF_6)_2$ complexes are shown in Figure 3.53 to 3.58.

3.4.5 1D and 2D Nuclear Magnetic Resonance spectroscopy

The ^{1}H, ^{13}C, DEPT 135, ^{1}H-^{1}H COSY, and ^{1}H-^{13}C HMQC NMR spectrum of the complexes, $[Ru(5mazpy)_2L](PF_6)_2$, $[Ru(5mazpy)_2L']$ $(PF_6)_2$ and $[Ru(L')_2 5mazpy](PF_6)_2$ (L = azpy, 5mazpy; L′ = bpy phen), were carried out in acetone-d_6 (500 MHz) and tetramethylsilane ($Si(CH_3)_4$) was used as internal reference. The 1D and 2D NMR studies of the $[Ru(5mazpy)_2L](PF_6)_2$, $[Ru(5mazpy)_2L'](PF_6)_2$ and $[Ru(L')_2 5mazpy](PF_6)_2$ complexes were described as below.

(a) Nuclear Magnetic Resonance spectroscopy of the $[Ru(5mazpy)_3](PF_6)_2$ complex

The ^{1}H and ^{13}C NMR spectroscopic data are listed in Table 3.27.

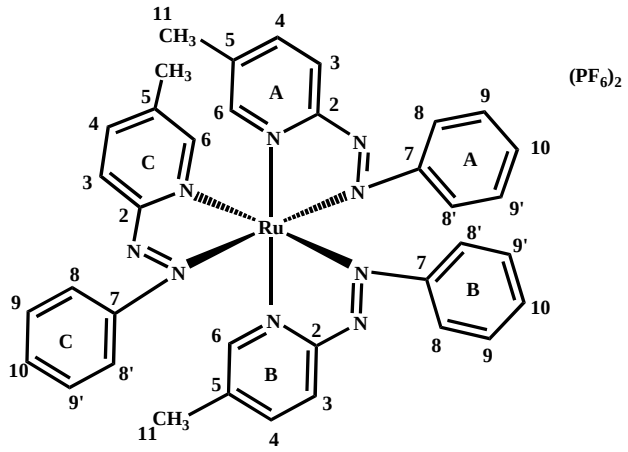

Table 3.27 ^{1}H and ^{13}C NMR of the $[Ru(5mazpy)_3](PF_6)_2$ complex

H-C Position	^{1}H NMR			^{13}C NMR
	δ (ppm)	J (Hz)	Number of H	δ (ppm)
3C	9.14 (*d*)	8.5	1	132.05
6C	8.67 (*s*)	8.0	1	153.59
3A	8.60 (*d*)	8.0	1	131.28

Table 3.27 (continued)

H-C Position	^{1}H NMR			^{13}C NMR δ (ppm)
	δ (ppm)	J (Hz)	Number of H	
3B	8.59 (*d*)	8.0	1	131.23
4C	8.50 (*d*)	8.0	1	143.14
6A	8.42 (*s*)	-	1	151.65
4B	8.34 (*d*)	8.0	1	143.31
4A	8.26 (*d*)	8.0	1	143.27
6B	8.21 (*s*)	-	1	152.39
10A	7.63 (*t*)	8.0, 8.0	1	134.15
10C	7.61 (*t*)	8.0, 8.0	1	134.09
9,9′A, 10B	7.51 (*m*)	-	3	130.86, 134.09
9,9′C, 8,8′A	7.44 (*m*)	-	4	130.80, 123.64
8,8′C	7.37 (*dd*)	8.5, 1.0	2	123.55
9,9′B	7.32 (*dd*)	8.0, 8.5	2	130.96
8,8′B	7.04 (*dd*)	9.0, 1.0	2	123.39
11C	2.52 (*s*)	-	3	18.56
11	2.48 (*s*)	-	3	18.44
11	2.47 (*s*)	-	3	18.40
Quaternary Carbons				163.42, 163.13, 162.45, 156.60, 153.52, 152.94, 144.86, 144.71, 144.34

d = doublet, *dd = doublet of doublet*, *m = multiplet*, *s = singlet*, and *t = triplet*

The ^{1}H NMR spectrum of $[Ru(5mazpy)_3](PF_6)_2$ is shown in Figure 3.59. As the complex of $[Ru(5mazpy)_3](PF_6)_2$ has C_1 symmetry, all the three 5mazpy

ligands are inequivalent, resulting in eighteen resonances in aromatic region, which have been fully assigned using ^{1}H-^{1}H COSY NMR spectroscopy (Figure 3.60). From ^{1}H-^{1}H COSY NMR, the three sets of 5mazpy pyridine signals and three sets of 5mazpy phenyl signals have been distinguished. The protons on pyridine ring (H3, H4, and H5) appear at lower field than phenyl ring (H8, H9, and H10) due to the electron withdrawing, N atom on pyridine. Since two of the three 5mazpy pyridine ring (A, B) are trans to each other, the positions of protons are slightly different similar to the situation of the $[Ru(azpy)_3](PF_6)_2$ complex (Hotze *et al*., 2005). While, the chemical shifts of the protons of 5mazpy pyridine ring C appear at the lowest field, because this pyridine ring trans to N=N azo function. The complex of $[Ru(5mazpy)_3](PF_6)_2$ contains three 5mazpy ligands in molecule. Thus, this complex is expected to exhibit three methyl signals of equal intensities at 2.52, 2.48, and 2.47 ppm. In addition, the methyl signal at 2.52 ppm is due to the methyl on the pyridine ring C because trans to N=N azo group.

The ^{13}C NMR spectrum (Figure 3.61) provides direct information about the carbon skeleton of the molecule. The ^{13}C NMR signals have been fully assigned using ^{1}H-^{13}C HMQC NMR spectroscopy (Figure 3.63) which is generally used for studing large and complicated molecules. The ^{13}C NMR spectrum shows eighteen signals from twenty-four methine carbons, three signals from three methyl carbons, and nine signals from nine quaternary carbons which support by the results from DEPT 135 NMR spectrum (Figure 3.62). The carbon atoms neighbouring the nitrogen atom shift to downfield due to a decrease electron density resulting from the presence of electronegative nitrogen atom. The quaternary carbons are found at 163.42, 163.13, 162.45, 156.60, 153.52, 152.94, 144.86, 144.71, and 144.34 ppm which refer to the C2, C7, and C5, respectively. These results correlate with ^{1}H-^{13}C HMQC NMR spectrum which it absence of any contours at these positions. The carbons signals at 18.56, 18.44, and 18.40 ppm refer to methyl carbons from three 5mazpy ligands. These signals are due to their interaction with proton resonances at 2.52, 2.48, and 2.47 ppm. It is noted that chemicals shifts of the complex move to downfield compared to those of the free ligand.

(b) Nuclear Magnetic Resonance spectroscopy of the $[Ru(5mazpy)_2azpy](PF_6)_2$ complex

The ^1H and ^{13}C NMR spectroscopic data are listed in Table 3.28.

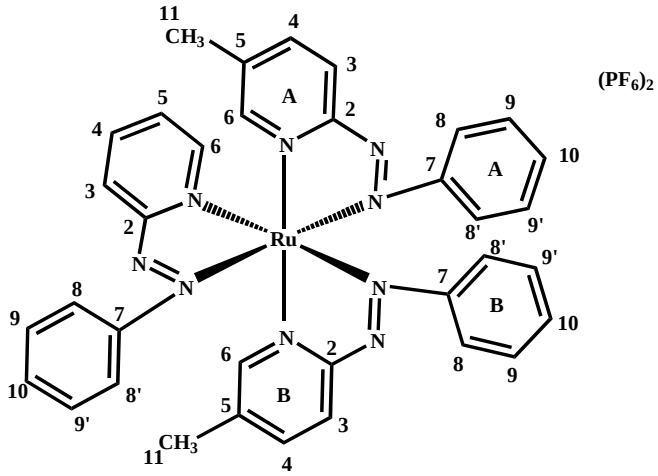

Table 3.28 ^1H and ^{13}C NMR of the $[Ru(5mazpy)_2azpy](PF_6)_2$ complex

H-C Position	^1H NMR			^{13}C NMR
	δ (ppm)	J (Hz)	Number of H	δ (ppm)
3(azpy)	9.26 (*d*)	8	1	130.97
6(azpy)	8.77 (*d*)	5.5	1	153.63
4(azpy)	8.69 (*ddd*)	8, 8, 1.5	1	143.12
3(5mazpy)	8.62 (*d*)	8	1	131.63
3(5mazpy)	8.61 (*d*)	8	1	131.44
6(5mazpy)	8.43 (*d*)	2	1	151.81
4(5mazpy)	8.35 (*dd*)	8, 1.5	1	143.39
4(5mazpy)	8.27 (*dd*)	8, 1.5	1	143.21
6(5mazpy)	8.22 (*d*)	2	1	152.49
5(azpy)	7.99 (*ddd*)	8, 8, 1.5	1	132.64

Table 3.28 (continued)

H-C Position	^{1}H NMR			^{13}C NMR δ(ppm)
	δ(ppm)	J (Hz)	Number of H	
10	7.66 (*t*)	8	1	134.36
10	7.61 (*t*)	8	1	134.17
9,9′	7.54 (*d*)	8	2	130.97
10B(5mazpy)	7.52 (*t*)	8	1	134.17
8,8′, 8,8′, 9,9′	7.42 (*m*)	-	6	123.73, 123.46, 130.56
9,9′B(5mazpy)	7.33 (*d*)	8	2	130.47
8,8′B(5mazpy)	7.06 (*d*)	8	2	123.39
11A	2.51 (*s*)	-	3	19.18
11B	2.48 (*s*)	-	3	19.13
Quaternary Carbons				164.33, 163.38, 163.04, 156.73, 153.03, 152.31 144.91, 144.89

d = doublet, *dd = doublet of doublet*, *ddd = doublet of doublet of doublet*, *m = multiplet*, *s = singlet*, and *t = triplet*

The ^{1}H NMR spectrum (Figure 3.64) of [Ru(5mazpy)$_2$azpy](PF$_6$)$_2$ shows three sets of pyridine ring signals and three set of phenyl ring signals. The assignments of all signals were made from ^{1}H-^{1}H COSY NMR spectroscopy (Figure 3.65). The ^{1}H NMR spectrum of this complex in acetone-d_6 contains nineteen signals from twenty-five aromatic protons and two signals from aliphatic protons. The signals of pyridine ring appear in the range 7.99-9.26 ppm and signals of phenyl ring are observed in the range 7.06-7.66 ppm. The methyl signals (2.51 and 2.48 ppm) are particularly useful to account for the configuration of N(py) and N(azo) orientation from starting complex, *ctc*-[Ru(5mazpy)$_2$Cl$_2$]. The proton H3 (9.26 ppm, *doublet*, *J* =

8 Hz) on pyridine ring of azpy ligand occurs at the lowest field which is due to trans to azo group. The methyl groups are useful to support the structure of the complexes. Two 5mazpy ligands in this complex give two sets of separate signals of methyl which resonances at 2.51 and 2.48 ppm. This suggests that the ligands chelated around Ru(II) are unsymmetrically disposed.

The ^{13}C NMR spectrum (Figure 3.66) displays nineteen methine carbons, two methyl carbons, and eight quaternary carbons. The signals of quaternary can not be observed in DEPT 135 NMR spectrum (Figure 3.67) which support ^{13}C NMR results. Eight quaternary carbons, C2A, C5A, C7A, C2B, C5B, C7B, C2(azpy), and C7(azpy), are observed. The carbon C2(azpy) occurs at the lowest field because this position located next to N=N azo group and the pyridine ring C trans to N=N azo group of 5mazpy (B) ligand. In addition, the quaternary carbons unable to show any direct ^{1}H-^{13}C heteronuclear multiple quantum coherence. The $[Ru(5mazpy)_2azpy](PF_6)_2$ complex contains two 5mazpy ligands, thus two methyl carbons are observed at 19.18 and 19.13 ppm. This results consist with the proton of methyl group. This is because, they belong to the non-proonated carbon atoms on the pyridine, phenyl rings. Figure 3.68 shows ^{1}H-^{13}C HMQC NMR spectrum of this complex.

(c) Nuclear Magnetic Resonance spectroscopy of the $[Ru(5mazpy)_2bpy](PF_6)_2$ complex

The ^1H and ^{13}C NMR spectroscopic data are listed in Table 3.29.

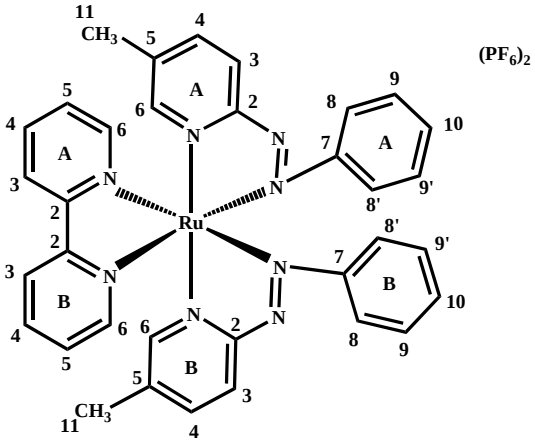

Table 3.29 ^1H and ^{13}C NMR of the $[Ru(5mazpy)_2bpy](PF_6)_2$ complex

H-C Position	^1H NMR			^{13}C NMR δ(ppm)
	δ(ppm)	*J* (Hz)	Number of H	
3(bpy)	8.97 (*d*)	8.0	1	126.34
3(5mazpy)	8.66 (*d*)	8.5	1	130.22
4(bpy)	8.44 (*ddd*)	8.0, 8.0, 1.0	1	141.28
6(bpy)	8.38 (*d*)	5.5	1	153.90
6(5mazpy)	8.32 (*s*)	-	1	150.97
4(5mazpy)	8.22 (*dd*)	8.0, 2.0	1	142.24
5(bpy)	7.77 (*td*)	7.5, 5.5	1	129.79
10(5mazpy)	7.57 (*m*)	-	1	133.58
9,9′, 8,8′(5mazpy)	7.41 (*m*)	-	2	130.31, 123.45
11	2.87 (*s*)	-	3	19.06

Table 3.29 (continued)

H-C Position	^{1}H NMR			^{13}C NMR
	δ (ppm)	J (Hz)	Number of H	δ (ppm)
Quaternary Carbons				163.96, 156.11, 153.97, 143.53

d = doublet, *dd = doublet of doublet*, *ddd = doublet of doublet of doublet*, *m = multiplet*, *s = singlet*, and *td = triplet of doublet*

The ^{1}H NMR spectrum of [Ru(5mazpy)$_2$bpy](PF$_6$)$_2$ (Figure 3.69) shows ten signals in aromatic region and one signal in aliphatic region. Due to the C_2 axis present in this complex, the two 5mazpy ligands are equivalent. The spectrum displays distinct eleven signals corresponding to one 5mazpy ligand and one pyridine ring of bpy ligand. The proton on pyridine ring in 5mazpy ligand exhibits at the higher field than in bpy ligand. Owing to the 5mazpy contains the methyl group which is electron donating group. This may be increase electron density on pyridine ring of 5mazpy. In addition, the bpy ligand is trans to N=N electron withdrawing group, azo(N=N). The proton H3 and H6 of bpy appear as *doublet* at 8.97, and 8.38 ppm, respectively. This H6 (J = 5.5 Hz) is easily recognised from the smaller J coupling in comparison to the J coupling of the H3 (J = 8 Hz). The signal of proton H6 of 5mazpy is found at 8.32 ppm as *singlet*. The methyl signal (2.87 ppm) is observed only one signal due to the symmetry of molecule. The ^{1}H-^{1}H COSY NMR spectrum in acetone-d_6 is displayed in Figure 3.70.

The ^{13}C NMR spectrum (Figure 3.71) shows ten methine carbons, one methyl carbon, and four quaternary carbons. These data are confirmed by using DEPT 135 NMR (Figure 3.72). The methyl carbon, appears at 2.87 ppm. In addition, the signal of quaternary carbons occurs at 163.96, 156.11, 153.97, and 143.53 ppm. The ^{13}C NMR signal assignments were based on the ^{1}H-^{13}C HMQC NMR spectroscopy (Figure 3.73). The observed peak at 19.06 ppm is assigned to the methyl carbon, due to the symmetry of molecule. Only one carbon from methyl group is found.

(d) Nuclear Magnetic Resonance spectroscopy of the [Ru(5mazpy)$_2$phen](PF$_6$)$_2$ complex

The ^{1}H and ^{13}C NMR spectroscopic data are listed in Table 3.30.

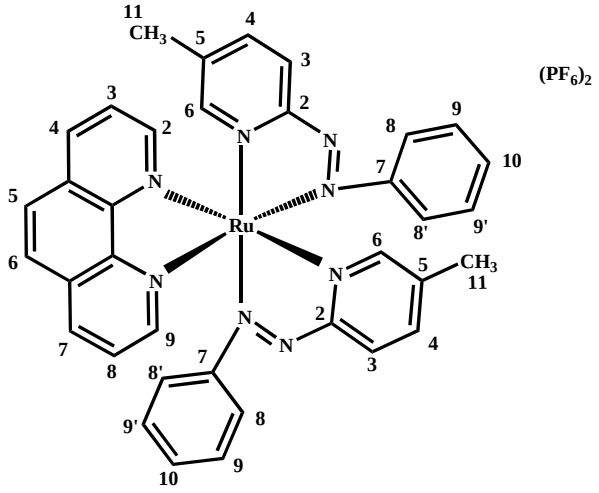

Table 3.30 ^{1}H and ^{13}C NMR of the [Ru(5mazpy)$_2$phen](PF$_6$)$_2$ complex

H-C Position	^{1}H NMR			^{13}C NMR δ (ppm)
	δ (ppm)	J (Hz)	Number of H	
3(5mazpy)	9.08 (*d*)	8	1	130.73
3(5mazpy)	9.05 (*d*)	8	1	130.52
7(phen)	8.97 (*dd*)	8, 1.5	1	140.59
5(phen)	8.69 (*d*)	8	1	139.57
2(phen)	8.65 (*d*)	5	1	153.40
4(5mazpy)	8.55 (*dd*)	8, 1.5	1	143.88
4(5mazpy)	8.33 (*d*)	8	1	143.37
6(phen)	8.29 (*d*)	8	1	128.91
6(5mazpy)	8.25 (*d*)	1.5	1	152.79

Table 3.30 (continued)

H-C Position	^{1}H NMR			^{13}C NMR δ (ppm)
	δ (ppm)	J (Hz)	Number of H	
4(phen)	8.14 (*d*)	9.5	1	128.81
6(5mazpy)	8.12 (*s*)	-	1	151.19
8(phen)	8.10 (*dd*)	8.5, 5.5	1	128.40
9(phen)	8.01 (*dd*)	5.5, 1.5	1	152.72
3(phen)	7.99 (*dd*)	8.5, 5.5	1	127.86
10(5mazpy)	7.69 (*t*)	8	1	133.46
9, 9′(5mazpy)	7.62 (*dd*)	8, 8	2	130.95
8, 8′(5mazpy)	7.39 (*dd*)	8, 1.5	2	123.62
10(5mazpy)	7.04 (*t*)	8	1	131.95
9, 9′(5mazpy)	6.80 (*dd*)	8, 8	2	129.32
8, 8′(5mazpy)	6.36 (*dd*)	8, 1.5	2	121.73
11	2.49 (*s*)	-	3	19.24
11	2.18 (*s*)	-	3	18.92
Quaternary Carbons				164.39, 162.78, 158.19, 153.92, 146.71, 146.37, 143.35, 142.55, 131.49, 131.41

d = doublet, *dd = doublet of doublet*, *m = multiplet*, *s = singlet*, and *t = triplet*

The ^{1}H NMR spectrum (Figure 3.74) of the $[Ru(5mazpy)_2phen](PF_6)_2$ complex shows many sharp resonances. In total twenty-two resonances are observed for thirty hydrogens present in this complex. The ^{1}H NMR spectrum shows two sets of 5mazpy signals, and one set of phen signals which is indicated that this molecules

lack C_2 symmetry. The assignment of all signals is made from ^{1}H-^{1}H COSY NMR spectroscopic data (Figure 3.75). The pyridine protons appear in the range 9.08-7.99 ppm and the phenyl protons display in the range 7.69-6.36 ppm. The proton H3 of both 5mazpy ligands occurs at 9.08 and 9.05 ppm as *doublet* (J = 8.0 Hz). The methyl signal of the 5mazpy ligand is particularly useful to confirm the number of 5mazpy ligand. This spectrum shows two methyl signals at 2.49 and 2.18 ppm which equal heights. The appearance of two signals refer to the presence of two 5mazpy ligands in this molecule, resulting in nonequivalent 5mazpy ligands.

The ^{13}C NMR signals (Figure 3.76) are assigned and compared with DEPT 135 NMR spectrum (Figure 3.77). The assignments of carbons on ligands are based on ^{1}H-^{13}C HMQC NMR spectroscopy (Figure 3.78). Ten quaternary carbons are observed at 164.39, 162.78, 158.19, 153.92, 146.71, 146.37, 143.35, 142.55, 131.49, and 131.41 ppm. In addition, the two methyl carbon signals appear at 19.24 and 18.92 ppm which are corroborated with the presence of two 5mazpy ligands in molecule. In addition, these signals show contours with proton at 2.49 and 2.18 ppm, respectively.

(e) Nuclear Magnetic Resonance spectroscopy of the $[Ru(bpy)_2 5mazpy](PF_6)_2$ complex

The ^1H and ^{13}C NMR spectroscopic data are listed in Table 3.31.

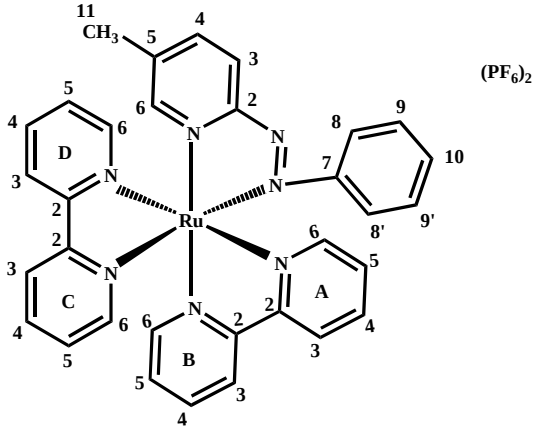

Table 3.31 ^1H and ^{13}C NMR of the $[Ru(bpy)_2 5mazpy](PF_6)_2$ complex

H-C Position	^1H NMR			^{13}C NMR δ (ppm)
	δ (ppm)	J (Hz)	Number of H	
3(bpy)	8.94 (*d*)	8	1	126.20
3(bpy)	8.92 (*d*)	8	1	125.88
3(5mazpy)	8.90 (*d*)	8.5	1	129.65
3(bpy)	8.62 (*d*)	8	1	125.34
3(bpy)	8.47 (*d*)	8	1	125.08
4(bpy), 4(bpy), 4(bpy), 6(bpy)	8.35 (*m*)	-	4	141.13, 140.82, 140.62, 154.20
4(5mazpy)	8.26 (*d*)	8	1	141.82
6(5mazpy)	8.19 (*s*)	-	1	151.89
4(bpy)	8.10 (*ddd*)	8, 8, 1.5	1	140.05

Table 3.31 (continued)

H-C Position	^{1}H NMR			^{13}C NMR δ (ppm)
	δ (ppm)	J (Hz)	Number of H	
6(bpy), 6(bpy)	7.99 (*d*)	5.5	2	151.89, 151.63
5(bpy), 5(bpy), 5(bpy), 6(bpy)	7.71 (*m*)	-	4	128.96, 129.14, 129.37, 153.34
5(bpy)	7.53 (*dd*)	8, 6	1	129.71
10(5mazpy)	7.40 (*t*)	8	1	131.80
9,9′(5mazpy)	7.23 (*dd*)	8, 8	2	130.04
8,8′(5mazpy)	7.15 (*d*)	8	2	123.01
11	2.31 (*s*)	-	3	19.19
Quaternary Carbons				165.38, 157.76, 157.29, 157.04, 156.03, 155.54, 141.85

d = doublet, *dd = doublet of doublet*, *ddd = doublet of doublet of doublet*, *m = multiplet*, *s = singlet*, and *t = triplet*

The ^{1}H NMR spectrum of the $[Ru(bpy)_2 5mazpy](PF_6)_2$ complex (Figure 3.79) shows signals in aromatic region and aliphatic region. Five sets of pyridine ring and one set of phenyl ring are observed. Due to the C_1 axis present in this complex, the two bpy ligands are nonequivalent. In each pyridine ring, proton H3 appears at the most downfield. The resonances have been assigned using ^{1}H-^{1}H COSY NMR spectroscopy (Figure 3.80). The resonances corresponding to the H6 of both 5mazpy and bpy ligands have a smaller *J* coupling than the resonances corresponding to the H3. The proton H6 on 5mazpy ligand appears at 8.19 ppm as *singlet*. This is due to absence of any proton near proton H6. The resonance at 2.31 ppm (*singlet*), which is attributable to the proton at the methyl group from 5mazpy.

The ^{13}C NMR spectrum (Figure 3.81) of the two bpy ligands are nonequivalent resulting in twenty-two methine carbons, one methyl carbon, and seven quaternary carbons. This results support by DEPT 135 NMR spectroscopy (Figure 3.82). The chemical shift of methyl carbon of 5mazpy is observed at 19.19 ppm which high field than that free 5mazpy ligand. The ^{13}C NMR signals assignments were based on the ^{1}H-^{13}C HMQC NMR spectrum (Figure 3.83), which exhibit correlation between ^{1}H NMR spectrum and ^{13}C NMR spectrum.

d) Nuclear Magnetic Resonance spectroscopy of the [Ru(phen)$_2$5mazpy](PF$_6$)$_2$ complex

The ^{1}H and ^{13}C NMR spectroscopic data are listed in Table 3.32.

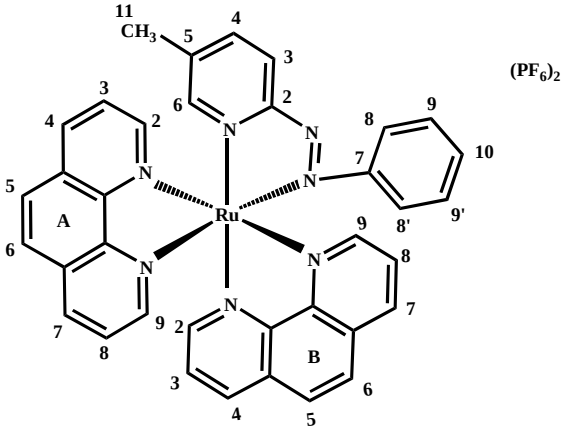

Table 3.32 ^{1}H and ^{13}C NMR of the [Ru(phen)$_2$5mazpy](PF$_6$)$_2$ complex

H-C Position	^{1}H NMR			^{13}C NMR δ(ppm)
	δ(ppm)	*J* (Hz)	Number of H	
7(phen)	9.03 (*d*)	8.5, 1.5	1	140.04
4(phen)	8.99 (*dd*)	8.5, 1.5	1	139.58
2(phen)	8.98 (*d*)	5.5	1	155.59
3(5mazpy)	8.93 (*dd*)	8	1	128.84
4(phen)	8.90 (*dd*)	8, 1.5	1	139.58
7(phen)	8.63 (*dd*)	8.5, 1	1	138.70
5, 6(phen)	8.50 (*m*)	-	2	129.30, 129.16
5(phen)	8.33 (*dd*)	8	1	128.86
9(phen)	8.28 (*dd*)	5.5, 1.5	1	154.68
2(phen)	8.27 (*dd*)	5.5, 1.5	1	153.15

Table 3.32 (continued)

H-C Position	^{1}H NMR			^{13}C NMR
	δ (ppm)	J (Hz)	Number of H	δ (ppm)
4(5mazpy)	8.24 (*d*)	8	1	141.70
6(phen)	8.21 (*d*)	8	1	129.49
9(phen), 6(5mazpy)	8.16 (*m*)	-	2	151.26, 153.73
8(phen)	8.15 (*dd*)	8, 8	1	127.94
3(phen)	8.09 (*dd*)	8, 8	1	128.02
3(phen)	7.84 (*dd*)	8, 8	1	127.58
8(phen)	7.66 (*dd*)	8, 8	1	127.31
10(5mazpy)	7.17 (*t*)	8	1	131.34
8,8′(5mazpy)	7.07 (*dd*)	8, 1.5	2	122.55
9,9′(5mazpy)	6.99 (*t*)	8, 8	2	129.57
11	2.19 (*s*)	-	3	19.57
Quaternary Carbons				165.67, 155.46, 148.18, 147.83, 147.58, 146.77, 141.64, 132.47, 132.34, 131.89, 131.63

d = doublet, *dd = doublet of doublet*, *m = multiplet*, *t = triplet*, *s = singlet*

The ^{1}H NMR spectrum of [Ru(phen)$_2$5mazpy](PF$_6$)$_2$ is depicted in Figure 3.84. As this complex has C_1 symmetry, two phen ligands are inequivalent, resulting in twenty-two resonances in aromatic region, which have been fully assigned using ^{1}H-^{1}H COSY NMR spectroscopy (Figure 3.85). From ^{1}H-^{1}H COSY NMR spectrum the 5mazpy signals display at the highest field which separate from the pyridine signal. In the spectrum, a singlet corresponding to three protons is observed

at 2.19 ppm. Appearance of the protons of methyl group as a *singlet* suggest that one 5mazpy ligand in this complex. The high field shift of the methyl group (0.23 ppm) compares to the free ligand indicated a position of this group in the shielding region of the pyridine ring of phen.

The ^{13}C NMR spectrum (Figure 3.86) consists with the DEPT 135 NMR spectrum (Figure 3.87). This suggests that eleven quaternary carbons in molecule. The carbon signal at 19.57 ppm is assigned to methyl carbon. The carbon chemical shifts of this complex have been assigned by using ^{1}H-^{13}C HMQC NMR spectroscopy (Figure 3.88).

3.4.6 Cyclic voltammetry

The electrochemical activity of the $[Ru(5mazpy)_2L](PF_6)_2$, $[Ru(5mazpy)_2L']$ $(PF_6)_2$ and $[Ru(L')_2 5mazpy](PF_6)_2$ complexes (L = azpy, 5mazpy; L′ = bpy, phen), was studied in CH_3CN solution by cyclic voltammetry at a scan rate of 100 mVs^{-1}. The voltammetric data are given in Table 3.33 and representative voltammograms are shown in Figure 3.89 to 3.94. Voltammograms of complexes display metal oxidation on the positive potential and ligand reductions on the negative potential with respect to ferrocene. The one electron nature of oxidation or reduction is establihsed by comparing its current heights with those of standard ferrocene-ferrocenium couple under identical experiment.

Table 3.33 Cyclic voltammetric data of the $[Ru(5mazpy)_2L](PF_6)_2$, $[Ru(5mazpy)_2L'](PF_6)_2$ and $[Ru(L')_2 5mazpy](PF_6)_2$ complexes in CH_3CN (0.1 M TBAH) at scan rate 100 mVs^{-1}

Complexes	[a] $E_{1/2}$, V (ΔE_p (mV))					
	Oxidation	Reduction				
	Ru(II)/Ru(III)	I	II	III	IV	V
$[Ru(5mazpy)_3](PF_6)_2$	n	-0.52 (60)	-0.84 (70)	-1.31 (60)	-1.98 (75)	-2.47 (160)
$[Ru(5mazpy)_2azpy](PF_6)_2$	n	-0.49 (60)	-0.80 (65)	-1.30 (65)	-1.95 (70)	-2.45 (160)
$[Ru(5mazpy)_2bpy](PF_6)_2$	n	-0.64 (60)	-1.13 (70)	-1.89 (60)	-2.16 (70)	-2.51 (125)
$[Ru(5mazpy)_2phen](PF_6)_2$	n	-0.68 (100)	-1.12 (80)	-1.87 (75)	-2.14 (75)	-2.46 (150)
$[Ru(bpy)_2 5mazpy](PF_6)_2$	1.14(65)	-1.03 (65)	-1.76 (80)	-2.16 (60)	-2.50 (95)	n

Table 3.33 (continued)

Complexes	$E_{1/2}$, V (ΔE_p (mV))					
	Oxidation	Reduction				
	Ru(II)/Ru(III)	I	II	III	IV	V
$[Ru(phen)_2 5mazpy](PF_6)_2$	1.11(100)	-1.07 (70)	-1.81 (65)	-2.24 (65)	-2.61 (85)	n

n = cannot be observed; [a] = $E_{1/2} = (E_{pa} + E_{pc})/2$, where E_{pa} and E_{pc} are anodic and chathodic peak potentials, respectively; $\Delta E_p = E_{pa} - E_{pc}$

Oxidation potential

The oxidation potenial range 0 to +1.50 V at scan rate 100 mVs^{-1} one redox couple is observed for the $[Ru(L')_2 5mazpy](PF_6)_2$ (L′ = bpy, phen) complexes while the $[Ru(5mazpy)_2 L](PF_6)_2$, $[Ru(5mazpy)_2 L'](PF_6)_2$ (L = azpy, 5mazpy; L′ = bpy, phen) complexes are not observed because the redox of Ru(II)/Ru(III) is too positive to be observed within the solvent window.

For the $[Ru(bpy)_2 5mazpy](PF_6)_2$ complex, the oxidation couple at 1.14 V is reversible which is nature as in evident from the peak-to-peak separation, $\Delta E_p \leq$ 100 mV while the redox potential of Ru(II)/Ru(III) in $[Ru(bpy)_3](PF_6)_2$ (Tempiam, S., 2002) are found to be reversible at 0.91 V (ΔE_p = 85 mV) which lower than that $[Ru(bpy)_2 5mazpy](PF_6)_2$. The $[Ru(phen)_2 5mazpy](PF_6)_2$ complex undergo oxidation at 1.11 V (ΔE_p = 100 mV). The response is attributed to the Ru(II)/Ru(III) couple. The oxidation potential of this complex is compared with $[Ru(phen)_3](PF_6)_2$. Results show that the potential of $[Ru(phen)_2 5mazpy](PF_6)_2$ more positive than that in the $[Ru(phen)_3](PF_6)_2$ (0.89 V, ΔE_p = 75 mV) (Rattanawit, N., 2002). The results from this study and the reported oxidation potential values demonstrate that π acceptance of 5mazpy is greater than bpy and phen. Thus the azopyridine ligand (L) can act as a

much better stabiliser of Ru(II) ion compare to the bpy and phen ligand, which is of course due to the stronger π-acid property of L. This results is in accordance with the earlier observations on other metal complexes of L. (Goswami *et al.*, 1983).

Reduction potential

The reduction potential range 0 to -2.65 V at scan rate 100 mVs^{-1}. Four or five successive reductions are observable within this potential window. The azopyridines are well known electron-transfer centres. Thus each ligand can accommodate two electrons in one electrochemically accessible lowest unoccupied molecular orbital (LUMO) which is primarily azo character (Goswami *et al.*, 1983). In addition, the bpy ligand can successively accept two electrons in its lowest unoccupied molecular orbital. Since the ruthenium complexes contain three electroactive ligands, in principle, six successive reductions are expected for each complex.

For the $[Ru(5mazpy)_2L](PF_6)_2$ and $[Ru(5mazpy)_2L'](PF_6)_2$ complexes, only five of the six couples are detected in this experiment. The interpretation of CV data may be carried out on comparison with the redox properties of *ctc*-$[Ru(5mazpy)_2Cl_2]$, $[Ru(azpy)_3](PF_6)_2$ (Changsaluk, U., 2002), $[Ru(bpy)_3](PF_6)_2$, $[Ru(bpy)_2azpy](PF_6)_2$ (Tempiam, S., 2002), $[Ru(phen)_3](PF_6)_2$, $[Ru(phen)_2azpy](PF_6)_2$ (Rattanawit, N., 2002). These are assigned to reductions of the coordinated ligands. Redox data in Table 3.34 reveal that the first reduction potential of the coordinated ligand occurs at a much less negative potential than that of other response and the oxidation potential of metal ion. The first reduction may be expected to involve the ligand having the most stable lowest unoccuiped molecular orbital (Dinda *et al.*, 2006), which is dominated by azo function of azpy and 5mazpy than bpy and phen. The formal potential of the first reduction of the $[Ru(5mazpy)_3](PF_6)_2$, $[Ru(5mazpy)_2azpy](PF_6)_2$, $[Ru(5mazpy)_2bpy](PF_6)_2$, and $[Ru(5mazpy)_2phen](PF_6)_2$ complexes is -0.52 V (ΔE_p = 60 mV), -0.49 V (ΔE_p = 60 mV), -0.64 V (ΔE_p = 60 mV) and -0.68 V (ΔE_p = 100 mV), respectively. Five couples at negative side of $[Ru(L')_25mazpy](PF_6)_2$ are assigned to gradual addition of electron into one azoimine chelate from 5mazpy and two imine chelates ring in the complexes. In addition, the first reduction potential in $[Ru(bpy)_25mazpy]$

$(PF_6)_2$ and $[Ru(phen)_2 5mazpy](PF_6)_2$ is -1.03 V (ΔE_p = 70 mV) and -1.07 V (ΔE_p = 65 mV), respectively.

Table 3.34. Cyclic voltammetric data of the ruthenium complexes with the azoimine and imine ligands in CH_3CN (0.1 M TBAH) at scan rate 100 mVs^{-1}

Complexes	$E_{1/2}$, V (ΔE_p (mV))	
	Oxidation Ru(II)/Ru(III)	First Reduction
ctc-$[Ru(5mazpy)_2Cl_2]$	0.65 (65)	-1.17 (95)
$[Ru(5mazpy)_3](PF_6)_2$	n	-0.52 (60)
$[Ru(azpy)_3](PF_6)_2$ [a]	n	-0.44 (70)
$[Ru(bpy)_2 5mazpy](PF_6)_2$	1.14 (65)	-1.03 (65)
$[Ru(bpy)_2 azpy](PF_6)_2$ [b]	1.21 (100)	-0.87 (65)
$[Ru(bpy)_3](PF_6)_2$ [b]	0.91 (85)	-1.14 (85)
$[Ru(phen)_2 5mazpy](PF_6)_2$	1.11 (100)	-1.07 (70)
$[Ru(phen)_2 azpy](PF_6)_2$ [c]	1.20 (105)	-0.88 (70)
$[Ru(phen)_3](PF_6)_2$ [c]	0.89 (72)	-1.93 (100)

n = can not be observed, [a] (Changsaluk, U., 2002),
[b] (Tempiam, S., 2002), [c] (Rattanawit, N., 2002)

The first reduction potential in all ruthenium complexes, $[Ru(5mazpy)_2 L](PF_6)_2$, $[Ru(5mazpy)_2 L'](PF_6)_2$ and $[Ru(L')_2 5mazpy](PF_6)_2$, is more positive than the free 5mazpy ligand (-1.62 V, ΔE_p = 94 mV) which due to the positive charge of the metal ion. In the presence of methyl group (in 5mazpy) may shift ligand dominated orbitals to higher energy side than azpy ligand. From this table shows that, the relative values of the potential suggest that the π-acidity order is azpy > 5mazpy

> bpy ~ phen.

The reduction potentials data of $[Ru(5mazpy)_3](PF_6)_2$ are listed in equation (7)-(11).

$$[Ru^{II}(5mazpy)(5mazpy)(5mazpy)]^{2+} + e^- \rightarrow [Ru^{II}(5mazpy)(5mazpy)(5mazpy^{1-})]^{+} \quad (7)$$

$$[Ru^{II}(5mazpy)(5mazpy)(5mazpy^{1-})]^{+} + e^- \rightarrow [Ru^{II}(5mazpy)(5mazpy^{1-})(5mazpy^{1-})]^{0} \quad (8)$$

$$[Ru^{II}(5mazpy)(5mazpy^{1-})(5mazpy^{1-})]^{0} + e^- \rightarrow [Ru^{II}(5mazpy^{1-})(5mazpy^{1-})(5mazpy^{1-})]^{-} \quad (9)$$

$$[Ru^{II}(5mazpy^{1-})(5mazpy^{1-})(5mazpy^{1-})]^{-} + e^- \rightarrow [Ru^{II}(5mazpy^{1-})(5mazpy^{1-})(5mazpy^{2-})]^{2-} \quad (10)$$

$$[Ru^{II}(5mazpy^{1-})(5mazpy^{1-})(5mazpy^{2-})]^{2-} + e^- \rightarrow [Ru^{II}(5mazpy^{1-})(5mazpy^{2-})(5mazpy^{2-})]^{3-} \quad (11)$$

Another one expected reduction is not observed presumably due to solvent cut off. The reduction for $[Ru(5mazpy)_2azpy](PF_6)_2$ have been observed. The reductions are actually observed in experiments, equations (12)-(16).

$$[Ru^{II}(5mazpy)(5mazpy)(azpy)]^{2+} + e^- \rightarrow [Ru^{II}(5mazpy)(5mazpy)(azpy^{1-})]^{+} \quad (12)$$

$$[Ru^{II}(5mazpy)(5mazpy)(azpy^{1-})]^{+} + e^- \rightarrow [Ru^{II}(5mazpy)(5mazpy^{1-})(azpy^{1-})]^{0} \quad (13)$$

$$[Ru^{II}(5mazpy)(5mazpy^{1-})(azpy^{1-})]^{0} + e^- \rightarrow [Ru^{II}(5mazpy^{1-})(5mazpy^{1-})(azpy^{1-})]^{-} \quad (14)$$

$$[Ru^{II}(5mazpy^{1-})(5mazpy^{1-})(azpy^{1-})]^{-} + e^- \rightarrow [Ru^{II}(5mazpy^{1-})(5mazpy^{1-})(azpy^{2-})]^{2-} \quad (15)$$

$$[Ru^{II}(5mazpy^{1-})(5mazpy^{1-})(azpy^{2-})]^{2-} + e^- \rightarrow [Ru^{II}(5mazpy^{1-})(5mazpy^{2-})(azpy^{2-})]^{3-} \quad (16)$$

The reduction potentials of the $[Ru(5mazpy)_2L'](PF_6)_2$ complexes (L′ = bpy, phen) are listed in equation (17)-(21).

$$[Ru^{II}(L')(5mazpy)(5mazpy)]^{2+} + e^- \rightarrow [Ru^{II}(L')(5mazpy)(5mazpy^{1-})]^{+} \quad (17)$$

$$[Ru^{II}(L')(5mazpy)(5mazpy^{1-})]^{+} + e^- \rightarrow [Ru^{II}(L')(5mazpy^{1-})(5mazpy^{1-})]^{0} \quad (18)$$

$$[Ru^{II}(L')(5mazpy^{1-})(5mazpy^{1-})]^{0} + e^- \rightarrow [Ru^{II}(L')(5mazpy^{1-})(5mazpy^{2-})]^{-} \quad (19)$$

$$[Ru^{II}(L')(5mazpy^{1-})(5mazpy^{2-})]^{-} + e^- \rightarrow [Ru^{II}(L')(5mazpy^{2-})(5mazpy^{2-})]^{2-} \quad (20)$$

$$[Ru^{II}(L')(5mazpy^{2-})(5mazpy^{2-})]^{2-} + e^- \rightarrow [Ru^{II}(L'^{-1})(5mazpy^{2-})(5mazpy^{2-})]^{3-} \quad (21)$$

The reduction potentials data of the $[Ru(L')_2 5mazpy](PF_6)_2$ (L′ = bpy, phen) complexes only four reductions are observed with one electron transfer in each equation (22)-(25).

$$[Ru^{II}(L')_2(5mazpy)]^{2+} + e^- \rightarrow [Ru^{II}(L')_2(5mazpy^{1-})]^{+} \quad (22)$$

$$[Ru^{II}(L')_2(5mazpy^{1-})]^{+} + e^- \rightarrow [Ru^{II}(L')_2(5mazpy^{2-})]^{0} \quad (23)$$

$$[Ru^{II}(L')_2(5mazpy^{2-})]^{0} + e^- \rightarrow [Ru^{II}(L')(L'^{1-})(5mazpy^{2-})]^{-} \quad (24)$$

$$[Ru^{II}(L')(L'^{1-})(5mazpy^{2-})]^{-} + e^- \rightarrow [Ru^{II}(L'^{1-})_2(5mazpy^{2-})]^{2-} \quad (25)$$

The first reduction potential of the $[Ru(5mazpy)_2L](PF_6)_2$ and $[Ru(5mazpy)_2L'](PF_6)_2$ complexes (L = azpy, 5mazpy; L′ = bpy, phen) was compared. Therefore, the $[Ru(5mazpy)_2azpy](PF_6)_2$ complex could accept electron better than the $[Ru(5mazpy)_3](PF_6)_2$ and $[Ru(5mazpy)_2bpy](PF_6)_2 \approx [Ru(5mazpy)_2phen](PF_6)_2$ complexes, respectively. This is in accorded with the π-acidity order of the ligands: bipyridine < azopyridine (Santra *et al.*, 1999).

3.4.7 X-ray Crystallography

The structure of the $[Ru(5mazpy)_2bpy](PF_6)_2$ complex was confirmed by X-ray crystallographic technique.

(a) X-ray structure of the $[Ru(5mazpy)_2bpy](PF_6)_2$ complex

The single crystals of $[Ru(5mazpy)_2bpy](PF_6)_2$ were grown by slow diffusion of ethanol into acetone solution of the $[Ru(5mazpy)_2bpy](PF_6)_2$ complex. The detailed measurement consitions and the crystal data are listed in Table 3.35. The selected bond lengths and bond angles are given in Table 3.36. Figure 3.95 shows the ORTEP and atom numbering scheme for the $[Ru(5mazpy)_2bpy](PF_6)_2$ complex. This complex was crystallized from methanol

Table 3.35 Crystallographic data of the $[Ru(5mazpy)_2bpy](PF_6)_2$complex

Empirical formula	$C_{34}H_{30}F_{12}P_6N_8Ru$
Formula weight	941.73
Crystal system	Monoclinic
Z	4
Space group	*C*2/*c*
a = 24.3405(15) Å	$\alpha = 90^o$
b = 14.0049(8) Å	$\beta = 123.86(1)^o$
c = 16.3346(10) Å	$\gamma = 90^o$
Temperature	293(2) K
Wavelength	0.71073 Å
Volume	4626.3(8) $Å^3$
Density (calculated)	1.352 Mg/m^3
Completeness to theta	24.00^o
Goodness-of-fit on F^2	1.169
Refinement method	Full-matrix least-squares on F^2

Table 3.35 (continued)

R indices (all data)	*R1* = 0.0780, *wR2* = 0.107
Measurement: Bruker SMART CCD diffractometer	
Program system: SHELX-97	
Structure determination: Direct methods (SHELXS-97)	
Refinement: full-matrix least-squares (SHELXL-97)	

Table 3.36 Selected bond lengths (Å) and bond angles (°) of the $[Ru(5mazpy)_2bpy](PF_6)_2$ complex

Ru(1)-N(1)	2.15(2)	Ru(1)-N(2)	2.06(2)
Ru(1)-N(4)	2.05(2)	C(7)-C(71)	1.56(6)
N(1)-C(1)	1.30(5)	N(1)-C(5)	1.30(3)
N(2)-C(6)	1.37(4)	N(2)-C(10)	1.26(3)
C(10)-N(3)	1.38(5)	N(3)-N(4)	1.26(3)
N(4)-C(11)	1.40(5)		
N(1)-Ru(1)-N(1)	78.1(7)	N(2)-Ru(1)-N(4)	74.2(9)
N(2)-Ru(1)-N(2)	169.5(8)	N(1)-Ru(1)-N(4)	174.8(8)
N(1)-Ru(1)-N(4)	100.4(9)	N(1)-Ru(1)-N(2)	100.5(9)
N(1)-Ru(1)-N(2)	87.7(8)	N(2)-Ru(1)-N(4)	97.4(9)
N(4)-Ru(1)-N(4)	81.7(9)		

The ruthenium ion of this complex is six-coordinated. The coordination geometry around ruthenium(II) is distorted octahedral with coordinating from two *N*-donor centers of bpy and four *N*-donor centers of two 5mazpy units. The pyridine rings of 5mazpy are at the *cis* position and the two pyridine rings of bpy ligand are *trans* to the azo groups of the 5mazpy ligands. The trans-angles around the ruthenium center in the plane ranged from 169.5(8) to 174.8(8)° indicating distortions

from the rectilinear geometry. The chelate angles extended by two 5mazpy and one bpy are 74.2(9), and 78.1 (7)°, respectively.

The Ru-N(azo) (2.05(2)Å) distances are shorter than Ru-N(pyridine) of 5mazpy (2.06(2)Å). The shortening may be due to greater π-backbonding, dπ(Ru) $\rightarrow\pi^*$ (azo). In this complex the N-N distances of 5mazpy are 1.264(3)Å which are slightly longer than those of free 5mazpy ligand (N=N 1.228(2)Å, and azpy (N=N 1.248(2)Å, Panneerselvam *et al*., 2000). In addition, the N=N distances of 5mazpy in tris complex, $[Ru(5mazpy)_2bpy](PF_6)_2$, are shorter than that in starting complex, *ctc*-$[Ru(5mazpy)_2Cl_2]$ (N=N 1.284(3)Å). The coordination could lead to a decrease in the N-N bond order due to σ-donor and π-acceptor character of the ligands. The Ru-N(pyridine) of bpy is 2.15(2)Å which longer than Ru-N(pyridine) distances in 5mazpy. Owing to pyridine rings of bpy is trans to azo function of 5mazpy. The results from the molecular structure of the this complex confirm that 5mazpy is a better π-acceptor than bpy. The chelate angles extend by 5mazpy were 74.2(9)° reveal a considerable distorsion of octahedron, as was found for the complexes $[Ru(azpy)_2$ bpy$](PF_6)_2$ (75.7(16)°, 76.8(17)°) (Kanidtha *et al*., 2007). As a consequence of the constraint of the bite angle, the ligands are bent back from the coordinated chlorides.

3.5 Syntheses of the $[Ru(5mazpy)_2L](NO_3)_2$, $[Ru(5mazpy)_2L']Cl_2$, and $[Ru(L')_25mazpy]Cl_2$ complexes (L = azpy, 5mazpy; L′ = bpy, phen)

Reaction of the *ctc*-$[Ru(5mazpy)_2Cl_2]$ complex with L ligands (azpy, 5mazpy) in the presence of $AgNO_3$ in methanol afforded tris-complexes, $[Ru(5mazpy)_2L](NO_3)_2$, as shown in equation (26).

$$\textit{ctc}\text{-}[Ru(5mazpy)_2Cl_2] \xrightarrow[MeOH,\ L]{AgNO_3} [Ru(5mazpy)_2L](NO_3)_2 \qquad (26)$$

The $[Ru(5mazpy)_2L']^{2+}$ complexes (L′ = bpy, phen) were isolated as chloride salt, $[Ru(5mazpy)_2L']Cl_2$, by the reaction of $[Ru(5mazpy)L'](PF_6)_2$ with tetra-*n*-butylammoniumchloride in acetone. The synthetic route is shown in equation (27).

$$[Ru(5mazpy)_2L'](PF_6)_2 \xrightarrow[acetone]{NBu_4Cl} [Ru(5mazpy)_2L']Cl_2 \qquad (27)$$

Addition of the saturated tetra-*n*-butylammoniumchloride in acetone to an acetone solution of the complexes $[Ru(L')_25mazpy](PF_6)_2$ (L′ = bpy, phen) had eliminated PF_6^- and gave $[Ru(L')_25mazpy]Cl_2$ (equation (28)).

$$[Ru(L')_25mazpy](PF_6)_2 \xrightarrow[acetone]{NBu_4Cl} [Ru(L')_25mazpy]Cl_2 \qquad (28)$$

The complexes of $[Ru(5mazpy)_2L](NO_3)_2$, $[Ru(5mazpy)_2L']Cl_2$, and $[Ru(L')_25mazpy]Cl_2$ (L = 2-(phenylazo)pyridine (azpy), 5-methyl-2-(phenylazo)pyridine (5mazpy), L′ = 2,2′-bipyridine (bpy), 1,10-phenanthroline (phen)) are readily soluble in water. These complexes were synthesized to study DNA-binding. All the

experiments involving the interaction of the complexes with DNA which were carried out using Tris buffer. The physical properties of these complexes are listed in Table 3.37.

Table 3.37 The physical properties of the $[Ru(5mazpy)_2L](NO_3)_2$, $[Ru(5mazpy)_2L']Cl_2$, and $[Ru(L')_25mazpy]Cl_2$ complexes

Complexes	Physical properties		
	Appearance	Color	Melting point (°C)
$[Ru(5mazpy)_3](NO_3)_2.5H_2O$	Solid	Red-brown	230-232
$[Ru(5mazpy)_2azpy](NO_3)_2.4H_2O$	Solid	Red-brown	232-235
$[Ru(5mazpy)_2bpy]Cl_2.6H_2O$	Solid	Dark-Red	245-248
$[Ru(5mazpy)_2phen]Cl_2.7H_2O$	Solid	Dark-Red	280-253
$[Ru(bpy)_25mazpy]Cl_2.6H_2O$	Solid	Red-brown	242-244
$[Ru(phen)_25mazpy]Cl_2.9H_2O$	Solid	Red-brown	248-252

3.6 Characterization of the $[Ru(5mazpy)_2L](NO_3)_2$, $[Ru(5mazpy)_2L']Cl_2$, and $[Ru(L')_25mazpy]Cl_2$ complexes (L = azpy, 5mazpy; L′ = bpy, phen)

All complexes were characterized by following techniques:

3.6.1 Elemental analysis

3.6.2 Infrared spectroscopy

3.6.3 1D and 2D Nuclear Magnetic Resonance spectroscopy

3.6.1 Elemental analysis

The elemental analysis data of the complexes were in very good agreement with the calculated values and thus confirmed the composition. The results are summarized in Table 3.38.

Table 3.38 Elemental analysis data of the $[Ru(5mazpy)_2L](NO_3)_2$, $[Ru(5mazpy)_2L']Cl_2$, and $[Ru(L')_25mazpy]Cl_2$ complexes

Complexes	%C		%N		%H	
	Calc.	Found	Calc.	Found	Calc.	Found
$[Ru(5mazpy)_3](NO_3)_2.5H_2O$	47.08	47.85	17.26	17.74	4.63	4.21
$[Ru(5mazpy)_2azpy](NO_3)_2.4H_2O$	48.05	48.84	17.61	17.71	4.49	4.43
$[Ru(5mazpy)_2bpy]Cl_2.6H_2O$	49.16	49.58	13.49	13.86	5.10	4.95
$[Ru(5mazpy)_2phen]Cl_2.7H_2O$	49.54	49.99	12.84	12.50	5.08	5.68
$[Ru(bpy)_25mazpy]Cl_2.6H_2O$	48.67	48.61	12.41	11.76	4.97	4.50
$[Ru(phen)_25mazpy]Cl_2.9H_2O$	48.49	48.44	10.99	10.83	5.08	4.16

3.6.2 Infrared Spectroscopy

IR spectral data were collected in the range 4000-370 cm^{-1} using KBr discs and characteristic group frequencies are given in Table 3.39. The IR spectra of the $[Ru(5mazpy)_3](NO_3)_2.5H_2O$, $[Ru(5mazpy)_2azpy](NO_3)_2.4H_2O$, $[Ru(5mazpy)_2bpy]Cl_2.6H_2O$, $[Ru(5mazpy)_2phen]Cl_2.7H_2O$, $[Ru(bpy)_25mazpy]Cl_2.6H_2O$, and $[Ru(phen)_25mazpy\ ]Cl_2.9H_2O$ complexes are shown in Figure 3.96 to 3.101.

Table 3.39 Infrared spectroscopic data of the $[Ru(5mazpy)_2L](NO_3)_2$,

$[Ru(5mazpy)_2L']Cl_2$, and $[Ru(L')_25mazpy]Cl_2$ complexes

Vibration modes	$[Ru(5mazpy)_2L](NO_3)_2$		$[Ru(5mazpy)_2L']Cl_2$		$[Ru(L')_25mazpy]Cl_2$	
	5mazpy	azpy	bpy	phen	bpy	phen
C=C, C=N stretching	1599(m) 1670(m) 1455(s)	1598(m) 1570(m) 1456(s)	1601(s) 1570(m) 1469(s) 1447(s)	1600(m) 1570(m) 1454(m) 1429(m)	1604(s) 1467(m) 1445(s)	1603(m) 1585(m) 1517(m) 1430(s)
N=N stretching	1363(s)	1360(s)	1341(s)	1338(s)	1325(s)	1326(s)
C-H bending in mono substituted benzene	554(s) 693(s) 779(s)	557(s) 691(s) 779(s)	576(m) 694(s) 768(s)	576(s) 690(s) 853(s)	557(s) 722(s) 840(s)	704(s) 771(s)
NO_3^-	1386(s)	1384(s)	-	-	-	-

s = strong, m = medium

The IR spectral data of the $[Ru(5mazpy)_2L](NO_3)_2$, $[Ru(5mazpy)_2L']Cl_2$, and $[Ru(L')_25mazpy]Cl_2$ complexes (L = azpy, 5mazpy; L′ = bpy, phen) were recorded in the range 4000-370 cm^{-1}. The complexes exhibit a broad bands assignable to the water in molecule. at 3500-3400 cm^{-1} The IR spectra of the $[Ru(5mazpy)_2L](NO_3)_2$, $[Ru(5mazpy)_2L']Cl_2$ complexes have compared with the spectra of *ctc*-$[Ru(5mazpy)_2Cl_2]$. An intense band observes in the range 1604-1429 cm^{-1} corresponds to C=C, C=N stretching modes.

The N=N stretching band of $[Ru(5mazpy)_3](NO_3)_2.5H_2O$, $[Ru(5mazpy)_2azpy](NO_3)_2.4H_2O$, $[Ru(5mazpy)_2bpy]Cl_2.6H_2O$, and $[Ru(5mazpy)_2phen]Cl_2.5H_2O$ is observed at 1363, 1360, 1341, and 1338 cm^{-1}, respectively. In *ctc*-$[Ru(5mazpy)_2Cl_2]$, the N=N band appears at 1334 cm^{-1}. However, this band shifts to

higher in the $[Ru(5mazpy)_2L](NO_3)_2$, and $[Ru(5mazpy)_2L']Cl_2$ complexes. This results can be implied that the third ligand is competition for the ruthenium t_{2g} electron and less π back-bonding to azo ligand raising the N=N bond order.

The $[Ru(L')_2 5mazpy]Cl_2$ complexes contain one azoimine ligand an two imine ligands. From the previous works, the azoimine ligand is the better π-acceptor than that the imine ligand. Therefore, we have observed that the N=N stretching mode in these complexes shifts to lower frequencies than that free 5mazpy ligand (1389 cm^{-1}) and $[Ru(5mazpy)_2L](NO_3)_2$, $[Ru(5mazpy)_2L']Cl_2$.

The $[Ru(5mazpy)_2L']Cl_2$, and $[Ru(L')_2 5mazpy]Cl_2$ complexes were synthesized from the reaction of tetra-*n*-butylammoniumchloride in acetone solution and the $[Ru(5mazpy)_2L'](PF_6)_2$, and $[Ru(L')_2 5mazpy](PF_6)_2$ complexes, respectively. The $\upsilon(PF_6^-)$ in complexes of $[Ru(5mazpy)_2L']Cl_2$, and $[Ru(L')_2 5mazpy]Cl_2$ disappears in the IR spectra. This results can be used to confirm that the PF_6^- counter ions were replaced by chloride ions.

3.6.3 1D and 2D Nuclear Magnetic Resonance spectroscopy

The ^{1}H, ^{13}C, DEPT 135, ^{1}H-^{1}H COSY, and ^{1}H-^{13}C HMQC NMR spectra of the $[Ru(5mazpy)_2L](NO_3)_2$, $[Ru(5mazpy)_2L']Cl_2$, and $[Ru(L')_2 5mazpy]Cl_2$ complexes were carried out in CD_3OD (500 MHz) and tetramethylsilane ($SiMe_4$) was used as internal reference. The 1D and 2D NMR data of these complexes were described as below.

a) Nuclear Magnetic Resonance spectroscopy of the $[Ru(5mazpy)_3](NO_3)_2.5H_2O$ complex

The ^{1}H and ^{13}C NMR spectroscopic data are listed in Table 3.40.

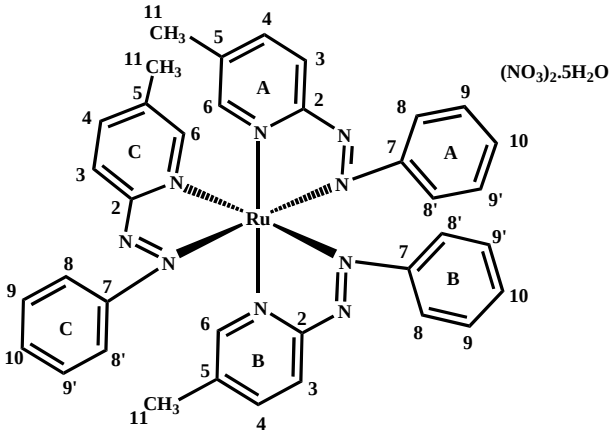

Table 3.40 ^{1}H and ^{13}C NMR of the $[Ru(5mazpy)_3](NO_3)_2.5H_2O$ complex

H-C Position	^{1}H NMR			^{13}C NMR δ (ppm)
	δ (ppm)	J (Hz)	Number of H	
3C	9.10 (*d*)	8	1	132.40
3A	8.50 (*d*)	8	1	131.67
3B	8.47 (*d*)	8	1	131.10

Table 3.40 (continued)

H-C Position	^{1}H NMR			^{13}C NMR δ (ppm)
	δ (ppm)	J (Hz)	Number of H	
4C	8.41 (*d*)	8	1	143.81
6C	8.33 (*d*)	1	1	153.45
4B	8.22 (*dd*)	8, 1	1	143.69
4A	8.15 (*dd*)	8.5, 1.5	1	143.44
6A	8.09 (*s*)	-	1	151.38
6B	7.96 (*s*)	-	1	152.83
10C	7.57 (*t*)	8	1	134.53
10A	7.55 (*t*)	8	1	134.53
9,9′C	7.46 (*dd*)	8, 8	2	131.21
10B	7.44 (*t*)	8	1	134.42
9,9′A	7.37 (*dd*)	8, 8	2	130.82
8,8′A	7.27 (*d*)	8	2	123.79
9,9′B	7.22 (*dd*)	8, 8	2	130.63
8,8′C	7.21 (*d*)	8	2	123.75
8,8′B	6.85 (*dd*)	8	2	123.59
11C	2.52 (*s*)	-	3	19.25
11A	2.51 (*s*)	-	3	19.19
11B	2.49 (*s*)	-	3	19.07
Quaternary Carbons				164.01, 163.74, 162.97, 157.06, 152.48, 134.56, 145.48, 145.14, 144.99

d = doublet, *dd = doublet of doublet*, *s = singlet*, and *t = triplet*

The ^{1}H NMR spectrum (Figure 3.102) of the $[Ru(5mazpy)_3](NO_3)_2.5H_2O$ complex shows three sets of pyridine ring and three sets of phenyl ring signals. As this complex has C_1 symmetry, all three 5mazpy ligands are inequivalent, resulting in eighteen resonances in aromatic region and three resonances in aliphatic region. The pyridine protons appear at the lower field (9.10 to 7.96 ppm) than that the phenyl protons (7.57 to 6.85 ppm). The proton H3 (9.10 ppm) in pyridine ring C occurs at the lowest field because this pyridine ring is trans to azo group. The protons H6 of 5mazpy ligand exhibit at 8.33 (*doublet*, J = 1 Hz), 8.09 (*singlet*), and 7.96 ppm (*singlet*) which are easily recognised from the smaller J coupling in comparison to the J coupling of the proton H3 and appear at 9.10 (*doublet*, J = 8 Hz), 8.50 (*doublet*, J = 8 Hz), and 8.47 ppm (*doublet*, J = 8 Hz). The methyl resonances of 5mazpy ligand in this complex are observed at 2.52, 2.51, and 2.49 ppm. The methyl signal has been particularly confirm that this complex contains three 5mazpy ligands. The assignment of all signals was made from ^{1}H-^{1}H COSY NMR spectroscopic data. The ^{1}H-^{1}H COSY NMR spectrum is shown in Figure 3.103. Results from 2D NMR, the three sets of 5mazpy pyridine signals and three sets of 5mazpy phenyl signals have been distinguish.

The ^{13}C NMR spectrum (Figure 3.104) shows eighteen methine carbons, nine quaternary carbons, and three methyl carbons which supports by the results from DEPT 135 NMR spectrum (Figure 3.105). Carbon atom neighbouring the nitrogen atom shifts to downfield due to the electronegative nitrogen atom. The protonated carbon atoms at C6 of 5mazpy moiety are shifted to downfield in the spectrum (153.45, 151.38, and 152.83 ppm). These signals are used to confirm that this molecule contains three 5mazpy ligand. The assignment of all signals was made from ^{1}H-^{13}C HMQC NMR spectroscopic data. Figure 3.106 displays ^{1}H-^{13}C HMQC NMR spectrum of the $[Ru(5mazpy)_3](NO_3)_2.5H_2O$ complex. The ^{1}H-^{13}C HMQC NMR spectrum provides information regarding the interaction between the protons and the carbon atoms which they are directly attached. In the present complex, the absence of any countours assign to the quaternary carbons. Therefore, this result corresponds to the ^{13}C NMR and DEPT 135 NMR spectroscopic data.

b) Nuclear Magnetic Resonance spectroscopy of the $[Ru(5mazpy)_2azpy](NO_3)_2.4H_2O$ complex

The ^{1}H and ^{13}C NMR spectroscopic data are listed in Table 3.41.

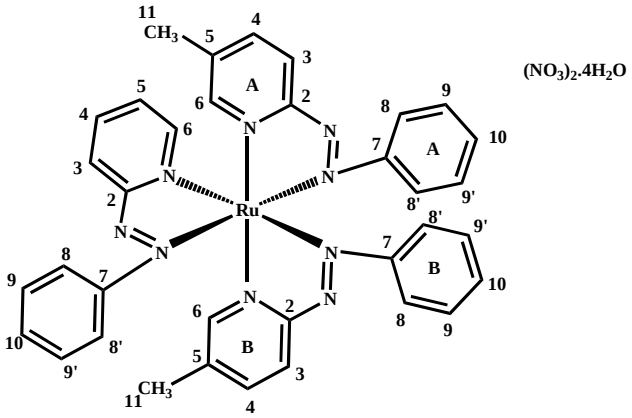

Table 3.41 ^{1}H and ^{13}C NMR of the $[Ru(5mazpy)_2azpy](NO_3)_2.4H_2O$ complex

H-C Position	^{1}H NMR			^{13}C NMR
	δ (ppm)	J (Hz)	Number of H	δ (ppm)
3(azpy)	9.22 (*d*)	8	1	134.74
4(azpy)	8.59 (*dd*)	8, 8	1	143.52
6(azpy)	8.53 (*dd*)	5.5, 1	1	153.56
3(5mazpy)	8.51 (*d*)	8	1	131.77
3(5mazpy)	8.48 (*d*)	8	1	131.74
4(5mazpy)	8.21 (*d*)	8	1	143.74
4(5mazpy)	8.14 (*d*)	8	1	143.42
6(5mazpy)	8.13 (*s*)	-	1	152.59
6(5mazpy)	7.96 (*d*)	1.5	1	151.71

Table 3.41 (continued)

H-C Position	^{1}H NMR			^{13}C NMR δ (ppm)
	δ (ppm)	J (Hz)	Number of H	
5(azpy)	7.86 (*dd*)	7.5, 6	1	131.25
10(5mazpy)	7.59 (*t*)	7.5	1	134.74
10(azpy)	7.55 (*t*)	8	1	134.57
9,9′A(5mazpy), 10(5mazpy)	7.46 (*m*)	-	3	131.20, 134.62
9,9′(azpy)	7.36 (*dd*)	8, 8	2	130.70
8,8′B(5mazpy), 8,8′(azpy),	7.26 (*m*)	8	4	123.96, 123.74
9B(5mazpy)	7.23 (*dd*)	8, 8	2	130.86
8B(5mazpy)	6.88 (*d*)	8	2	123.68
11A	2.50 (*s*)	-	3	19.10
11B	2.49 (*s*)	-	3	19.03
Quaternary Carbons				165.01, 164.01, 163.66, 157.21, 153.51, 152.89, 145.55, 145.35

d = doublet , *dd = doublet of doublet*, *m = multiplet*, *s = singlet*, and *t = triplet*

The ^{1}H NMR spectrum of $[Ru(5mazpy)_2azpy](NO_3)_2.4H_2O$ (Figure 3.107) in CD_3OD contains twenty-one proton resonances, which indicates the formation of the mixed-ligand complex. The pyridine protons appear at the lower field (9.22 to 7.86 ppm) than that phenyl protons (7.59 to 6.88 ppm) due to the nitrogen atom in pyridine ring. The protons on pyridine ring of azpy ligand occur at the lower field than protons on pyridine ring of 5mazpy due to trans to N=N azo

group. In addition, the 5mazpy ligand contains methyl group which is electron donating group. The signal at 9.22 ppm (*doublet*, J = 8 Hz) is assigned to the proton H3 of the azpy ligand because this signal has a bigger J coupling than the resonances corresponding to the proton H6 (8.53 ppm, *doublet of doublet*, J = 5.5, 1 Hz). Besides, the protons H3 on pyridine ring of the both 5mazpy ligand exhibit (8.51, 8.48 ppm) at the downfield than the other protons on pyridine ring. The assignment of individual proton resonances have been assigned using ^{1}H-^{1}H COSY NMR spectroscopy (Figure 3.108). The both pyridine rings of 5mazpy ligand in parent complex, *ctc*-[Ru(5mazpy)$_2$Cl$_2$], are trans. If the third ligand (unsymmetric ligand) coordinates to ruthenium ,the [Ru(5mazpy)$_2$azpy](NO$_3$)$_2$.4H$_2$O complex lacks of C_2-symmetry. Therefore, two methyl signals are observed (2.50 and 2.49 ppm).

The ^{13}C NMR spectrum (Figure 3.109) shows nineteen methine carbons, eight quaternary carbons, and two methyl carbons. This results are supported with DEPT 135 NMR spectroscopy (Figure 3.110). The two carbon signals in aliphatic region are observed at 19.10 and 19.03 ppm which are assigned to methyl carbons. All signals have been assigned using ^{1}H-^{13}C HMQC NMR spectroscopy. The ^{1}H-^{13}C HMQC NMR spectrum is displayed in Figure 3.111.

c) Nuclear Mmagnetic Resonance spectroscopy of the[Ru(5mazpy)$_2$bpy]Cl$_2$.6H$_2$O complex

The ^{1}H and ^{13}C NMR spectroscopic data are listed in Table 3.42.

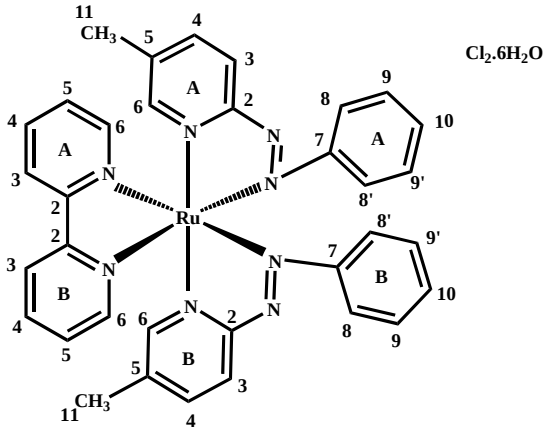

Table 3.42 ^{1}H and ^{13}C NMR of the [Ru(5mazpy)$_2$bpy]Cl$_2$.6H$_2$O complex

H-C Position	^{1}H NMR			^{13}C NMR
	δ (ppm)	*J* (Hz)	Number of H	δ (ppm)
3(bpy)	8.90 (*d*)	8	1	126.73
3(5mazpy)	8.58 (*d*)	8	1	130.63
4(bpy)	8.35 (*ddd*)	8, 8, 1	1	141.69
6(bpy)	8.14 (*d*)	5	1	153.70
4(5mazpy)	8.12 (*dd*)	8, 1.5	1	142.61
6(5mazpy)	7.93 (*s*)	-	1	150.68
5(bpy)	7.66 (*dd*)	8, 5	1	130.06
10(5mazpy)	7.52 (*t*)	8	1	134.04
9(5mazpy)	7.33 (*dd*)	8, 8	2	130.59

Table 3.42 (continued)

H-C Position	^{1}H NMR			^{13}C NMR δ(ppm)
	δ(ppm)	*J* (Hz)	Number of H	
8(5mazpy)	7.23 (*d*)	8	2	123.69
11	2.39 (*s*)	-	3	19.05
Quaternary Carbons				164.53, 156.52, 154.53, 144.03

d = doublet, *dd = doublet of doublet*, *ddd = doublet of doublet of doublet*, *s = singlet*, and *t = triplet*

The ^{1}H NMR spectrum of the [Ru(5mazpy)$_2$bpy]Cl$_2$.6H$_2$O complex (Figure 3.112) displays eleven protons resonances from thirty protons in molecule. Due to the C_2 axis present in this complex, the two 5mazpy ligands are equivalent (A=B) and even the two pyridine rings of bpy ligand are indistinguishable. Form ^{1}H-^{1}H COSY NMR spectrum (Figure 3.113), the two sets of pyridine (bpy and 5mazpy) are observed. They can be assigned using ^{1}H-^{1}H COSY NMR spectroscopy. The proton H3 (*doublet*, *J* = 8 Hz) of bpy ligand is easily recognised from the *J* coupling in comparison to the proton H6 (*doublet*, *J* = 5.5 Hz). The signal at 7.93 ppm (*singlet*) is assigned to proton H6 of 5mazpy, as this resonance exhibits weak COSY NMR cross peak with proton H4 (8.12 ppm, *doublet*, *J* = 1.5 Hz). The assignment of the resonances at 7.52 ppm (*triplet*, *J* = 8 Hz), 7.33 ppm (*doublet of doublet*, *J* = 8, 8 Hz), 7.23 ppm (*doublet*, *J* = 8 Hz) as proton H10, H9,9′, and H8,8′, respectively. Only one methyl signal iss observed at 2.39 ppm (*singlet*) because the effective C_2 symmetry is retained.

The ^{13}C NMR spectrum is illustrated in Figure 3.114. The DEPT 135 NMR spectrum (Figure 3.115) agrees with the carbon spectrum. As [Ru(5mazpy)$_2$ bpy]Cl$_2$.6H$_2$O has C_2 symmetry, ten methine carbons, four quaternary carbons and one methyl carbon are observed. The carbon signals at 153.70 and 150.68 ppm are

expected carbon C6(bpy) and C6(5mazpy), respectively. The ^{1}H-^{13}C HMQC NMR spectrum is shown in Figure 3.116. This ^{1}H-^{13}C HMQC NMR data are in correspondence with the ^{1}H and ^{13}C NMR spectroscopic data.

d) Nuclear Magnetic Resonance spectroscopy of the [Ru(5mazpy)$_2$phen]Cl$_2$.7H$_2$O complex

The ^{1}H and ^{13}C NMR spectroscopic data are listed in Table 3.43.

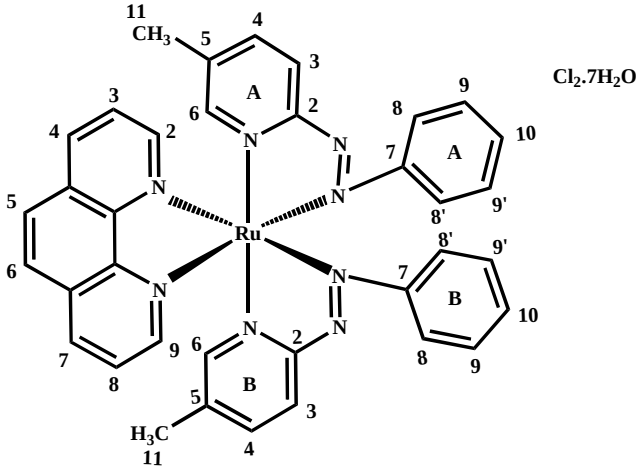

Table 3.43 ^{1}H and ^{13}C NMR of the [Ru(5mazpy)$_2$phen]Cl$_2$.7H$_2$O complex

H-C Position	^{1}H NMR			^{13}C NMR δ(ppm)
	δ(ppm)	*J* (Hz)	Number of H	
4(phen)	8.94 (*dd*)	8, 1	1	140.77
3(5mazpy)	8.61 (*d*)	8	1	130.71
2(phen)	8.60 (*dd*)	5, 1	1	154.90
5 (phen)	8.43 (*s*)	-	2	129.74
4(5mazpy)	8.06 (*dd*)	8, 1	1	142.51
3(phen)	8.01 (*dd*)	8, 8	1	128.36
6(5mazpy)	7.65 (*d*)	1.5	1	150.85
10(5mazpy)	7.53 (*t*)	8	1	133.92
9,9′(5mazpy)	7.37 (*dd*)	8, 8	2	130.65
8,8′(5mazpy)	7.31 (*dd*)	8, 1	2	123.72

Table 3.43 (continued)

H-C Position	^{1}H NMR			^{13}C NMR δ (ppm)
	δ (ppm)	J (Hz)	Number of H	
11(5mazpy)	2.19 (*s*)	-	3	18.82
Quaternary Carbons				164.52, 154.59, 146.82 143.91, 133.06

d = doublet, *dd = doublet of doublet*, *ddd = doublet of doublet of doublet*, *m = multiplet*, *s = singlet*, and *t = triplet*

The ^{1}H NMR spectrum of the $[Ru(5mazpy)_2phen]Cl_2.7H_2O$ complex (Figure 3.117) shows one set of 5mazpy and four protons of phen. The coordination of phen ligand (symmetric ligand) to the isomeric bis(ligand) complex, *ctc*-$[Ru(5mazpy)_2]$**,** results in a complex that has C_2 axis, resulting in equivalent 5mazpy ligand. The assignment of all signals was made from ^{1}H-^{1}H COSY NMR spectroscopic data. This spectrum is shown in Figure 3.118. The protons of pyridine ring from 5mazpy and phen are assigned by using ^{1}H-^{1}H COSY NMR spectroscopic technique, and NMR spectroscopic data of parent complex, *ctc*-$[Ru(5mazpy)_2Cl_2]$. The resonances corresponding to the proton H6 of 5mazpy (7.65 ppm, *doublet*, J = 1.5 Hz) and proton H2 (8.60 ppm, *doublet of doublet*, J = 5, 1 Hz) of phen have a smaller J coupling than resonances corresponding to the proton H3 of 5mazpy (8.61 ppm, *doublet*, J = 8 Hz) and proton H4 of phen (8.94 ppm, *doublet of doublet*, J = 8, 1 Hz). The proton H4 (8.94 ppm) of phen ligand occurs at the lowest field because of trans to the azo nitrogen of the 5mazpy ligand. The phenyl protons of $[Ru(5mazpy)_2phen]Cl_2.7H_2O$ display at the downfield (7.53 ppm (H10), 7.37 ppm (H9,9′), 7.31 ppm (H8,8′)) when compared with the *ctc*-$[Ru(5mazpy)_2Cl_2]$ (7.25 ppm (H10), 7.10 ppm (H9,9′), 6.80 ppm (H8,8′)). This results can be implied that the coordination of phen ligand. The phen ligand is σ-donor and π-acceptor while the Cl

ligand is σ-donor. Only one single sharp methyl signal is observed at 2.19 ppm (*singlet*). It is then resonable to assume that the effective C_2 symmetry is retained.

The ^{13}C NMR spectrum is displayed in Figure 3.119 which is used to support with DEPT 135 NMR spectrum (Figure 3.120). Ten methine carbons, five quaternary carbons and one methyl carbon are found. The carbon C2(phen) appears at 154.90 ppm and carbon C6(5mazpy) exhibits at 150.85 ppm due to the coordination of nitrogen atom to ruthenium. The carbon signal at 18.82 ppm is assigned to the methyl carbon. Appearance of the carbons of methyl group as one signal suggest that two methyl groups of this complex are magnetically equivalent. This observation is consistent with the ^{1}H, DEPT 135, ^{1}H-^{1}H COSY and ^{1}H-^{13}C HMQC NMR spectroscopic techniques. The ^{1}H-^{13}C HMQC NMR spectrum is illustrated in Figure 3.121.

e) Nuclear Magnetic Resonance spectroscopy of the [Ru(bpy)$_2$5mazpy]Cl$_2$.6H$_2$O complex

The ^{1}H and ^{13}C NMR spectroscopic data are listed in Table 3.44.

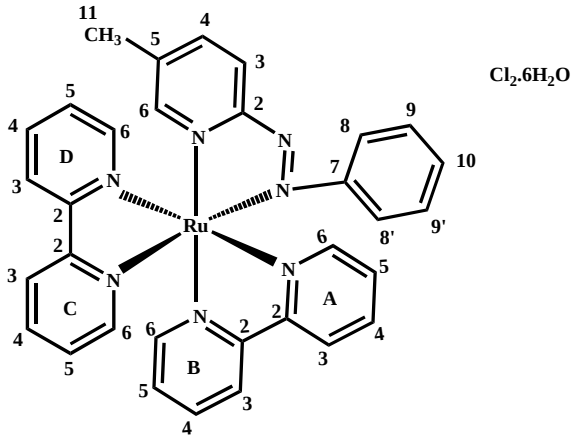

Table 3.44 ^{1}H and ^{13}C NMR of the [Ru(bpy)$_2$5mazpy]Cl$_2$.6H$_2$O complex

H-C Position	^{1}H NMR			^{13}C NMR
	δ (ppm)	J (Hz)	Number of H	δ (ppm)
3(bpy)	8.82 (*d*)	8	1	126.35
3(bpy)	8.81 (*d*)	8	11	126.03
3(5mazpy)	8.80 (*d*)	8	1	129.09
3(bpy)	8.47 (*d*)	8	1	125.43
3(bpy)	8.33 (*d*)	8	1	125.27
4(bpy), 4(bpy)	8.25 (*m*)	-	2	140.92
4(bpy)	8.21 (*dd*)	8, 8	1	140.74
4(5mazpy)	8.16 (*d*)	8	1	12.35
6(bpy)	8.15 (*d*)	6.5	1	154.04
4(bpy)	7.99 (*dd*)	8, 8	1	140.11

Table 3.44 (continued)

H-C Position	^{1}H NMR			^{13}C NMR δ (ppm)
	δ (ppm)	J (Hz)	Number of H	
6(5mazpy)	7.86 (*s*)	-	1	150.25
6(bpy), 6(bpy)	7.74 (*d*)	8	2	153.22, 152.44
5(bpy), 5(bpy) 5(bpy)	7.59 (*m*)	-	3	129.68, 129.56, 129.37
6(bpy)	7.46 (*d*)	6	1	151.69
5(bpy)	7.44 (*dd*)	8, 8	1	129.31
10(5mazpy)	7.33 (*t*)	8	2	131.98
9,9′(5mazpy)	7.16 (*dd*)	8, 8	2	130.15
8,8′(5mazpy)	7.16 (*dd*)	8, 8	2	123.04
11	2.34 (*s*)	-	3	19.02
Quaternary Carbons				165.71, 158.11, 157.55, 157.39, 156.31, 155.80, 141.98

d = doublet, *dd = doublet of doublet*, *ddd = doublet of doublet of doublet*, *m = multiplet*, *s = singlet*, and *t = triplet*

The downfield region (8.82 to 7.44 ppm) of ^{1}H NMR spectrum (Figure 3.122) exhibits five sets of pyridine ring. The fact that the two bpy ligand are non-equivalent upon coordination of 5mazpy. With the use of ^{1}H-^{1}H COSY NMR experiment, the bpy and 5mazpy signals are assigned. The protons on pyridine ring of 5mazpy was assigned using the cross peak at the ^{1}H-^{1}H COSY NMR spectrum (Figure 3.123). The proton H4 (8.16 ppm, *doublet*, J = 8 Hz) of 5mazpy displays intense cross peak with proton H3 (8.80 ppm, *doublet*, J = 8 Hz) and weak cross peak

with proton H6 (7.86 ppm, *singlet*) in COSY NMR spectrum. The proton H3 on pyridine ring C of bpy occurs at the lowest field (8.82 ppm) due to trans to nitrogen atom of azo group. The assignment is performed by comparison with $[Ru(bpy)_3](BF_4)_2$ (Tempiam, S., 2002). In pyridine ring of bpy, proton H3 appears at lowest field, this is similar to the $[Ru(bpy)_3](BF_4)_2$ complex. The phenyl protons occur at the highfield region (7.33 to 7.16 ppm). The triplet peak at 7.33 ppm corresponding to proton H10 are observed. The protons methyl signal are assigned at 2.34 ppm as *singlet* peak.

The ^{13}C NMR spectrum (Figure 3.124) consists with the DEPT 135 NMR spcetrum (Figure 3.125). Twenty-two methine carbons, seven quaternary carbons, and one methyl carbon are observed. The ^{1}H-^{13}C HMQC NMR spectrum (Figure 3.126) shows cross peak which supports the ^{1}H, ^{13}C, DEPT 135, and ^{1}H-^{1}H COSY NMR spectroscopic experiments.

f) Nuclear Magnetic Resonance spectroscopy of the $[Ru(phen)_2 5mazpy]Cl_2.9H_2O$ complex

The ^{1}H and ^{13}C NMR spectroscopic data are listed in Table 3.45.

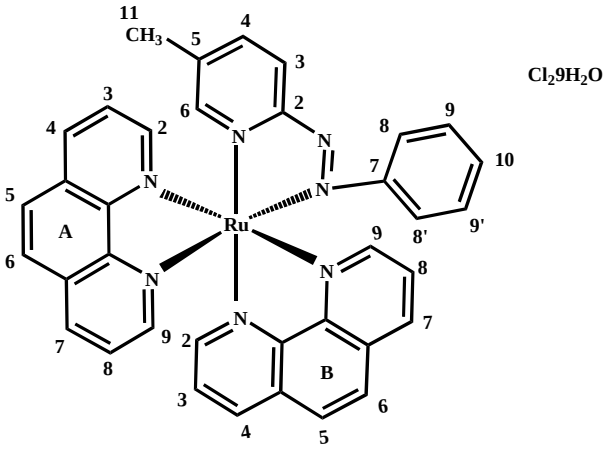

Table 3.45 ^{1}H and ^{13}C NMR of the $[Ru(phen)_2 5mazpy]Cl_2.9H_2O$ complex

H-C Position	^{1}H NMR			^{13}C NMR δ (ppm)
	δ (ppm)	J (Hz)	Number of H	
7A(phen)	8.90 (*d*)	8	1	141.98
4B(phen), 3(5mazpy)	8.85 (*d*)	8, 5	2	140.19, 129.50
4A(phen)	8.79 (*d*)	8	1	139.86
2B(phen)	8.76 (*d*)	5	1	155.73
7B(phen)	8.50 (*d*)	8.5	1	138.89
5,6A(phen)	8.40 (*m*)	-	2	129.31
5B(phen)	8.20 (*d*)	8	1	129.01
4(5mazpy)	8.16 (*d*)	7.5	1	142.31
6B(phen)	8.08 (*d*)	8	1	129.08

Table 3.45 (continued)

H-C Position	^{1}H NMR			^{13}C NMR δ (ppm)
	δ (ppm)	J (Hz)	Number of H	
9A(phen), 8A(phen) 2A(phen), 3B(phen)	8.04 (*m*)	-	4	154.52, 127.97, 152.87, 127.97
9B(phen)	7.89 (*d*)	6.5	1	150.82
6(5mazpy)	7.83 (*s*)	-	1	153.49
3A(phen)	7.76 (*dd*)	8, 8	1	127.64
8B(phen)	7.58 (*dd*)	8, 8	1	127.40
10(5mazpy)	7.09 (*m*)	-	1	131.63
8,8′(5mazpy), 9,9′(5mazpy)	6.92 (*m*)	-	4	125.55, 129.72
11	2.24 (*s*)	-	3	18.94
Quaternary Carbons				166.03, 155.45, 150.79 148.44, 147.99, 147.84 146.97, 132.88, 132.76 132.21, 132.05

d = doublet, *dd = doublet of doublet*, *m = multiplet*, *s = singlet*, and *t = triplet*

The ^{1}H NMR spectrum of [Ru(phen)$_2$5mazpy]Cl$_2$ is shown in Figure 3.127. As this complex has C_1 symmetry, all ligands are inequivalent. Twenty-two proton signals are observed at aromatic region, and one proton signals is found at aliphatic region. The ^{1}H-^{1}H COSY NMR spectrum is shown in Figure 3.128. Using COSY connectivities the other resonances are assigned. Assignments of proton resonances are made by spin-spin splitting, comparative integration and chemical

shift. The proton H7 of phen (A) is assigned the resonance at 8.90 ppm (*doublet*, J = 8 Hz) which occurs at the lowest field due to trans to the azo nitrogen. The 5mazpy signals are clearly present in the ^{1}H NMR spectrum, the proton H6 at 7.83 ppm (*singlet*), the proton H4 at 8.16 ppm (*doublet*, J = 7.5 Hz), and the proton H3 at 8.85 ppm (*doublet*, J = 8 Hz), and the methyl at 2.24 ppm, respectively. The phenyl protons occur at highfield region (7.09 ppm (H10), 6.92 ppm (H8,8′, H9,9′)) which are similarly to [Ru(phen)$_2$5mazpy)](PF$_6$)$_2$.

The ^{13}C NMR spectrum of this complex (Figure 3.129) correlates with the DEPT 135 NMR spectrum (Figure 3.130). There are twenty-two methine carbons, eleven quaternary carbons, and only one methyl carbon in this molecule. Besides, the assignments of all signals were made from ^{1}H-^{13}C HMQC NMR spectroscopy experiment. This spectrum is depicted in Figure 3.131.

3.7 DNA binding

The numerous biological experiments performed so far suggest that DNA is the main cellular target of antitumor drugs because the interaction between small molecules and DNA can cause DNA damage in cancer cells, blocking the division of cancer cells and resulting in cell date (Quiroga *et al*., 1998). In this experiment, we interested to study interaction of ruthenium complexes with calf thymus DNA (CT DNA). The DNA binding of ruthenium(II) complexes, $[Ru(5mazpy)_2L](NO_3)_2$, $[Ru(5mazpy)_2L']Cl_2$, and $[Ru(L')_25mazpy]Cl_2$ (L = azpy, 5mazpy; L′ = bpy, phen), with CT DNA had been monitored by absorption titration, competitive binding and viscosity measurements.

3.7.1 Absorption titration

Absorption spectral titration of the complexes with CT DNA was followed by monitoring the MLCT bands. The absorption spectra of the $[Ru(5mazpy)_3](NO_3)_2.5H_2O$, $[Ru(5mazpy)_2azpy](NO_3)_2.4H_2O$, $[Ru(5mazpy)_2bpy]Cl_2.6H_2O$, $[Ru(5mazpy)_2phen]Cl_2.7H_2O$, $[Ru(bpy)_25mazpy]Cl_2.6H_2O$, and $[Ru(phen)_25mazpy]Cl_2.9H_2O$ complexes in the absence and presence of increasing amounts of CT DNA are shown in Figure 3.132 to Figure 3.137. As the DNA concentration is increased, the MLCT transition bands of $[Ru(5mazpy)_3](NO_3)_2.5H_2O$, $[Ru(5mazpy)_2azpy](NO_3)_2.4H_2O$, $[Ru(bpy)_25mazpy]Cl_2.6H_2O$, and $[Ru(phen)_25mazpy]Cl_2.9H_2O$ at 494 nm and $Ru(5mazpy)_2bpy]Cl_2.6H_2O$, $[Ru(5mazpy)_2phen]Cl_2.7H_2O$ at 515 nm exhibited hypochromism. The binding constant (K_b) for binding of the ruthenium(II) complexes to CT DNA are summarizes in Table 3.46. In the all complexes, although no red shift is found, notable hypochromicities are observed. To compare quantitatively the binding strength of the six complexes, the intrinsic binding, K_b, was determined according to following equation (29) (Wolfe *et al*., 1987).

$$[DNA]/(\varepsilon_a-\varepsilon_f) = [DNA]/(\varepsilon_b-\varepsilon_f) + 1/(K_b(\varepsilon_b-\varepsilon_f)) \quad (29)$$

The ε_a, ε_f and ε_b correspond to $A_{obs}/[Ru]$, the extinction coefficient for the free ruthenium complex and the extinction coefficient for the ruthenium complex in fully bound form, respectively. The slope and y intercept of the linear fit of $[DNA]/(\varepsilon_a-\varepsilon_f)$ versus [DNA] are $1/(\varepsilon_b-\varepsilon_f)$ and $1/K_b(\varepsilon_b-\varepsilon_f)$, respectively. The binding constant (K_b) can be obtained from the slope to the y intercept.

Table 3.46 Absorption spectral data and binding constant (K_b) for binding of the $[Ru(5mazpy)_2L](NO_3)_2$, $[Ru(5mazpy)_2L']Cl_2$ and $[Ru(L')_2 5mazpy]Cl_2$ complexes with CT DNA

Complexes	MLCT λ_{max} (nm)	Hypochromism[a] (%)	K_b (M^{-1})
$[Ru(5mazpy)_3](NO_3)_2.5H_2O$	494	6.08	$1.5(\pm0.1)x10^5$
$[Ru(5mazpy)_2azpy](NO_3)_2.4H_2O$	494	7.73	$1.2(\pm0.2)x10^5$
$[Ru(5mazpy)_2bpy]Cl_2.6H_2O$	515	10.82	$8.5(\pm0.2)x10^4$
$[Ru(5mazpy)_2phen]Cl_2.7H_2O$	515	7.04	$9.0(\pm0.3)x10^4$
$[Ru(bpy)_2 5mazpy]Cl_2.6H_2O$	494	9.17	$6.5(\pm0.2)x10^4$
$[Ru(phen)_2 5mazpy]Cl_2.9H_2O$	494	9.01	$1.5(\pm0.2)x10^5$

[a]In MLCT band; Hypochromism, $[(A_{free}-A_{bound})/A_{free}]x100\%$

The complexes of $[Ru(5mazpy)_3](NO_3)_2.5H_2O$ and $[Ru(5mazpy)_2$ $azpy](NO_3)_2.4H_2O$ exhibit MLCT transition at 494 nm which show a decrease in intensity that a maximum value of 6.08% and 7.73%, respectively as the amount of DNA is increase. Intrinsic binding constants, K_b, of the $[Ru(5mazpy)_3](NO_3)_2$ $.5H_2O$ and $[Ru(5mazpy)_2azpy](NO_3)_2.4H_2O$ complexes are obtained as ca. $1.5(\pm0.1)x10^5$, and $1.2(\pm0.2)x10^5$ M^{-1}, respectively. Then the binding constants of $[Ru(5mazpy)_2bpy]$ $Cl_2.6H_2O$ and $[Ru(5mazpy)_2phen]Cl_2.7H_2O$ are calculated by the ration of slope to intercept as $8.5(\pm0.2)x10^4$ M^{-1} and $9.0(\pm0.3)x10^4$ M^{-1}, respectively.

In addition, the percentage hypochromicities of MLCT band upon binding to DNA are found to be 10.82% and 7.04% for $[Ru(5mazpy)_2bpy]Cl_2.6H_2O$ and $[Ru(5mazpy)_2phen]Cl_2.7H_2O$, respectively. The binding constants of $[Ru(bpy)_25mazpy]Cl_2.6H_2O$ and $[Ru(phen)_2\ 5mazpy]Cl_2.9H_2O$, with calf thymus DNA were determined from the decay of the absorbance monitor at 494 nm of both complexes. The determined binding constants are about $6.5(\pm0.2)x10^4\ M^{-1}$ (%H = 9.17) and $1.5(\pm0.2)x10^5\ M^{-1}$ (%H = 9.01) for $[Ru(bpy)_25mazpy]Cl_2.6H_2O$ and $[Ru(phen)_25mazpy]Cl_2.9H_2O$, respectively.

These values are comparable to that observed for $[Ru(phen)_2phi]^{2+}$ (phi = 9,10-phenanthrenequinonediimine) ($4.7x10^4\ M^{-1}$) (Pyle *et al.*, 1989), but smaller than those observed for $[Ru(bpy)_2(dppz)]^{2+}$ ($>10^6\ M^{-1}$) (Friedman *et al.*, 1990) and $[Ru(ip)_2(dppz)]^{2+}$ (ip = imidazo[4,5-*f*][1,10]phenanthroline) ($2.1x10^7\ M^{-1}$) (Jenkins *et al.*, 1992). The strength of the interaction of complexes with DNA increases in order $[Ru(5mazpy)_3](NO_3)_2.5H_2O$, $[Ru(phen)_2(5mazpy)]Cl_2.9H_2O$, $[Ru(5mazpy)_2azpy](NO_3)_2.4H_2O$, $[Ru(5mazpy)_2phen]Cl_2.7H_2O$, $[Ru(5mazpy)_2bpy]Cl_2.6H_2O$, and $[Ru(bpy)_25mazpy]Cl_2.6H_2O$. The moderate binding for these complexes was comparable to those observed for many ruthenium complexes (Zou *et al.*, 2001), but smaller than the classical interactions and metallointercalators whose binding constants are in the order of 10^7 (Cory *et al.*, 1985).

(a)

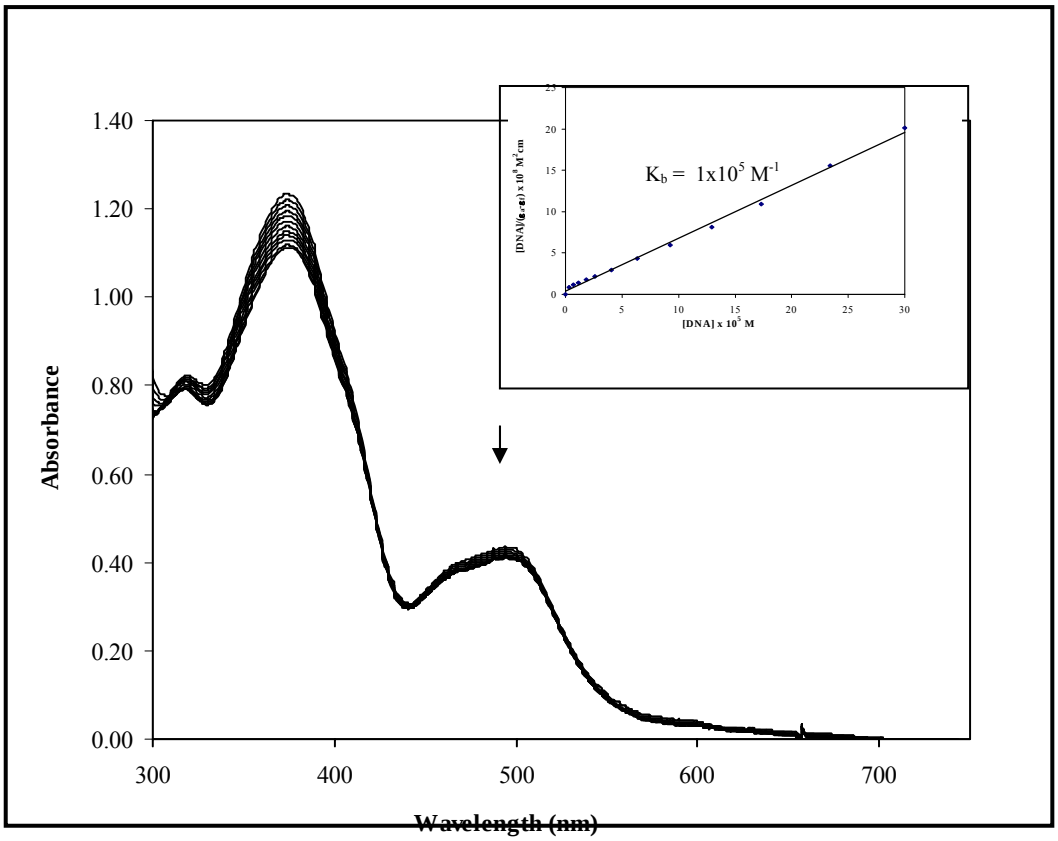

(b)

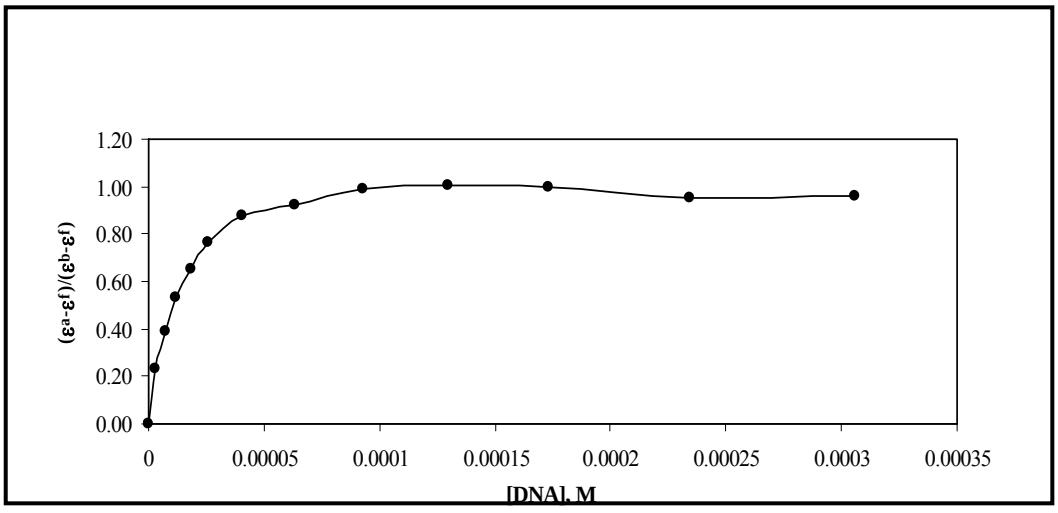

Figure 3.132 (a) Absorption spectra of the $[Ru(5mazpy)_3](NO_3)_2.5H_2O$ complex in tris base buffer pH 7.4 upon addition of CT DNA in the absence (top line) and presence of CT DNA; [Ru] = 40 μM. The arrow showing the intensity change upon increasing DNA concentration. Plot $[DNA]/(\varepsilon_a-\varepsilon_f)$ vs [DNA]. (b) Plots of $(\varepsilon_a-\varepsilon_f)/(\varepsilon_b-\varepsilon_f)$ vs [DNA].

(a)

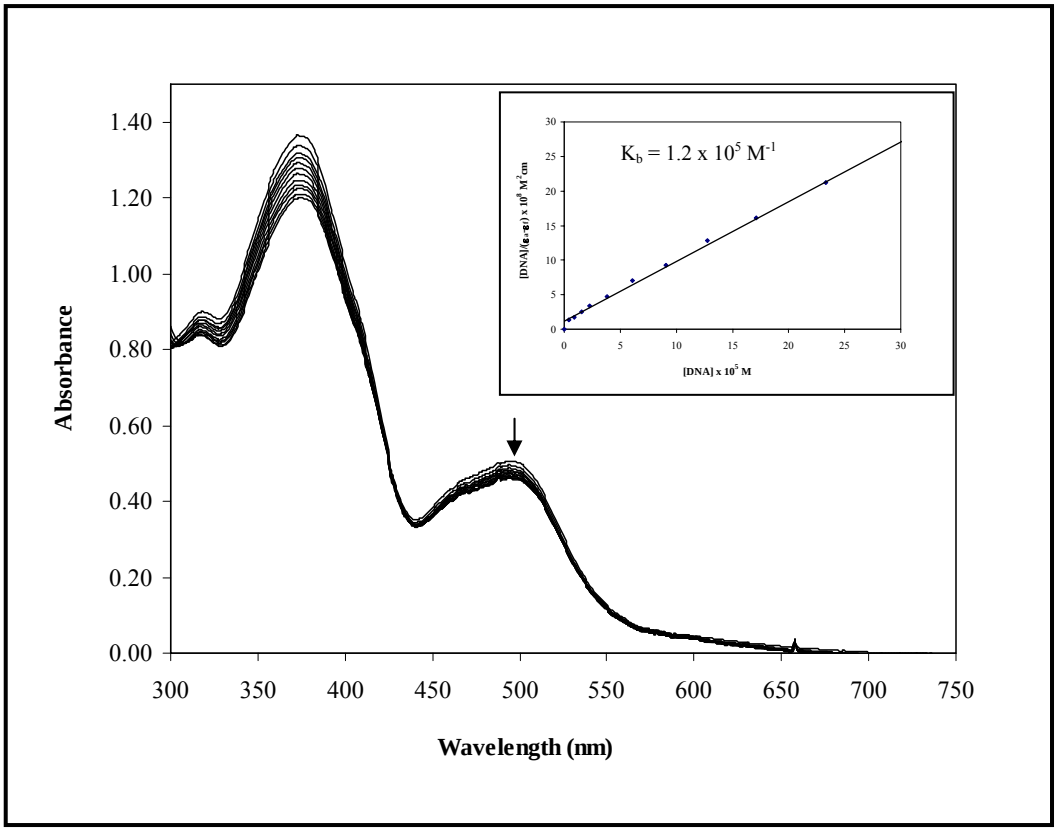

(b)

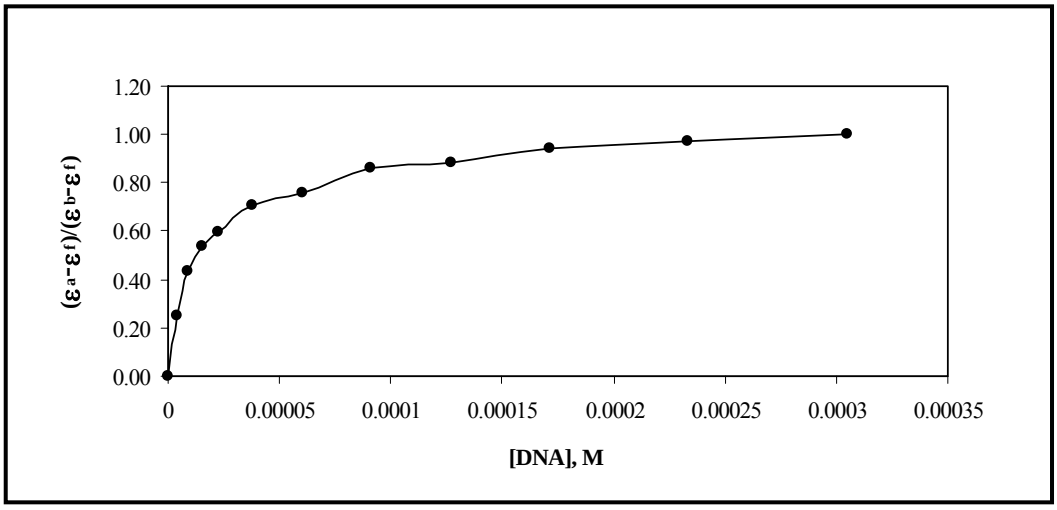

Figure 3.133 (a) Absorption spectra of the $[Ru(5mazpy)_2azpy](NO_3)_2.4H_2O$ complex in tris base buffer pH 7.4 upon addition of CT DNA in the absence (top line) and presence of CT DNA; [Ru] = 40 μM. The arrow showing the intensity change upon increasing DNA concentration. Plot [DNA]/(ε_a-ε_f) vs [DNA]. (b) Plots of (ε_a-ε_f)/(ε_b-ε_f) vs [DNA].

(a)

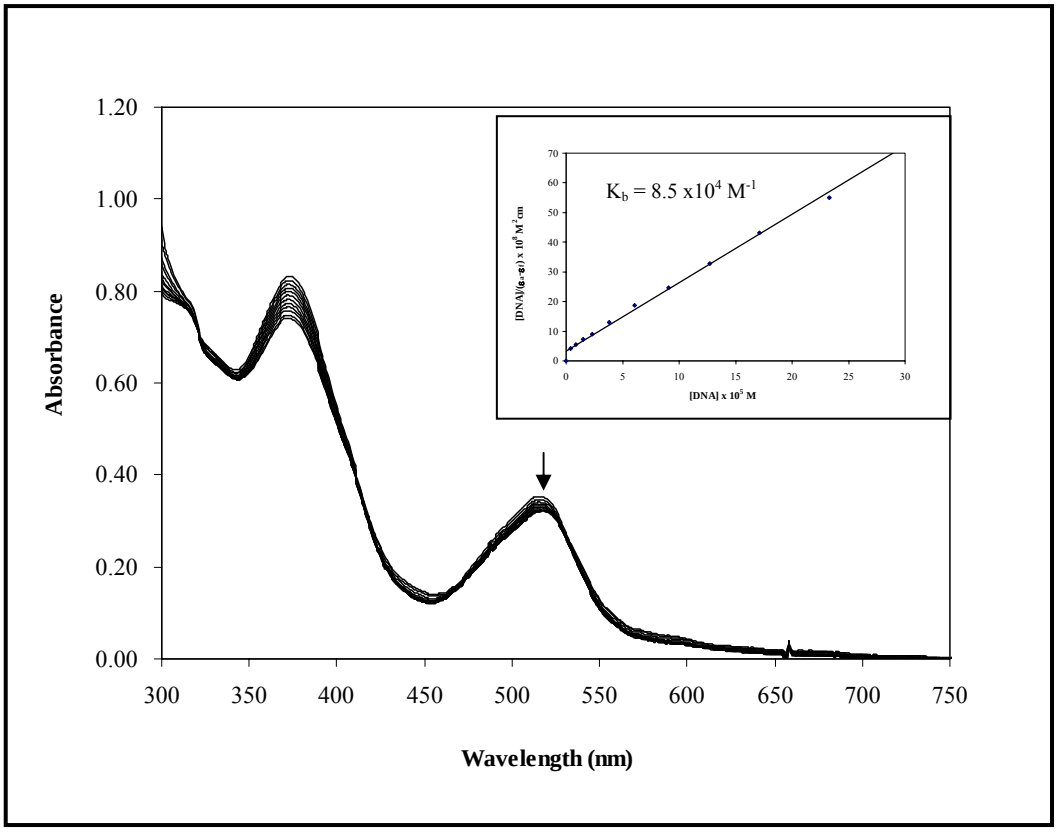

(b)

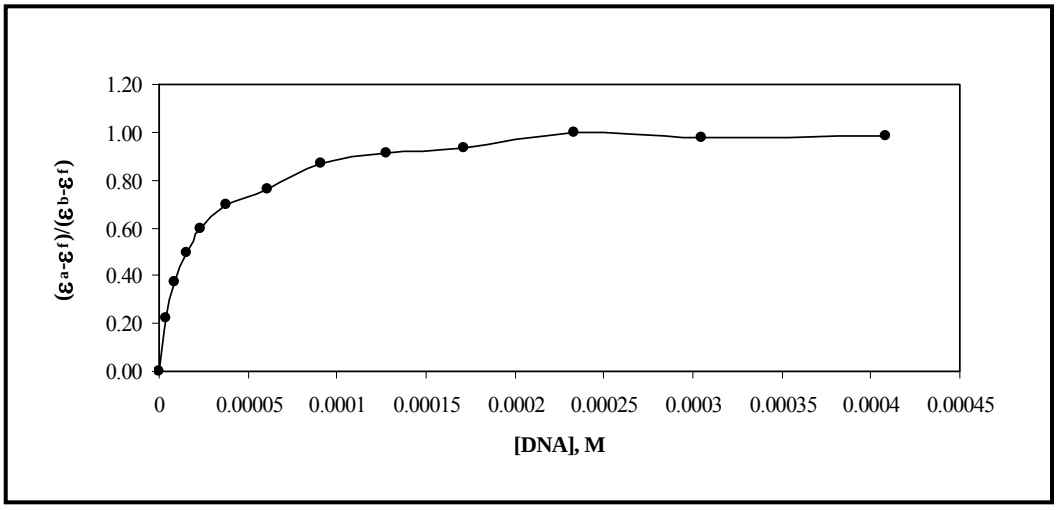

Figure 3.134 (a) Absorption spectra of the [Ru(5mazpy)$_2$bpy]Cl$_2$.6H$_2$O complex in tris base buffer pH 7.4 upon addition of CT DNA in the absence (top line) and presence of CT DNA; [Ru] = 40 μM. The arrow showing the intensity change upon increasing DNA concentration. Plot [DNA]/(ε_a-ε_f) vs [DNA]. (b) Plots of (ε_a-ε_f)/(ε_b-ε_f) vs [DNA].

(a)

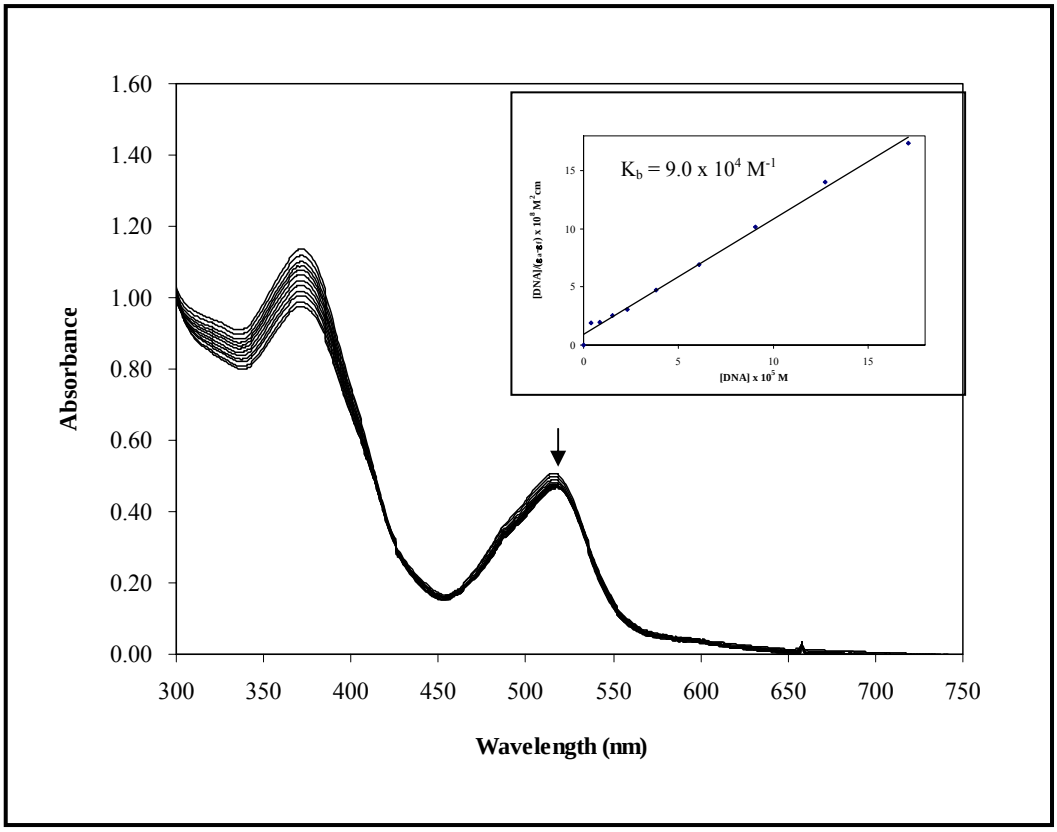

(c)

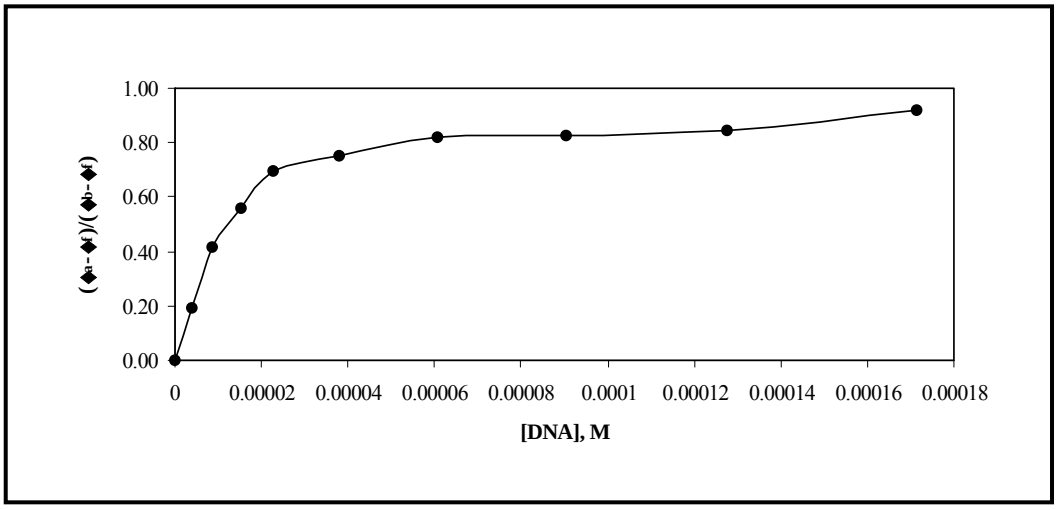

Figure 3.135 (a) Absorption spectra of the $[Ru(5mazpy)_2phen]Cl_2.7H_2O$ complex in tris base buffer pH 7.4 upon addition of CT DNA in the absence (top line) and presence of CT DNA; [Ru] = 40 μM. The arrow showing the intensity change upon increasing DNA concentration. Plot $[DNA]/(\varepsilon_a-\varepsilon_f)$ vs [DNA]. (b) Plots of $(\varepsilon_a-\varepsilon_f)/(\varepsilon_b-\varepsilon_f)$ vs [DNA].

(a)

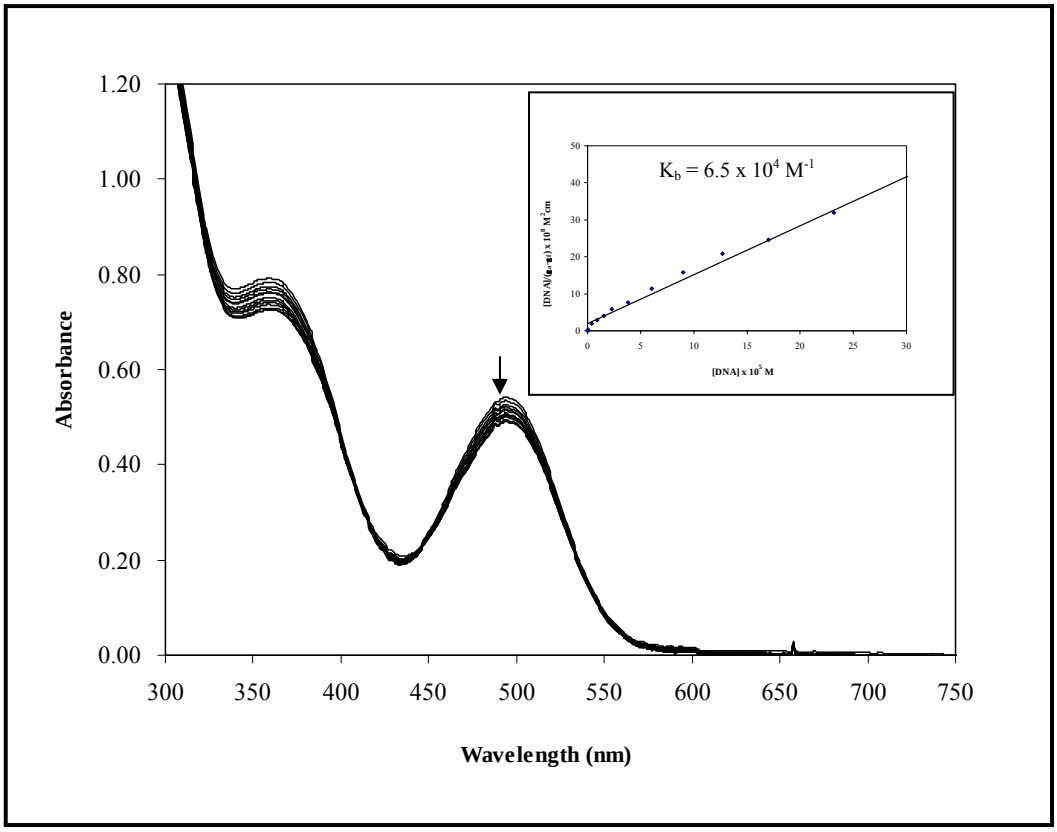

(b)

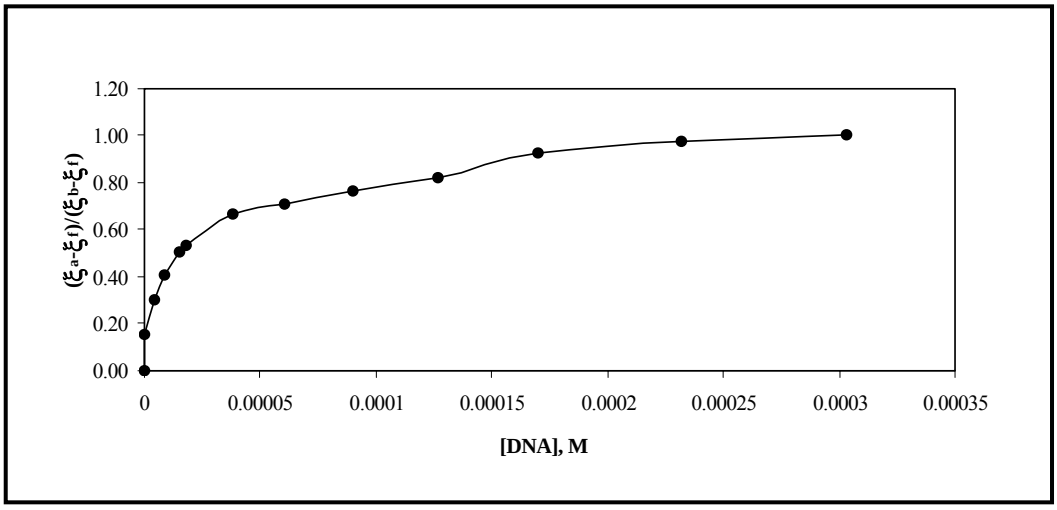

Figure 3.136 (a) Absorption spectra of the $[Ru(bpy)_2 5mazpy]Cl_2.6H_2O$ complex in tris base buffer pH 7.4 upon addition of CT DNA in the absence (top line) and presence of CT DNA; [Ru] = 40 μM. The arrow showing the intensity change upon increasing DNA concentration. Plot $[DNA]/(\varepsilon_a-\varepsilon_f)$ vs [DNA]. (b) Plots of $(\varepsilon_a-\varepsilon_f)/(\varepsilon_b-\varepsilon_f)$ vs [DNA].

(a)

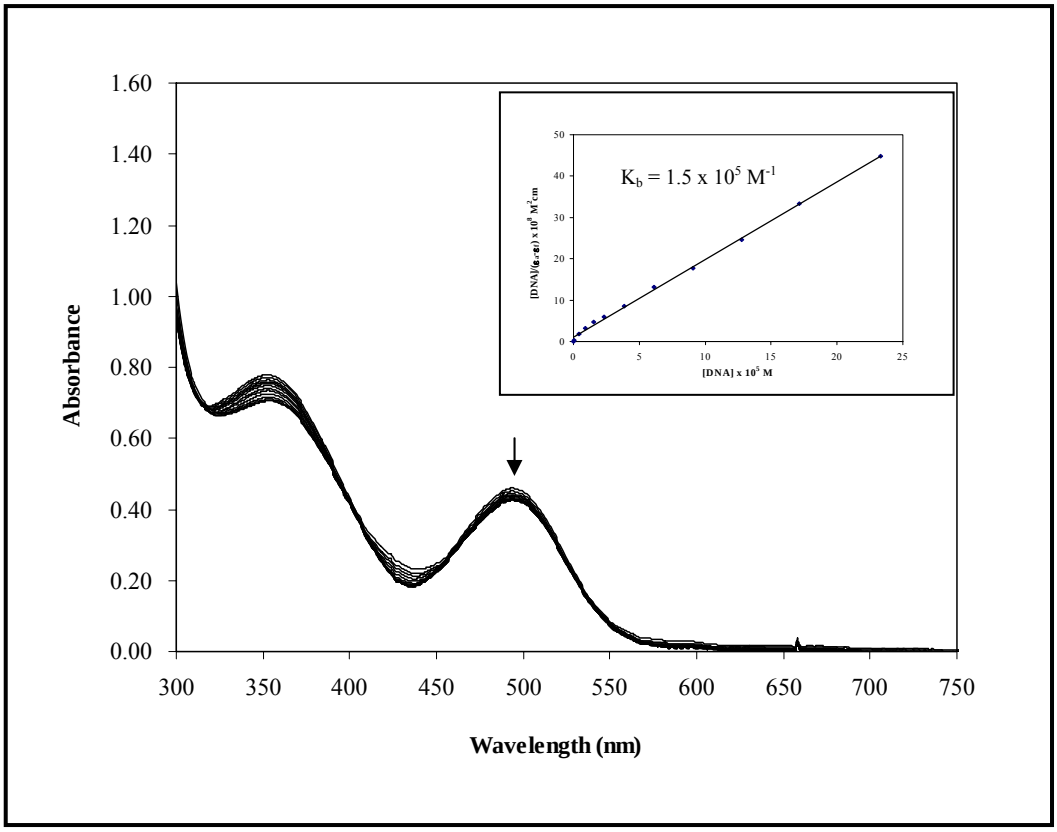

(b)

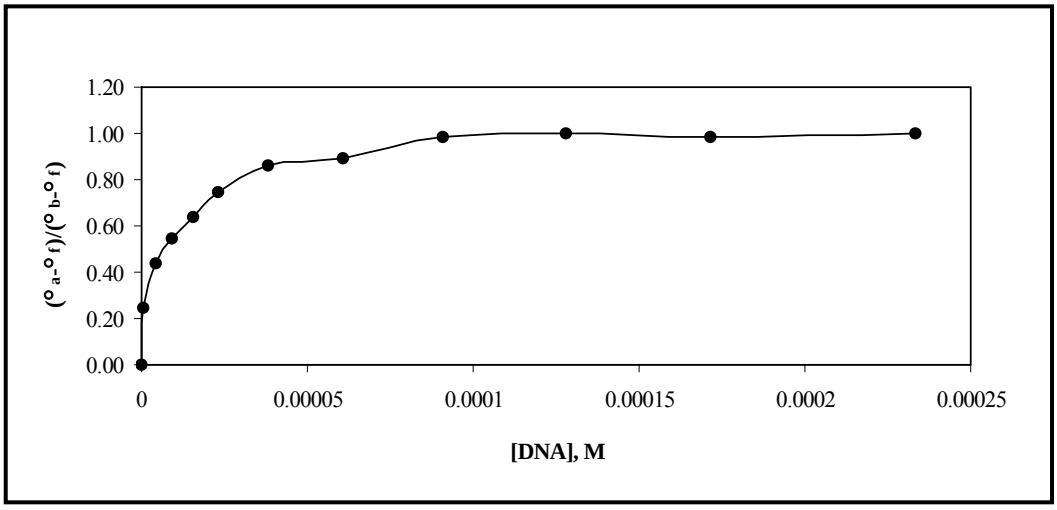

Figure 3.137 (a) Absorption spectra of the $[Ru(phen)_2 5mazpy]Cl_2.9H_2O$ complex in tris base buffer pH 7.4 upon addition of CT DNA in the absence (top line) and presence of CT DNA; [Ru] = 40 μM. The arrow showing the intensity change upon increasing DNA concentration. Plot $[DNA]/(\varepsilon_a-\varepsilon_f)$ vs [DNA]. (b) Plots of $(\varepsilon_a-\varepsilon_f)/(\varepsilon_b-\varepsilon_f)$ vs [DNA].

3.7.2 Competitive binding

No luminescence is observed for all of complexes, $[Ru(5mazpy)_3](NO_3)_2.5H_2O$, $[Ru(5mazpy)_2azpy](NO_3)_2.4H_2O$, $[Ru(5mazpy)_2bpy]Cl_2.6H_2O$, $[Ru(5mazpy)_2phen]Cl_2.7H_2O$, $[Ru(bpy)_25mazpy]Cl_2.6H_2O$, and $[Ru(phen)_25mazpy]Cl_2.9H_2O$ at room temperature in aqueous solution. Hence competitive binding studies using ethidium bromide (EB) bound to DNA were carried out for these complexes. The quenching extent of fluorescence of EB bound to DNA was used to determine the binding of complexes and DNA. Binding of complex results in the displacement of bound EB molecule with a reduction of emission intensity. The addition of the complexes to DNA pretreated with EB caused appreciable reduction in the emission intensity, indicating that the displacement of EB fluorophore by the complexes results in a decrease of the binding of EB to DNA. The data form this experiment were fited into the classical Stern-Volmer equation (30) (Lakowicz and Webber, 1973).

$$I_0/I = 1+Kr \qquad (30)$$

The I_0 and I are the luminescence intensities in the absence and presence of complex, respectively; K is a linear Stern-Volmer quenching constant; r is the ration of total concentration of complex to that of DNA.

The emission spectra of EB bound to DNA in the absence and presence of complex and the fluorescence quenching curves of EB bound to DNA by the ruthenium (II) complexes and are shown in Figure 3.138-3.143. The Emission spectral data and linear Stern-Volmer quenching constant (K) on binding to CT DNA are summarized in Table 3.47.

In the plot of I_0/I versus [Ru]/[DNA], K was given by the ratio of the slope to the intercept. The K values for $[Ru(5mazpy)_3](NO_3)_2.5H_2O$, $[Ru(5mazpy)_2azpy](NO_3)_2.4H_2O$ were estimated using equation (2) which are 4.92 (R = 0.997) and 4.47 (R = 0.992) respectively, and suggest that the interaction of the complex $[Ru(5mazpy)_3](NO_3)_2.5H_2O$ with DNA is strong as compared to that with $[Ru(5mazpy)_2azpy](NO_3)_2.4H_2O$ which is consistent with the above absorption spectral results.

In comparison of the $[Ru(5mazpy)_2bpy]Cl_2.6H_2O$ and $[Ru(5mazpy)_2phen]Cl_2.7H_2O$ complexes, the K of $[Ru(5mazpy)_2bpy]Cl_2.6H_2O$ and $[Ru(5mazpy)_2phen]Cl_2.7H_2O$ are 4.04 and 4.68, respectively; the R values of their linear fit plot of I_0/I versus [Complex]/[DNA] are 0.994 and 0.995, respectively. The data suggest that the interaction of $[Ru(5mazpy)_2phen]Cl_2.7H_2O$ with CT DNA is stronger than $[Ru(5mazpy)_2bpy]Cl_2.6H_2O$ which correspond to the data absorption titration.

The K values for the complexes $[Ru(bpy)_25mazpy]Cl_2.6H_2O$ and $[Ru(phen)_25mazpy]Cl_2.9H_2O$ were 4.37 and 4.46, respectively. According to these data, the magnitude of binding affinity of both complexes with DNA is $[Ru(bpy)_25mazpy]Cl_2.6H_2O$ < $[Ru(phen)_25mazpy]Cl_2.9H_2O$. All of these results are consistent with the above absorption spectral results.

Table 3.47 Emission spectral data and linear Stern-Volmer quenching constants (K) for binding of the $[Ru(5mazpy)_2L](NO_3)_2$, $[Ru(5mazpy)_2L]Cl_2$ and $[Ru(L')_25mazpy]Cl_2$ complexes with CT DNA

Complexes	I_0	I	I_0/I	K	%H
$[Ru(5mazpy)_3](NO_3)_2.5H_2O$	395	335	1.18	4.92	15.19
$[Ru(5mazpy)_2azpy](NO_3)_2.4H_2O$	385	329	1.17	4.74	14.55
$[Ru(5mazpy)_2bpy]Cl_2.6H_2O$	378	330	1.15	4.04	12.70
$[Ru(5mazpy)_2phen]Cl_2.7H_2O$	386	332	1.17	4.68	13.99
$[Ru(bpy)_25mazpy]Cl_2.6H_2O$	401	348	1.15	4.37	13.22
$[Ru(phen)_25mazpy]Cl_2.9H_2O$	384	330	1.16	4.46	14.06

(a)

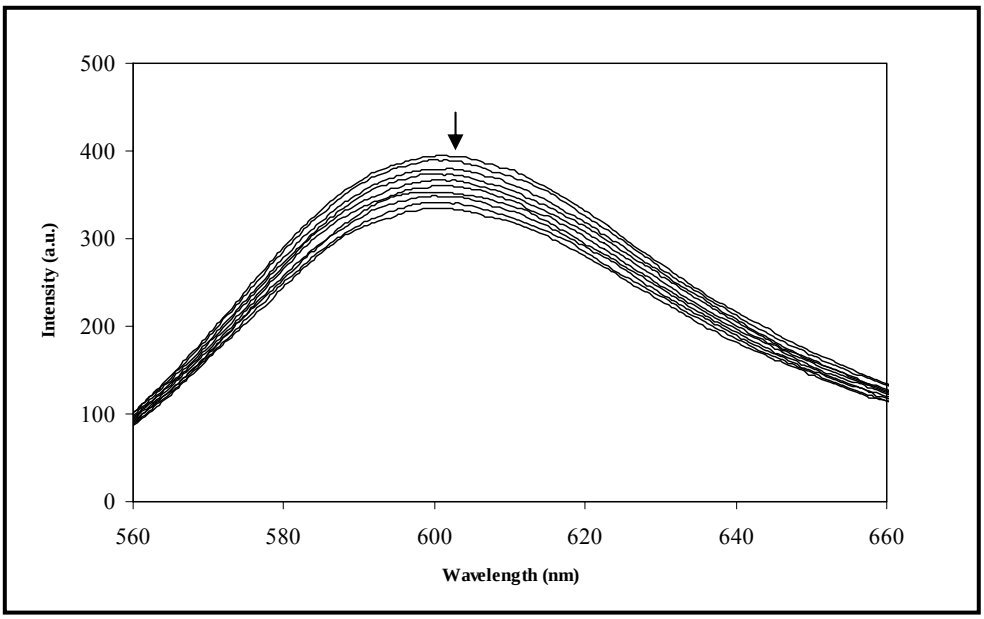

(b)

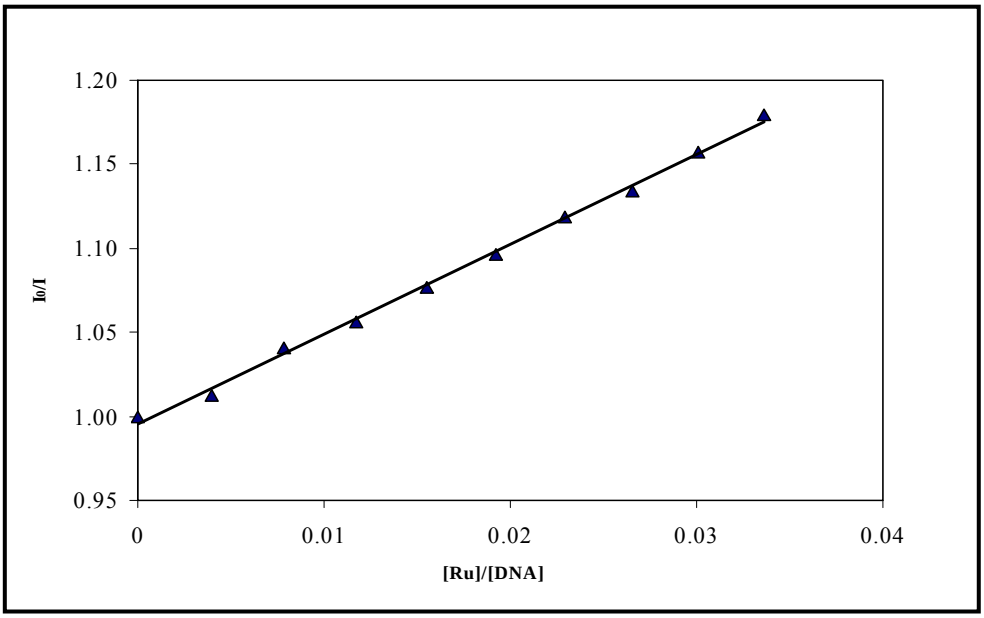

Figure 3.138 (a) Emission spectra (λ_{ex} = 340 nm) of EB in Tris-base buffer in the absence (top line) and presence of increasing of concentrations of the $[Ru(5mazpy)_3](NO_3)_2.5H_2O$ complex. Arrow shows that the intensity changes upon increasing concentrations. (b) Fluorescence quenching curves of EB bound to DNA by $[Ru(5mazpy)_3](NO_3)_2.5H_2O$ ([EB] = 2 μM, [DNA] = 40 μM, [Ru] = 20 μM; λ_{ex} = 340 nm)

(a)

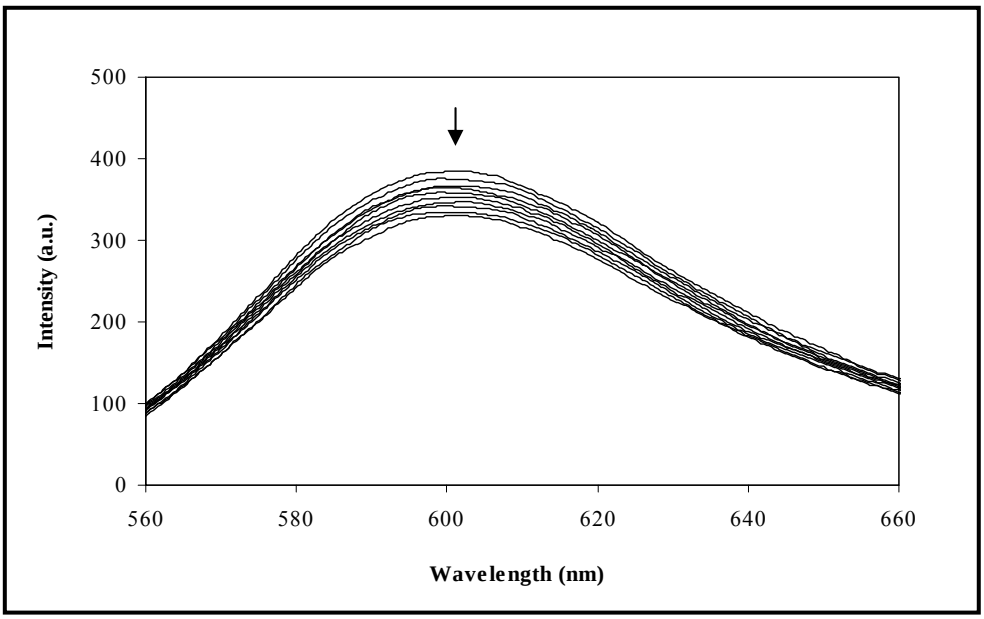

(b)

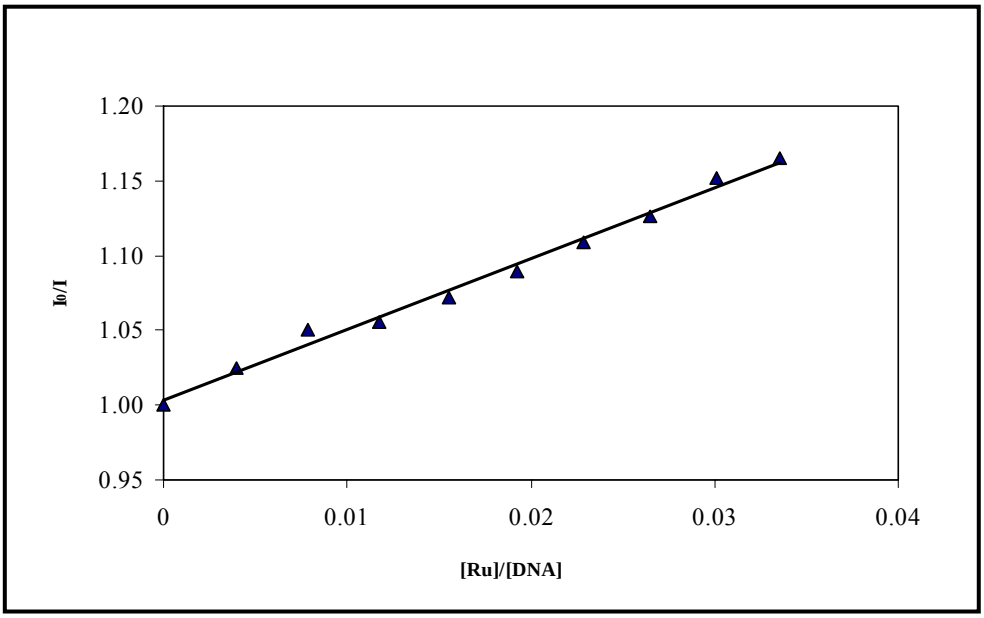

Figure 3.139 (a) Emission spectra (λ_{ex} = 340 nm) of EB in Tris-base buffer in the absence (top line) and presence of increasing of concentrations of the $[Ru(5mazpy)_2azpy](NO_3)_2.4H_2O$ complex. Arrow shows that the intensity changes upon increasing concentrations. (b) Fluorescence quenching curves of EB bound to DNA by $[Ru(5mazpy)_2azpy](NO_3)_2 .4H_2O$ ([EB] = 2 μM, [DNA] = 40 μM, [Ru] = 20 μM; λ_{ex} = 340 nm)

(a)

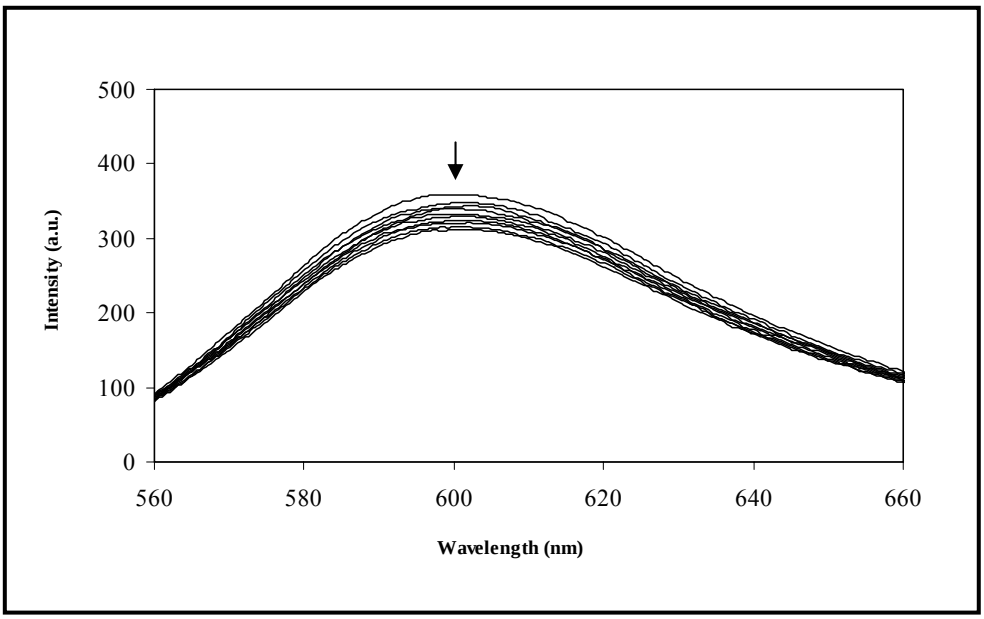

(b)

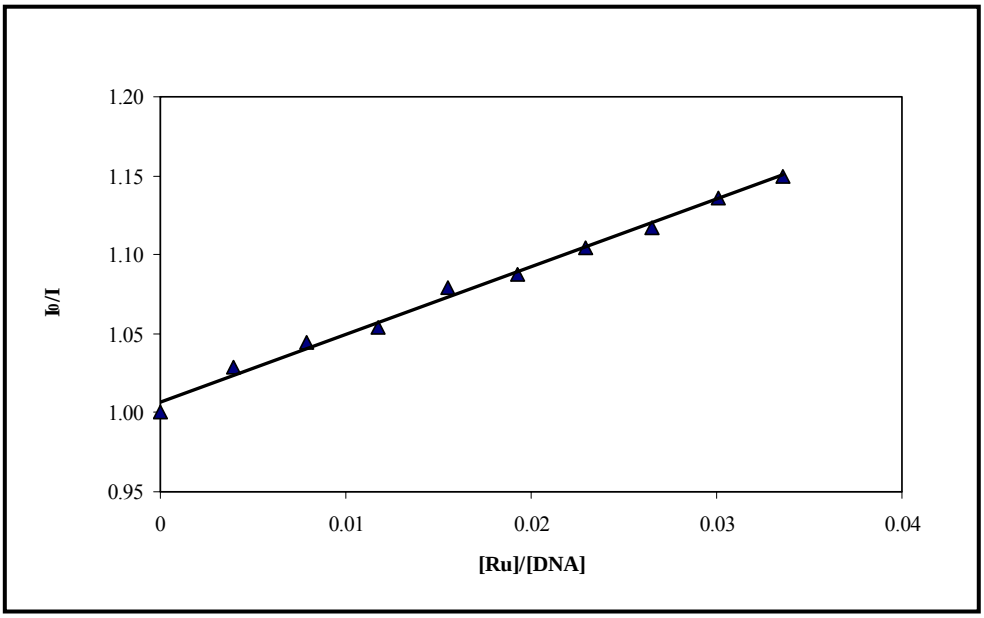

Figure 3.140 (a) Emission spectra (λ_{ex} = 340 nm) of EB in Tris-base buffer in the absence (top line) and presence of increasing of concentrations of the $[Ru(5mazpy)_2bpy]Cl_2.6H_2O$ complex. Arrow shows that the intensity changes upon increasing concentrations. (b) Fluorescence quenching curves of EB bound to DNA by $[Ru(5mazpy)_2bpy]Cl_2.6H_2O$ ([EB] = 2 μM, [DNA] = 40 μM, [Ru] = 20 μM; λ_{ex} = 340 nm)

(a)

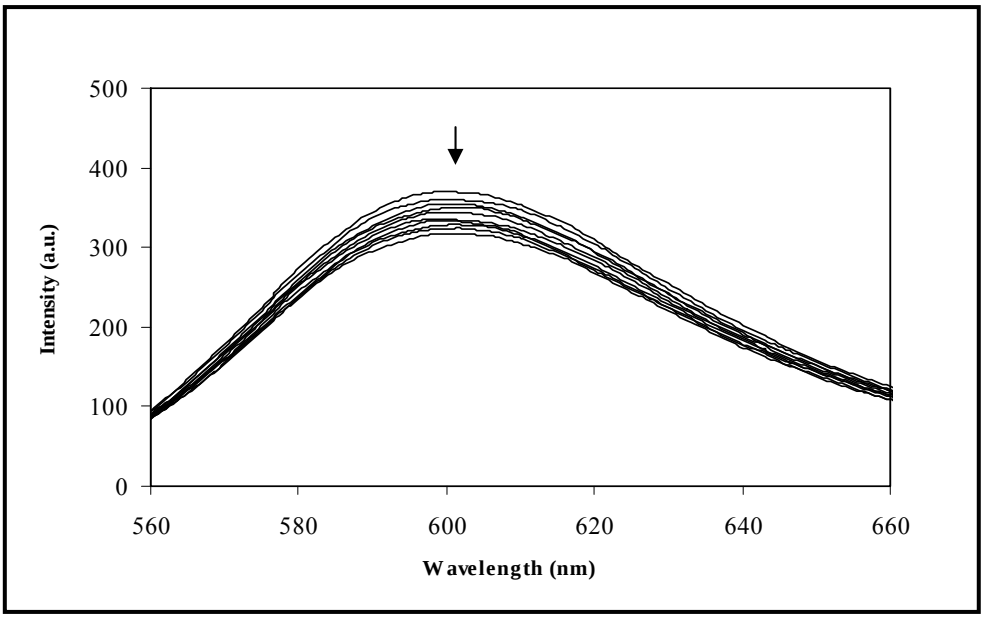

(b)

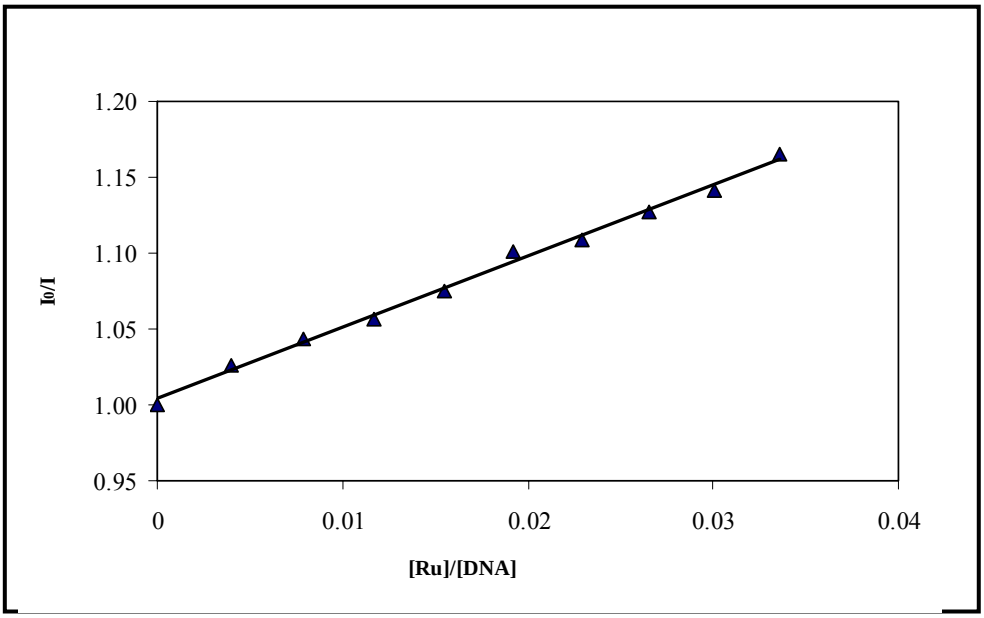

Figure 3.141 (a) Emission spectra (λ_{ex} = 340 nm) of EB in Tris-base buffer in the absence (top line) and presence of increasing of concentrations of the $[Ru(5mazpy)_2phen]Cl_2.7H_2O$ complex. Arrow shows that the intensity changes upon increasing concentrations. (b) Fluorescence quenching curves of EB bound to DNA by $[Ru(5mazpy)_2phen]Cl_2.7H_2O$ ([EB] = 2 μM, [DNA] = 40 μM, [Ru] = 20 μM; λ_{ex} = 340 nm)

(a)

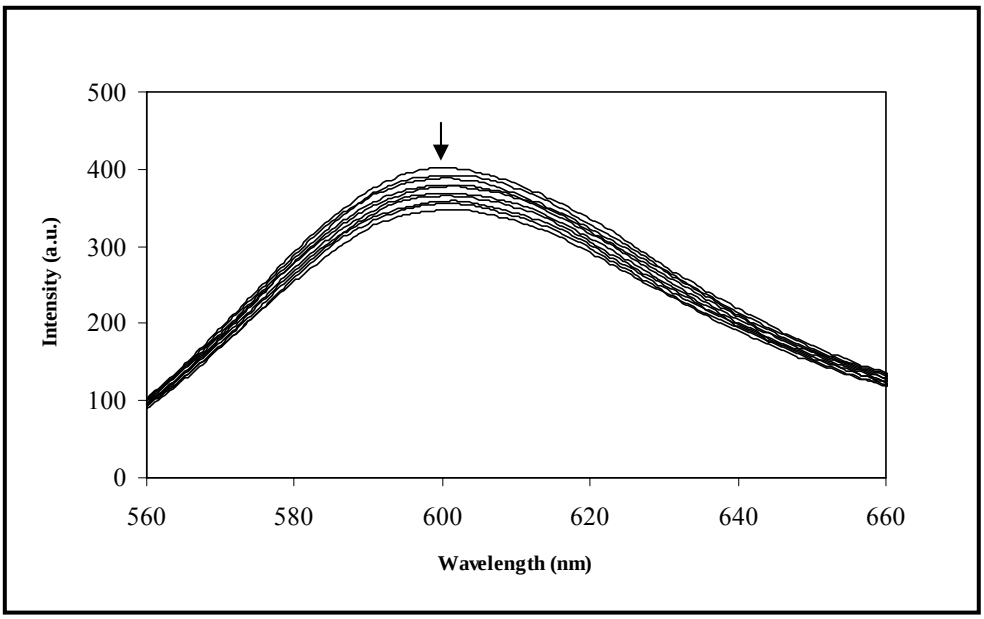

(b)

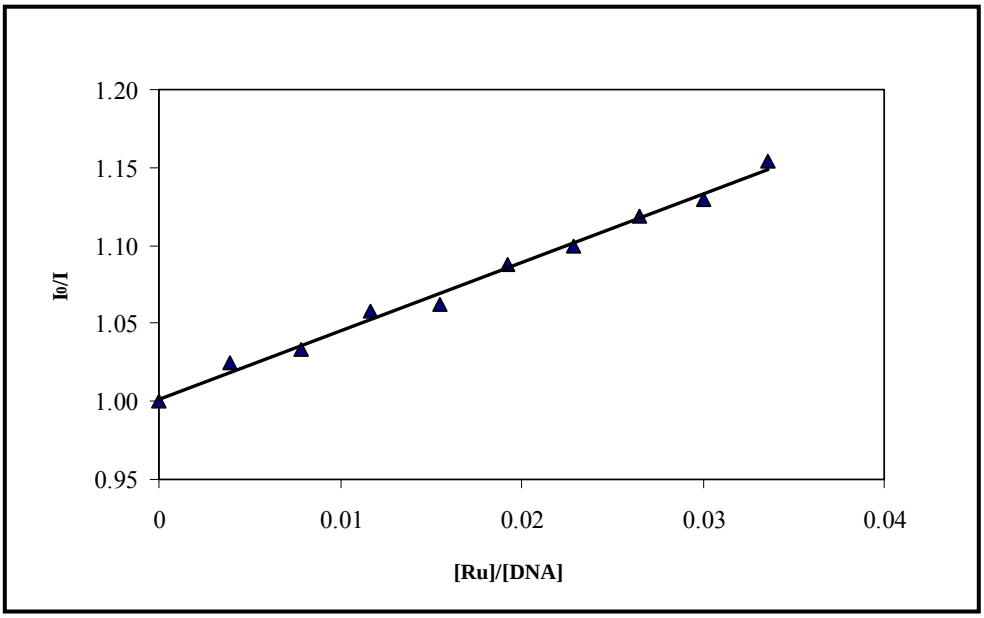

Figure 3.142 (a) Emission spectra (λ_{ex} = 340 nm) of EB in Tris-base buffer in the absence (top line) and presence of increasing of concentrations of the $[Ru(bpy)_2 5mazpy]Cl_2.6H_2O$ complex. Arrow shows that the intensity changes upon increasing concentrations. (b) Fluorescence quenching curves of EB bound to DNA by $[Ru(bpy)_2 5mazpy]Cl_2.6H_2O$ ([EB] = 2 μM, [DNA] = 40 μM, [Ru] = 20 μM; λ_{ex} = 340 nm)

(a)

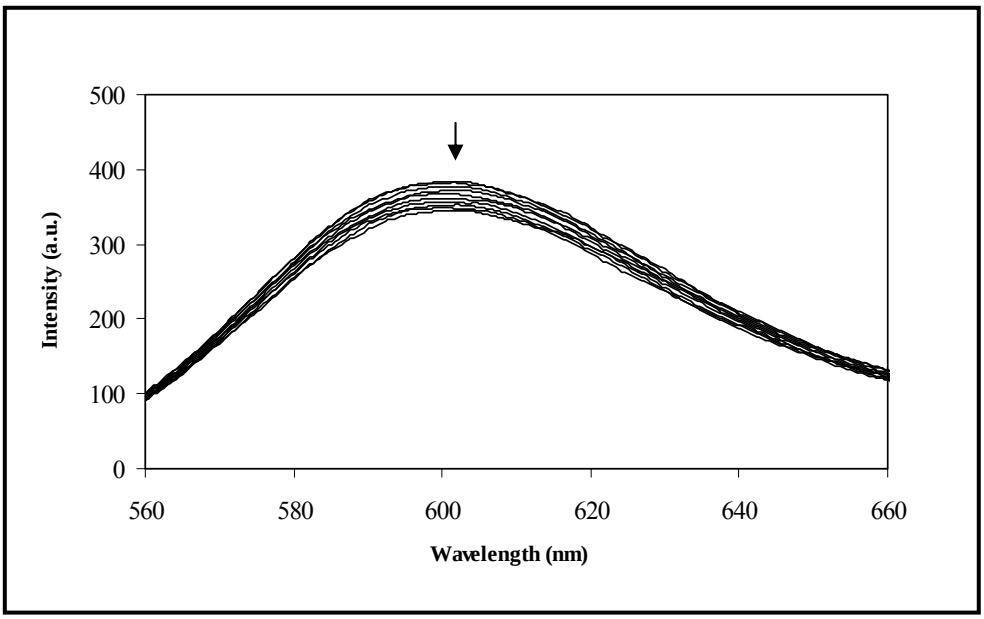

(b)

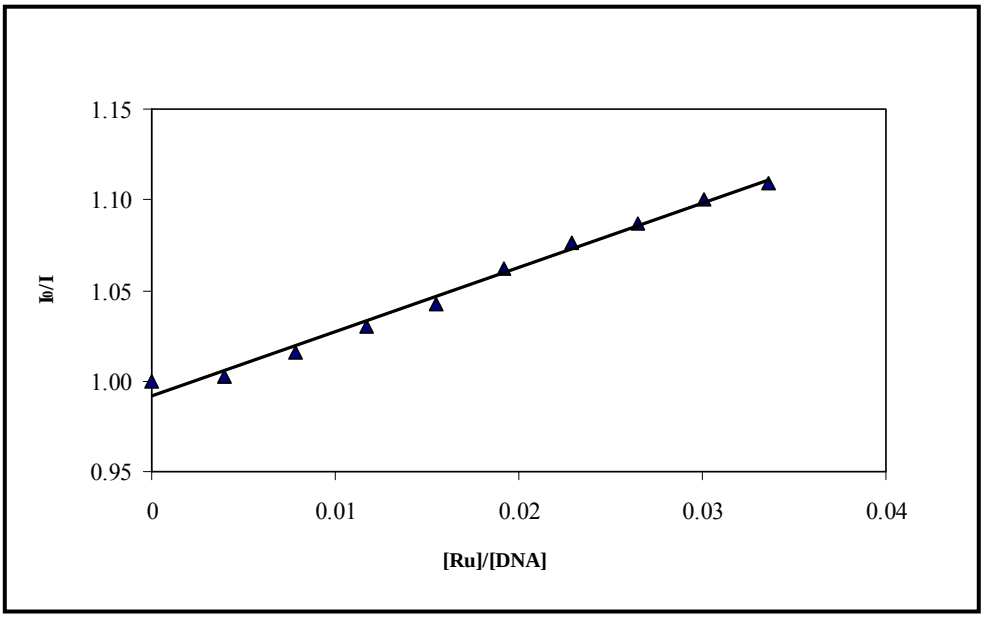

Figure 3.143 (a) Emission spectra (λ_{ex} = 340 nm) of EB in Tris-base buffer in the absence (top line) and presence of increasing of concentrations of the $[Ru(phen)_2 5mazpy]Cl_2.9H_2O$ complex. Arrow shows that the intensity changes upon increasing concentrations. (b) Fluorescence quenching curves of EB bound to DNA by $[Ru(phen)_2 5mazpy]Cl_2.9H_2O$ ([EB] = 2 μM, [DNA] = 40 μM, [Ru] = 20 μM; λ_{ex} = 340 nm)

3.7.3 Viscosity measurements

Further clarification of the interaction between the ruthenium complexes and DNA was carried out by viscosity measurements. Hydrodynamic measurements that are sensitive to length change (i.e., viscosity, sedimentation) and are regarded as the least ambiguous and the most critical tests of binding in solution in the absence of crystallographic structural data. A classical intercalation model results in lengthening the DNA helix, as base pairs are separated to accommodate the binding ligand, leading to the increase of DNA viscosity. In contrast, a partial and/or non-classical intercalation of ligand could bind (or kink) the DNA helix, reducing its effective length and, concomitantly, its viscosity (Satyanarayana *et al.*, 1992). Effects of the complexes together with $[Ru(bpy)_3]Cl_2.7H_2O$ and Eithidium Bromide EB on the viscosity are shown in Figure 3.144-3.146. Ethidium bromide (EB) is a known DNA classical intercalator and increase the relative specific viscosity for the lengthening of the DNA double helix through the intercalation mode; while for complex $[Ru(bpy)_3]^{2+}$ which has been well known to bind with DNA only through the electrostatic mode, it exerts essentially no effect on DNA viscosity.

The effects of $[Ru(5mazpy)_3](NO_3)_2.5H_2O$, $[Ru(5mazpy)_2azpy](NO_3)_2.4H_2O$ on the viscosity of CT DNA is shown in Figure 3.144. The viscosity of CT DNA bound with the both complexes and EB increase dramatically, indicating that both complexes intercalate the base pairs of DNA but is still smaller than those bound with EB. The experimental results suggest that the relative viscosity of CT DNA increase, which follows the order EB > $[Ru(5mazpy)_3](NO_3)_2.5H_2O$ > $[Ru(5mazpy)_2azpy](NO_3)_2.4H_2O$.

The effects of the $[Ru(5mazpy)_2bpy]Cl_2.6H_2O$, together with $[Ru(5mazpy)_2phen]Cl_2.7H_2O$, on the viscosity of rod-like DNA are shown in Figure 3.145. Upon increasing concentration of $[Ru(5mazpy)_2bpy]Cl_2.6H_2O$ and $[Ru(5mazpy)_2phen]Cl_2.7\ H_2O$, the viscosity of the DNA also increase but is smaller than those bound with EB. The results indicat that $[Ru(5mazpy)_2phen]Cl_2.7H_2O$ can intercalate into DNA base pairs slightly stronger than $[Ru(5mazpy)_2bpy]Cl_2.6H_2O$.

Figure 3.146 shows the effects of $[Ru(bpy)_25mazpy]Cl_2.6H_2O$ and $[Ru(phen)_25mazpy]Cl_2.9H_2O$ on the viscosity of CT DNA. On increasing the

amounts of $[Ru(bpy)_2 5mazpy]Cl_2.6H_2O$ and $[Ru(phen)_2 5mazpy]Cl_2.9H_2O$, the relative viscosity of DNA increase steadily, this is similar to the behavior of EB. The increase degree of viscosity, which may depend on its affinity to DNA, follows the order of EB > $[Ru(phen)_2 5mazpy]Cl_2.9H_2O$ > $[Ru(bpy)_2 5mazpy]Cl_2.6H_2O$. The results from the viscosity are consistent with the spectroscopic results.

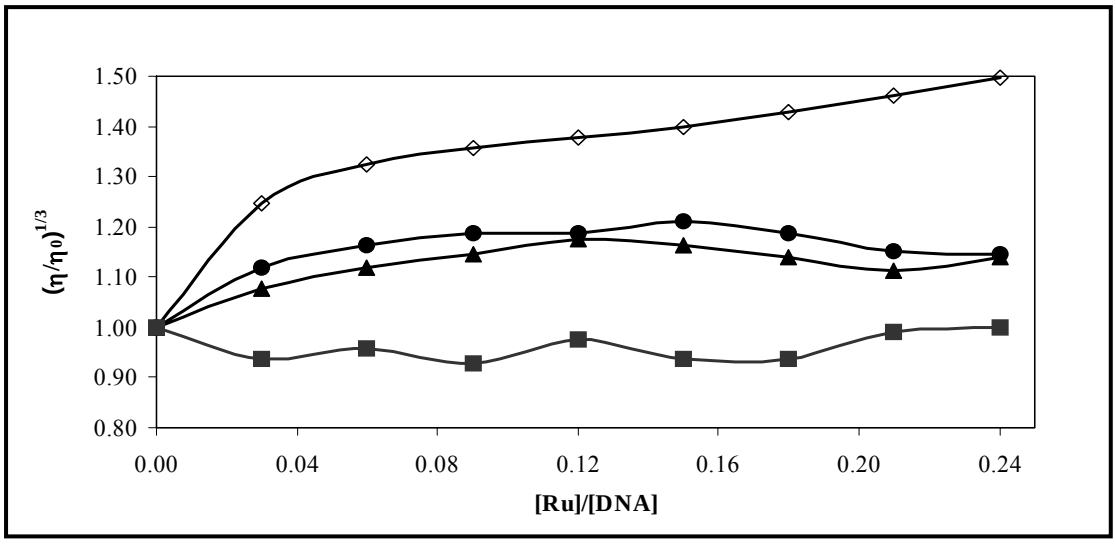

Figure 3.144 Effects of increasing amount of the complexes of $[Ru(5mazpy)_3](NO_3)_2.5H_2O$ (●), $[Ru(5mazpy)_2azpy](NO_3)_2.4H_2O$ (▲), $[Ru(bpy)_3]Cl_2.6H_2O$ (■) and Ethidium Bromide (◇) on relative viscosities of CT DNA at 25°C. ([DNA] = 300 μM, [Ru]/[DNA] = 0 to 0.24 μM)

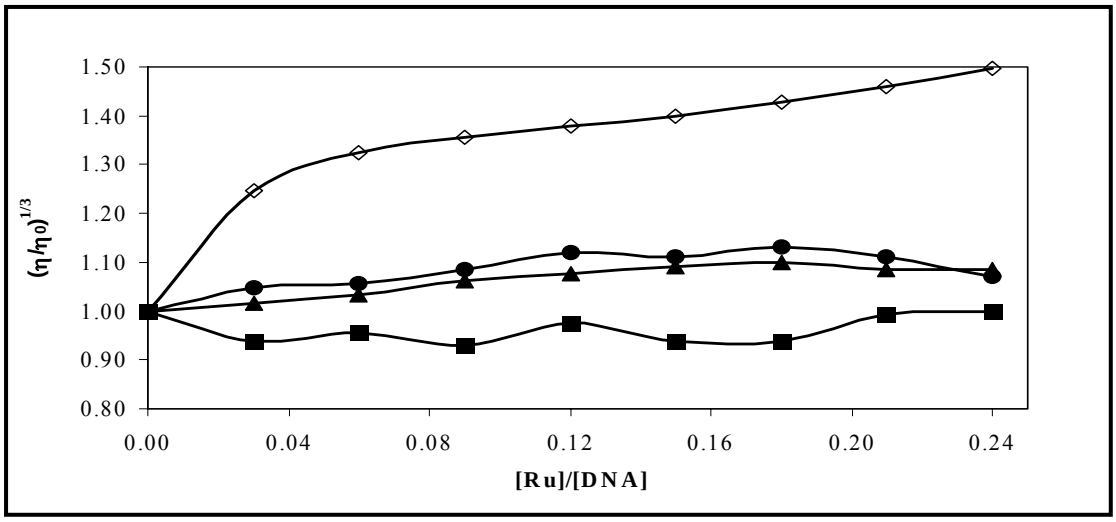

Figure 3.145 Effects of increasing amount of the complexes of $[Ru(5mazpy)_2bpy]Cl_2.6H_2O$ (▲), $[Ru(5mazpy)_2phen]Cl_2.7H_2O$ (●), $[Ru(bpy)_3]Cl_2.6H_2O$ (■) ,and Ethidium Bromide (◇)on relative viscosities of CT DNA at 25°C. ([DNA] = 300 μM, [Ru]/[DNA] = 0 to 0.24 μM)

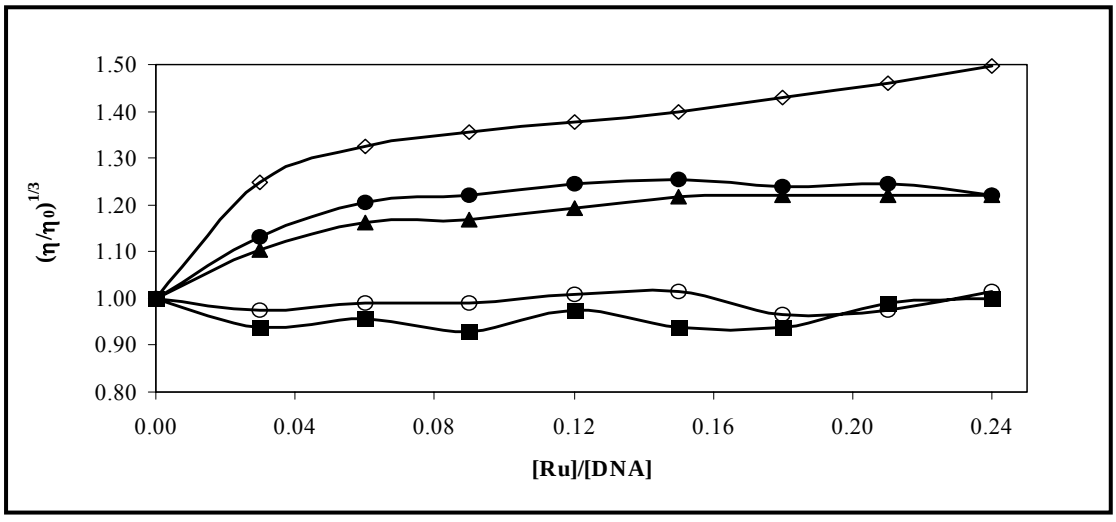

Figure 3.146 Effects of increasing amount of the $[Ru(bpy)_25mazpy]Cl_2.6H_2O$ (▲), $[Ru(phen)_25mazpy]Cl_2.9H_2O$ (●), $[Ru(bpy)_3]Cl_2.6H_2O$ (■), $[Ru(phen)_3]Cl_2.7H_2O$ (○) complexes and Ethidium Bromide (◇)on relative viscosities of CT DNA at 25°C. ([DNA] = 300 μM, [Ru]/[DNA] = 0 to 0.24 μM)

3.7.4 Cyclic voltammetry

The application of electrochemical methods to study of metallointercalation and coordination of metal ions and chelates to DNA provides a useful complement to the previously used methods of investigation, such as UV-Visible spectroscopy. A summary of the voltammetric results is given in Table 3.48 and typical CV responses of ruthenium complexes in Tris-base buffer in the presence and absence of CT DNA are shown in Figure 3.147 to Figure 3.152.

On the addition of DNA (R = 5) to all the complexes, the peak potential seperation ΔE_p decrease or increase depending on the ligand. The $E_{1/2}$ values of the DNA-bound complexes follow the same order as that for free complexes. Analogous to the treatment of the association of small molecules with micelles (Kaifer and Bard 1985). In addition, the positive shifts of peak potentials indicate that this interaction mode may be intercalation between ruthenium complex and DNA (Carter and Bard, 1987). The formal potentials, ($E_{1/2}$) were taken as the average of the anodic (E_{pa}) and cathodic peak potentials (E_{pc}) obtained from cyclic voltammetry. The net shift in $E_{1/2}$ can be used to estimate the ratio of equilibrium constants for the binding of Ru(II) and Ru(III) complexes to DNA using the equation (31) (Maheswari and Palaniandavar, 2004).

$$E^{0\prime}{}_b - E^{0\prime}{}_f = 0.059 \log(K_{2+}/K_{3+}) \qquad (31)$$

The $E^{0\prime}{}_b$ and $E^{0\prime}{}_f$ are the formal potentials of the 3+/2+ couple in the free and bound forms, respectively, and K_{2+} and K_{3+} are the binding constants for the respective binding of 2+ and 3+ species to DNA.

All of complexes, the cyclic voltammetric data of complexes in the absence and presence of DNA showed only reduction peak. In this work, the first reduction peak was used to estimated the K_{2+}/K_{3+} value. In the absence of DNA, the ligand based reduction is observed at -0.53 V and -0.54 V for $[Ru(5mazpy)_3](NO_3)_2 .5H_2O$ (Figure 3.147) and $[Ru(5mazpy)_2azpy](NO_3)_2.4H_2O$ (Figure 3.148), respectively. In the absence of DNA this peak shifts to -0.50 V and -0.52 V for the former and latter complexes, respectively .

The cyclic voltammograms of $[Ru(5mazpy)_2bpy]Cl_2.6H_2O$ and $[Ru(5mazpy)_2phen]Cl_2.7H_2O$ in the absenc and presence of DNA are displayed in Figure 3.149 and 3.150, respectively. In the absence of DNA, the E_{pc} of -0.71 V for $[Ru(5mazpy)_2bpy]Cl_2.6H_2O$, -0.67 V $[Ru(5mazpy)_2phen]Cl_2.7H_2O$ and the E_{pa} of both complexes occurs at -0.64 V and -0.61 V, respectively. The formal potential $E_{1/2}$, take as the average of E_{pc}, are -0.64, and -0.63 V, respectively. In the presence of DNA, the formal potential $E_{1/2}$ of $[Ru(5mazpy)_2bpy]Cl_2.6H_2O$ and $[Ru(5mazpy)_2phen]Cl_2.7H_2O$ are -0.57, and -0.55 V, respectively. In the solution at the same concentration of both complexes caused a shift to positive potential.

The $[Ru(bpy)_25mazpy]Cl_2.6H_2O$ (Figure 3.151) and $[Ru(phen)_25mazpy]Cl_2.9H_2O$ (Figure 3.152) complexes shows the irreversible wave peak. The anodic peak potential in the absence of DNA of $[Ru(bpy)_25mazpy]Cl_2.6H_2O$ and $[Ru(phen)_25mazpy]Cl_2.9H_2O$ at -0.96 V, and -0.98 V, respectively. The anodic peak potential of the reduction of ligand has been found to shift to a more positive value of -0.92 V ($[Ru(bpy)_25mazpy]Cl_2.6H_2O$) and -0.90 V ($[Ru(phen)_25mazpy]Cl_2.9H_2O$) in the presence of DNA.

Table 3.48 Cyclic voltammetric data behaviour[a] of the $[Ru(5mazpy)_2L]Cl_2$, $[Ru(5mazpy)_2L']$$(NO_3)_2$ and $[Ru(L')_25mazpy]Cl_2$ complexes in the absence and presence of CT DNA

Complexes	R [b]	E_{pa} (V)	E_{pc} (V)	ΔE_p (mV)	$E_{1/2}$ (V)	K_{2+}/K_{3+} [c]
$[Ru(5mazpy)_3](NO_3)_2.5H_2O$	0	-0.49	-0.56	70	-0.53	3.24
	5	-0.46	-0.54	80	-0.50	
$[Ru(5mazpy)_2azpy](NO_3)_2.4H_2O$	0	-0.50	-0.57	70	-0.54	2.19
	5	-0.48	-0.56	80	-0.52	
$[Ru(5mazpy)_2bpy]Cl_2.6H_2O$	0	-0.57	-0.71	136	-0.64	15.49
	5	-0.50	-0.64	138	-0.57	
$[Ru(5mazpy)_2phen]Cl_2.7H_2O$	0	-0.60	-0.67	64	-0.63	22.91
	5	-0.53	-0.58	52	-0.55	

Table 3.48 (continued)

Complexes	R[b]	E_{pa} (V)	E_{pc} (V)	ΔE_p (mV)	$E_{1/2}$ (V)	K_{2+}/K_{3+}[c]
$[Ru(bpy)_2 5mazpy]Cl_2.6H_2O$	0	-0.96	-	-	-0.96	4.79
	5	-0.92	-	-	-0.92	
$[Ru(phen)_2 5mazpy]Cl_2.9H_2O$	0	-0.98	-	-	-0.98	22.91
	5	-0.90	-	-	-0.90	

[a] Measured vs ferrocene methanol, scan rate 100 mVs^{-1}; supporting electrolyte (pH 7.1); complex concentration $5x10^{-4}$ M.

[b] R = [DNA]/[Ruthenium]

[c] Based on $E_{1/2}$ values from cyclic voltammetry measurements.

On the addition of DNA (R = 5) to all the complexes, the reduction peak shifts to less negative potential and slightly drop of the voltammetric currents which can be attributed to diffusion of the metal complexes bound to the large, slowly diffusing DNA molecule. The results parallel to the above spectroscopic and viscosity data.

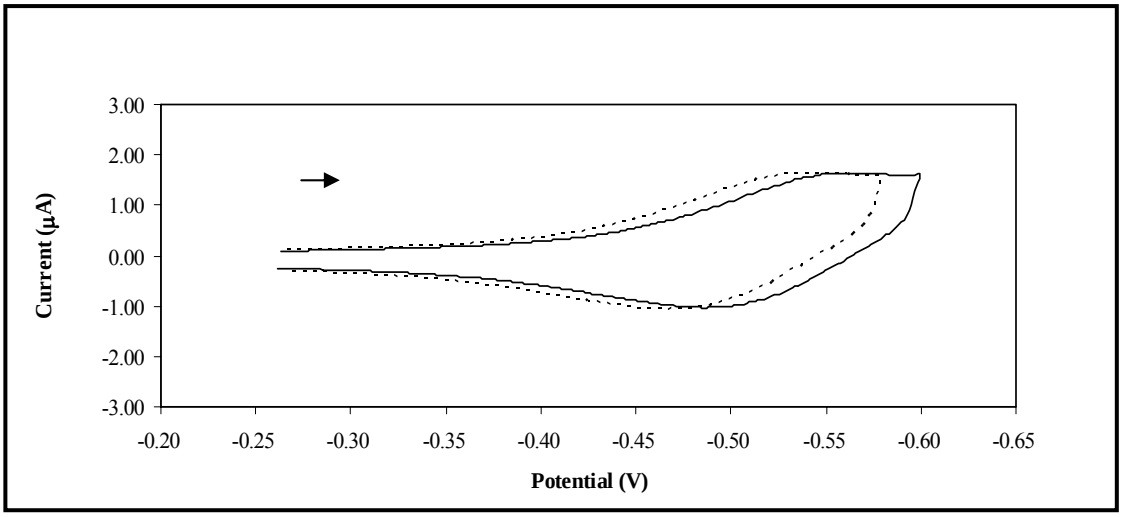

Figure 3.147 Cyclic voltammograms of the $[Ru(5mazpy)_3](NO_3)_2.5H_2O$ complex in absence (solid line) and presence (dash line) of CT DNA in 5 mM Tris/50 mM NaCl buffer (pH 7.2) at scan rate 100 mVs^{-1}.

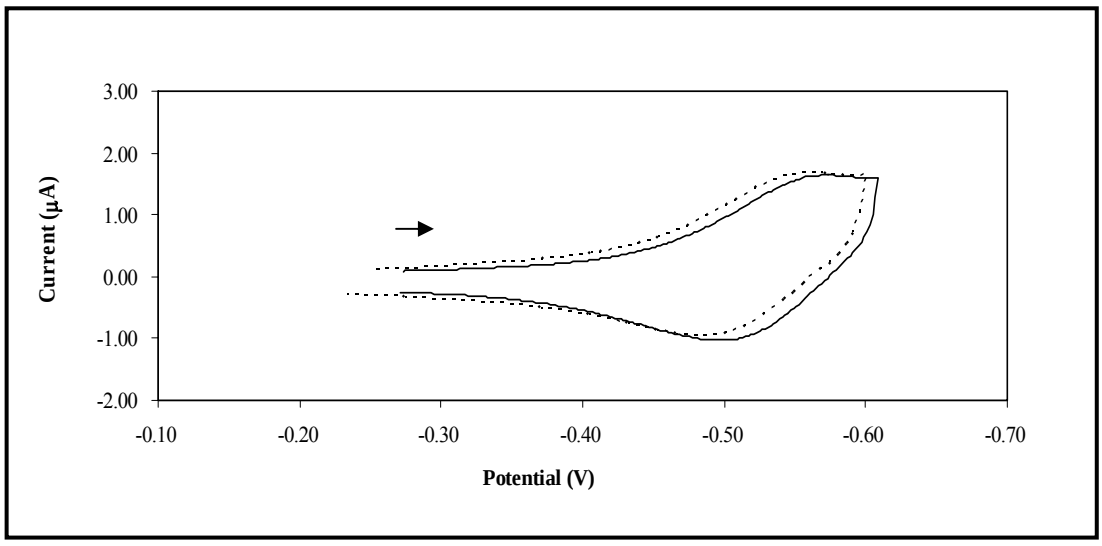

Figure 3.148 Cyclic voltammograms of the $[Ru(5mazpy)_2azpy](NO_3)_2.4H_2O$ complex in absence (solid line) and presence (dash line) of CT DNA in 5 mM Tris /50 mM NaCl buffer (pH 7.2) at scan rate 100 mVs^{-1}.

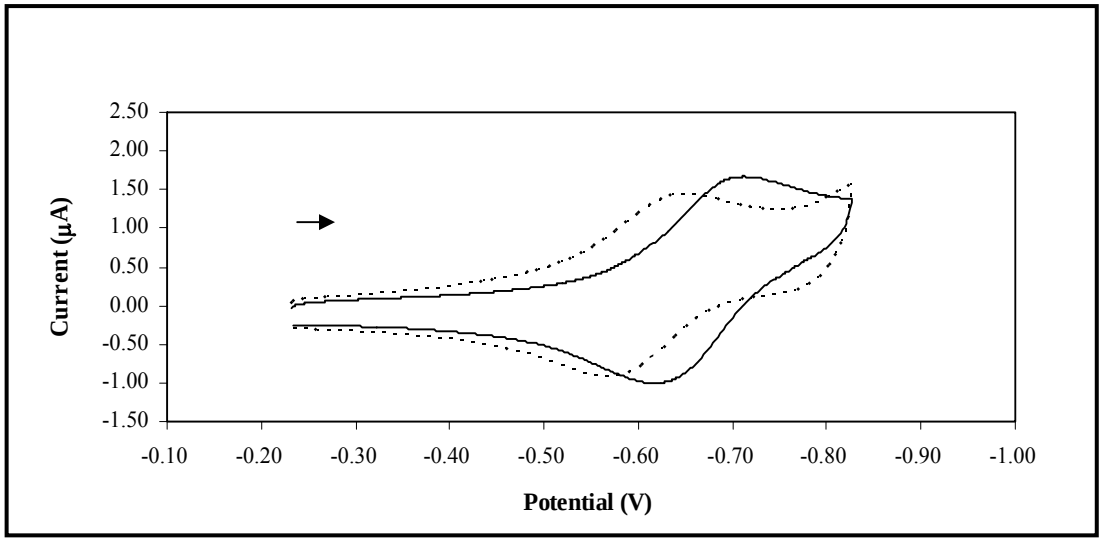

Figure 3.149 Cyclic voltammograms of the $[Ru(5mazpy)_2bpy]Cl_2.6H_2O$ complex in absence (solid line) and presence (dash line) of CT DNA in 5 mM Tris /50 mM NaCl buffer (pH 7.2) at scan rate 100 mVs^{-1}.

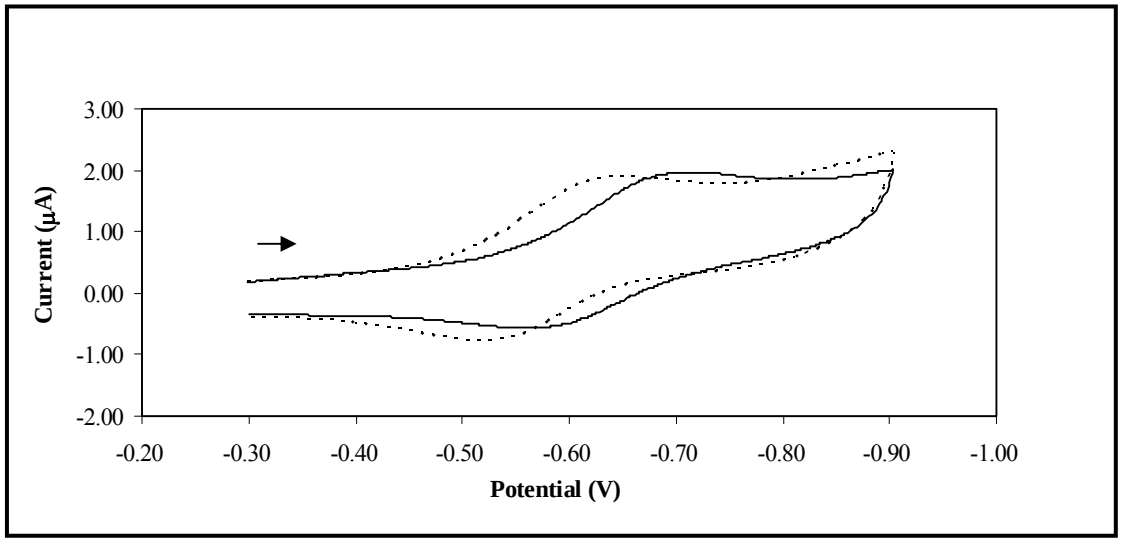

Figure 3.150 Cyclic voltammograms of the $[Ru(5mazpy)_2phen]Cl_2.7H_2O$ complex in absence (solid line) and presence (dash line) of CT DNA in 5 mM Tris/50 mM NaCl buffer (pH 7.2) at scan rate 100 mVs^{-1}.

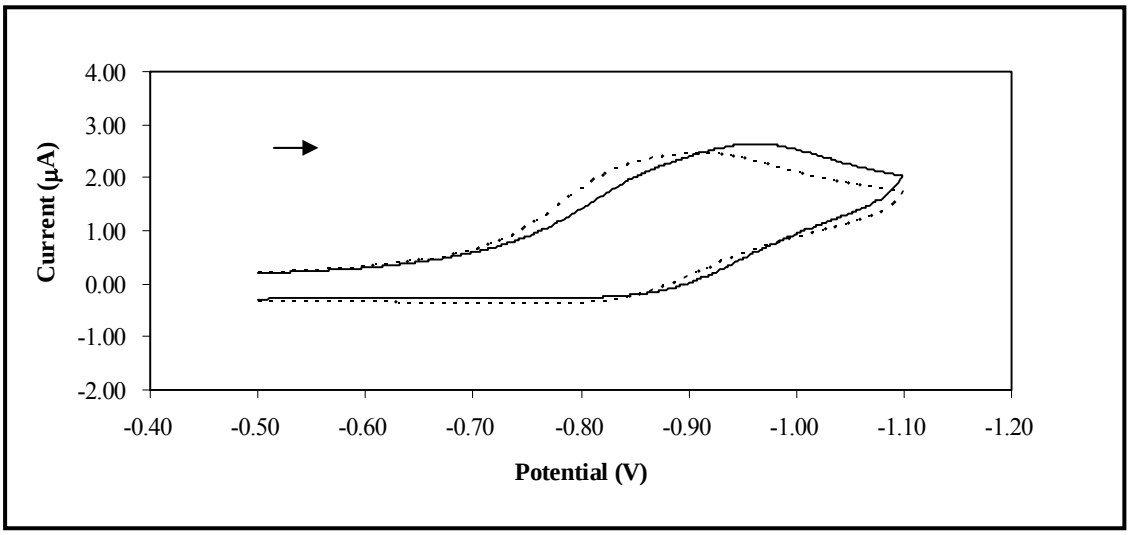

Figure 3.151 Cyclic voltammograms of the $[Ru(bpy)_2 5mazpy]Cl_2.6H_2O$ complex in absence (solid line) and presence (dash line) of CT DNA in 5 mM Tris /50 mM NaCl buffer (pH 7.2) at 100 scan rate mVs^{-1}.

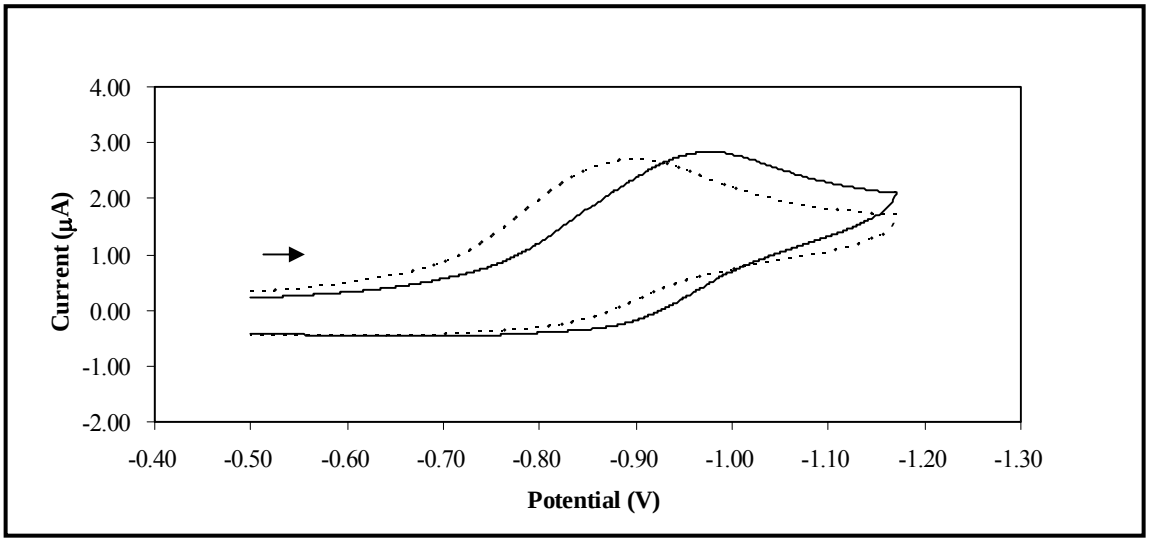

Figure 3.152 Cyclic voltammograms of the $[Ru(phen)_2 5mazpy]Cl_2.9H_2O$ complex in absence (solid line) and presence (dash line) of CT DNA in 5 mM Tris /50 mM NaCl buffer (pH 7.2) at scan rate 100 mVs^{-1}.

3.7.5 DNA cleavage study

The potential of the present complexes to cleave DNA was studied by gel electrophoresis using pBIND DNA in TAE buffer. When circular plasmid DNA was subjected to electrophoresis, relatively. Fast migration will be observed for the intact supercoil form (Form I, ccc form). If scission occurs on one strand (nicking), the supercoiled will relax to generate a slower-moving open circular form (Form II, OC form). If the both strands are cleaved, a linear form (Form III) will be generated (Selvakumar *et al.*, 2006).

Figure 3.153 reveals the conversion of Form I, II and III in the presence of varying concentrations of $[Ru(5mazpy)_3](NO_3)_2.5H_2O$ and $[Ru(5mazpy)_2azpy](NO_3)_2.4H_2O$. No DNA cleavage is observed for controls in which the complex was absent (lane 0) with increasing concentration of $[Ru(5mazpy)_3](NO_3)_2.5H_2O$ (lane 1-5) diminish gradually, whereas Form II increase. In addition, linear form, Form III, are observed.

Figure 3.154 shows the gel electrophoretic seperation of pBIND DNA with different concentrations of $[Ru(5mazpy)_2bpy]Cl_2.6H_2O$ and $[Ru(5mazpy)_2phen]Cl_2.7H_2O$. Control experiment (lane 0) suggests that untreated DNA does not show any cleavage, with increasing concentration of rutenium(II) complexes (lane 1-5 for $[Ru(5mazpy)_2bpy]Cl_2.6H_2O$, lane 6-10 for $[Ru(5mazpy)_2phen]Cl_2.7H_2O$). The amount of Form I of pBIND DNA decreases whereas that of Form II increase and slightly increase Form III. Under comparable experimental conditions, $[Ru(5mazpy)_2phen]Cl_2.9H_2O$ exhibits more effective DNA cleavage activity than $[Ru(5mazpy)_2bpy]Cl_2.6H_2O$.

Figure 3.155 exhibits gel electrophoresis separation of pBIND DNA after incubation with $[Ru(bpy)_25mazpy]Cl_2.6H_2O$ and $[Ru(phen)_25mazpy]Cl_2.9H_2O$. For pBIND untreated with complex, no cleavage is observed (lane 0). On the other hand, formation of the open circular form, Form II, of DNA is found when DNA is treated with $[Ru(bpy)_25mazpy]Cl_2.6H_2O$ (lane 1-5) and $[Ru(phen)_25mazpy]Cl_2.9H_2O$ (lane 6-10). The different DNA cleavage efficiency of the six complexes is due to the different binding affinity of the complexes to DNA.

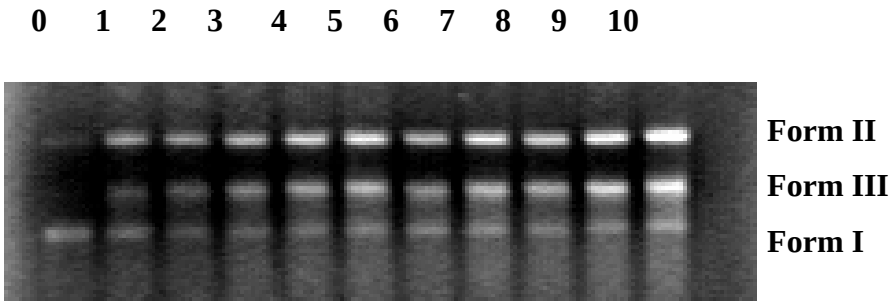

Figure 3.153 Electrophoresis behavior of the pBIND DNA in the presence of complexes on 1% agarose gel electrophoresis. Lane 0: plasmid DNA; lane 1-5: plasmid DNA was incubated with 20, 40, 60, 80, and 100 μM of $[Ru(5mazpy)_2azpy](NO_3)_2.4H_2O$, respectively; lane 6-10: plasmid DNA was incubated with 20, 40, 60, 80, and 100 μM of $[Ru(5mazpy)_3](NO_3)_2.5H_2O$ respectively. Form I, II and III refer to supercoil form, open circular form, and linear form, respectively.

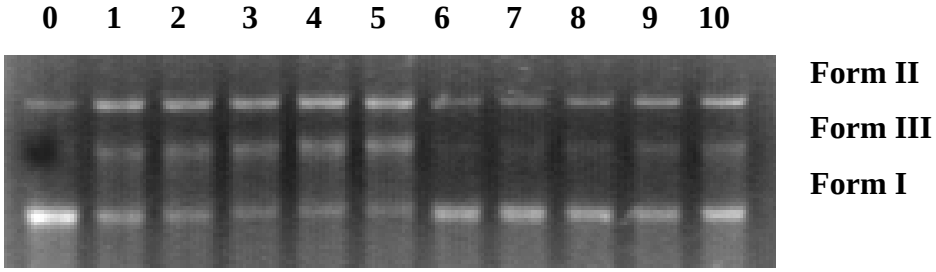

Figure 3.154 Electrophoresis behavior of the pBIND DNA in the presence of complexes on 1% agarose gel electrophoresis. Lane 0: plasmid DNA; lane 1-5: plasmid DNA was incubated with 20, 40, 60, 80, and 100 μM of $[Ru(5mazpy)_2phen]Cl_2.7H_2O$, respectively; lane 6-10: plasmid DNA was incubated with 20, 40, 60, 80, and 100 μM of $[Ru(5mazpy)_2bpy]Cl_2.6H_2O$ respectively. Form I, II and III refer to supercoil form, open circular form, and linear form, respectively.

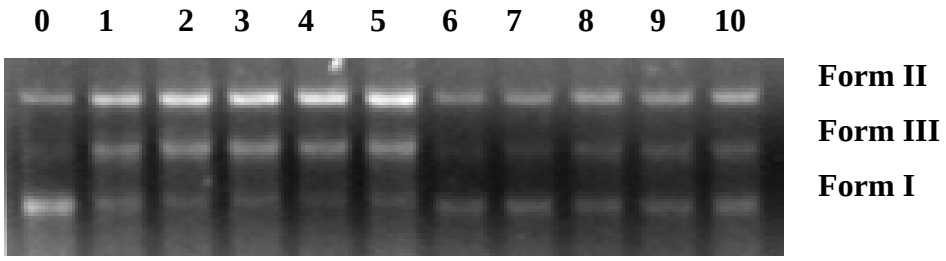

Figure 3.155 Electrophoresis behavior of the pBIND DNA in the presence of complexes on 1% agarose gel electrophoresis. Lane 0: plasmid DNA; lane 1-5: plasmid DNA was incubated with 20, 40, 60, 80, and 100 μM of $[Ru(phen)_2 5mazpy]Cl_2.9H_2O$, respectively; lane 6-10: plasmid DNA was incubated with 20, 40, 60, 80, and 100 μM of $[Ru(bpy)_2 5mazpy]Cl_2.6H_2O$ respectively. Form I, II and III refer to supercoil form, open circular form, and linear form, respectively.

3.8 Cytotoxicity assay

The ruthenium(II) complexes exhibit a widely applied foreground in the search of new anticancer drugs (Velders *et al*, 2000; Hotze *et al*, 2004). Recently, some ruthenium(II) complexes, *ctc*-[Ru(azpy)$_2$Cl$_2$] (α), *ccc*-[Ru(azpy)$_2$Cl$_2$] (β), *tcc*-[Ru(azpy)$_2$ Cl$_2$] (γ), have been reported. The α-[Ru(azpy)$_2$Cl$_2$] complex shows a very pronounced cytotoxicity, higher than that of cisplatin in all cell lines. The β-[Ru(azpy)$_2$Cl$_2$] complex was approximately a factor of 10 less active than the α-[Ru(azpy)$_2$Cl$_2$] and, in contrast to literature data (Velders *et al*, 2000), γ-[Ru(azpy)$_2$Cl$_2$] showed an activity comparable to that of the α-[Ru(azpy)$_2$Cl$_2$]. To further investigate the cytotoxic activity, the rutenium(II) complexes with 5-methyl-2-(phenylazo)pyridine ligand have been studied. The first part of cytotoxicity was studied at Cancer Drug Resistance Group, Centenary Institute of Cancer Medicine & Cell Biology, University of Sydney, Australia. There were several human tumor cell lines (A549, CEM, IGROV, MCF-7, PC3, SK-MEL-28, and WIDR). The compounds in the second part were tested IC_{50} at National Center for Genetic Engineering and Biotechnology, Bangkok, Thailand, with three cell lines (Anti-NCI-H187, BC, and KB).

The in vitro cytotoxicity effects of the parent complexes, α,β,γ-[Ru(azpy)$_2$Cl$_2$], and the α,β,γ-[Ru(5mazpy)$_2$Cl$_2$] complexes were compared with cisplatin (positive control), in a series of human tumor cell lines are listed in Table 3.49. A DMSO stock solution was used in the cytotoxicity tests of all complexes, as these complexes are poorly water soluble. The IC_{50} values represent the concentration of a drug that is required for 50% reduction of cellular growth. The α-[Ru(5mazpy)$_2$Cl$_2$] complex is more active in all cell lines, while γ-[Ru(5mazpy)$_2$Cl$_2$] is less active in all cell lines. In addition, the α-[Ru(5mazpy)$_2$ Cl$_2$] complex shows higher activity in the lung cancer (A549) and colon cancer cell lines (WIDR) cell lines than that of cisplatin. However, this isomer shows activity slightly below that of cisplatin in ovarian cencer (IGROV), breast cancer (MCF-7), and prostate cancer (PC3), melanoma cancer (SK-MEL-28), and leukemia (CEM) cell lines. In comparison to the parent complexes, α,β,γ-[Ru(azpy)$_2$Cl$_2$], the α,β,γ-[Ru(5mazpy)$_2$

Cl_2] complexes show a lower activity than the α,β,γ-[Ru(azpy)$_2$Cl$_2$] complexes in most cell lines. The IC_{50} curves of α,β,γ-[Ru(azpy)$_2$Cl$_2$], α,β,γ-[Ru(5mazpy)$_2$Cl$_2$], and cisplatin are illustrated in Figure 3.156-3.162, respectively. Results from these data showed that the α-isomer of [Ru(L)$_2$Cl$_2$] (L = azpy, 5mazpy) displayed a high cytotoxicity.

Table 3.49 IC_{50} values[a] (μM) of a series of ruthenium(II) complexes and cisplatin against a resies of tumor cell lines (A549, CEM, IGROV, MCF-7, PC3, SK-MEL-28, and WIDR)

Complexes	Cell lines						
	A549	CEM	IGROV	MCF-7	PC3	SK-MEL-28	WIDR
α-[Ru(azpy)$_2$Cl$_2$]	0.13	0.60	0.14	0.29	0.26	0.15	0.20
β-[Ru(azpy)$_2$Cl$_2$]	2.05	10.39	1.97	3.39	8.84	4.50	4.66
γ-[Ru(azpy)$_2$Cl$_2$]	0.01	0.15	0.016	0.053	0.039	0.028	0.045
α-[Ru(5mazpy)$_2$Cl$_2$]	0.50	1.41	0.71	1.48	1.37	1.03	0.78
β-[Ru(5mazpy)$_2$Cl$_2$]	17.25	13.07	16.61	19.23	18.55	8.87	8.38
γ-[Ru(5mazpy)$_2$Cl$_2$]	>26	>26	>26	>26	>26	>26	>26
cisplatin	0.90	2.97	0.40	0.41	0.52	0.94	4.64

[a]method: cytotoxicity assay at Cancer Drug Resistance Group, Centenary Institute of Cancer Medicine & Cell Biology, University of Sydney, Australia. A549: lung cancer; CEM: leukemia; IGROV: ovarian cancer; MCF-7: breast cancer; PC3: prostate cancer; SK-MEL-28: melanoma cancer; WIDR: colon cancer.

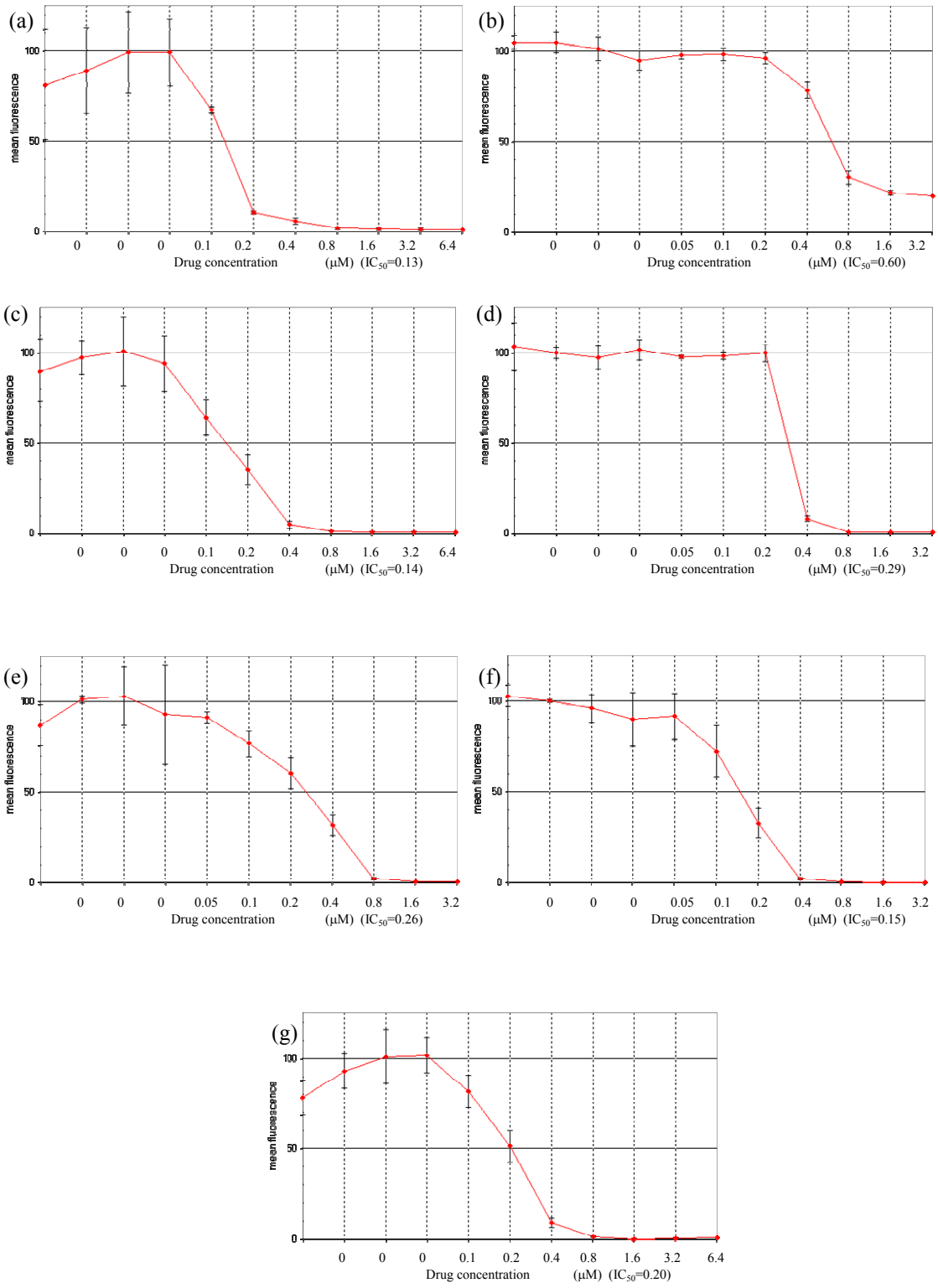

Figure 3.156 IC_{50} curves of the α-$[Ru(azpy)_2Cl_2]$ complex against a resies of tumor cell lines A549 (a), CEM (b), IGROV (c), MCF-7 (d), PC3 (e), SK-MEL-28 (f) and WIDR (g)

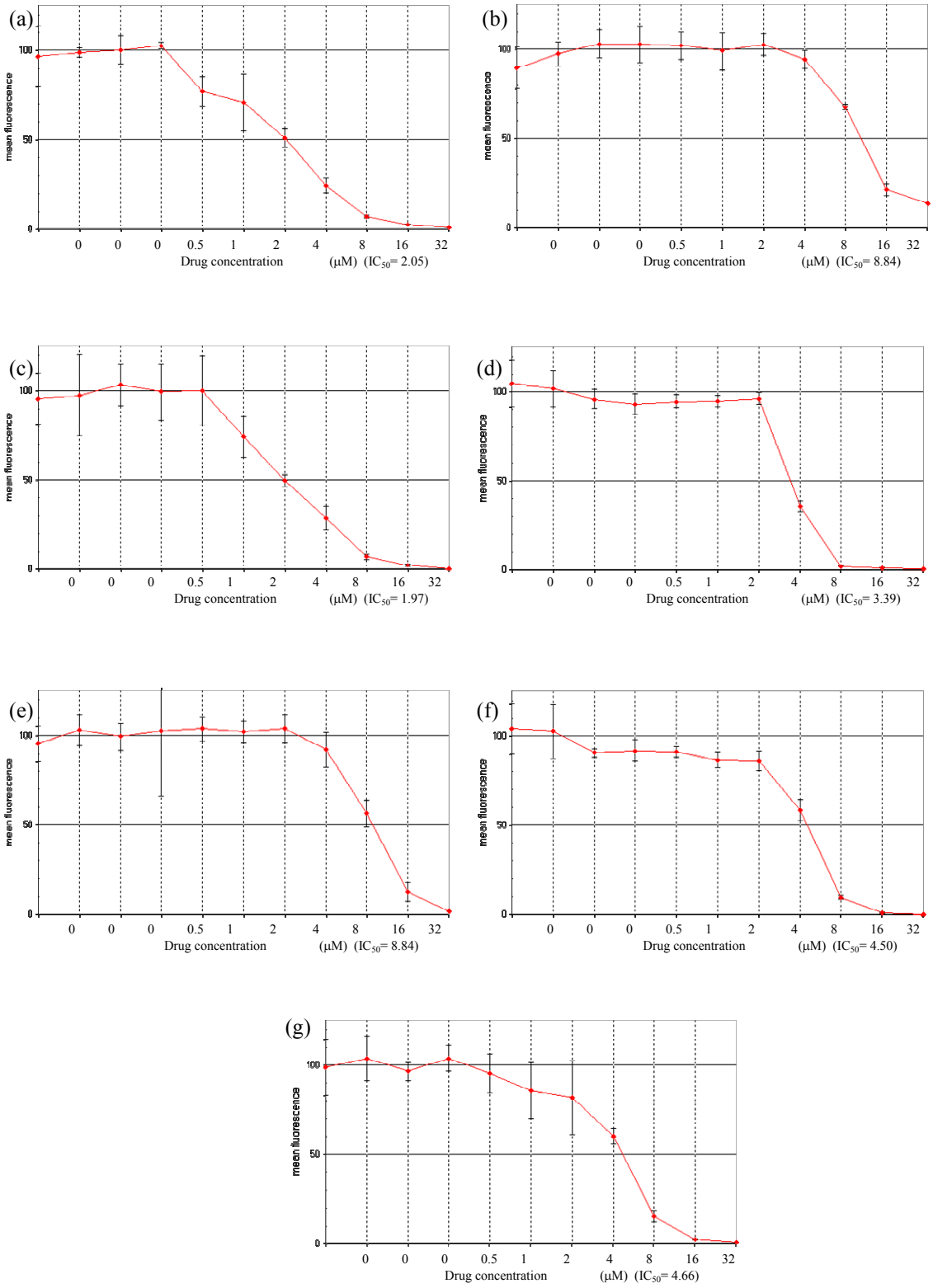

Figure 3.157 IC_{50} curves of the β-$[Ru(azpy)_2Cl_2]$ complex against a resies of tumor cell lines A549 (a), CEM (b), IGROV (c), MCF-7 (d), PC3 (e), SK-MEL-28 (f) and WIDR (g)

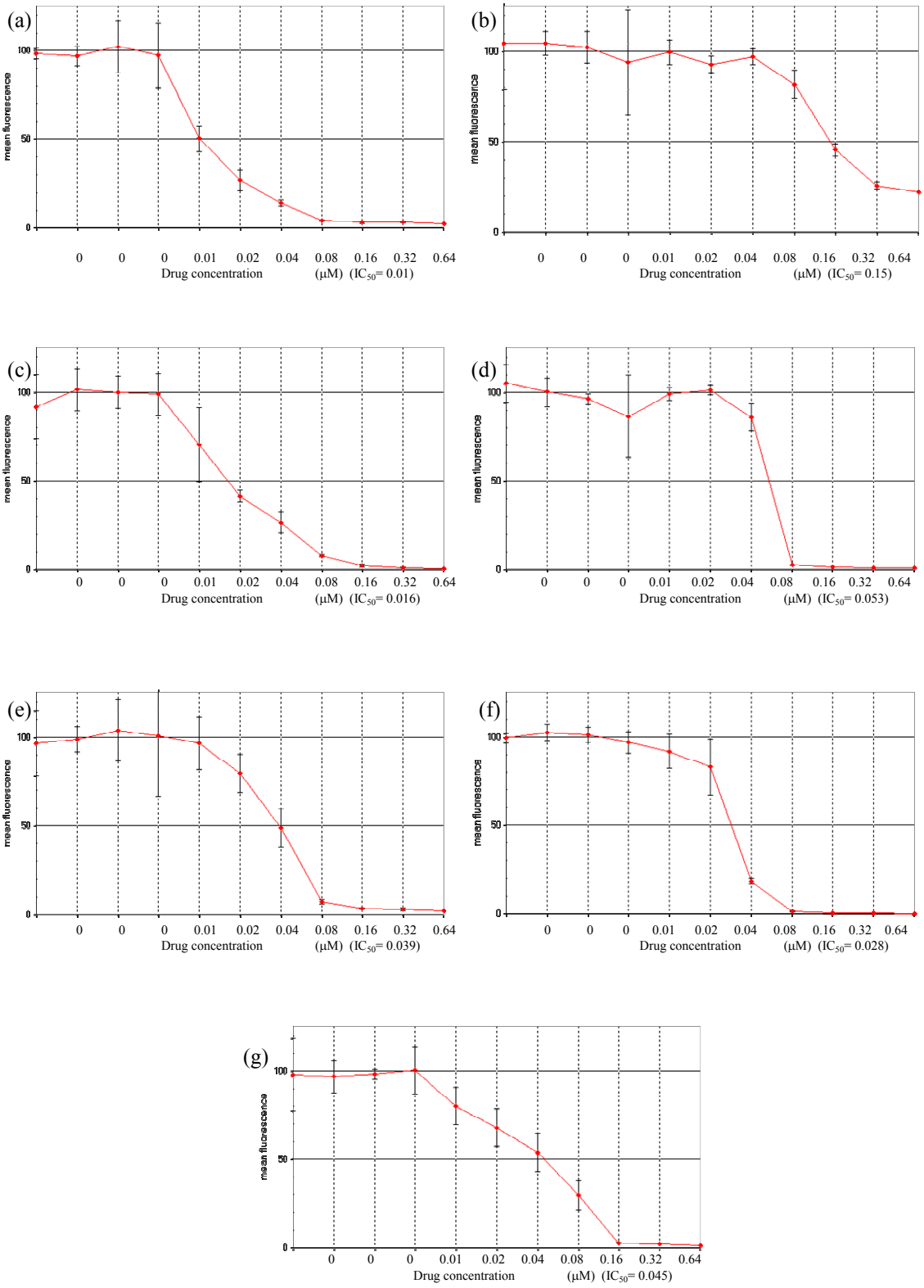

Figure 3.158 IC_{50} curves of the γ-$[Ru(azpy)_2Cl_2]$ complex against a resies of tumor cell lines A549 (a), CEM (b), IGROV (c), MCF-7 (d), PC3 (e), SK-MEL-28 (f) and WIDR (g)

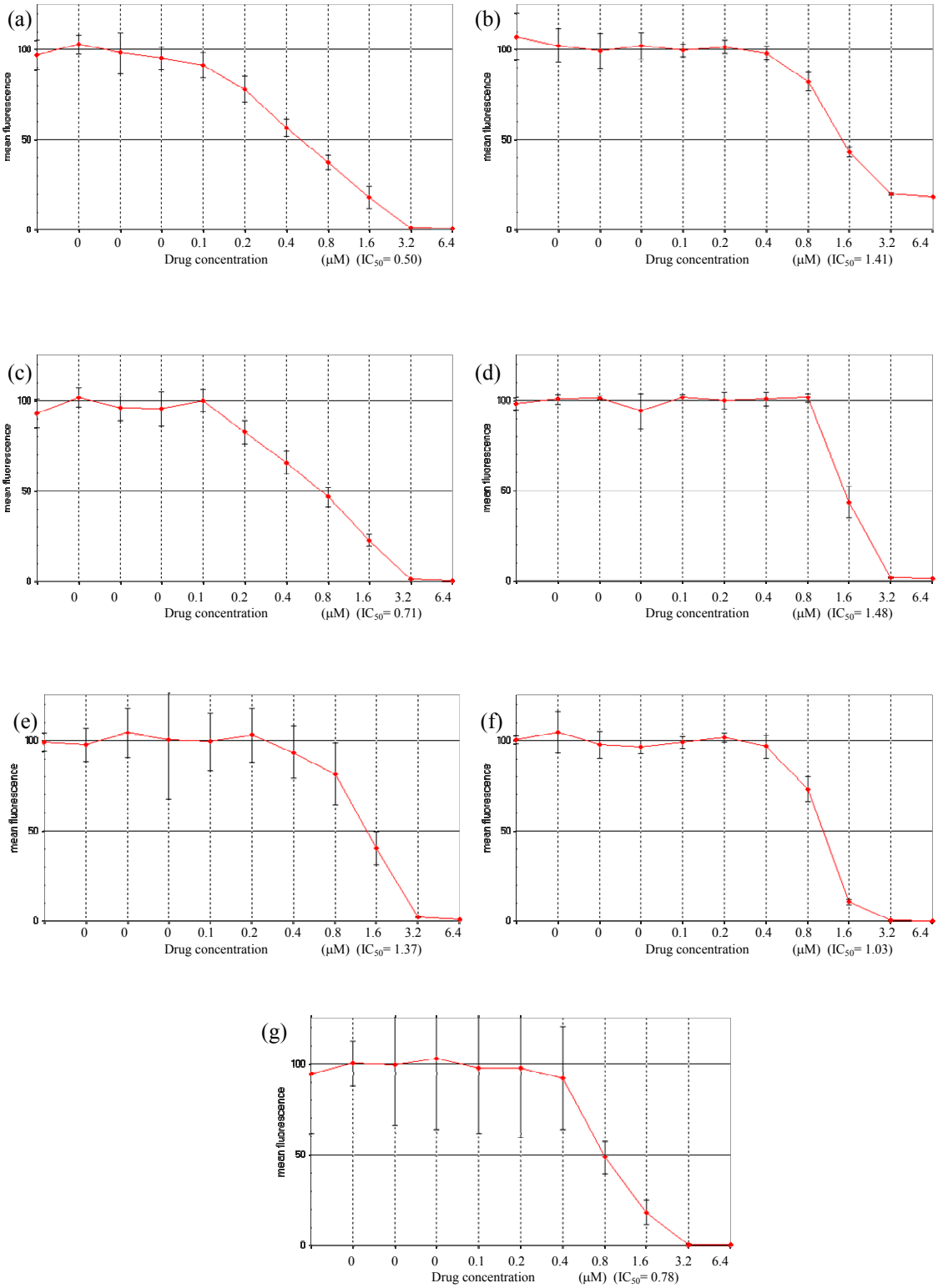

Figure 3.159 IC_{50} curves of the α-$[Ru(5mazpy)_2Cl_2]$ complex against a resies of tumor cell lines A549 (a), CEM (b), IGROV (c), MCF-7 (d), PC3 (e), SK-MEL-28 (f) and WIDR (g)

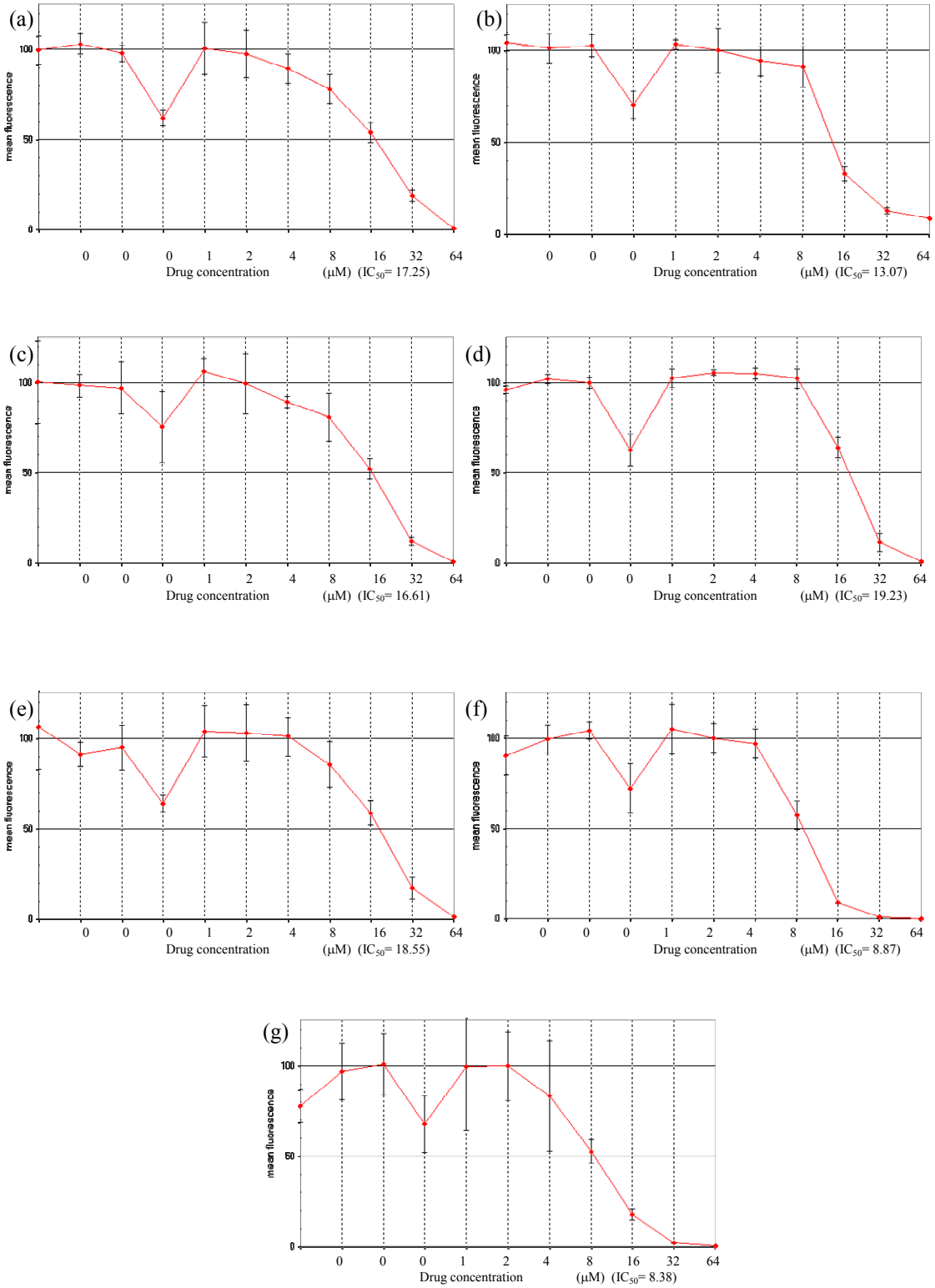

Figure 3.160 IC_{50} curves of the β-$[Ru(5mazpy)_2Cl_2]$ complex against a resies of tumor cell lines A549 (a), CEM (b), IGROV (c), MCF-7 (d), PC3 (e), SK-MEL-28 (f) and WIDR (g)

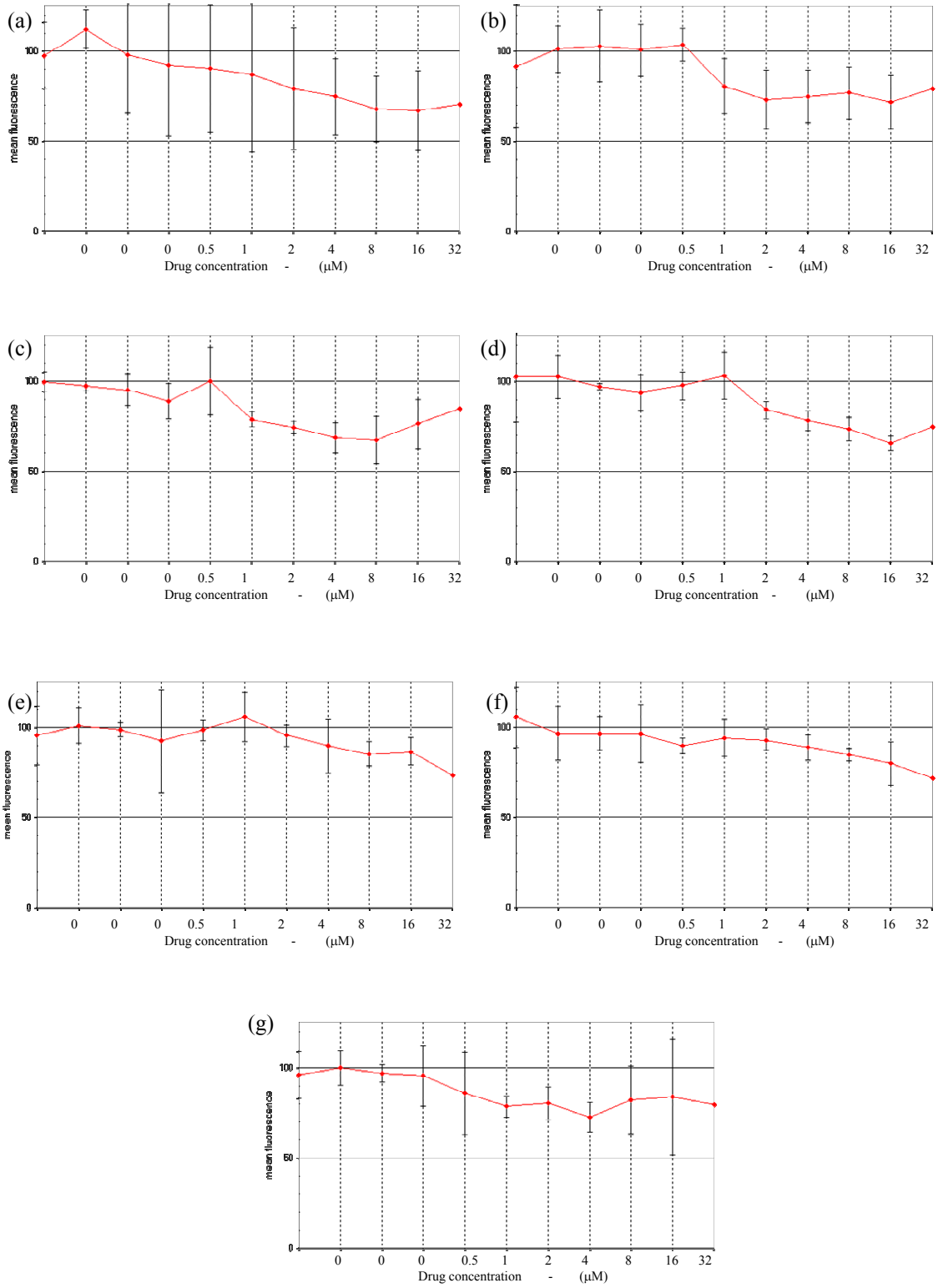

Figure 3.161 IC_{50} curves of the γ-$[Ru(5mazpy)_2Cl_2]$ complex against a resies of tumor cell lines A549 (a), CEM (b), IGROV (c), MCF-7 (d), PC3 (e), SK-MEL-28 (f) and WIDR (g)

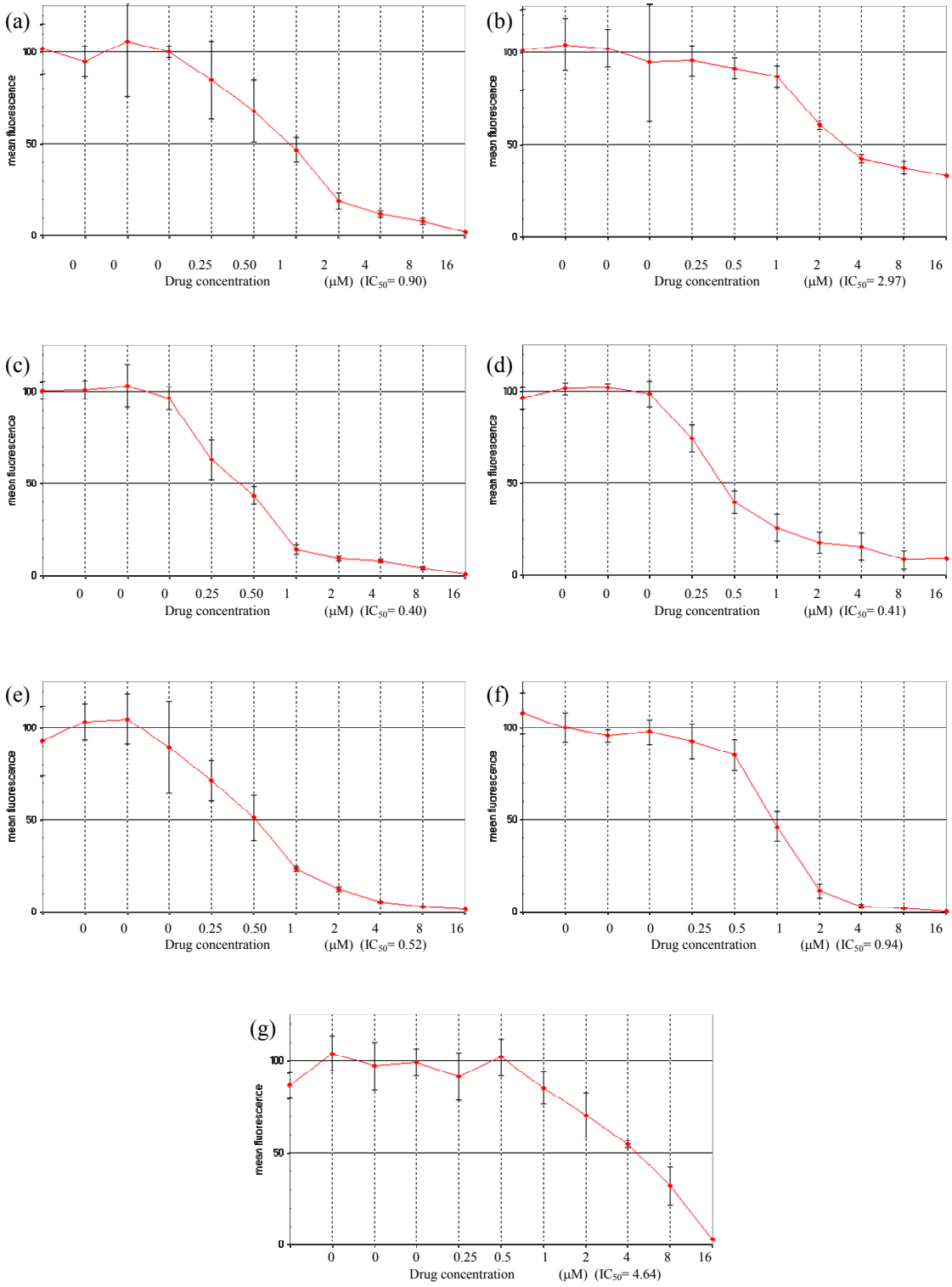

Figure 3.162 IC_{50} curves of cisplatin against a resies of tumor cell lines A549 (a), CEM (b), IGROV (c), MCF-7 (d), PC3 (e), SK-MEL-28 (f) and WIDR (g)

Besides, the IC_{50} values of ruthenium(II) complexes, in small cell lung cancer (Anti-NCI-H187), breast cancer (BC), and oral human epidermal carcinoma (KB) cell lines were determined. The cytotoxicity of ruthenium(II) complexes in a series of human tumor cell lines are listed in Table 3.50. In comparison to the parent complexes, α,β,γ-$[Ru(azpy)_2Cl_2]$, the γ-$[Ru(5mazpy)_2Cl_2]$ complex is slightly active only in small cell lung cancer cell line. In addition, the γ isomer shows a higher activity than ellipticine which is positive control. The α,β,γ-$[Ru(5mazpy)_2Cl_2]$ complexes are inactive in oral human epidermal carcinoma and breast cancer. The tris chelates complexes, $[Ru(5mazpy)_3](PF_6)_2$, $[Ru(5mazpy)_2azpy](PF_6)_2$, $[Ru(5mazpy)_3](NO_3)_2.5H_2O$, and $[Ru(5mazpy)_2azpy](NO_3)_2.4H_2O$, are active in all cell lines (Anti-NCI-H187, BC, KB). The $[Ru(5mazpy)_2bpy](PF_6)_2$ and $[Ru(phen)_25mazpy](PF_6)_2$ complexes show weakly active in small cell lung cancer. The $[Ru(5mazpy)_2phen](PF_6)_2$ complex displays moderatly active (IC_{50} = 7.64 μg/mL) in oral human epidermal carcinoma. The complexes of $[Ru(5mazpy)_2bpy]Cl_2.6H_2O$ and $[Ru(5mazpy)_2phen]Cl_2.9H_2O$ show weakly active in oral human epidermal carcinoma with IC_{50} 17.64 and 15.41 μg/mL, respectively.

Table 3.50 IC_{50} values[a] (μg/mL) of a series of ruthenium(II) complexes and cisplatin against a resies of tumor cell lines (Anti-NCI-H187, BC, and KB)

Complexes	Cell lines			Vero cell
	Anti-NCI-H187	BC	KB	
5mazpy	5.34 (m)	inactive	inactive	12.90
α-$[Ru(5mazpy)_2Cl_2]$	0.24 (s)	inactive	inactive	>50
β-$[Ru(5mazpy)_2Cl_2]$	inactive	inactive	inactive	-
γ-$[Ru(5mazpy)_2Cl_2]$	0.49 (s)	inactive	inactive	>50
α-$[Ru(azpy)_2Cl_2]$	inactive	1.27 (s)	4.28 (s)	>50
β-$[Ru(azpy)_2Cl_2]$	inactive	0.98 (s)	inactive	>50
γ-$[Ru(azpy)_2Cl_2]$	1.12 (s)	0.278 (s)	0.401 (s)	>50

Table 3.50 (continued)

Complexes	Cell lines			Vero cell
	Anti-NCI-H187	BC	KB	
$[Ru(5mazpy)_3](PF_6)_2$	5.23 (m)	3.88 (s)	1.03 (s)	>50
$[Ru(5mazpy)_2azpy](PF_6)_2$	5.03 (m)	8.71 (m)	2.09 (s)	>50
$[Ru(5mazpy)_2bpy](PF_6)_2$	17.85 (w)	Inactive	Inactive	>50
$[Ru(5mazpy)_2phen](PF_6)_2$	Inactive	Inactive	7.64 (m)	>50
$[Ru(bpy)_25mazpy](PF_6)_2$	Inactive	Inactive	Inactive	-
$[Ru(phen)_25mazpy](PF_6)_2$	10.35 (w)	Inactive	Inactive	>50
$[Ru(5mazpy)_3](NO_3)_2.5H_2O$	4.23 (s)	4.93 (s)	1.20 (s)	>50
$[Ru(5mazpy)_2azpy](NO_3)_2.4H_2O$	4.38 (s)	8.90 (m)	2.01 (s)	>50
$[Ru(5mazpy)_2bpy]Cl_2.6H_2O$	Inactive	Inactive	17.64 (w)	>50
$[Ru(5mazpy)_2phen]Cl_2.7H_2O$	Inactive	Inactive	15.41 (w)	>50
$[Ru(bpy)_25mazpy]Cl_2.6H_2O$	16.01 (w)	Inactive	Inactive	>50
$[Ru(phen)_25mazpy]Cl_2.9H_2O$	Inactive	Inactive	Inactive	-
Doxorubicin	0.029	0.140	0.103	-
Ellipticine	0.618	0.134	0.413	0.5

[a] method: sulforhodamine B (SRB) assay at National Center for Genetic Engineering and Biotechnology, Bangkok, Thailand. Anti-NCI-H187: small cell lung cancer; BC: Breast cancer; KB: Oral human epidermal carcinoma

IC_{50} (μg/mL)	Activity
> 20	Inactive
> 10-20	Weakly active
5 – 10	Moderately active
< 5	Strongly active

CHAPTER 4
CONCLUSION

The new a symmetric bidentate ligand, 5-methyl-2-(phenylazo) pyridine (5mazpy), was synthesized and it reacted with $RuCl_3.3H_2O$ in ethanol under refluxing condition. Three isomers of $[Ru(5mazpy)_2Cl_2]$ were isolated by column chromatography. There are *cis-trans-cis* (*ctc*, α), *cis-cis-cis* (*ccc*, β), and *trans-cis-cis* (*tcc*, γ) by the order of coordinating pairs of Cl, N(py), and N(azo), respectively. In addition, the $[Ru(5mazpy)_2L](PF_6)_2$, $[Ru(5mazpy)_2L'](PF_6)_2$, and $[Ru(L')_2 5mazpy](PF_6)_2$ complexes (L = 2-(phenylazo)pyridne (azpy), 5-methly-2-(phenylazo)pyridne (5mazpy); L′ = 2, 2′-bipyridine (bpy), and 1,10-phenanthroline (phen)) were also synthesized. They have been characterized by elemantal analysis, mass spectrometry, UV-Visible absorption spectroscopy, infrared spectroscopy, ^1H, ^{13}C, DEPT 135, ^1H-^1H COSY, and ^1H-^{13}C HMQC NMR spectroscopy and their electrochemical properties were also studied by cyclic voltammetry. The structures of 5mazpy, *ctc*-, *ccc*-, *tcc*-$[Ru(5mazpy)_2Cl_2]$, and $[Ru(5mazpy)_2bpy](PF_6)_2$ have been confirmed by X-ray crystallography.

Results from X-ray crystallography show that the N-N distances in *ctc*-, *ccc*-, *tcc*-$[Ru(5mazpy)_2Cl_2]$, and $[Ru(azpy)_2bpy](PF_6)_2$ are longer than those in the free 5mazpy ligand. In addition, the average Ru-N(azo) distances are shorter than average Ru-N(py) distances. The 5mazpy ligand exhibits a sharp band at 1389 cm^{-1}, corresponding to N=N stretching mode. In the *ctc*-, *ccc*-, and *tcc*-$[Ru(5mazpy)_2Cl_2]$ complexes the $\upsilon_{(N=N)}$ is red shifted by 1299-1334 cm^{-1}, which is a good indication of N-coordination. The $\upsilon_{(N=N)}$ in $[Ru(5mazpy)_2L](PF_6)_2$, $[Ru(5mazpy)_2L'](PF_6)_2$, and $[Ru(L')_2 5mazpy](PF_6)_2$ is also shifted to lower energy than that of the free ligand. In addition, in $[Ru(5mazpy)_2L'](PF_6)_2$ (L′ = bpy, phen), N=N stretching mode occurs at lower energy than $[Ru(5mazpy)_2L](PF_6)_2$ (L = azpy , 5mazpy). As the $[Ru(5mazpy)_2 L](PF_6)_2$ complexes contain more azoimine group than the $[Ru(5mazpy)_2L'](PF_6)_2$ complexes. Besides the $\upsilon_{(N=N)}$ in $[Ru(L')_2 5mazpy](PF_6)_2$ (L′ = bpy ,phen) appears at lower frequencies than that $[Ru(5mazpy)_2L'](PF_6)_2$ because the former complexes

contain one azo imine ligand and the latter complexes contain two azoimine ligands. Solution electronic spectra of the complexes revealed that the *ctc*-, and *ccc*-[Ru(5mazpy)$_2$Cl$_2$] complexes exhibit highly intense MLCT transitions at higher energy than the *tcc*-[Ru(5mazpy)$_2$Cl$_2$] complex. Only one intense band is observed in the visible region for [Ru(5mazpy)$_2$L](PF$_6$)$_2$, [Ru(5mazpy)$_2$L′](PF$_6$)$_2$, and [Ru(L′)$_2$ 5mazpy](PF$_6$)$_2$. The ^{1}H, ^{13}C, DEPT 135, ^{1}H-^{1}H COSY, and ^{1}H-^{13}C HMQC NMR spectroscopy are used to supported the structure of compounds. All the three isomers of [Ru(5mazpy)$_2$Cl$_2$] exhibit one reversible peak and one irriversible peak. Furthermore, The reduction potential in negative region shifts from the free ligand value. In [Ru(5mazpy)$_2$L](PF$_6$)$_2$, [Ru(5mazpy)$_2$L′](PF$_6$)$_2$, and [Ru(L′)$_2$5mazpy](PF$_6$)$_2$, the [Ru(5mazpy)$_2$azpy](PF$_6$)$_2$ complex can accept electron better than those of [Ru(5mazpy)$_3$](PF$_6$)$_2$ and [Ru(5mazpy)$_2$bpy](PF$_6$)$_2$ ≈ [Ru(5mazpy)$_2$phen](PF$_6$)$_2$.

The water soluble complexes, [Ru(5mazpy)$_2$L](NO$_3$)$_2$, [Ru(5mazpy)$_2$ L′]Cl$_2$, and [Ru(L′)$_2$5mazpy]Cl$_2$ (L = azpy, 5mazpy; L′ = bpy, phen) were also synthesized for study DNA binding properties. The interaction of a series of mixed ligand complexes with Calf thymus DNA has been monitored by absorption titration, competitive binding, viscosity measurements and cyclic voltammetry. Furthermore, the cleavage experiment was also investigated by argarose gel electrophoresis.

The *ctc*, *ccc*, *tcc*-[Ru(5mazpy)$_2$Cl$_2$], [Ru(5mazpy)$_2$L](PF$_6$)$_2$, [Ru(L′)$_2$ 5mazpy](PF$_6$)$_2$, [Ru(5mazpy)$_2$L′](PF$_6$)$_2$, [Ru(5mazpy)$_2$L](NO$_3$)$_2$, [Ru(5mazpy)$_2$L′]Cl$_2$, and [Ru(L′)$_2$5mazpy]Cl$_2$ complexes were investigated the activity against a series of tumor cell lines (A549, CEM, IGROV, MCF-7, PC3, SK-MEL-28, WIDR, Anti-NCI-H187, BC, and KB). The results show that the *ctc*-[Ru(5mazpy)$_2$Cl$_2$] complex is high activity than that *ccc*- and *tcc*-[Ru(5mazpy)$_2$Cl$_2$] in all cell lines.

REFERENCES

Al-Noaimi, M. Z., Saadeh, H., Haddad, S. F., El-Barghouthi, M. I., El-khateeb, M. and Crutchley, R. J. 2007. Syntheses, Crystallography and Spectroelectrochemical Studies of Ruthenium Azomethine Complexes. *Polyhedron* 26, 3675-3685.

Bag, N., Pramanik, A., Lahiri, G. K. and Chakravorty, A. 1992. Chemistry of the $[Ru(RQ)(tap)_2]^z$ Family: Authentic Catecholates, Reduction Potentials, and Spectra (RQ = Quinone/Semiquinone/Catecholate; tap = 2-(*m*-Tolylazo)pyri dine; z = 0, ±, ±2). *Inorganic Chemistry* 31, 40-45.

Boelrijk, A, E. M., Jorna, A. M. J. and Reedijk, J. 1995. Oxidation of octyl α-D-Glucuronic acid, Catalyzed by Several Ruthenium Complexes, Containing a 2-(Phenylazo)pyridine or a 2-(Nitrophenyl)azopyridine Ligand. *Journal of Molecular Catalysis A: Chemical* 103, 73-85.

Byabartta, P., Jasimuddin, S. K., Mostafa, G., Lu, T.-H. and Sinha, C. 2003. The Synthesis, Spectral Studies and Electrochemistry of 1,10-(Phenanthroline)-bis-{1-alkyl-2-(arylazo)imidazole}ruthenium(II) perchlorate. Singel Crystal X-ray Structure of $[Ru(phen)(HaaiMe)_2](ClO_4)_2$ [phen = 1,10-phenanthro- line, HaaiMe = 1-methyl-2-(phenylazo)imidazole]. *Polyhedron* 22, 849-859.

Byabartta, P. 2007. Heteroleptic Tris-Chelates of Ruthenium(II): Synthesis, Spectral Characterisation and Electrochemical Properties. *Spectrochimica Acta Part A* 66, 521-533.

Carter, M. T. and Bard, A. J. 1987. Voltammetric Studies of the Interaction of Tris (1,10-phenanthroline)cobalt(III) with DNA. *Journal of the American Chemical Society* 109, 7528-7530.

Changsaluk, U. 2002. Chemistry of Bis[2-(phenylazo)pyridine] Ruthenium(II) Complexes with 1,10-Phenanthroline and other Ligands. Master of Science Thesis, Prince of Songkla University, Songkhla, Thailand.

Changsaluk, U. and Hansongnern, K. 2005. Dichlorobis(5-methyl-2-(phenylazo)pyridine)ruthenium(II) complex: Characterization and NMR spectroscopy. *Songklanakarin Journal of Science and Technology* 27, 739-749.

Choudhury, S., Kakoti, M., Deb, A. K. and Goswami, S. 1992. Isomeric Complexes of Ruthenium(II) with Neutral Heterocyclic Schiff Base Ligands. High Resolution Proton Resonance Spectra of Trans-Cis Isomeric Pairs of RuX_2L_2 (L = 2-Aryl- pyridinecarboxaldimine, X = Cl, Br) and Comparison of their Physical Properties. *Polyhedron* 24, 3183-3190.

Chen, J. C., Li, J., Qian, L. and Zheng, K. C. 2005. Electronic Structures and SARS of the Isomeric Complexes α-, β-, γ-$[Ru(mazpy)_2Cl_2]$ with Different Antitumor Activities. *Journal of Molecular Structure: THEOCHEM* 728, 93-101.

Chen, J., Li, J., Wu, W. and Zheng, K. 2006. Structures and Anticancer Activities of a Series of Isomeric Complexes $Ru(azpy)_2Cl_2$. *Acta Physico-Chimica Sinica* 22, 391-396.

Cory, M., McKee, D. D., Kagan, J., Henry, D. W. and Miller, J. A. 1985. Design, Synthesis, and DNA Binding Properties of Bifunctional Intercalators. Comparison of Polymethylene and Diphenyl Ether Chains Connecting Phenanthridine. *Journal of the American Chemical Society* 107, 2528-2536.

Deng, H., Xu, H., Yang, Y., Li, H., Zou, H., Qu, L.-H. and Ji, L.-N. 2003. Synthesis, Characterization, DNA-Binding and Cleavage Studies of $[Ru(bpy)_2(actatp)]^{2+}$ and $[Ru(phen)_2(actatp)]^{2+}$ (actatp = acenephthereno[1,2-*b*]-1,4,8,9-tetraazariphenylence). *Journal of Inorganic Biochemistry* 97, 207-214.

Deng, H., Li, J., Zheng, K. C., Yang, Y., Chao, H. and Ji, L.-N. 2005. Synthesis, Characterization, Structure DNA-Binding Properties of Complexes [Ru $(bpy)_2(L)]^{2+}$ (L = ptdb, ptda and ptdp) with Asymmetric Intercalative Ligands. *Inorganica Chimica Acta* 358, 3430-3440.

Dinda, J., Senapoti, S., Mondal, T., Jana, A. D., Chiang, M. Y., Lu, T.-H. and Sinha, C. 2006. Synthesis, Spectral Sharacterisation, and Electrochemistry of bis-(2,2′-bipyridine)(1-alkyl-2-(napthylazo)imidazole)ruthenium(II) Complexes: X-ray Crystal Structure of [bis-(2,2′-bipyridine)-{1-ethyl-2-(napthyl-α-azo) imidazole}ruthenium(II) perchlorate. *Polyhedron* 25, 1125-1132.

Dougan, S. J., Melchart, M., Hebtemariam, A., Parsons, S. and Sadler, P. J. 2006. Phenylaz-pyridine and Phenylazo-pyrazole Chlorido Ruthenium(II) Arene Complexes: Arene Loss, Aquation, and Cancer Cell Cytotoxicity. *Inorganic Chemistry* 45, 10882-10894.

Friedman, A. E., Chambron, J. C., Sauvage, J. P., Turro, N. J. and Barton, J. K. 1990. A Molecular Light Switch for DNA: $Ru(bpy)_2(dppz)^{2+}$. *Journal of the American Chemical Society* 112, 4960-4962.

Goswami, S., Chakravorty, A. R. and Chakravorty, A. 1981. Chemistry of Ruthenium. 2.[1] Synthesis, Structure, and Redox Properties of 2-(Arylazo)py-ridine Complexes. *Inorganic Chemistry* 20, 2246-2250.

Goswami, S., Mukherjee, R. and Chakravorty, A. 1983. Chemistry of Ruthenium. 12.[1] Reactions of Bidentate Ligands with Diaquobis[2-(arylazo)pyridine] ruthenium(II) Cation. Stereoretensive Synthesis of Tris Chelates and Their Characterization: Metal Oxidation, Ligand Reduction, and Spectroelectro-Chemical Correlation. *Inorganic Chemistry* 22, 2825-2832.

Hansongnern, K., Tempiam, S., Liou, J.-C., Liao, F.-L. and Lu, T.-H. 2003. Crystal structure of 2-(4′-N,N-Diethylaminophenylazo)pyrimidine. *Analytical Sciences* 19, x13-x14.

Harada, J., Ogawa, K. and Tomoda, S. 1997. Molecular Motion and conformational Interconversion of Azobenzenes in Crystal as studied by X-ray Diffraction. *Acta Crystallographica Section B53*, 662-672.

Hotze, A. C. G., Velders, A. H., Ugozzoli, F., Biagini-Cingi, M., Manotti-Lanfredi, A. M., Haasnoot, J. G. and Reedijk, J. 2000. Synthesis, Characterization, and Crystal Structure of α-$[Ru(azpy)_2(NO_3)_2]$ (azpy = 2-(Phenylazo)pyridine) and the Products of Its Reactions with Guanine Derivatives. *Inorganic Chemistry* 39, 3838-3844.

Hotze, A. C. G., Broekhuisen, M. E. T., Velders, A. H., Kooij, H., Spek, A. L., Haasnoot, J. G. and Reedijk, J. 2002. Crystallographic and NMR Evidence of the Unusual *N6*,*N7*-didentate Chelation of 3-Methyladenine Coordinated to the Cytotoxic α-Dichloro Bis(2-phenylazopyridine)Ruthenium(II) Complex. *Journal of Chemical Society, Dalton Transaction*, 2809-2810.

Hotze, A. C. G., Broekhuisen, M. E. T., Velders, A. H., Schilden, K., Haasnoot, J. G. and Reedijk, J. 2002. Unusual Coordination of the Rare Neutral Imine Tautomer of 9-Methyladenine Chelating in the *N6*,*N7*-Mode to Ruthenium (II) Complexes. *European Journal of Inorganic Chemistry*, 369-376.

Hotze, A. C. G., Bacac, M., Velders, A. H., Jansen, B. A. J., Kooijman, H., Spek, A. L., Haasnoot, J. G. and Reedijk, J. 2003. New Cytotoxic and Water-Soluble Bis-(2-phenylazopyridine)ruthenium(II) Complexes. *Journal of Medicinal Chemistry* 46, 1743-1750.

Hotze, A. C. G., Kooijman, H., Spek, A. L., Haasnoot, J. G. and Reedijk, J. 2004. Synthesis and Characterization of Ruthenium(II) Complexes with the New

Ligand 2-Phenylazopyridine-5-sulfonic Acid (Hsazpy): In Search for New Anticancer Agents. *New Journal of Chemistry* 28, 565-569.

Hotze, A. C. G., Geer, E. P, L., Caspers, S. E., Kooijman, H., Spek, A. L., Haasnoot, J. G. and Reedijk, J. 2004. Coordination of 9-Ethylguanine to the Mixed-Ligand Compound α-[Ru(azpy)(bpy)Cl_2] (azpy = 2-Phenylazopyridine and bpy = 2,2′-Bipyridine). An Unprecedented Ligand Positional Shift, Correlated to te Cytotoxicity of This Type of [Ru$(L)_2Cl_2$] (with L = azpy or bpy) Complex. *Inorganic Chemistry* 43, 4935-4943.

Hotze, A. C. G., Caspers, S. E., Vos, D., Kooijman, H., Spek, A. L., Flamigni, A., Bacac, M., Sava, G., Haasnoot, J. G. and Reedijk, J. 2004. Structure-Dependent in Vitro Cytotoxicity of the Isomeric Complexes [Ru$(L)_2Cl_2$] (L = *o*-Tolylazopyridine and 4-Methyl-2-phenylazopyridine) in Comparison to [Ru$(azpy)_2Cl_2$]. *Journal of Biological Inorganic Chemistry* 9, 354-364.

Hotze, A. C. G., Geer, E. P, L., Kooijman, H., Spek, A. L., Haasnoot, J. G. and Reedijk, J. 2005. Characterization by NMR Spectroscopy, X-ray Analysis and Cytotoxic Activity of the Ruthenium(II) Compounds [RuL′$_2$L′′]$(PF_6)_2$ (L′ , L′′ = 2-Phenylazopyridine, 2,2′-Bipyridine). *European Journal of Inorganic Chemistry*, 2648-2657.

Jasimuddin, S., Byabartta, P., Mostafa, G., Lu, T.H. and Sinha, C. 2004. Synthesis, Spectral Studies, Crystal Structure and Redox Properties of Homoleptic Tris-Chelated Ruthenium(II)-Arylazoimidazoles. *Polyhedron* 23, 727-733.

Jasimuddin, S., Mostafa, G. and Sinha, C. 2004. Mixed Ligand Complexes of Osmium(II)-2,2′-bipyridine: Synthesis, Spectral Characterization and Electro chemical Properties of Bis-chelated-arylazoimidazole-bipyridine-osmium(II) and X-ray Crystal Structure of [(2,2′-bipyridine)-bis-{1-methyl-2-(*p*-tolylazo

)imidazole}osmium(II) hexafluorophosphate. *Inorganica Chimica Acta* 357, 1975-1984.

Jasimuddin, S., Mathur, T. and Sinha, C. 2005. Bis-chelated-arylazoimidazole-1,10-phenanthroline-osmium(II) Complexes. Structure, Spectra and Electrochemistry. *Inorganica Chimica Acta* 358, 3601-3609.

Jenkins, Y., Friedman, A. E., Turro, N. J. and Barton, J. K. 1992. Characterization of Dipyridophenazine Complexes of Ruthenium(II): The Light Switch Effect as a Function of Nucleic Acid Seuence and Conformation. *Biochemistry* 31, 10809-10816.

Jiang, C.-W., Chao, H., Li, H., and Ji, L.-N. 2003. Syntheses, Characterization and DNA-Binding Studies of Ruthenium(II) Terpyridine Complexes: [Ru(tpy)(PHBI)]$^{2+}$ and [Ru(tpy)(PHNI)]$^{2+}$. *Journal of Inorganic Biochemistry* 93, 247-255.

Kaifer, A. E. and Bard, A. J. 1985. Micellar Effects on the Reductive Electrochemistry of Methylviologen. *Journal of Physical Chemistry* 89, 4876-4880.

Kooijman, H., Hotze, A. C. G., Caspers, S. E., Haasnoot, J. G., Reedijk, J. and Spek, A. L. 2004. α-Dichlorobis(2-phenylazo-4,6-dimethylpyridine)Ruthenium(II) chlo- roform Solvate. *Acta Crystallographica Section E* 60, m247-m249.

Krause, R. A. and Krause, K. 1980. Chemistry of Bipyridine-like Ligands. Isomeric Complexes of Ruthenium(II) with 2-(Phenylazo)pyridine. *Inorganic Chemistry* 19, 2600-2603.

Krause, R. A. and Krause, K. 1982. Chemistry of Bipyridine-like Ligands. Mixed Complexes of Ruthenium(II) with 2-(Phenylazo)pyridine: A New π-Bonding Probe. *Inorganic Chemistry* 21, 1714-1720.

Lakowicz, J. R. and Weber, G. 1973. Quenching of Fluorescence by Oxygen. Probe for Structural Fluctuations in Macromolecules. *Biochemistry* 12, 4161-4170.

Liu, J.-G., Ye, B.-H., Zhang, Q.-L., Zou, X.-H. Zhen, Q.-X., Tian, X. and Ji, L.-N. 2000. Enantiometric Ruthenium(II) Complexes Binding to DNA: Binding Modes and Enantioselectivity. *Journal of Biological Inorganic Chemistry* 5, 119-128.

Lu, T-H., Misra, T. K., Lin, P-C., Liao, F-L. and Chung, C-S. 2003. Synthesis and X-ray Characterization of Two Isomeric Dichloro bis-{1-(Phenylazo)isoqui noline}Complexes of Ruthenium. *Polyhedron* 22, 535-541.

Maheswari, P. U. and Palaniandavar, M. 2004. DNA binding and Cleavage Activity of $[Ru(NH_3)_4(diimine)]Cl_2$ Complexes. *Inorganica Chimica Acta* 357, 901-912.

Marmur, J. 1961. A Procedure for the Isolation of Deoxyribonucleic Acid from Micro-organisms. *Journal of Molecular Biology* 3, 208-218.

Mazumder, U. K., Gupta, M., Karki, S. S., Bhattacharya, S., Rathinasamy, S. and Sivakumar, T. 2005. Synthesis and Pharmacological Activities of Some Mononuclear Ru(II) Complexes. *Bioorganic and Medicinal Chemistry* 13, 5766-5773.

Michalski, J., Kucharska, E., Wandas, M., Hanuza, J., Waskowska, A., Maczka, M., Talik, Z., Olejniczak, S., Potrzebowski, M. J. 2005. Crystal structure, vibrational and NMR studies and chemical quantum calculations of 2-phenyl azo-5-nitro-6-methyl-pyridine ($C_{12}H_{10}N_4O_2$). *Journal Molecular Structure* 744-747, 377-392.

Misra, T. K., Das, D., Sinha, C., Ghosh, P. and Pal, C. K. 1998. Chemistry of: Synthesis, Spectral Characterization, Electrochemical Studies, and X-ray Crystal

Structures of Isomeric DichloroBis[1-alkyl-2-(arylazo)imidazole]Complex- es of Ruthenium(II). *Inorganic Chemistry* 37, 1672-1678.

Muaksang, K. 2005. Synthesis and characterization of Ruthenium(II) Complexes with 4-Metyl-2(phenylazo)pyridine Ligands. Master of Science Thesis, Prince of Songkla University, Songkhla, Thailand.

Nagababu, P., Latha, J. N. L. and Satyanarayana, S. 2006. DNA-Binding Studies of Mixed-Ligand (Ethylenediamine)Ruthenium(II) Complexes. *Chemistry and Biodiversity* 3, 1219-1229.

Nair, R. B., Teng, E. S., Kirkland, S. L. and Murphy, C. J. 1998. Synthesis and DNA -Binding Properties of $[Ru(NH_3)_4dppz]^{2+}$. *Inorganic Chemistry* 37, 139-141.

Panneerselvam, K., Hansongnern, K., Rattanawit, N., Liao, F.-L. and Lu, T.-H. 2000. Crystal Structure of the [Protonated 2-(phenylazo)pyridine and Protonated 2-(4-hydroxyphenylazo)pyridine(3:1)]tetrafluoroborate. *Analytical Sciences* 16, 1107-1108.

Pyle, A. M., Rehmann, J. P., Meshoyrer R., Kumar, C. V., Turro, N. J. and Barton, J. K. 1989. Mixed-Ligand Complexes of Ruthenium(II): Factors Governing Binding to DNA. *Journal of the American Chemical Society* 111, 3051-3058.

Quiroga, A. G., Perez, J. M., Lopez-Solera, I., Montero, E. I., Masaguer, J. R., Alonso, C. and Navarro-Ranninger, C. 1998. Binuclear Chloro-Bridged Palladated and Platinated Complexes Derived from *p*-Isopropylbenzaldehyde Thiosemicarba- zone with Cytotoxicity Against Cisplatin Resistant Tumor Cell lines. *Journal of Inorganic Biochemistry* 69, 275-281.

Rattanawit, N. 2002. Chemistry of Ruthenium with 1,10-Phenanthroline, 2-(Phenyl azo)pyridine and Derivatives of 2-(Phenylazo)pyridine. Master of Science Thesis, Prince of Songkla University, Songkhla, Thailand.

Sahavisit, L. and Hansongnern, K. 2005. Synthesis, Spectral Studies and Electrochemical Properties of Ruthenium(II) Complex with New Bidentate Ligand 5-Chloro-2-(phenylazo)pyridine. *Songklanakarin Journal of Science and Technology* 27, 751-759.

Santra, P. K., Misra, T. K., Das, D., Sinha, C., Slawin, A. M. Z. and Woollins, J. D. 1999. Chemistry of Azopyridines. Part II. Synthesis, Spectral, Electrochemistry and X-ray Crystal Structures of Isomeric Dichloro Bis[2-(arylazo)pyrimidine] Complexes of Ruthenium(II). *Polyhedron* 18, 2869-2878.

Satyanarayana, S., Dabrowiak, J. C. and Chaires, J. B. 1993. Tris(phenanthroline) Ruthenium(II) Enantiomer Interactions with DNA: Mode and Specificity of Binding. *Biochemistry* 32, 2573-2584.

Seal, A. and Ray, S. 1984. Structures of Two Isomers of Dichlorobis(2-Phenylazo) pyridine)Ruthenium(II), $[RuCl_2(C_{11}H_9N_3)_2]$. *Acta Crystallographica Section C* 40, 929-932.

Selvakumar, B., Rajendiran, V., Maheswari, P. U., Stoeckli-Evans, H. and Palaniandavar, M. 2006. Structures, Spectra, and DNA-Binding Properties of Mixed Ligand Copper(II) Complexes of Iminodiacetic Acid: The novel role of Diimine Co-Ligands on DNA Conformation and Hydrolytic and Oxidative Double Strand DNA Cleavage. *Journal of Inorganic Biochemistry* 100, 316-330.

Sullivan, B. P., Salmon, D. J. and Meyer, T. J. 1978. Mixed Phosphine 2,2′-Bipyridine Complexes of Ruthenium. *Inorganic Chemistry* 17, 3334-3341.

Tan. L.-F., Chao, H., Liu, Y.-J., Li, H., Sun, B. and Ji, L.-N. 2005. DNA-Binding and Photocleavage Studies of $[Ru(phen)_2(NMIP)]^{2+}$. *Inorganica Chimica Acta* 358, 2191-2198.

Tempiam, S. 2002. Synthesis and Characterization of Ruthenium(II) Complexes with 2,2′-Bipyridine, 2-(4′-N,N-Dimethylaminophenylazo)pyridine and 2-(4′-N,N -Diethylaminophenylazo)pyridine Ligands. Master of Science Thesis, Prince of Songkla University, Songkhla, Thailand.

Vaidyanathan, V. G. and Nair, B. U. 2002. Synthesis, Characterization and DNA Binding Studies of a Ruthenium(II) Complex. *Journal of Inorganic Biochemistry* 91, 405-412.

Vaidyanathan, V. G. and Nair, B. U. 2003. Oxidative Cleavage of DNA by Tridentate Copper(II) Complex. *Journal of Inorganic Biochemistry* 93, 271-276.

Velders, A. H., Kooijman, H., Spek, A. L., Haasnoot, J. G., Vos, D. D. and Reedijk. J. 2000. Strong Difference in the in Vitro Cytotoxicity of Three Isomeric Dichloro bis(2-Phenylazopyridine)ruthenium(II) Complexes. *Inorganic Chemistry* 39, 2966-2967.

Velders, A. H., Schilden, K., Hotze, A., Reedijk. J., Kooijman, H. and Spek, A. L. 2004. Dichlorobis-(2-phenylazopyridine)Ruthenium(II) Complexes: Characterization, Spectroscopic and Structural Properties of Four Isomer. *Dalton Transactions*, 448-455.

Wang, X.-L., Chao, H., Li, H., Hong, X.-L., Liu, Y.-J., Tan, L.-F. And Ji, L.-N. 2004. DNA Interactions of Cobalts (III) Mixed-Polypyridyl Complexes containing Asymmetric Ligands. *Journal of Inorganic Biochemistry* 98, 1143-1150.

Wolfe, A., Shimer, G. H. and Meehan, T. 1987. Polycyclic Aromatic Hydrocarbons Physically Intercalate Into Duplex Regions of Denatured DNA. *Biochemistry* 26, 6392-6396.

Xu, Z.-D., Lui, H.-L., Xiao, S.-L., Yang, M. and Bu, X.-H. 2002. Synthesis, Crystal Structure, Antitumor Activity and DNA-Binding Study on the Mn(II)

Complex of 2*H*-5-hydroxy-1,2,5-oxadiazo[3,4-f]1,10-phenanthroline. *Journal of Inorganic Biochemistry* 90, 79-84.

Zhen, Q.-X., Ye, B.-H., Zhang, Q.-L., Liu, J.-G., Li, H., Ji, L.-N. and Wang, L. 1999. Synthesis, Characterization and the Effect of Ligand Planarity of $[Ru(bpy)_2 L]^{2+}$ on DNA Binding Affinity. *Journal of Inorganic Biochemistry* 76, 47-53.

Zhou, C.-Y., Zhao, J., Wu, Y.-B., Yin, C.-X. and Yang, P. 2007. Synthesis, Characterization and Studies on DNA-Binding of a New Cu(II) Complex with N^1, N^8-Bis(1-methyl-4-nitropyrrole-2-carbonyl)triethylenetetraamine. *Journal of Inorganic Biochemistry* 101, 10-18.

Zou, X.-H., Ye, B.-H., Li, H., Zhang, Q.-L., Chao, H., Liu, J.-G., Ji, L.-N. and Li, X.-Y. 2001. The Design of New Molecular Light Switches for DNA. *Journal of Biological Inorganic Chemistry* 6, 143-150.

APPENDIX

Cut off solvents

Table A.1 The solvents for UV-Visible spectrum and the their cut-off

Solvents	λ(nm)
CH_2Cl_2	230
CH_3COCH_3	330
DMF	270
DMSO	265
C_2H_5OH	195
CH_3OH	195
CH_3CN	195

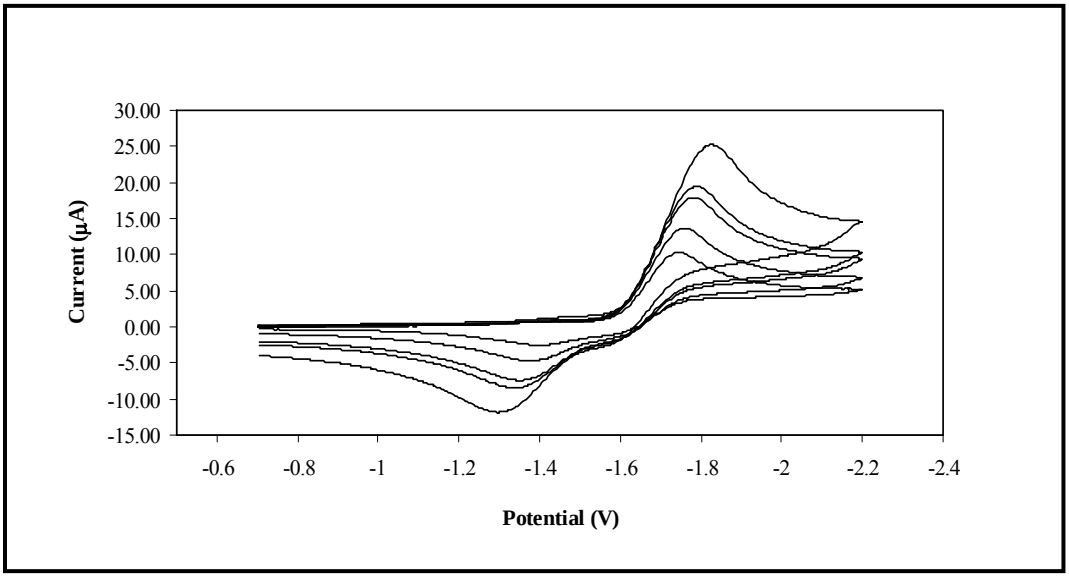

Figure A.1 Cyclic voltammograms of the 5mazpy ligand in the reduction range with various scan rates (50-1000 mVs^{-1})

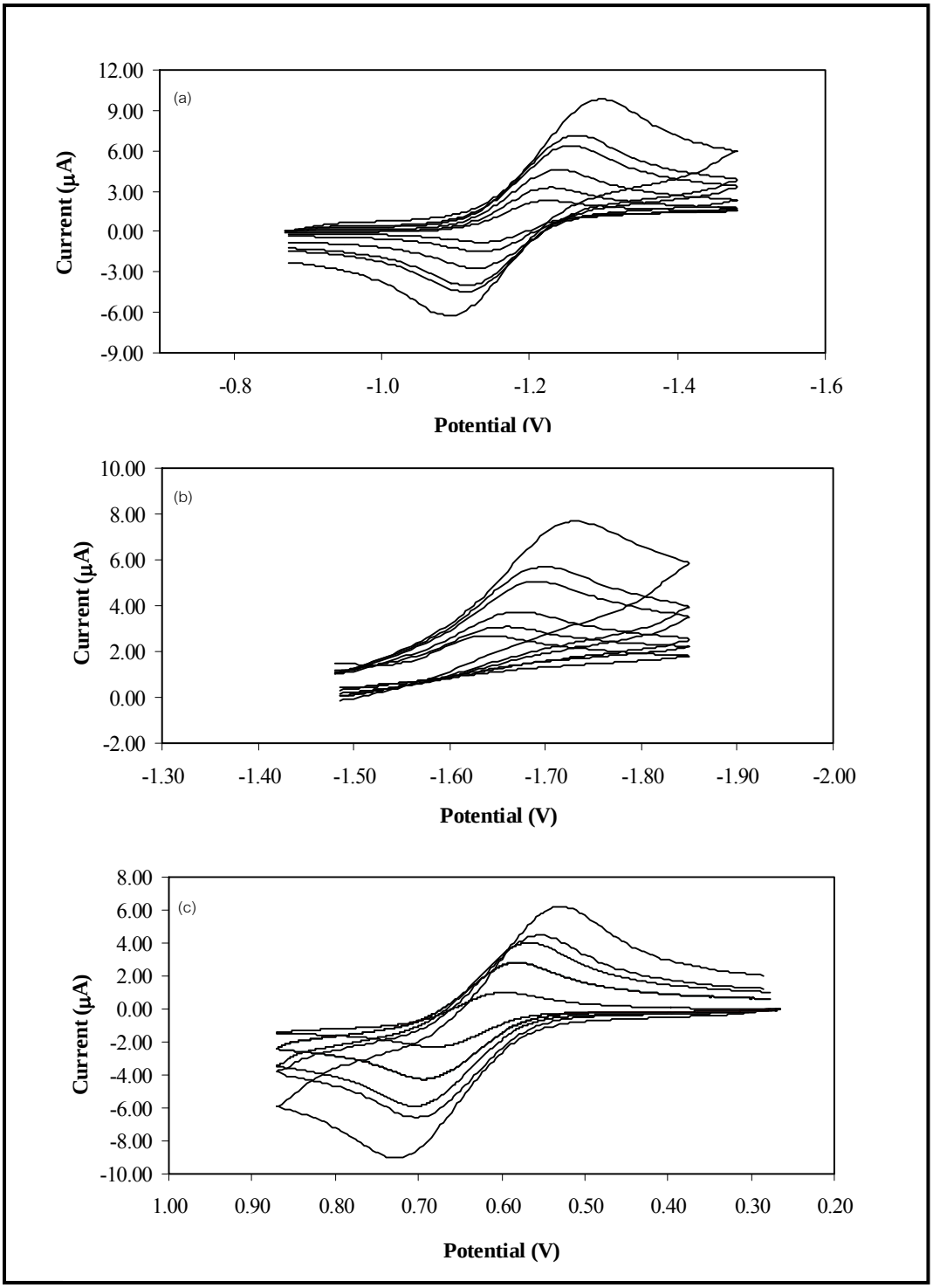

Figure A.2 Cyclic voltammograms of the *ctc*-[Ru(5mazpy)$_2$Cl$_2$] complex – couple (a), couple II (b) in the reduction range and couple Ru(II/III) (c) in oxidation range with various scan rates (50-1000 mVs^{-1})

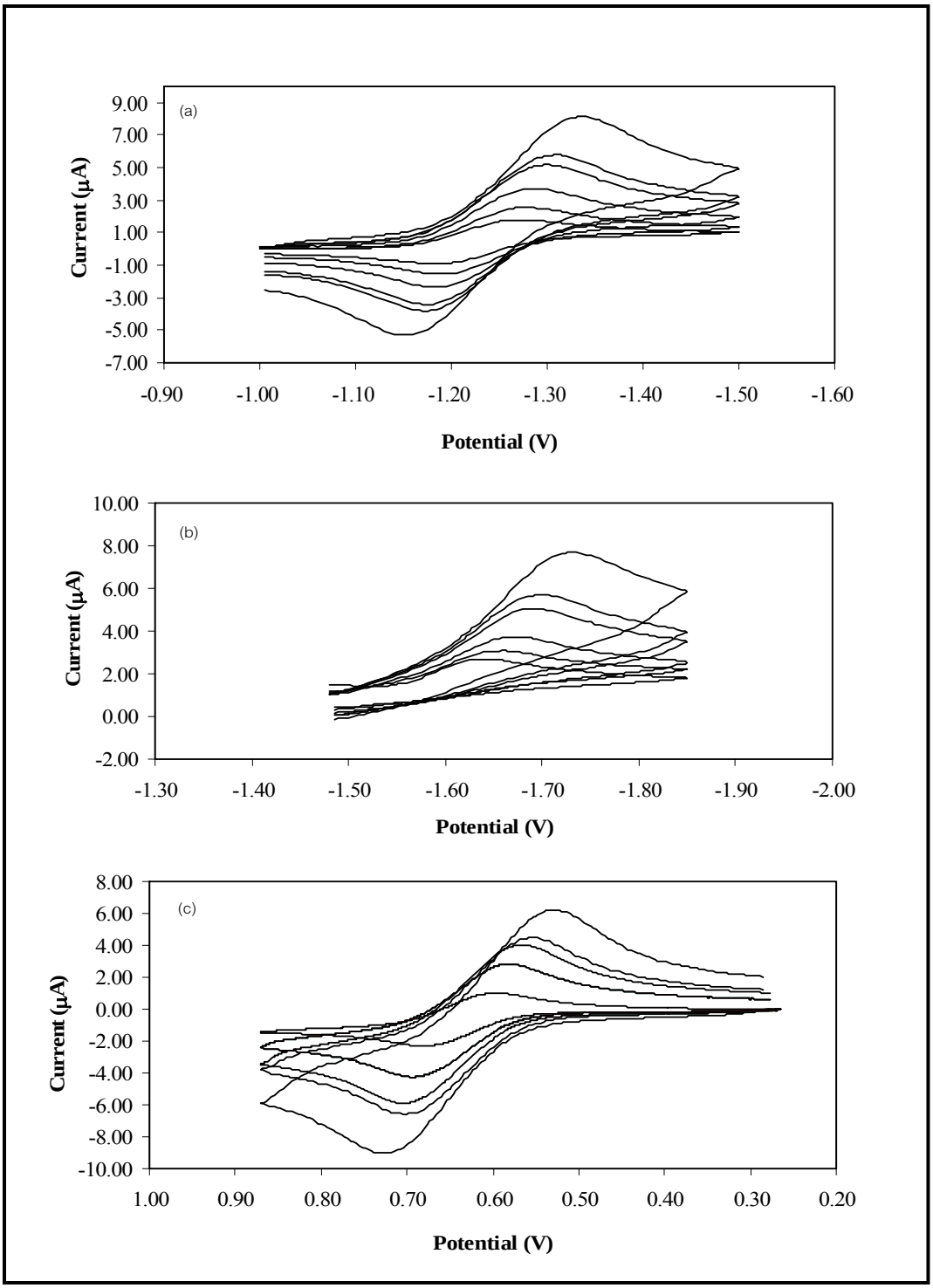

Figure A.3 Cyclic voltammograms of the *ccc*-[Ru(5mazpy)$_2$Cl$_2$] complex - couple I (a), couple II (b) in the reduction range and couple Ru(II/III) (c) in oxidation range with various scan rates (50-1000 mVs^{-1})

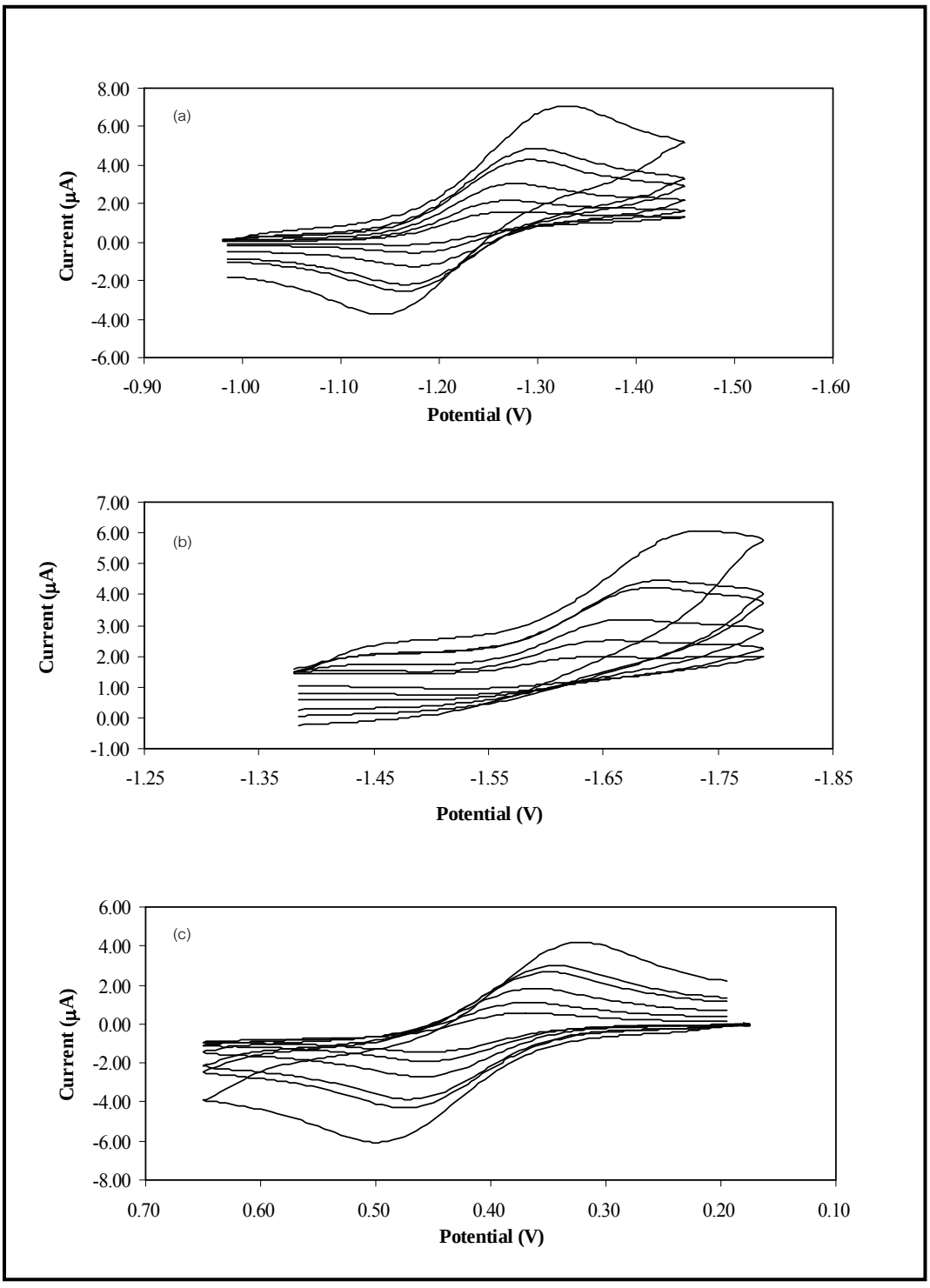

Figure A.4 Cyclic voltammograms of the *tcc*-[Ru(5mazpy)$_2$Cl$_2$] complex - couple I (a), couple II (b) in the reduction range and couple Ru(II/III) (c) in oxidation range with various scan rates (50-1000 mVs^{-1})

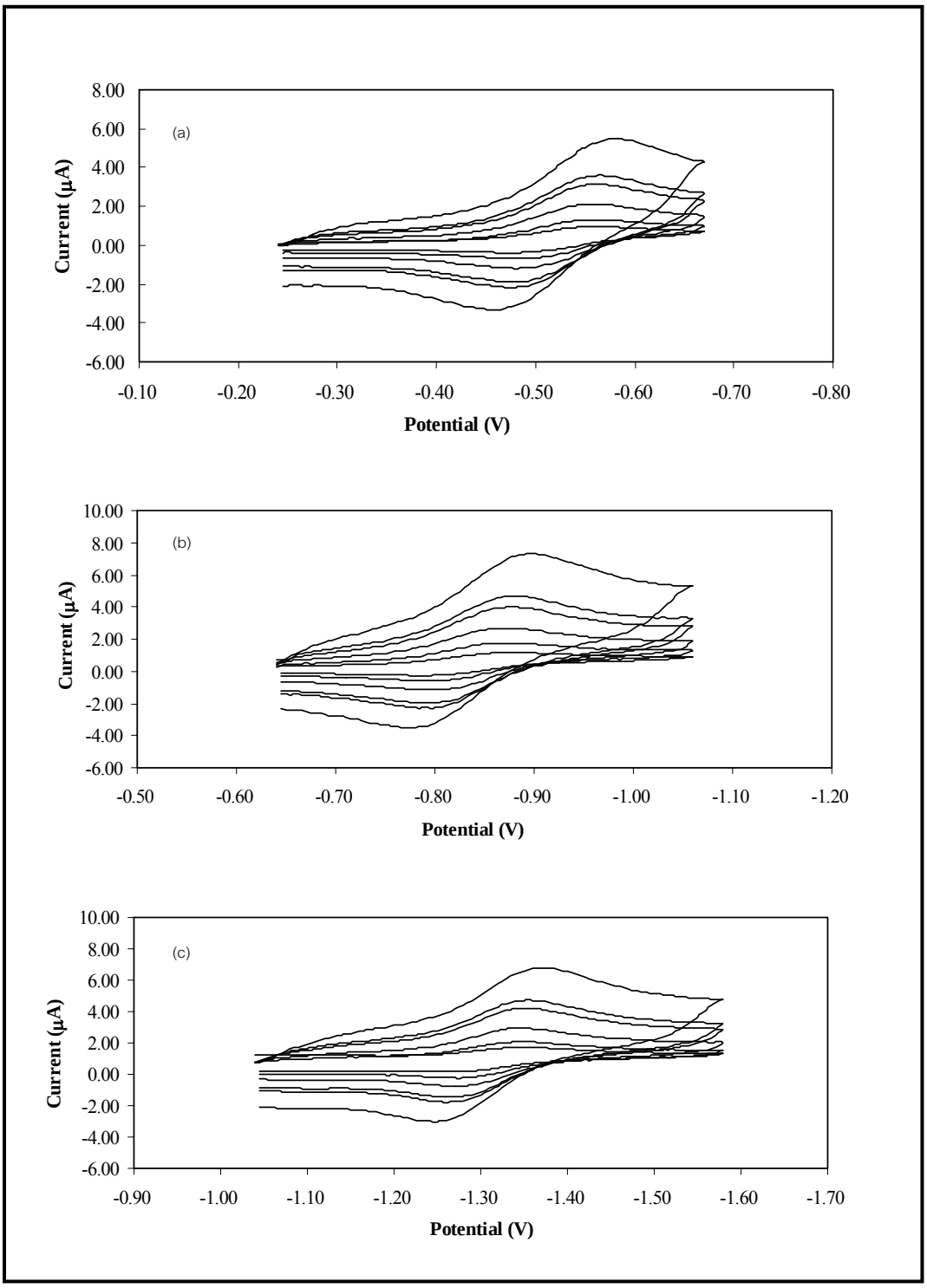

Figure A.5 Cyclic voltammograms of the $[Ru(5mazpy)_3](PF_6)_2$ complex - couple I (a), couple II (b), and couple III (c) in the reduction range with various scan rates (50-1000 mVs^{-1})

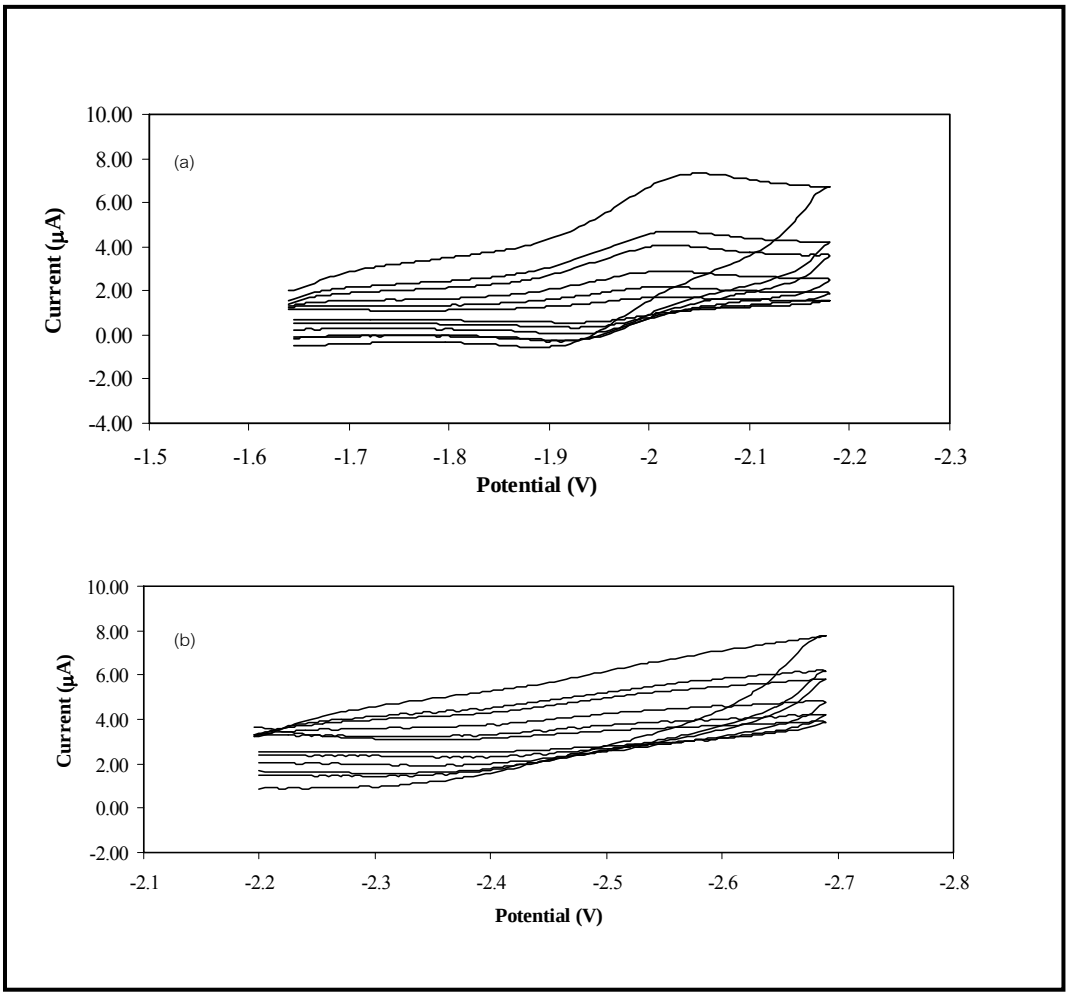

Figure A.6 Cyclic voltammograms of the $[Ru(5mazpy)_3](PF_6)_2$ complex - couple IV (a), and couple V (b) in the reduction range with various scan rates (50-1000 mVs^{-1})

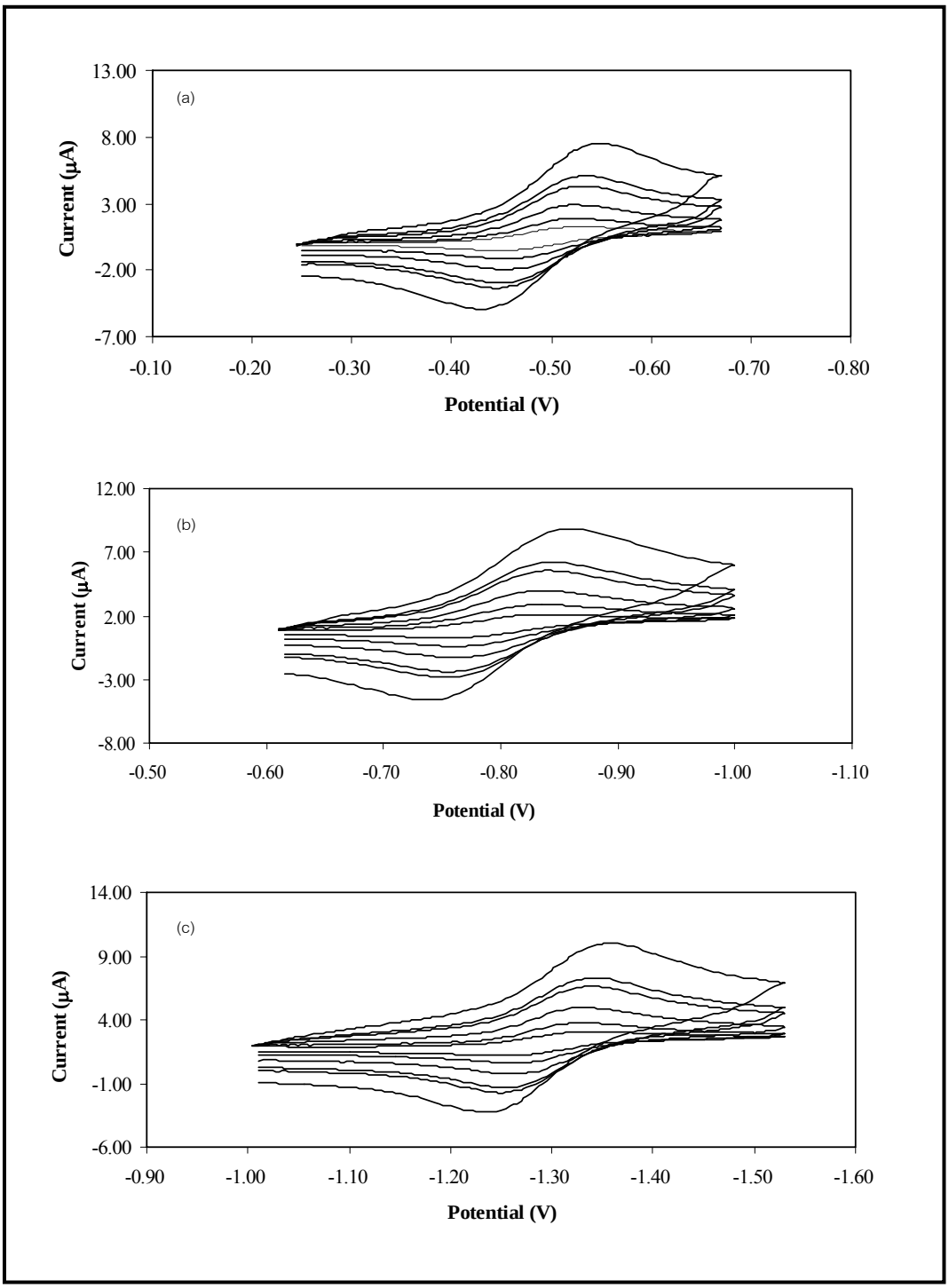

Figure A.7 Cyclic voltammograms of the $[Ru(5mazpy)_2azpy](PF_6)_2$ complex - couple I (a), couple II (b), and couple III (c) in the reduction range with various scan rates (50-1000 mVs^{-1})

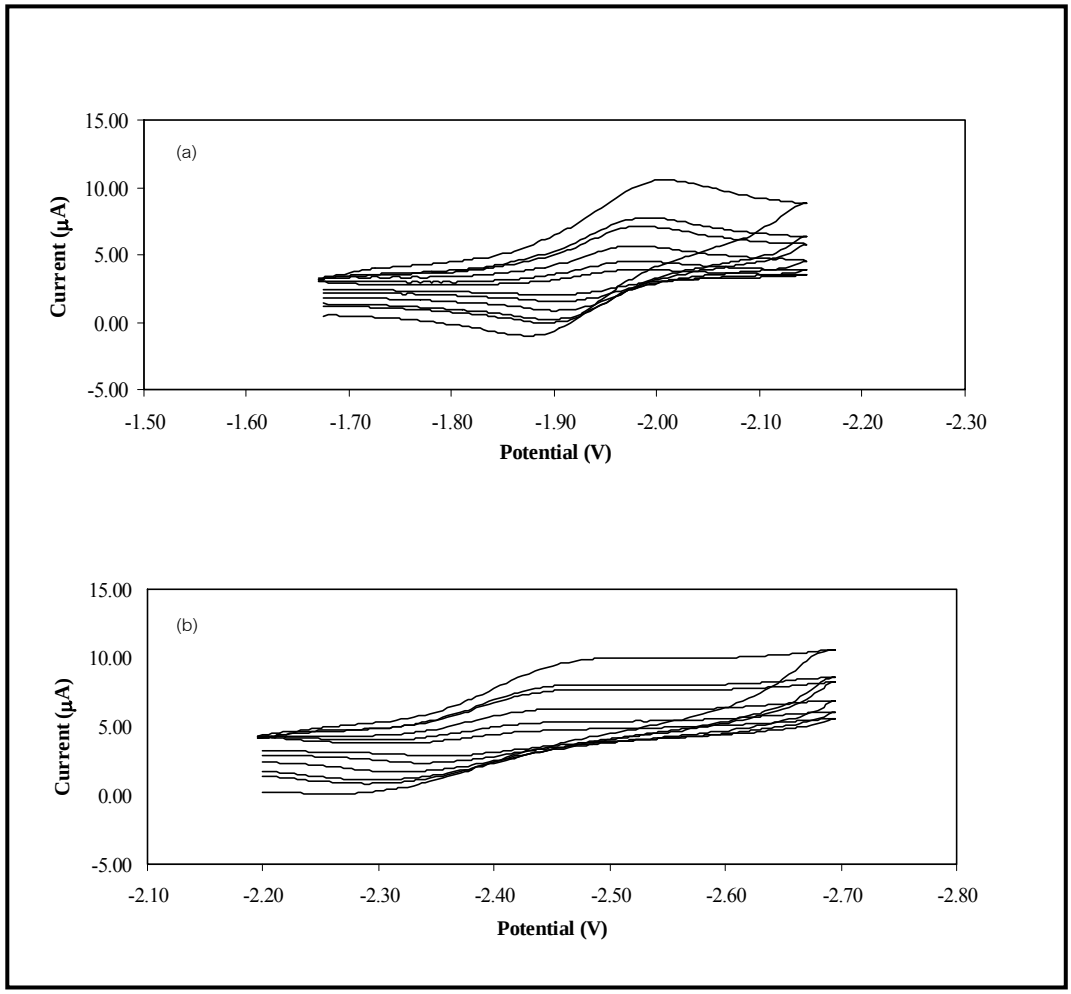

Figure A.8 Cyclic voltammograms of the $[Ru(5mazpy)_2azpy](PF_6)_2$ complex - couple IV (a), and couple V (b) in the reduction range with various scan rates (50-1000 mVs^{-1})

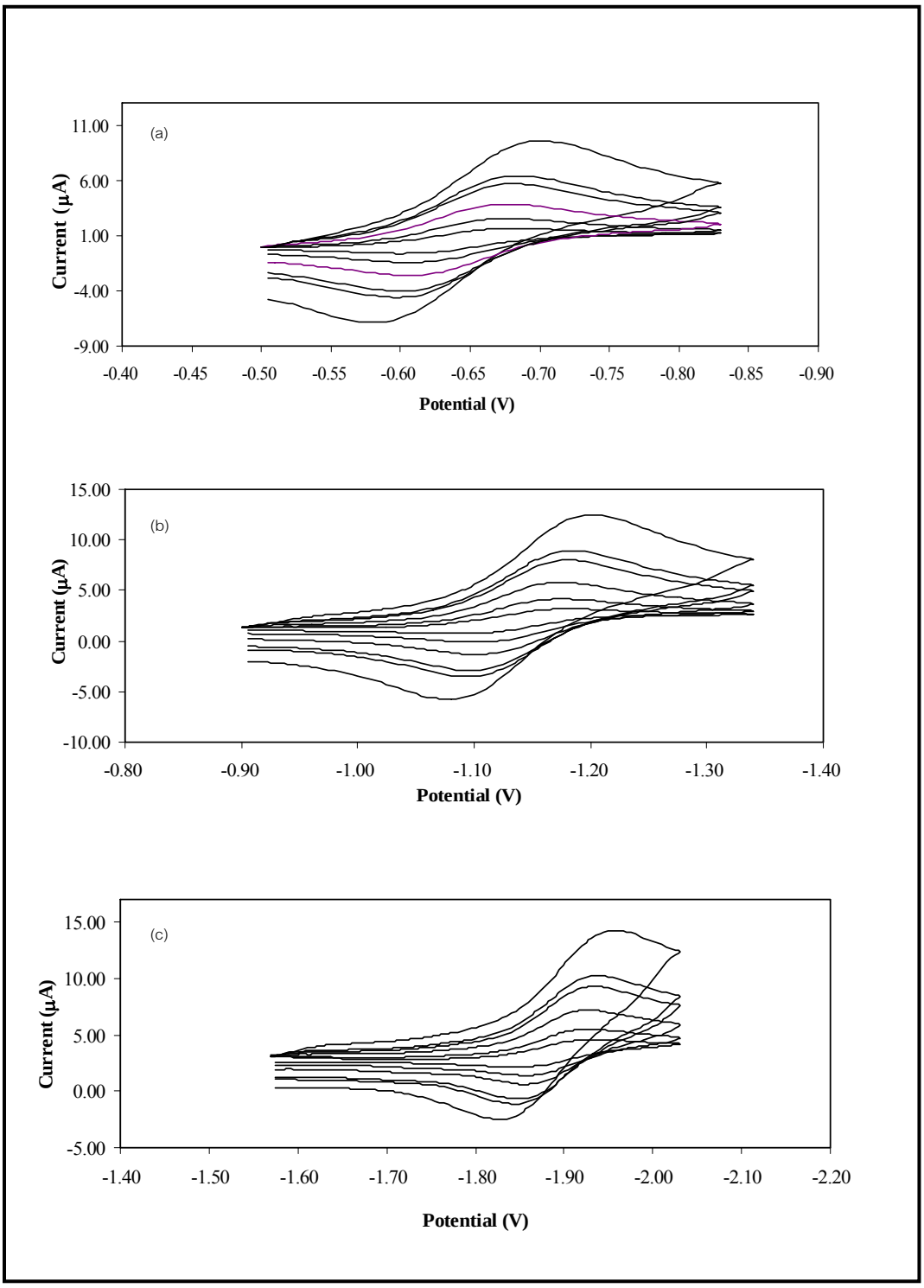

Figure A.9 Cyclic voltammograms of the $[Ru(5mazpy)_2bpy](PF_6)_2$ complex - couple I (a), couple II (b), and couple (III) (c) in the reduction range with various scan rates (50-1000 mVs^{-1})

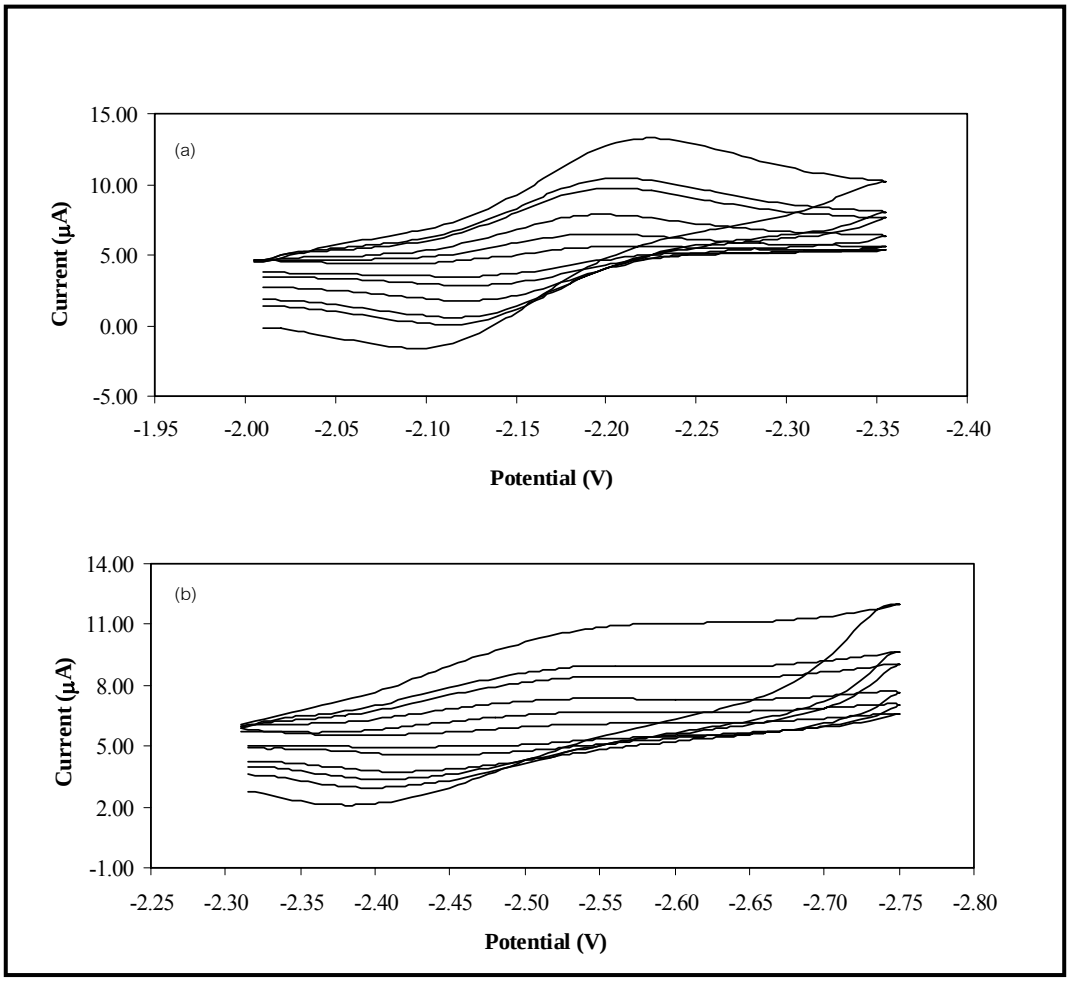

Figure A.10 Cyclic voltammograms of the $[Ru(5mazpy)_2bpy](PF_6)_2$ complex - couple IV (a), and couple V (b) in the reduction range with various scan rates (50-1000 mVs^{-1})

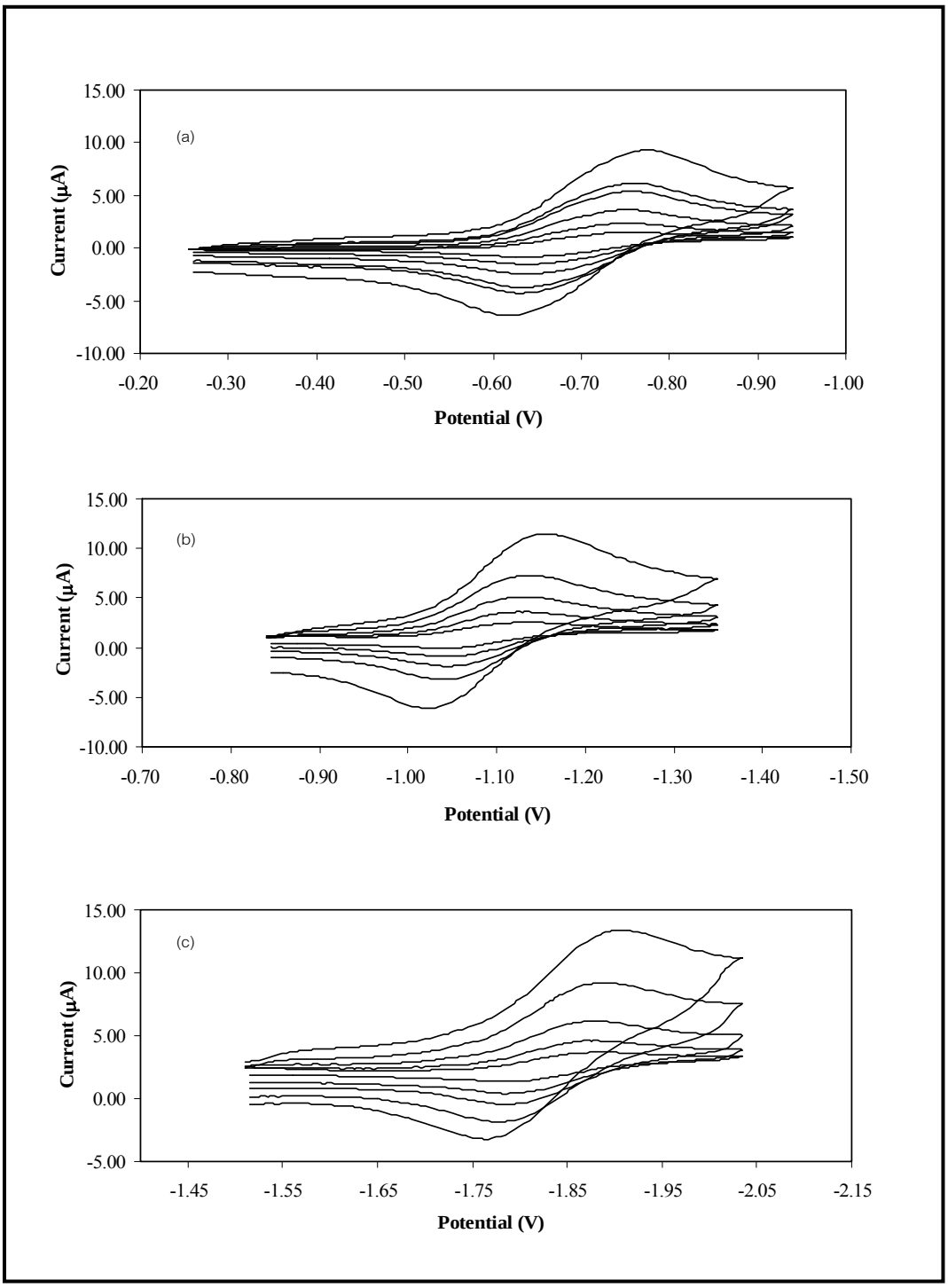

Figure A.11 Cyclic voltammograms of the $[Ru(5mazpy)_2phen](PF_6)_2$ complex - couple I (a), couple II (b), and couple (III) (c) in the reduction range with various scan rates (50-1000 mVs^{-1})

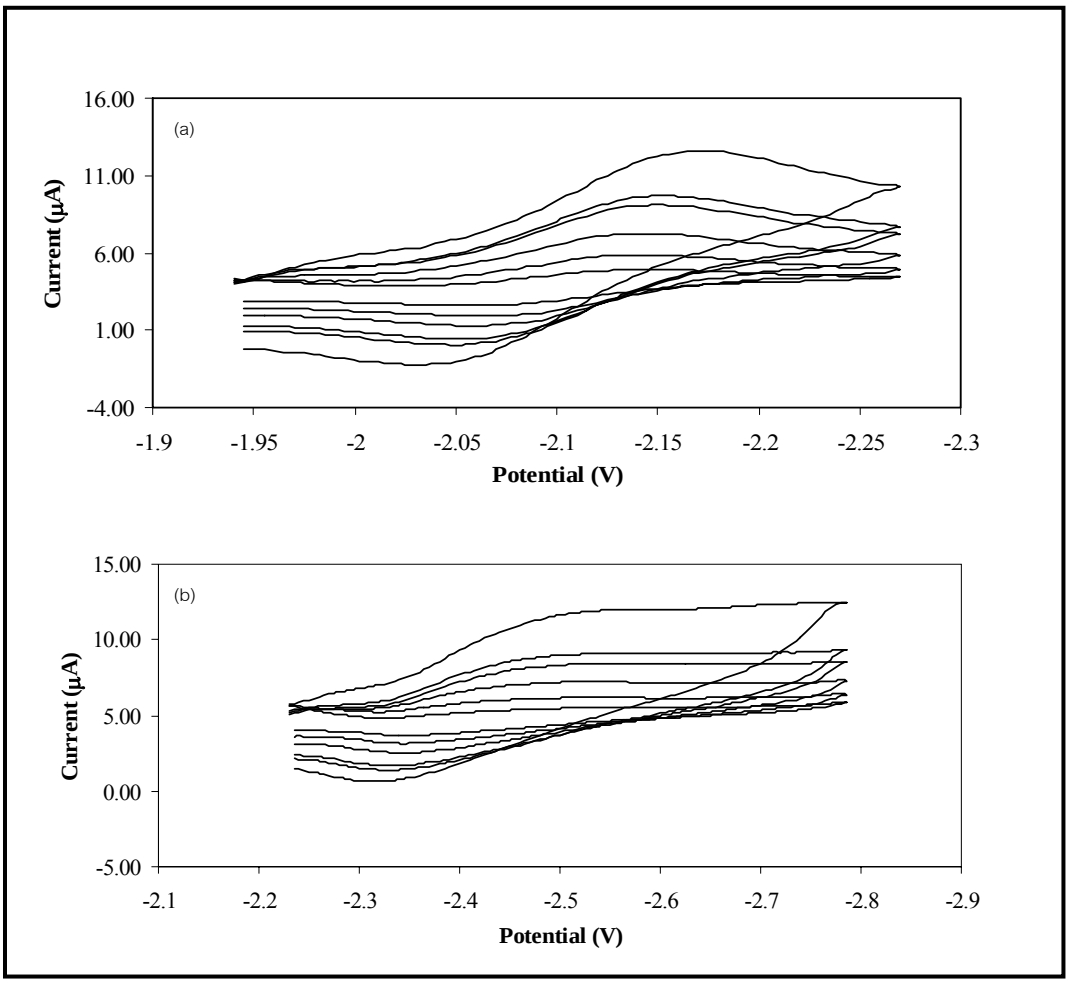

Figure A.12 Cyclic voltammograms of the $[Ru(5mazpy)_2phen](PF_6)_2$ complex - couple IV (a), and couple V (b) in the reduction range with various scan rates (50-1000 mVs^{-1})

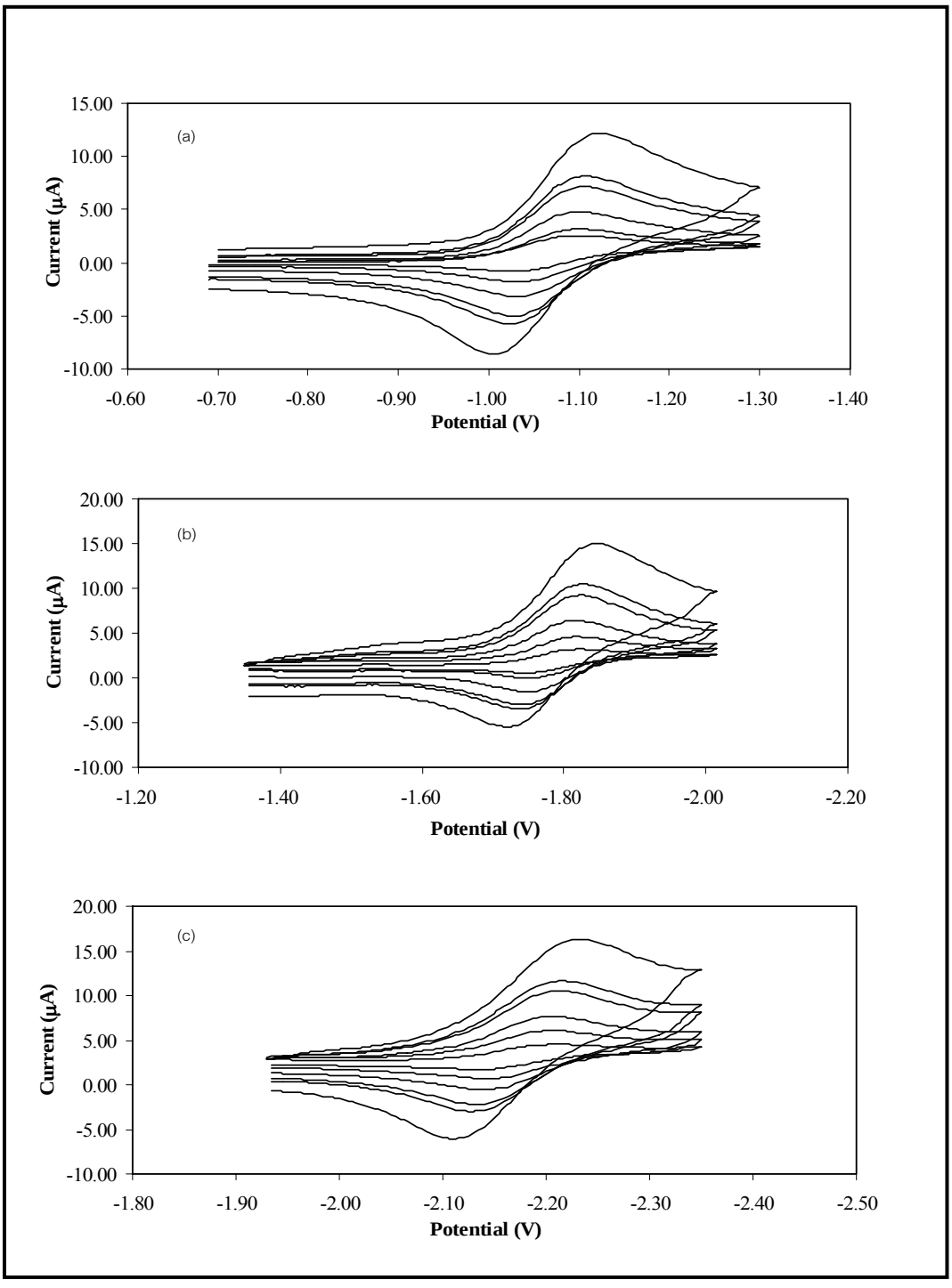

Figure A.13 Cyclic voltammograms of the $[Ru(bpy)_2 5mazpy](PF_6)_2$ complex - couple I (a), couple II (b), and couple (III) (c) in the reduction range with various scan rates (50-1000 mVs^{-1})

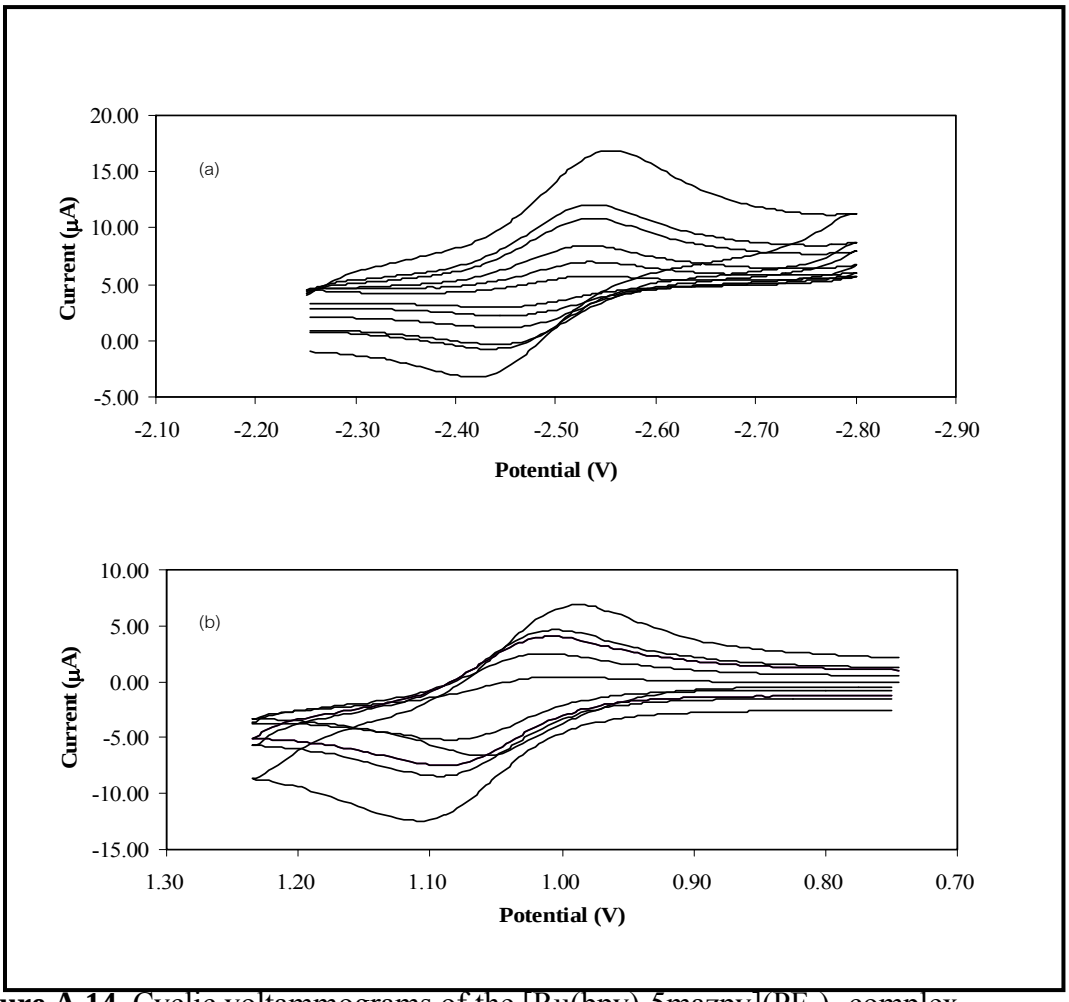

Figure A.14 Cyclic voltammograms of the $[Ru(bpy)_2 5mazpy](PF_6)_2$ complex - couple IV (a), in the reduction range and couple Ru(II/III) (b) in oxidation range with various scan rates (50-1000 mVs^{-1})

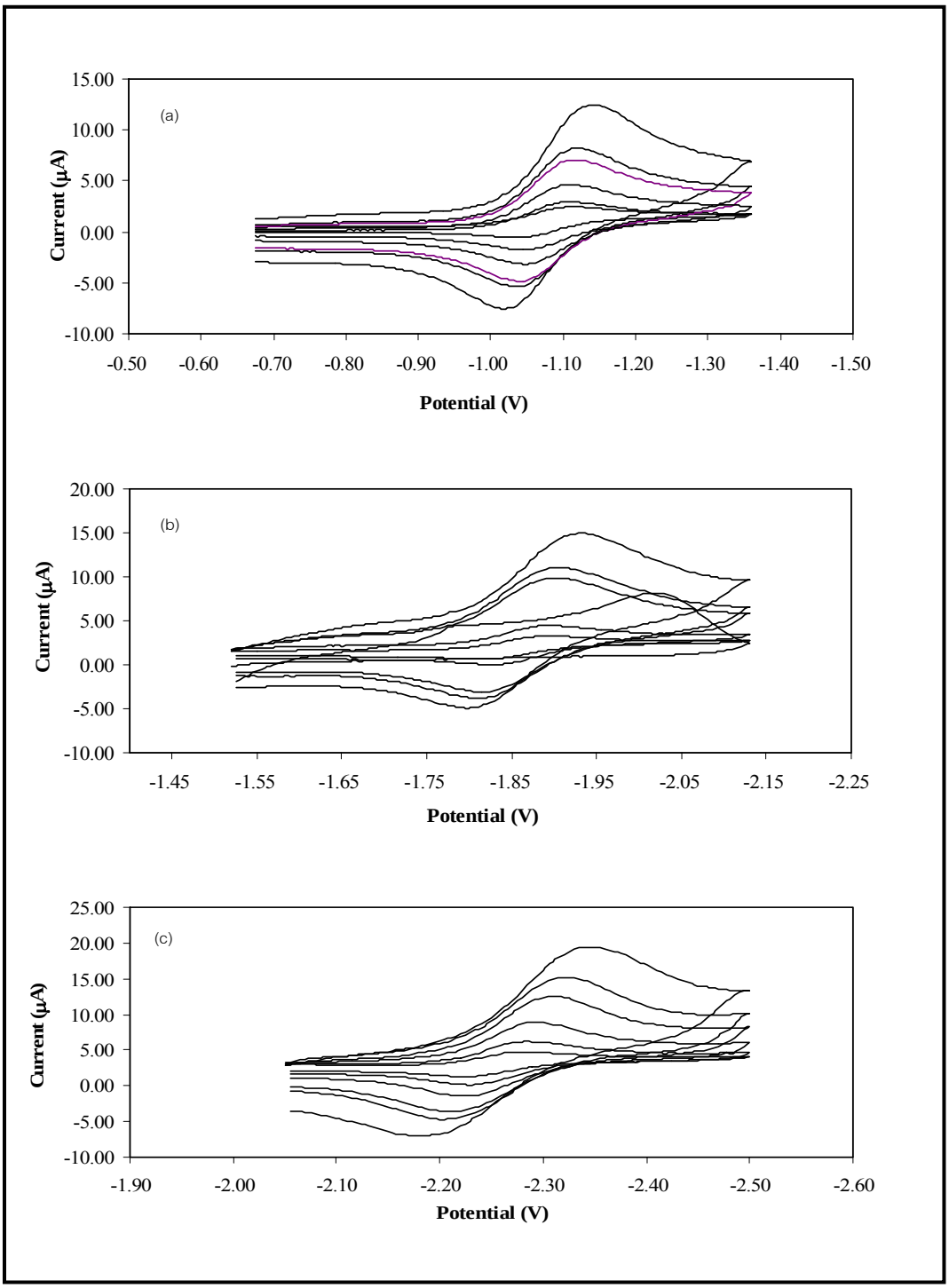

Figure A.15 Cyclic voltammograms of the $[Ru(phen)_2 5mazpy](PF_6)_2$ complex - couple I (a), couple II (b), and couple (III) (c) in the reduction range with various scan rates (50-1000 mVs^{-1})

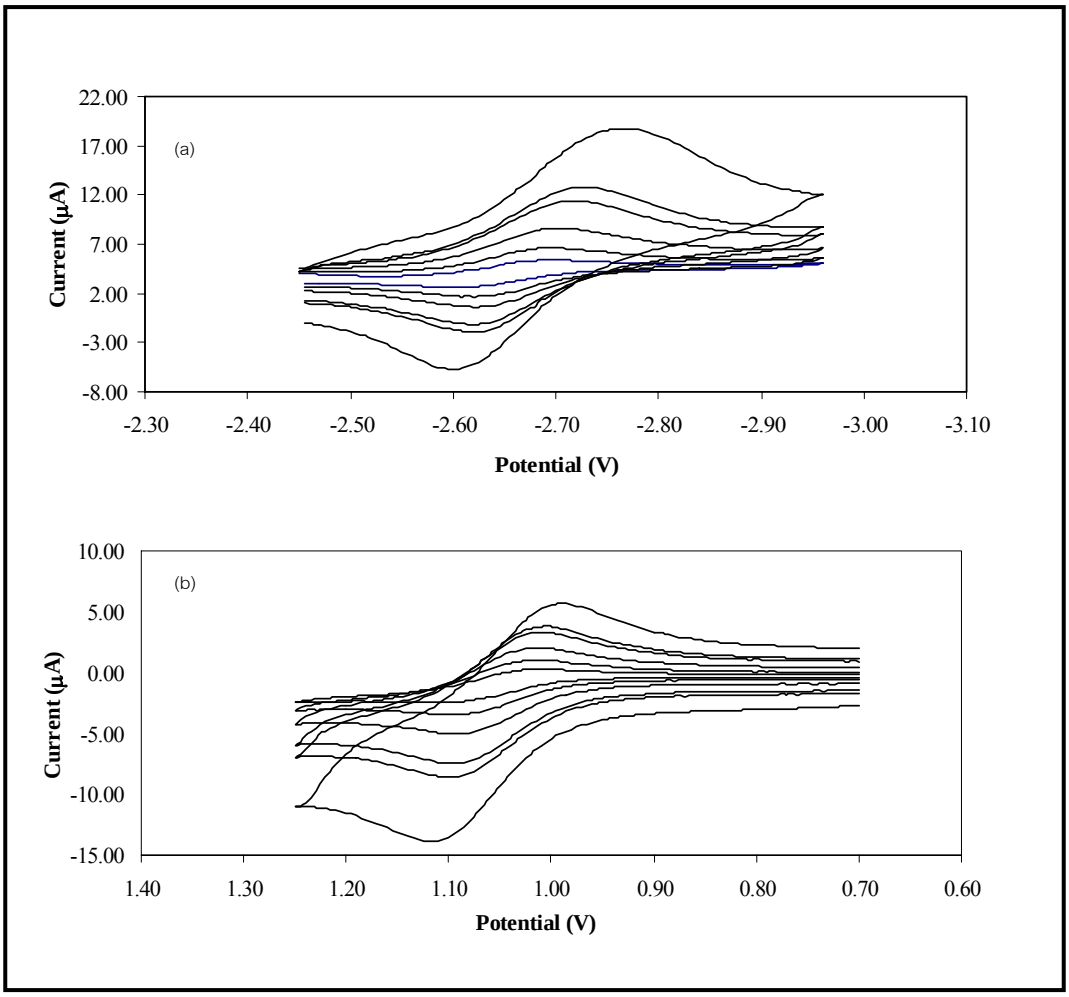

Figure A.16 Cyclic voltammograms of the $[Ru(phen)_2 5mazpy](PF_6)_2$ complex - couple IV (a), in the reduction range and couple Ru(II/III) (b) in oxidation range with various scan rates (50-1000 mVs^{-1})

Table A.2 Bond lengths (Å) and angles (°) of the 5mazpy ligand

Bond lengths (Å)

Atoms	Distances (Å)
N(1)-C(5)	1.329(2)
N(1)-C(1)	1.330(3)
N(2)-N(3)	1.228(2)
N(2)-C(5)	1.442(3)
N(3)-C(6)	1.445(3)
C(1)-C(2)	1.381(3)
C(2)-C(3)	1.382(3)
C(2)-C(12)	1.500(3)
C(3)-C(4)	1.373(3)
C(4)-C(5)	1.385(3)
C(6)-C(7)	1.379(3)
C(6)-C(11)	1.381(3)
C(7)-C(8)	1.379(3)
C(8)-C(9)	1.378(4)
C(9)-C(10)	1.376(4)
C(10)-C(11)	1.371(3)

Bond angles (°)

Atoms	Angles (°)
C(5)-N(1)-C(1)	116.45(18)
N(3)-N(2)-C(5)	112.75(17)
N(2)-N(3)-C(6)	113.70(18)
N(1)-C(1)-C(2)	125.8(2)
C(1)-C(2)-C(3)	115.75(19)
C(11)-C(6)-N(3)	124.90(19)

Table A.2 (continued)

Atoms	Angles (°)
C(8)-C(7)-C(6)	120.0(2)
C(9)-C(8)-C(7)	119.9(2)
C(10)-C(9)-C(8)	119.8(2)
C(11)-C(10)-C(9)	120.6(3)
C(10)-C(11)-C(6)	119.6(2)
C(1)-C(2)-C(12)	121.8(2)
C(3)-C(2)-C(12)	122.5(2)
C(4)-C(3)-C(2)	120.44(19)
C(3)-C(4)-C(5)	118.38(19)
N(1)-C(5)-C(4)	123.13(19)
N(1)-C(5)-N(2)	111.88(17)
C(4)-C(5)-N(2)	125.00(18)
C(7)-C(6)-C(11)	120.0(2)
C(7)-C(6)-N(3)	115.1(2)

Table A.3 Bond lengths (Å) and angles (°) of the *ctc*-[Ru(5mazpy)$_2$Cl$_2$] complex

Bond lengths (Å)

Atoms	Distances (Å)
Ru(1)-Cl(1)	2.4102(7)
Ru(1)-N(1)	2.043(2)
Ru(1)-N(3)	1.972(2)
Ru(1)-Cl(1)	2.4102(7)
Ru(1)-N(1)	2.043(2)
Ru(1)-N(3)	1.972(2)

Table A.3 (continued)

Atoms	Distances (Å)
N(1)-C(1)	1.344(3)
N(1)-C(6)	1.356(3)
N(2)-N(3)	1.284(3)
N(2)-C(6)	1.391(3)
N(3)-C(7)	1.439(3)
C(1)-C(2)	1.387(4)
C(2)-C(3)	1.500(5)
C(2)-C(4)	1.385(4)
C(4)-C(5)	1.369(4)
C(5)-C(6)	1.389(4)
C(7)-C(8)	1.375(4)
C(7)-C(12)	1.378(4)
C(8)-C(9)	1.411(5)

Bond angles (^{o})

Atoms	Angles (^{o})
Cl(1)-Ru(1)-N(1)	88.70(6)
Cl(1)-Ru(1)-N(3)	171.64(6)
Cl(1)-Ru(1)-Cl(1)	91.24(2)
Cl(1)-Ru(1)-N(1)	95.53(6)
Cl(1)-Ru(1)-N(3)	85.17(6)
N(1)-Ru(1)-N(3)	99.14(8)
N(1)-Ru(1)-Cl(1)	95.53(6)
N(1)-Ru(1)-N(1)	173.96(8)
N(1)-Ru(1)-N(3)	76.87(8)
N(3)-Ru(1)-Cl(1)	85.17(6)

Table A.3 (continued)

Atoms	Angles (^{o})
N(3)-Ru(1)-N(1)	76.87(8)
N(3)-Ru(1)-N(3)	99.36(8)
Cl(1)-Ru(1)-N(1)	88.70(6)
Cl(1)-Ru(1)-N(3)	171.64(6)
N(1)-Ru(1)-N(3)	99.14(8)
Ru(1)-N(1)-C(1)	130.14(17)
Ru(1)-N(1)-C(6)	112.17(16)
C(1)-N(1)-C(6)	117.7(2)
N(3)-N(2)-C(6)	111.6(2)
Ru(1)-N(3)-N(2)	120.98(16)
Ru(1)-N(3)-C(7)	124.88(16)
N(2)-N(3)-C(7)	113.2(2)
N(1)-C(1)-C(2)	122.9(2)
C(1)-C(2)-C(3)	120.8(3)
C(1)-C(2)-C(4)	118.2(2)
C(3)-C(2)-C(4)	121.0(3)
C(2)-C(4)-C(5)	120.2(3)
C(4)-C(5)-C(6)	118.4(3)
N(2)-C(6)-N(1)	117.8(2)
N(2)-C(6)-C(5)	119.6(2)
N(1)-C(6)-C(5)	122.7(2)
N(3)-C(7)-C(8)	119.8(2)
N(3)-C(7)-C(12)	119.3(2)
C(8)-C(7)-C(12)	120.9(3)
C(7)-C(8)-C(9)	118.0(3)
C(8)-C(9)-C(10)	120.7(4)
C(9)-C(10)-C(11)	120.6(3)
C(10)-C(11)-C(12)	120.7(4)

Table A.3 (continued)

Atoms	Angles (°)
C(7)-C(12)-C(11)	119.1(3)

Table A.4 Bond lengths (Å) and angles (°) of the *ccc*-[Ru(5mazpy)$_2$Cl$_2$] complex

Bond lengths (Å)

Atoms	Distances (Å)
Ru(1)-N(1)	2.028(3)
Ru(1)-N(3)	2.009(3)
Ru(1)-N(4)	2.060(3)
Ru(1)-N(6)	1.982(3)
Ru(1)-Cl(1)	2.397(1)
Ru(1)-Cl(2)	2.397(1)
N(1)-C(1)	1.339(4)
N(1)-C(6)	1.355(5)
N(2)-N(3)	1.286(4)
N(2)-C(6)	1.387(4)
N(3)-C(7)	1.446(4)
N(4)-C(13)	1.347(4)
N(4)-C(18)	1.344(5)
N(5)-N(6)	1.288(5)
N(5)-C(18)	1.386(5)
N(6)-C(19)	1.433(4)
C(1)-C(2)	1.386(6)
C(2)-C(3)	1.505(6)
C(2)-C(4)	1.397(6)

Table A.4 (continued)

Atoms	Distances (Å)
C(4)-C(5)	1.365(6)
C(5)-C(6)	1.384(6)
C(7)-C(8)	1.373(5)
C(7)-C(12)	1.393(5)
C(8)-C(9)	1.389(6)
C(9)-C(10)	1.360(6)
C(10)-C(11)	1.372(7)
C(11)-C(12)	1.375(7)
C(13)-C(14)	1.381(6)
C(14)-C(15)	1.500(6)
C(14)-C(16)	1.375(8)
C(16)-C(17)	1.368(6)
C(17)-C(18)	1.391(7)
C(19)-C(20)	1.377(6)
C(19)-C(24)	1.383(6)
C(20)-C(21)	1.384(6)
C(21)-C(22)	1.363(8)
C(22)-C(23)	1.366(8)
C(23)-C(24)	1.380(7)

Bond angles (^{o})

Atoms	Angles (^{o})
N(1)-Ru(1)-N(3)	76.8(1)
N(1)-Ru(1)-N(4)	96.6(1)
N(1)-Ru(1)-N(6)	89.5(1)
N(1)-Ru(1)-Cl(1)	88.59(9)

Table A.4 (continued)

Atoms	Angles (^{o})
N(1)-Ru(1)-Cl(2)	177.58(8)
N(3)-Ru(1)-N(4)	171.9(1)
N(3)-Ru(1)-N(6)	98.6(1)
N(3)-Ru(1)-Cl(1)	90.98(9)
N(3)-Ru(1)-Cl(2)	100.83(8)
N(4)-Ru(1)-N(6)	76.6(1)
N(4)-Ru(1)-Cl(1)	93.46(9)
N(4)-Ru(1)-Cl(2)	85.79(8)
N(6)-Ru(1)-Cl(1)	169.59(9)
N(6)-Ru(1)-Cl(2)	90.65(9)
Cl(1)-Ru(1)-Cl(2)	91.65(4)
Ru(1)-N(1)-C(1)	129.0(3)
Ru(1)-N(1)-C(6)	113.0(2)
C(1)-N(1)-C(6)	118.0(3)
N(3)-N(2)-C(6)	112.5(3)
Ru(1)-N(3)-N(2)	119.4(2)
Ru(1)-N(3)-C(7)	129.0(2)
N(2)-N(3)-C(7)	111.6(3)
Ru(1)-N(4)-C(13)	129.6(3)
Ru(1)-N(4)-C(18)	112.4(2)
C(13)-N(4)-C(18)	117.9(4)
N(6)-N(5)-C(18)	112.3(3)
Ru(1)-N(6)-N(5)	120.7(2)
Ru(1)-N(6)-C(19)	126.3(3)
N(5)-N(6)-C(19)	112.8(3)
N(1)-C(1)-C(2)	123.6(4)
C(1)-C(2)-C(3)	120.5(4)
C(1)-C(2)-C(4)	117.0(3)

Table A.4 (continued)

Atoms	Angles (^{o})
C(3)-C(2)-C(4)	122.5(4)
C(2)-C(4)-C(5)	120.4(4)
C(4)-C(5)-C(6)	119.1(4)
N(1)-C(6)-N(2)	117.6(3)
N(1)-C(6)-C(5)	121.9(3)
N(2)-C(6)-C(5)	120.3(4)
N(3)-C(7)-C(8)	119.1(3)
N(3)-C(7)-C(12)	120.3(3)
C(8)-C(7)-C(12)	120.6(4)
C(7)-C(8)-C(9)	119.2(4)
C(8)-C(9)-C(10)	120.7(4)
C(9)-C(10)-C(11)	119.8(4)
C(10)-C(11)-C(12)	121.2(4)
C(7)-C(12)-C(11)	118.6(4)
C(7)-C(12)-C(11)	118.6(4)
N(4)-C(13)-C(14)	123.3(4)
C(13)-C(14)-C(15)	120.6(4)
C(13)-C(14)-C(16)	117.4(4)
C(15)-C(14)-C(16)	122.0(4)
C(14)-C(16)-C(17)	120.4(5)
C(16)-C(17)-C(18)	119.0(3)
C(20)-C(21)-C(22)	121.0(3)
C(21)-C(22)-C(23)	119.0(4)
C(22)-C(23)-C(24)	120.3(5)
C(19)-C(24)-C(23)	119.0(5)

Table A.5 Bond lengths (Å) and angles (^{o}) of the *tcc*-[Ru(5mazpy)$_2$Cl$_2$] complex

Bond lengths (Å)

Atoms	Distances (Å)
Ru(1)-N(3)	1.990(5)
Ru(1)-N(3)	1.990(5)
Ru(1)-N(1)	2.102(5)
Ru(1)-N(1)	2.102(5)
Ru(1)-Cl(1)	2.377(2)
Ru(1)-Cl(1)	2.377(2)
N(1)-C(6)	1.342(7)
N(1)-C(1)	1.344(8)
N(2)-N(3)	1.286(7)
N(2)-C(6)	1.390(8)
N(3)-C(7)	1.448(8)
N(4)-C(14)	0.784(19)
C(1)-C(2)	1.377(9)
C(2)-C(4)	1.369(9)
C(2)-C(3)	1.507(10)
C(4)-C(5)	1.385(10)
C(5)-C(6)	1.387(9)
C(7)-C(8)	1.365(8)
C(7)-C(12)	1.385(9)
C(8)-C(9)	1.390(9)
C(9)-C(10)	1.362(11)
C(10)-C(11)	1.357(12)
C(11)-C(12)	1.385(10)
C(13)-C(14)	2.00(2)

Table A.5 (Continued)

Bond angles (^{o})

Atoms	Angles (^{o})
N(3)-Ru(1)-N(3)	105.2(3)
N(3)-Ru(1)-N(1)	75.5(2)
N(3)-Ru(1)-N(1)	179.31(19)
N(3)-Ru(1)-N(1)	179.31(19)
N(3)-Ru(1)-N(1)	75.5(2)
N(1)-Ru(1)-N(1)	103.9(3)
N(3)-Ru(1)-Cl(1)	95.26(15)
N(3)-Ru(1)-Cl(1)	88.40(14)
N(1)-Ru(1)-Cl(1)	91.33(14)
N(1)-Ru(1)-Cl(1)	84.94(14)
N(3)-Ru(1)-Cl(1)	88.40(14)
N(3)-Ru(1)-Cl(1)	95.27(15)
N(1)-Ru(1)-Cl(1)	84.94(14)
N(1)-Ru(1)-Cl(1)	91.33(14)
Cl(1)-Ru(1)-Cl(1)	173.97(9)
C(6)-N(1)-C(1)	116.9(5)
C(6)-N(1)-Ru(1)	111.2(4)
C(1)-N(1)-Ru(1)	131.6(4)
N(3)-N(2)-C(6)	112.1(5)
N(2)-N(3)-C(7)	109.5(5)
N(2)-N(3)-Ru(1)	121.0(4)
C(7)-N(3)-Ru(1)	129.5(4)
N(1)-C(1)-C(2)	124.6(6)
C(4)-C(2)-C(1)	117.7(6)
C(4)-C(2)-C(3)	121.5(6)
C(1)-C(2)-C(3)	120.7(6)

Table A.5 (continued)

Atoms	Angles (^{o})
N(1)-Ru(1)-Cl(1)	120.7(6)
C(2)-C(4)-C(5)	119.4(6)
C(4)-C(5)-C(6)	119.3(6)
N(1)-C(6)-C(5)	122.1(6)
N(1)-C(6)-N(2)	118.1(5)
C(5)-C(6)-N(2)	119.6(5)
C(8)-C(7)-C(12)	121.1(6)
C(8)-C(7)-N(3)	119.0(5)
C(12)-C(7)-N(3)	119.9(6)
C(7)-C(8)-C(9)	119.2(6)
C(10)-C(9)-C(8)	119.6(7)
C(11)-C(10)-C(9)	121.3(7)
C(10)-C(11)-C(12)	120.0(7)
C(7)-C(12)-C(11)	118.7(7)
N(4)-C(14)-C(13)	160.5(19)

Table A.6 Bond lengths (Å) and angles (^{o}) of the $[Ru(5mazpy)_2bpy](PF_6)_2$ complex

Bond lengths (Å)

Atoms	Distances (Å)
Ru(1)-N(1)	2.15(2)
Ru(1)-N(2)	2.06(2)
Ru(1)-N(4)	2.05(2)
Ru(1)-N(1)	2.15(2)
Ru(1)-N(2)	2.06(2)
Ru(1)-N(4)	2.05(2)

Table A.6 (continued)

Atoms	Distances (Å)
N(1)-C(1)	1.30(5)
N(1)-C(5)	1.30(3)
C(1)-C(2)	1.41(5)
C(2)-C(3)	1.38(5)
C(3)-C(4)	1.35(6)
C(4)-C(5)	1.34(4)
C(5)-C(5)	1.57(4)
N(2)-C(6)	1.37(4)
N(2)-C(10)	1.26(3)
C(6)-C(7)	1.36(4)
C(7)-C(71)	1.56(6)
C(7)-C(8)	1.33(5)
C(8)-C(9)	1.39(6)
C(9)-C(10)	1.39(4)
C(10)-N(3)	1.38(5)
N(3)-N(4)	1.26(3)
N(4)-C(11)	1.40(5)
C(11)-C(12)	1.51(4)
C(11)-C(16)	1.40(6)
C(12)-C(13)	1.39(9)
C(13)-C(14)	1.2(1)
C(14)-C(15)	1.43(9)
C(15)-C(16)	1.43(8)
P(1)-F(1)	1.54(1)
P(1)-F(2)	1.54(1)
P(1)-F(3)	1.54(1)
P(1)-F(4)	1.45(1)
P(1)-F(5)	1.461(9)

Table A.6 (continued)

Bond angles (^{o})

Atoms	Angles (^{o})
N(1)-Ru(1)-N(2)	87.7(8)
N(1)-Ru(1)-N(4)	100.4(9)
N(1)-Ru(1)-N(1)	78(1)
N(1)-Ru(1)-N(2)	100.5(9)
N(1)-Ru(1)-N(4)	174.8(8)
N(2)-Ru(1)-N(4)	74.2(9)
N(2)-Ru(1)-N(1)	100.5(9)
N(2)-Ru(1)-N(2)	169.5(8)
N(2)-Ru(1)-N(4)	97.4(9)
N(4)-Ru(1)-N(1)	174.8(8)
N(4)-Ru(1)-N(2)	97.4(9)
N(4)-Ru(1)-N(4)	81.7(9)
N(1)-Ru(1)-N(2)	87.7(8)
N(1)-Ru(1)-N(4)	100.4(9)
N(2)-Ru(1)-N(4)	74.2(91)
Ru(1)-N(1)-C(1)	121(2)
Ru(1)-N(1)-C(5)	115(2)
C(1)-N(1)-C(5)	124(3)
N(1)-C(1)-C(2)	116(3)
C(1)-C(2)-C(3)	121(3)
C(2)-C(3)-C(4)	117(3)
C(3)-C(4)-C(5)	121(3)
N(1)-C(5)-C(4)	120(3)
N(1)-C(5)-C(5)	116(2)
C(4)-C(5)-C(5)	123(3)
Ru(1)-N(2)-C(6)	126(1)

Table A.6 (continued)

Bond angles (^{o})

Atoms	Angles (^{o})
C(6)-N(2)-C(10)	121(3)
N(2)-C(6)-C(7)	118(2)
C(6)-C(7)-C(71)	123(3)
C(6)-C(7)-C(8)	121(4)
C(71)-C(7)-C(8)	116(3)
C(7)-C(8)-C(9)	120(3)
C(8)-C(9)-C(10)	116(3)
N(2)-C(10)-C(9)	123(3)
N(2)-C(10)-N(3)	123(3)
C(9)-C(10)-N(3)	114(3)
C(10)-N(3)-N(4)	110(2)
Ru(1)-N(4)-N(3)	120(2)
Ru(1)-N(4)-C(11)	121(2)
N(3)-N(4)-C(11)	119(2)
N(4)-C(11)-C(12)	114(4)
N(4)-C(11)-C(16)	124(3)
C(12)-C(11)-C(16)	122(4)
C(11)-C(12)-C(13)	113(4)
C(12)-C(13)-C(14)	128(5)
C(13)-C(14)-C(15)	120(6)
C(14)-C(15)-C(16)	121(6)
C(11)-C(16)-C(15)	115(4)

VITAE

Name Miss Uraiwan Changsaluk

Student ID 4623017

Educational Attainment

Degree	Name of Institution	Year of Graduation
Bachelor of Science (Chemistry)	Prince of Songkla University	2001
Master of Science (Inorganic Chemistry)	Prince of Songkla University	2002

Scholarship Awards during Enrolment

1. Center for Innovation in Chemistry: Postgraduate Education and Research Program in Chemistry (PERCH-CIC) (2003-2005).
2. Teaching Assistant

List of Publication and Proceeding

Publications

1. Hansongnern, K., Changsaluk, U., and Pakawatchai, C. Crystal Structure of 5-Methyl- 2-(phenylazo)pyridine *Analytical Sciences*, Accepted for publication.

2. Hansongnern, K., Changsaluk, U., and Pakawatchai, C. Crystal Structure of the *ccc*- $[Ru(5mazpy)_2Cl_2]$ Complex *Analytical Sciences*, submitted.

3. Hansongnern, K., Changsaluk, U., Wu, J.-S., and Lu, T.-H., Crystal Structure of the $[Ru(azpy)_2(bpy)](PF_6)_2$ Complex (azpy = 2-(phenylazo) pyridine, bpy = 2,2′-bipyridine) *Analytical Sciences*, 2007, **23**, x131-x132.

4. Changsaluk, U., and Hansongnern, K. Dichlorobis(5-Methyl-2-phenylazopyridine) Ruthenium(II) Complex: Characterization and NMR Spectroscopy *Songklanakarin J. Sci. Technol* , 2005, **27**, 739-749